

# Cellular Nanoparticle Delivery by G-Protein Coupled Receptors

Dissertation to obtain the Degree of Doctor of Natural Sciences  
(Dr. rer. nat.)  
from the Faculty of Chemistry and Pharmacy  
University of Regensburg



Presented by  
**Wolfgang Hild**  
from Landshut

March 2010

This work was carried out from May 2005 until April 2009 at the Department of Pharmaceutical Technology of the University of Regensburg.

The thesis was prepared under supervision of Prof. Dr. Achim Göpferich.

Submission of the PhD application:		19.03.2010
Date of examination:		07.05.2010
Examination board:	Chairman:	Prof. Dr. S. Elz
	1. Expert:	Prof. Dr. A. Göpferich
	2. Expert:	Prof. Dr. J. Heilmann
	3. Examiner:	Prof. Dr. F.-M. Matysik

To my family

---

A pessimist sees the difficulty in every opportunity, an optimist sees the opportunity  
in every difficulty - *Winston Churchill*

# Table of contents

<b>Chapter 1</b>	Introduction .....	7
<b>Chapter 2</b>	Goals of the Thesis .....	51
<b>Chapter 3</b>	Synthesis of Quantum Dots – Comparison Between Non-coordinating and Coordinating Solvents.....	55
<b>Chapter 4</b>	Solubilization and Characterization of Quantum Dots for Biological Applications .....	79
<b>Chapter 5</b>	Characterization of Aqueous Quantum Dot Dispersions using Asymmetrical Flow Field-flow Fractionation (AF4) .....	105
<b>Chapter 6</b>	Cell-culture Characterization of Quantum Dots.....	121
<b>Chapter 7</b>	G-Protein Coupled Receptor Targeted Micelles.....	137
<b>Chapter 8</b>	G-protein Coupled Receptor Targeted Nanoparticles Allow for Choosing between Membrane Binding and Cellular Uptake .....	155
	Supporting Information.....	175
<b>Chapter 9</b>	Towards the Characterization of the Mechanism of Internali- zation of QDs Targeted to Neuropeptide Y Y <sub>1</sub> -receptors .....	185
<b>Chapter 10</b>	Summary and Conclusions .....	203
<b>Appendix</b>	Abbreviations .....	211
	Curriculum Vitae .....	215
	List of Publications .....	216
	Acknowledgements.....	218



# Chapter 1

## Introduction:

### **Quantum dots – Nano-sized Probes for the Exploration of Cellular and Intracellular Targeting**

W. A. Hild, M. Breunig, A. Göpferich

Department of Pharmaceutical Technology, University of Regensburg,  
Universitätsstraße 31, 93040 Regensburg, Germany

**Abstract**

Nanoparticles emerged as promising tool in drug targeting, since, after appropriate modification, they are able to deliver their payload to specific sites, like tissues, cells, or even certain cellular organelles. In this context, the delivery of nanoparticles from the circulation into the target cells represents a crucial step. Here, model drug delivery systems such as quantum dots are ideal candidates to elucidate this process in more detail, since they provide outstanding features like a small and uniform size, unique optical properties for most sensitive detection and modifiable surfaces.

Recent progress in the surface chemistry of quantum dots expanded their use in biological applications, reduced their cytotoxicity and rendered quantum dots a powerful tool for the investigation of distinct cellular processes, like uptake, receptor trafficking and intracellular delivery.

In this review, we will not only describe the ideal attributes of QDs for biological applications and imaging but also their distinct specific and non-specific pathways into the cells as well as their intracellular fate.



## 1. Introduction

In contemporary drug therapy, most drugs are designed to bind to specific receptors or receptor subtypes. However, these drugs still lack selectivity for specific sites in the human body, namely specific cells, tissues or organs since the receptors may be expressed at various sites of the body. In addition, modern drugs tend to have unfavorable pharmacokinetic properties. As a consequence, the dose of the drug has to be increased. However, this raises the cost of the therapy as well as side-effects. In some cases, the design of prodrugs can improve this situation but, so far, we are far from a general solution.

A more promising solution to this problem can be expected by targeted nanoparticles for site-specific drug delivery [1]. Under ideal circumstances, these drug carriers, mediated by a targeting sequence, should deliver their payload only to specific target cells, tissues or organs [2].

Nanoparticles are tools that can compensate for unfavorable physico-chemical properties of the drug and therefore may optimize the bioavailability and the biodistribution of the drug. However, after their application to the circulation such particles face several obstacles until they are able to reach their destination. First, the particles have to escape from the reticulo endothelial system (RES) consisting of phagocytosing cells. These are mainly located in the liver, the spleen and the bone marrow, which rapidly remove “foreign” particles from the circulation. The recognition of nanoparticles by the RES can be reduced by modifying the surface of the particles with “protein repulsive” molecules, such as polyethylene glycol (PEG) [3,4]. Apart from that, the particles will have to pass biological barriers like the endothelium or they will have to penetrate tissues. Both processes, however, require small, nanoparticulate drug delivery systems of optimal size. Additionally, targeting sequences on the particle surfaces are needed to address the drug carrier to specific cells [5]. Last but not least, when the nanoparticles have reached the target cell, the final question still remains unanswered: How can the drug be delivered into the cell, in case of an intracellular site of action?

To obtain detailed information on the particle design for optimized intracellular drug delivery, well-defined model colloids are necessary, since the pathways for nanoparticles into cells strongly depend on the properties of the colloid itself like its

size. The importance of this is emphasized by the fact that the different pathways for the cellular uptake of a colloid already determine its fate inside the cell [6]. Another crucial parameter is the surface composition of the nanoparticles. As an example, protein repulsive molecules on the surface of the colloid, like PEGs, can mask the particles for cells. As a consequence, non-specific cellular particle uptake [7] beyond specific mechanisms, like receptor-mediated endocytosis, can be reduced. This fact is crucial to obtain specific targeting to the desired cell type. A last, obvious requirement for the model colloid is that it must be easily detectable, e.g. by fluorescence, in order to follow its cellular uptake and intracellular accumulation in certain organelles.

Unfortunately, conventional nanoparticles, like polymer-based ones, often possess quite broad size distributions, which limit the use of these particles for the examination of the cellular uptake and intracellular distribution. When these particles are tagged with fluorescent dyes, this can also change the physico-chemical properties of the particles significantly.

Quantum dots (QDs), fluorescent, semiconductor nanoparticles, overcome these problems due to their small size, narrow size distribution, and unique optical properties. This enables the investigation of size-dependence of cellular uptake and the detection of the particles due to their fluorescence. Furthermore, these nanoparticles can be modified with a number of targeting ligands. Taken together, these properties render QDs ideal model colloids to study the cellular uptake and intracellular targeting of nanoparticles.

In this review, we show that QDs are used to answer particular questions in the realm of cellular nanoparticle delivery, like *what is the optimal size of a particle for endocytosis* [8], *how can non-specific uptake of particles be reduced by surface PEGylation* [9], or *which receptors can mediate specific uptake of colloids* [10,11]? Other approaches focus on how specific organelles can be targeted by QDs, once the particles have arrived inside a cell [12,13]. Dividing the complex field of drug targeting with nanoparticles into such distinct questions, which can be answered by using well-defined, QD-based colloids, will promote the progress in this research area.

The review is structured as follows: after a short overview of the properties and advantages of QDs, we will show how these particles can be modified in order to use them for the analysis of specific cellular uptake. This will be followed by a

presentation of the distinct pathways for cellular uptake and intracellular delivery of nanoparticles. In the next section, an overview of approaches of cellular uptake studies as well as of organelle targeting with QDs will be given. Finally, possibilities for further developments in intracellular drug targeting using QDs will be presented.

## **2. Non-invasive imaging using nanoparticles**

For the development of drug targeting systems, non-invasive imaging technologies play a key-role, since they allow for following the fate of nanoparticles inside biological systems, like cells, tissues or whole organisms.

Non-invasive imaging of nanoparticles includes a number of techniques, like positron emission tomography (PET), single photon emission computed tomography (SPECT), magnetic resonance imaging (MRI) and optical imaging. These techniques differ concerning their sensitivity, resolution complexity and demands on personnel and equipment (for more detailed information see [14, 19])

In order to investigate the interactions between nanoparticles and biological systems, particles of well-defined size and size distribution are required, as presented above. Three widely used systems provide these properties: colloidal gold [14], superparamagnetic iron oxide particles (SPIONs) [15] and semiconductor nanocrystals (QDs) [10]. However, these particles show great differences in their detectability, which is the second, important demand on a model colloid. All of these particles can be detected by transmission electron microscopy. Yet, this technique requires the fixation of the cells which does not allow for studies of dynamic processes in living cells. SPIONs can additionally be detected by MRI. This technique proves especially favorable in deep-tissue and *in vivo* imaging. Though, the resolution of this technique is not suitable for the investigation of processes on the cellular level (see table 1).

QDs, on the other hand, offer some advantages in imaging cell-particle interactions. They can be detected easily by (confocal) fluorescence microscopy which is most preferable for the observation of distinct cellular processes, like endocytosis and intracellular trafficking. The high resolution, sensitivity and versatility of fluorescence detection render QDs the most suitable of these three systems for the described application.

	<i>Transmission electron microscopy (TEM)</i>	<i>Magnetic resonance imaging (MRI)</i>	<i>Fluorescence laser scanning microscopy (CLSM)</i>
applications	<i>in vitro</i> imaging (cell fixation required)	deep-tissue <i>in vivo</i> -imaging [16]	intracellular imaging <i>In vivo</i> imaging [17]
resolution	visualization of sub-cellular distribution [18]	sensitivity and resolution (10-100 $\mu$ m) not for sub-cellular processes [19]	high resolution (to the single molecule level) [11,20]
imaged nanoparticles	gold, superparamagnetic iron oxide, quantum dots	superparamagnetic iron oxide	quantum dots

*Table 1: Comparison of imaging technologies for different types of nanocrystals*

### 3. Properties of QDs for optical imaging

QDs -small (1-10 nm) semiconductor nanocrystals- have attracted increasing attention due to their unique optical properties as compared to conventional organic fluorescent dyes. QDs possess a bright fluorescence, which means that they can absorb light efficiently due to their large extinction coefficient together with high quantum yields (up to 85% [21]), which is the ratio of the number of photons emitted to the number of photons absorbed. Together with their high stability with regard to photobleaching as compared to conventional fluorophores, QDs enable high sensitive detection and long observation times in fluorescence microscopy [22]. What is more, QDs have a large Stokes shift, which is the difference between the wavelength of absorbed and emitted light. They also exhibit narrow emission spectra [23] as compared to conventional organic fluorescent dyes. As a consequence, the fluorescence signal of QDs can easily be separated from the light of the excitation source. In addition, these unique optical properties allow for multiple-color imaging without crosstalk between different detection channels in fluorescence microscopes. Additionally, QDs of different emission maxima can be excited by one single wavelength [24], which eliminates the need for numerous excitation sources in the instrumental setup. The relatively long fluorescence lifetime (20-50 ns [25]) enables time-resolved detection of the QD-fluorescence which can significantly increase the signal-to-background ratio (factor of 15) relative to cell auto-fluorescence [26].

The range of the fluorescence maxima of QDs is determined by their elemental composition and extends over the whole visible spectrum (e.g. CdS and CdSe) to the

near infrared (NIR; e.g. CdTe). Furthermore, within the emission range given by the elemental composition, the emission maximum of QDs can be tuned precisely by adjusting the size of the QDs. Smaller QDs emit light of lower wavelengths than larger particles. For example, the emission maxima of CdSe nanocrystals of 3 and 7 nm in diameter are approximately 550 and 650 nm, respectively [27]. The so-called QD cores then usually are covered by a shell of another semiconductor, mostly ZnS [21,28,29] (figure 1). The thus generated core-shell QDs provide enhanced quantum yields as compared to the blank cores [30]. An interesting phenomenon is the so-called “blinking”, an on-off behaviour of the luminescence signal of the QDs. This phenomenon is caused by charge trapping and un-trapping at surface defects during excitation and results in an alternation of bright and dark states during which no photons are emitted [31]. Blinking can be a limiting factor for detection but can also represent a useful fingerprint, for example to follow trafficking of receptors labeled with QDs [20].

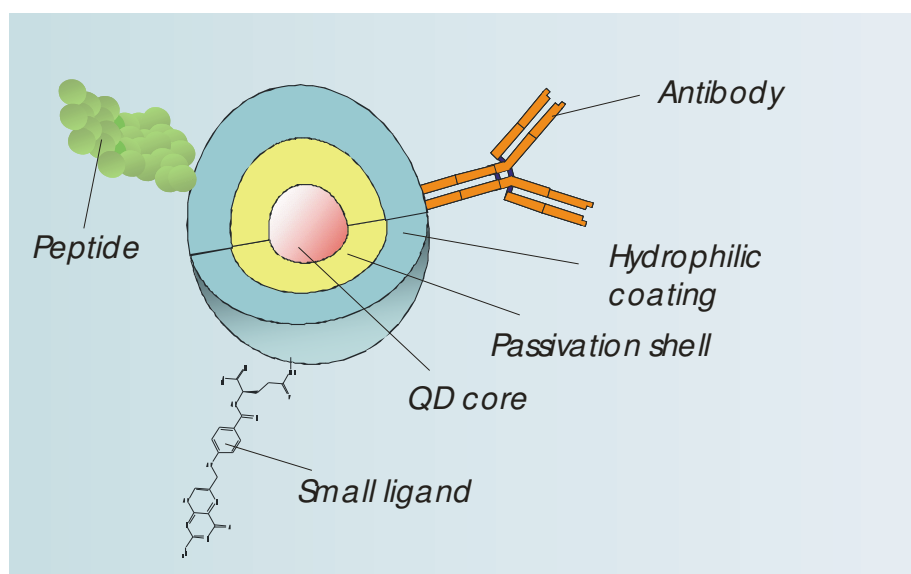


**Figure 1: Scheme of a QD for biological application.** The nanocrystal core (e.g. CdSe) is passivated by another semiconductor shell (e.g. ZnS). The QD-surface is covered by a hydrophilic coating which enables conjugation to biological active compounds (e.g. antibodies, peptides or small ligands, here depicted for folic acid).

Recent developments in QD technology also expanded the applicability in the field of *in vivo* imaging, especially of small animals. Important advances in this field have been achieved by the use of NIR emitting QDs [32] since the penetration of NIR light into tissues is significantly higher than light of lower wavelengths, which is scattered

and absorbed by the tissue [33; 34]. An increase in detectability can also be achieved by combining the unique optical properties of the QDs with MRI traceability [35,36,37], which further enhances the possibility of tissue imaging. Another approach to improve the detectability of QDs *in-vivo* is given by so-called self-illuminating QDs. Here, no excitation source is needed since using the phenomenon of bioluminescence resonance energy transfer (BRET), a bioluminescent molecule coupled to QDs serves for the excitation of the QDs. As a consequence, the sensitivity of detection and the signal-to-background ratio *in vivo* is enhanced [38].

#### **4. Surface modifications and bioconjugation of QDs**

Unmodified QDs cannot be used for cellular studies since, after most of the QD synthesis strategies, the particles are water-insoluble. Therefore, to make use of their unique properties, the particles have to be modified on the surface. Additionally, the particles have to be conjugated with cell-specific biomolecules like proteins or peptides, in order to investigate specific uptake mechanisms and intracellular targeting.

QDs are mostly synthesized in non-polar organic solvents and are solubilized in these solvents by hydrophobic surface ligands like aliphatic phosphines and phosphine oxides, fatty acids and aliphatic amines. For solubilisation in aqueous buffers, the hydrophobic QD-surface needs to be modified by a hydrophilic coating (figure 1). This coating additionally has to prevent aggregation of the QDs, e.g. by electrostatic stabilization or by steric repulsion between the particles mediated by a polymer coating. The hydrophobic surface ligands can be exchanged by thiol-containing molecules [10,39], oligomeric phosphines [40], dendrons [41], or peptides [42,43]. Other approaches encapsulate the QDs in a silica shell [44] or use hydrophobic interactions between the QDs and amphiphilic polymers [45,46] or phospholipids [47] for modification (for a more detailed review, see [48]).

Since the QDs are supposed to be used for the investigation of distinct cellular uptake processes, the particles have to be connected to biomolecules like peptides or proteins, which can address the colloid to certain structures on the cell surface, like receptors. Therefore, the surface of the QD colloid must also provide functional groups or other reactive sites which can react with the biomolecules (figure 1).

There are several possibilities for the attachment of biomolecules to QDs. A commonly used strategy is the use of QDs containing streptavidin because they can

easily be linked to biotin-tagged biomolecules [11,20,24,49] (figure 2A). Yet, since streptavidin is quite bulky (~ 60 kDa) and can bind four biotin molecules, steric and size aspects have to be considered. Hence, small covalent linkages are often preferred when the particle size of the QD bioconjugate is critical for the application, for example when intracellular pores have to be crossed or cellular transport proteins are targeted. Such covalent bonds can be formed by carboxylic acids, for instance provided by a mercapto acid coating of the QDs. The mercapto groups of such acids can bind to the QDs while the carboxylic acid functions can form stable amide bonds with amines in presence of coupling reagents, like carbodiimides and *N*-hydroxysuccinimides (NHS) [10,50] (figure 2B).

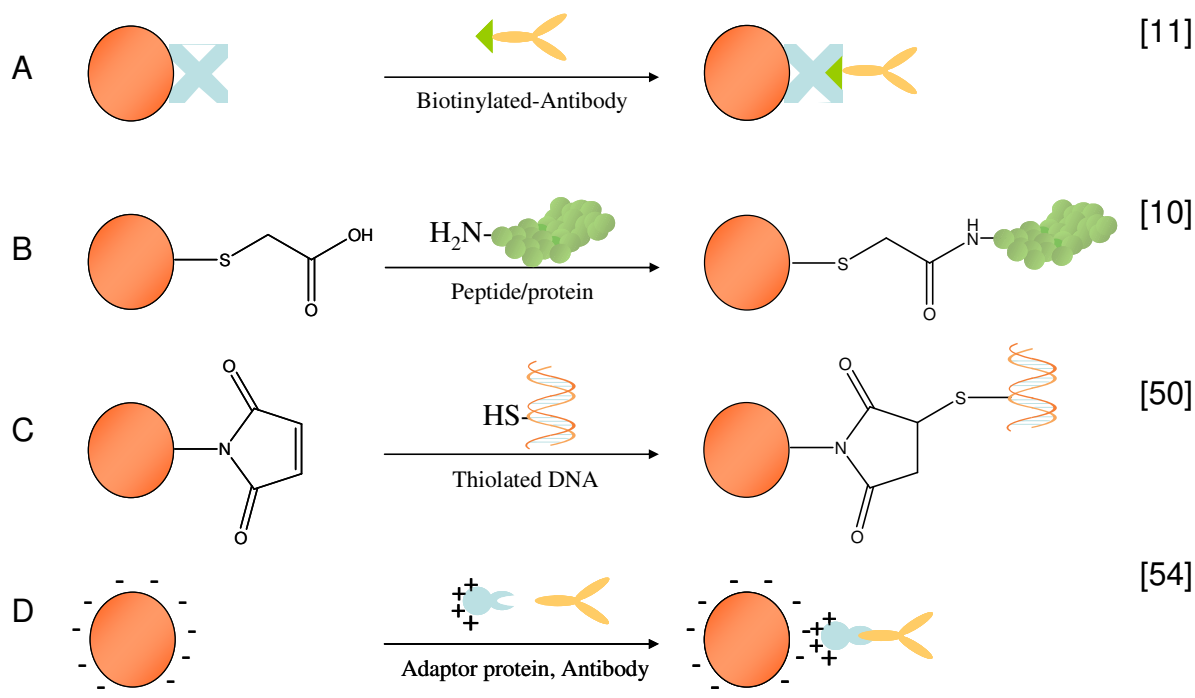


**Figure 2: Examples for bioconjugation of differently functionalized QDs to biomolecules by various strategies. For details, please see text.**

Stable, covalent bonds can also be formed between maleimides and thiols, resulting in a thioether between QDs and biomolecules [47,49,51] (figure 2C). Heterobifunctional crosslinkers, like sulfosuccinimidyl-4-(*N*-maleimidomethyl)-cyclohexane-1-carboxylate (sulfo-SMCC), can be used to couple thiol-containing biomolecules with amine-coated QDs [47], or vice versa [52]. Thiol groups in proteins or peptides are provided by cystein residues or, after thiolation, e.g. by iminothiolane

[53]. Functionalization of QDs stabilized with thiols can also be achieved by a thiol-exchange with biomolecules containing a sulfhydryl group [53]. After incubation, equilibrium of the thiols on the QD surface is achieved resulting in partial substitution of the initial coating molecules by the biomolecules. Electrostatic interactions between the QD-surface and peptides or proteins (figure 2D) can also be used for coating and linkage [54,55] (for reviews see [56,57]).

## 5. Cytotoxicity of QDs

Since QDs are supposed to be used for studies at living cells and organisms, these particles have to be characterized concerning their biocompatibility. As compared to other nanoparticles, like gold or iron nanoparticles, which have been used for several decades and which proved to be biocompatible [58,59], QDs are quite new materials and have not been completely characterized with regard to their toxicity. Most of the QDs used for biological applications contain the heavy metal cadmium, known to cause toxic effects, when in contact with cells. Derfus *et al.* showed for hepatocytes that oxidation of Cd on the QD surface and subsequent Cd<sup>2+</sup> release, e.g. mediated by air or UV light, is one possible mechanism responsible for QD cytotoxicity [60]. Consequently, the next step was to protect the QD core, as described above, by a shell of much lower toxicity, in most cases ZnS, which resulted in a significant reduction of cytotoxic effects [60,61]. As this layer also improves the optical properties, core-shell systems have become standard in most biological applications. But the introduction of capping layers was still not sufficient to solve the problem of cytotoxicity completely. Various other factors, like the aggregation of particles on the cell surface [62] and even the stabilizing QD surface ligands were shown to impair cell viability [63]. Hence, choosing an appropriate surface coating is also important, since simple coatings, like thiol containing carboxylic acids, present a minor diffusion barrier for Cd<sup>2+</sup>. Additionally, thiol-coated QDs, in addition, are known for their poor colloidal stability [44,64], and therefore, the introduction of inert and stable, macromolecular or cross-linked surface coatings was an important improvement. This concept has been realized by several workgroups. For instance, Dubertret *et al.* integrated QDs in PEG-containing phospholipid micelles and microinjected them into early-stage *Xenopus* embryos [47]. The development of the embryos was observed and it did not show toxic effects when  $2 \times 10^9$  QDs per cell were injected. However, at



higher concentrations ( $>5 \times 10^9$  QDs per cell) abnormalities (cell size, cell death, cell movement and axis elongation) became apparent. Other coatings, like silica encapsulation or polymer coating [62], can also serve for fairly non-toxic modifications. Finally, the recent replacement of the toxic elements of the semiconductors by more biocompatible ones is a next step towards low-toxic QDs [61,69].

Besides the toxic effects of the elemental building blocks, cell death can be induced by the formation of reactive oxygen species (ROS) [70-72], since QDs can transfer absorbed optical energy to oxygen molecules. Free radicals can cause damage to DNA [73] and other cellular components and as a consequence induce apoptosis and necrosis.

Surprisingly, in most of the studies of QDs in live cells there was no significant influence on cell viability, morphology, function or development in the used concentrations (ranging from nM to  $\mu$ M) [24,51,54,65-68]. So far, few data on the toxicity of QDs, especially for *in vivo* applications, are available. Therefore, this toxicity remains the main limitation for the use of QDs. Several questions remain unanswered, like the clearance of the particles from the circulation and tissues and if there are long-term effects on gene expression. First gene arrays after the incubation of fibroblasts with silanized, PEGylated QDs, however, indicate low cytotoxicity when the QDs have an appropriate surface modification [74].

## **6. Cellular particle uptake – a decisive step for intracellular particle delivery**

When nanoparticles in general or QDs as model colloids have to be delivered into specific cells, two aspects have to be considered: first, specific cell-surface structures have to be addressed and, second, an appropriate pathway into the cell must be found.

As numerous factors influence the uptake and the intracellular delivery of particles, like the size and the surface charge of the particles [75], the particle design requires a profound understanding of the cellular mechanisms. Additionally, there are many ways leading inside a cell but the pathway chosen for delivery itself can already determine the fate of the colloid inside the cell [76]. After clathrin dependent uptake, for instance, particles are trapped in endosomes and can further be degraded in

lysosomes or be exocytosed [7]. Hence, for a better understanding of these processes, in the following section the most widely used cellular uptake-mechanisms for delivery of nanoparticles will be described. After this general section, concrete approaches of non-specific and specific cell targeting with QDs will be presented.

### *6.1 Gateways for cellular uptake and QD delivery*

For intracellular delivery of nanoparticles, it is helpful to take a closer look at the uptake-mechanisms of the cells which are subsumed under the global term *endocytosis*. By this process, macromolecules and small particles are transported across the plasma membrane. Cells use these pathways for the supply with nutrients, for intercellular communication and for immune response as well as for other essential functions, but these highly-developed routes can also be exploited to deliver other kinds of freights, like drug-loaded nanoparticles or QDs. According to the mechanism of endocytosis, this process can be subdivided into two major categories: *phagocytosis*, which is the uptake of large particles, and *pinocytosis*, which is the uptake of fluid and solutes (figure 3; for review, see [76]). While the first mechanism is only typical for specialized mammalian cells, like macrophages, monocytes and neutrophils, pinocytosis can be found at every cell. Pinocytosis can be further classified into at least four mechanisms: macropinocytosis, clathrin-mediated endocytosis, caveolae-mediated endocytosis and clathrin- and caveolae-independent endocytosis (figure 3). Macropinocytosis represents an efficient route for non-selective endocytosis of solute macromolecules. The formation of macropinosomes (diameter up to 5  $\mu\text{m}$ ) is started by actin-driven ruffling of the cell membrane which is induced by growth factors or other signals. The membrane protrusions engulf large volumes of extracellular fluid [78]. Micropinocytosis is preferred for the uptake of smaller particles. The different uptake-mechanisms result in differently sized vesicles and can be classified into clathrin- (~120 nm), caveolin- (~60 nm) or clathrin- and caveolin-independent endocytosis (~90 nm). Clathrin-mediated endocytosis (specified later) is the most important mechanism for receptor-mediated uptake, occurs in all mammalian cells and plays an important physiological role, for example in mediating the uptake of low-density lipoprotein (LDL). Caveolae, small flask-shaped invaginations in the plasma membrane, can most notably be found in endothelial cells, smooth muscle cells and adipocytes. Their physiological role is still being discussed (e.g. cholesterol uptake, solute transport and tumor

suppression) [79]. Pathogens, e.g. the SV40 virus [80], are also able to enter cells via caveolae which do not fuse with lysosomes after endocytosis, which enables their entry into the cell without impairing their activity in the acidic environment of lysosomes. This fact makes endocytosis via caveolae interesting for nanoparticle delivery, since compared to other mechanisms, the particles are neither entrapped in endosomes nor degraded in lysosomes and therefore can directly head for their intracellular targets. However, it is more complicated as caveolae uptake can also result in delivery to the Golgi complex and to the endoplasmic reticulum as well as in discharge of the particles by transcytosis [81].

Clathrin- and caveolin-independent endocytosis is only described for a few examples, e.g. for the recovery of membrane proteins in neurons or the internalization of the interleukin-2 (IL-2) receptor on lymphocytes [76]. It is still unclear how this not clearly defined way of endocytosis can be selectively addressed by nanoparticles. QD-based colloids could help to investigate these ways of uptake due to their small size, narrow size distribution and easy detectability.

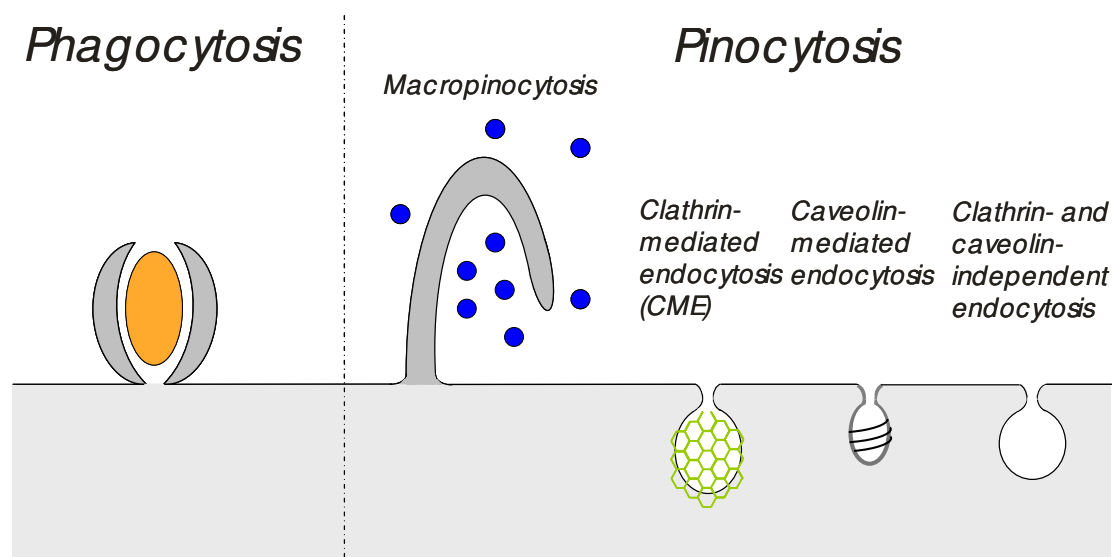


**Figure 3: Survey of different endocytic pathways.** The pathways can be classified by the mechanism of vesicle formation, the nature and the size of the cargo (for details, please see text). Adopted from [75].

## 6.2 Receptor-mediated endocytosis

One pathway for active and selective transport of nanoparticulate systems into the cell is exploited in many applications – the receptor mediated endocytosis [82-84].

This is due to the fact that a number of ligands specific for certain receptors is known and that this pathway allows for a 1000-fold increase of the intracellular concentration of macromolecules, rendering this form of uptake very effective. The most frequent form of receptor-mediated endocytosis is the clathrin-mediated endocytosis (CME) [77] (figure 4). This process begins with the binding of a ligand to a specific cell surface receptor, followed by the clustering of the ligand-receptor complexes in *coated pits*, which are formed by the assembly of cytosolic coat proteins, mainly clathrin. The coated pits then invaginate and pinch off of the plasma membrane, aided by dynamin, to form intracellular clathrin coated vesicles (CCVs). After depolymerisation of clathrin, the endosomes are acidified due to proton influx which leads to late endosomes. In this state, the ligands dissociate from the receptors and are subsequently either released from the endosome or degraded after the fusion of the late endosomes with lysosomes [7,76,85]. A crucial prerogative for intracellular particle delivery is the endosomal release of the particles, otherwise the particles will be degraded. A possible solution to this problem can be the use of pH-sensitive polymeric building blocks for the nanoparticle design [86-89].

QDs which were delivered into cells by CME are for example connected to transferrin, growth factors or folic acid. Details of these approaches will be described later.

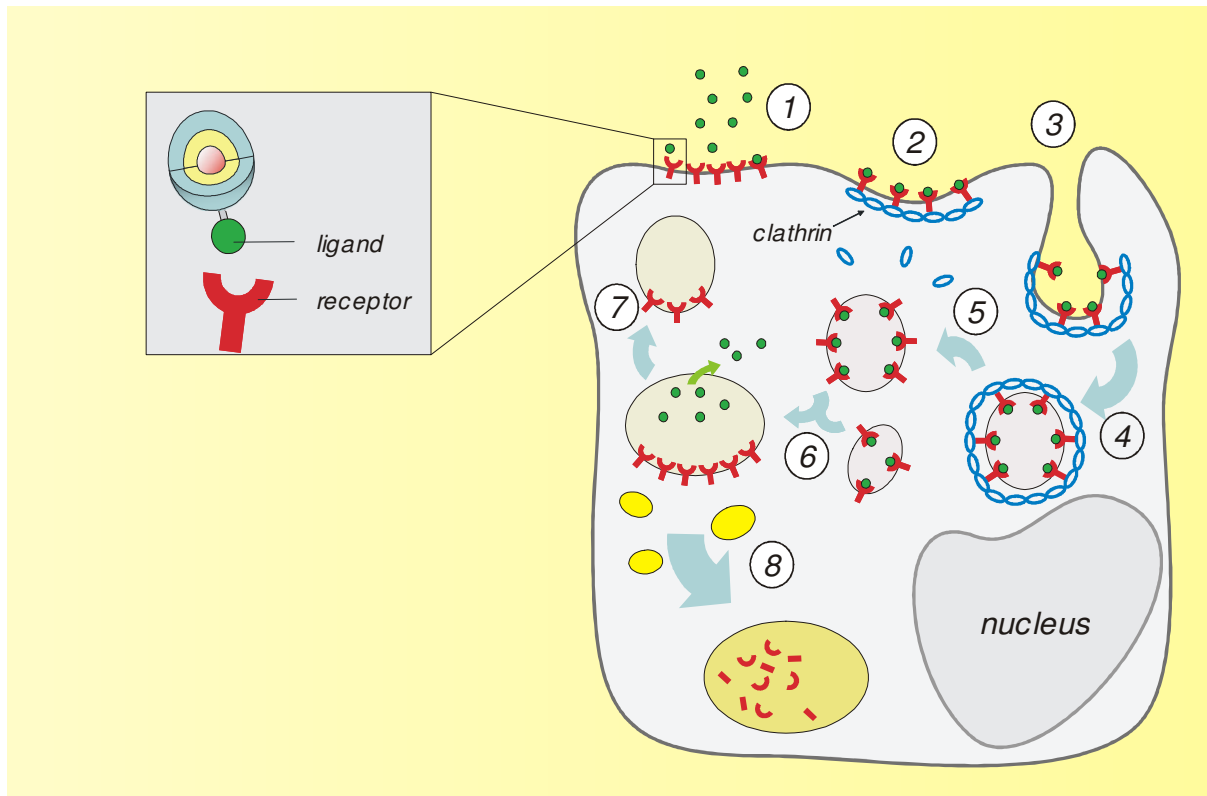


**Figure 4: Clathrin-mediated endocytosis.** (1) Ligand binds to a specific cell surface receptor. (2) Invagination of cell membrane, clustering of the ligand-receptor complexes and (3) formation of clathrin-coated pit. After pinching off of the cell membrane the ligand-receptor complexes are sequestered in clathrin-coated vesicles (4). Clathrin depolymerizes and proton influx acidifies the early endosomes (pH ~6) (5). Several early endosomes can fuse to build late endosomes (pH ~5) (6) from which the receptors can be recycled after release of the ligand (7) or fuse with lysosomes (8) leading to degradation. Adopted from [7].

### 6.3 Protein transduction domains

Another pathway into cells which is clathrin-independent and which attracted growing attention during the last decade is mediated by protein transduction domains (PTDs). This cell delivery system enables the transport of certain peptides and proteins [90], liposomes [91,92] and nanoparticles [93,94] across the cell membrane. QDs have also been successfully delivered via PTD, examples of which will be given later.

In literature, also the term *cell penetrating peptides* (CPPs) is used for both peptides and proteins of this class. For every cell type PTDs can be found which can deliver proteins into these cells. Additionally, PTDs are able to cross the blood brain barrier

and can even enter intracellular sites and the nucleus though the exact mechanism for the cellular uptake has not been completely resolved, yet [95,96].

An important sample is the TAT PTD [97], derived from the TAT protein from the human immunodeficiency virus (HIV-1), which is able to deliver proteins into cells. Other PTDs, like the third  $\alpha$ -helix of *Antennapedia* homeodomain and VP22 protein from herpes simplex virus, can also serve as vector for protein delivery *in vivo* [95].

Morris *et al.* enhanced the possibilities of peptide transfection by engineering the peptide carrier Pep-1. This 21-residue peptide consists of two domains which are separated by a spacer. A tryptophan-rich domain allows for efficient cell membrane translocation and the hydrophilic lysine-rich domain, derived from the simian virus 40 (SV-40) T large antigen nuclear localization sequence (NLS), facilitates solubility and intracellular delivery [98].

Contemporary research deals with the question, if delivery mediated by PTDs does not end in endosomes, unlike CME [95]. This would enable more effective intracellular delivery. However, this form of uptake is non-specific which may also be desirable if a collective of cells has to be addressed effectively, especially *in vitro*. But the lack of selectivity can also be a limiting factor for drug targeting *in vivo*.

## **7. Non-specific particle uptake**

Non-specific uptake of QDs, which is not mediated by certain targeting moieties, can be desirable for simply labeling a collective of cells, for example for *in vivo* applications in which cells are needed to be identified within an application. The following approaches demonstrate, how the unique properties of QDs can be used for effective whole-cell labeling.

Phagocytosis, a form of non-specific uptake, was exploited for the investigation of cell motility and migration of small epithelial cancer cells (phagokinetic tracks). After the deposition of small, non-PEGylated and silica-capped QDs on collagen coated substrates and seeding of cells, QDs were internalized by phagocytosis [99]. The change in fluorescence intensity and thus the migration of the cells was observed by confocal microscopy. By the use of QDs problems of other previous approaches could be overcome. Conventional fluorophores suffered from photobleaching, while large, submicrometer gold particles would probably show interactions with cell motility when more particles are ingested. The phagokinetic tracks are a powerful tool

for the classification of cancer cells [65]. In another approach, phagocytosis of albumin-coated QDs by peritoneal mouse macrophages was used for immune cell tracing. The QDs were rapidly incorporated by the macrophages and then applied to the peritoneum of mice. After hapten injection, accumulation of the QDs on the inflammation site could be observed after tissue resection, detected by a handheld UV-lamp [100]. QDs emitting light in the NIR were able to label sentinel lymph nodes for imaging during resection. After intradermal injection, non-specific uptake by the RES was exploited for mapping and subsequent resection of sentinel lymph nodes guided by *in vivo* imaging [32].

The process of non-specific uptake was further investigated by Osaki *et al.*, who proved that endocytosis is also an extremely size-dependent process. They investigated endocytosis by means of amphiphilic sugar-coated QDs (15 nm, determined by dynamic light scattering - DLS). Based upon fluorescence microscopy they suggest an optimum of particle incorporation at ~50 nm (shown for an artificial 'glycovirus' consisting of plasmid DNA and the amphiphilic sugar), while the smaller sugar-coated QDs and larger aggregates of the glycovirus (> 100 nm) were taken up at a smaller degree [8]. However, this influence of the size effects on endocytosis has to be further investigated for more detailed information. Non-specific uptake of QDs can also be triggered by translocation peptides [12,101-104], cationic liposomes [51,68] and dendrimers [12], or enhanced physically by electroporation [13]. These methods, together with microinjection [47], are often used for intracellular delivery and subsequent organelle tracking (this will be addressed later).

## 8. Reduction of non-specific binding and uptake

However, in applications where specific cell-particle interactions have to be investigated, non-specific interactions have to be reduced. Otherwise, targeting of specific cells cannot be achieved, as every cell, even the non-targeted ones, would be addressed. A solution can be to mask the surfaces of the QDs with PEG (stealth effect) [3,4] which significantly reduces non-specific particle uptake, e.g. by the RES [3].

To this end, Chang *et al.* showed at a human breast cancer cell line (SK-BR-3) that surface modification with PEG remarkably reduced non-specific QD uptake [105]. To this end, carboxylate-terminated QDs were used without modification or coupled to

PEGs of different molecular weights (750 to 6000 Da). Photoluminescence measurements after incubation with the differently modified QDs and after washing of the cells revealed significantly reduced non-specific uptake of PEG-coated particles as compared to the QDs without PEG (approximately by the factor of 10 after two hours of incubation). Quite interestingly, an increase of the molecular weight of the PEG only slightly reduced the uptake. Non-specific uptake was also shown to increase at prolonged incubation times and higher concentrations, despite the PEG-coating of the QDs.

Similar effects were observed in another study for non-specific binding of QDs to cells [106] when QDs of different degrees of PEGylation were used. Here, non-specific binding studies using different cell lines revealed that this effect is also strongly depending upon the cell type. Non-specific binding to HEK cells was the highest while 3T3 cells only slightly interacted with QDs. In addition, effective reduction of non-specific binding can also be achieved by a partial coating of the QDs. Here, reduction of PEG bound to the carboxyl-modified QDs to one third still sufficiently reduced non-specific binding. This partial PEGylation provides additional binding sites for biomolecules on the surface of the QDs. Ballou *et al.* demonstrated that the circulating half-lives of QDs in mice can be considerably improved by PEGylation which increase with longer molecular weights from 5 to 71 minutes [17]. However, phagocytosis and subsequent particle removal by the RES still remains a problem [107,108].

Gao *et al.* investigated passive targeting of tumor tissue by PEGylated polymer coated QDs *in vivo* exploiting the enhanced permeability and retention (EPR) of tumors [67]. Since the leaky tumor vasculature is permeable for macromolecules and tumors lack an effective lymphatic drainage system macromolecule or nanoparticle accumulation in these tissues is enforced [109]. The QDs were injected into mice in which prostate cancer cells were implanted. After this, the distribution of the QDs was observed by *in vivo* fluorescence imaging. Passive targeting was observed 6h after injection of 6.0 nmol of the QDs. However, when compared to active tumor targeting, which was also achieved in this study after the QDs were additionally linked to an antibody against PSMA (a prostate cancer marker) and applied in a dose of 0.4 nmol, passive targeting showed a lower accumulation in the tumor. Additionally, the accumulation, mediated by the antibody, was significantly faster (2h). These findings



show that active targeting of specific cells and tissues, here using an antibody, leads to more effective particle delivery to the target.

## 9. Specific cell-particle interactions

### 9.1 Cell surface antigens

In first approaches QDs were applied as fluorescent label of specific cells for analytical purposes. Many of them made use of antibodies [20,24,55,67,110], favored by the fact that antibodies against numerous cell-surface proteins are commercially available. In this technique, usually, a primary antibody specific for a cell-specific protein is applied. Subsequently, this antibody is addressed by a secondary antibody which can be connected to the QDs. The advantage of this method is that it is quite flexible, since the unit consisting of QDs and secondary antibodies can be used to bind to several primary antibodies.

However, it is obvious that large complexes consisting of primary and secondary antibodies and QDs can be excluded from such uptake pathways which discriminate larger particles. Therefore, antibodies are more suitable in diagnostics and in labeling than with regard to nanoparticle delivery into cells.

Wu *et al.* used QDs conjugated to antibodies to label cell surface cancer markers, the epidermal growth factor receptor Her2, on SK-BR-3 cells. The biotinylated secondary antibodies were conjugated to streptavidin-tagged polyacrylic acid-coated QDs. It was also possible to label intracellular structures, actin and microtubules, but this required fixation of the cells since the QD-antibody conjugates are not taken up into living cells [111].

An alternative to antibodies is presented by Howarth *et al.* They genetically attached an acceptor peptide to AMPA receptors (glutamate activated ion channels) of neurons [112]. Furthermore, *E. coli* biotin ligase was added to perform biotinylation of the acceptor peptide on the receptor. In a last step, streptavidin-coated QDs were addressed to the modified receptor in order to label it. This allowed following the trafficking of the QD-tagged receptors in the neurons by fluorescence microscopy. The advantage of this labeling strategy is that customized chemistry for each ligand and antibody are not required.

## 9.2 *The transferrin receptor*

Serum-transferrin, a 80 kDa glycoprotein, plays a crucial role in the maintenance of iron in the organism since it carries  $\text{Fe}^{3+}$ -ions from the sites of intake, the mucosa cells, into the systemic circulation to the cells and tissues. The transferrin receptor (TfR), a homodimeric membrane receptor of 90 kDa per subunit, is internalized after Tf binding, followed by endosomal release of iron and recycling of the Tf-TfR complex. As the TfR is highly expressed in rapidly dividing cells, like tumor cells, it provides a target for specific particle delivery [82].

Several approaches with transferrin-conjugated QDs were made to prove specific uptake [10,113-115]. In an early report, Chan and Nie demonstrated the use of QDs for bioimaging by coupling mercaptoacetic acid-coated QDs to Tf using EDC [10]. Fluorescence microscopy indicated specific uptake of Tf-QDs by HeLa cells, compared to non-conjugated QDs. The colloid was further improved by cross-linking the mercapto-acid-coating with lysine yielding higher stability in a large pH-range (regarding the quantum yields) and high salt concentrations (regarding the monodispersity of particle size distribution). To prove the monodispersity, blinking was investigated by epi-fluorescence microscopy as this phenomenon can only be observed for single QDs. Bioconjugation to Tf and subsequent uptake was achieved in a similar manner than before [113]. Two other approaches further confirmed Tf-mediated endocytosis of QDs by atomic force microscopy (AFM) and two-photon excitation CLSM [114,115].

## 9.3 *Tyrosine kinases*

In the family of transmembrane receptor tyrosine kinases (TRKs), growth factor receptors, especially the epidermal growth factor receptors (EGFRs), are of special interest concerning cancer targeting, since they are implicated in the development and progression of many human solid tumors [116]. There are numerous approaches investigating interactions of QDs with EGFRs [11,115,117,118]. Lidke *et al.* applied streptavidin-coated QDs for cellular uptake studies at the erbB1 receptor, one of four homologous receptor subtypes [11]. The receptor was expressed in CHO cells together with green fluorescent protein (GFP) as fusion protein. After binding of biotinylated EGF to the receptor, the streptavidin-QDs were added and accumulated at the cell membrane due to the strong streptavidin-biotin binding and could be

observed by confocal microscopy. The ligand-receptor complex quickly internalized at 37° C while at 4° C endocytosis could be blocked (figure 5). After endocytosis which was furthermore demonstrated to be clathrin-dependent by colocalization of transferrin-Alexa 633, fusion of the QD containing vesicles could be observed. Furthermore, the erbB1 was shown to be active after binding of EGF-linked QDs by staining with Cy5-anti-activated erbB1. These results indicate that the small QDs do not impair the biological function of the attached growth factor and the receptor trafficking. Incubation of the EGF-QDs with A431 cells which express the erbB1 constitutively unveiled a rapid movement of the ligand-receptor complexes along filopodia, thin extensions of the cell body, by a retrograde transport to the cell body. Similarly, the nerve growth factor receptor TrkA was targeted by QDs conjugated to anti-TrkA as well as by QDs attached to nerve growth factor (NGF), the naturally occurring ligand [119]. After binding of the QD-bioconjugates to the receptor on PC12 nerve cells, rapid internalization was observed by confocal microscopy. The shuttling of the endosomal QD-receptor complexes inside the cells was shown to be associated with microtubules. After addition of nocodazole, a microtubule inhibitor, the transport was inhibited.

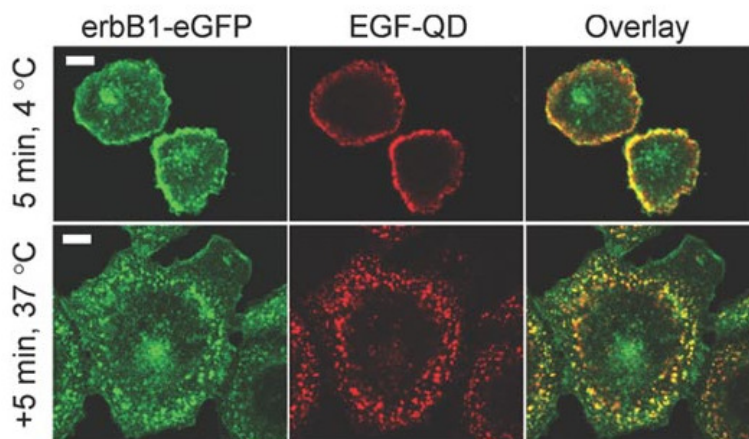


**Figure 5: Binding of EGF-QDs to EGFRs and endocytosis at erbB1-eGFP expressing CHO cells.** The EGFRs are marked by GFP, QDs show red fluorescence. Upper panels: After addition of biotin-EGF to the cells, QDs bind to the EGFRs and show colocalization with the receptor on the plasma membrane. Endocytosis is inhibited at 4° C. Lower panels: At 37° C endocytosis takes place. The ligand-receptor complexes are visible inside the cell in endocytic vesicles. Scale bars: 20  $\mu\text{m}$  (reprinted from [11]).

### 9.4 Integrins

Integrins are a family of  $\alpha,\beta$ -heterodimeric receptors that mediate dynamic linkages between extracellular adhesion molecules and the intracellular actin cytoskeleton [120]. Several integrins play an important role in angiogenesis and metastasis and are therefore upregulated in numerous tumor cell types. Integrins bind to the arginine-glycine-aspartic acid (RGD) peptide sequence present in many extracellular matrix proteins. This sequence binds for example to  $\alpha_v\beta_3$  and  $\alpha_v\beta_5$  integrins [121], which are overexpressed at the vasculature of tumors [122]. Therefore, these integrins are selective targets for cancer targeting. QDs attached to antibodies specific for the  $\alpha_v$  subunit as well as QDs bound to RGD were able to bind to the nerve cell line SK-N-SH [110]. NIR-emitting, PEG-coated QDs connected to cyclic RGD were targeted to integrin-positive cells *in vivo* [108]. At increasing receptor expression levels, depending on the respective tumor cell lines, staining of the cells became more visible, while the effect could be blocked by excess free RGD and did not occur when the blank QDs were applied. In the same study, these RGD-decorated QDs were also able to stain frozen tumor tissue *in vitro*, in contrast to QDs without RGD. Application to tumor bearing mice resulted in staining of the tumor vasculature, visualized by *in vivo* imaging (figure 6), but also in non-selective accumulation in the RES, mainly in liver, lymph nodes and bone-marrow, though the particles were PEG-coated. This approach shows that *in vivo* targeting with QDs on principle is feasible but for more selectivity of targeting the colloids still have to be improved.

Another approach proved specific uptake of QDs coated with paramagnetic phospholipids containing the MRI-traceable element Gadolinium [36]. Therefore, the colloid is in addition to the fluorescence of the QDs also detectable by MRI. Thiolated RGD was connected to the colloid via maleimide-linkage. The maleimide function was introduced by partial incorporation of maleimide-derivatized PEG-phospholipids into the coating. After incubation, HUVEC cells ( $\alpha_v\beta_3$  positive) showed increased uptake of the QDs compared to control (bare QDs without RGD), visualized by fluorescence microscopy. However, non-specific uptake of the bare QDs was also observed.

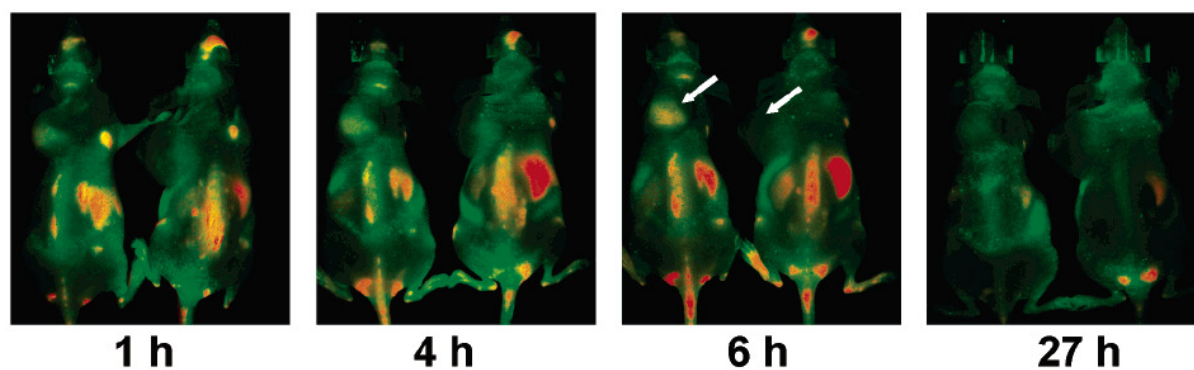


**Figure 6:** *In vivo* imaging of tumor bearing mice (left shoulder, arrows) after injection of RGD-QD (left sides) and QDs without RGD (right sides). After 6h location of RGD-QDs in the tumor is visible. Strong fluorescence in liver, bone marrow and lymph nodes indicates uptake by the RES (reprinted from [107]).

### 9.5 The folate receptor

The folate receptor (FR) represents an adequate target for intracellular nanoparticle delivery since it is overexpressed in many cancer cell-lines [123] due to the increased need of cancer cells for folic acid as this coenzyme is essential for the synthesis of amino acids as well as nucleic acids. Since folic acid can be easily connected to functionalized nanoparticles by carbodiimide/NHS chemistry and because of its cheap availability, several approaches have been made to exploit FRs for drug targeting [124,125]. After preliminary results presented by Chan *et al.* [126], Bharali *et al.* showed uptake of QDs by KB cells, a FR positive epithelial cancer cell line, when mercaptoacetic acid-coated InP-ZnS QDs decorated by folic acid were applied. The QD uptake was proven by confocal microscopy. However their control-experiments showed non-specific particle-uptake by FR-negative cells (A549 cells) which reduces the selectivity of the uptake of the QDs by FRs [69]. This problem of non-specific particle-uptake is already known and can be reduced by introducing PEG into the coating of the QDs, as mentioned before [105,106]. Hence, further experiments are necessary to ensure specific uptake after optimization of the QD surface.

### 9.6 Phage displayed peptides

Screening of phage displayed peptide libraries yielded a number of peptides which are selective for specific tumor tissues and have great potential for the development

of novel cancer-targeted drugs and could replace bulky antibodies in the future [127,128]. With this technique, phages are genetically engineered to display polypeptides on their surfaces which are encoded by their DNA which can be manipulated by insertion of randomized oligonucleotide fragments. The resulting phage displayed peptide libraries are subsequently screened for the binding affinity of the peptides to certain receptors (*biopanning*).

Akerman et al. applied three pre-scanned peptides from phage display, each connected to QDs [53]. These isolated peptides already have been proven to bind to specific sites in mice *in vivo* and were homing to membrane dipeptidase on endothelial cells in lung blood vessels, tumor blood vessels or lymphatic vessels and tumor cells, respectively [127]. After modification with iminothiolane to introduce a thiol group into the peptides, the compounds were subsequently bound to mercaptoacetic acid coated QDs via thiol exchange. Thiolated PEG was also attached for passivation of the QDs. Following injection into mice, the QDs were found in the respective tissues using fluorescent microscopy depending on the peptide attached. Tissue samples of liver and spleen revealed reduced uptake of PEGylated QDs by the RES compared to non-PEGylated ones.

In another approach, peptide from phage display was used to target QDs, which were attached via streptavidin, to a lung carcinoma cell line. The colloid was internalized by the cells, whereas QDs attached to a tetrameric control peptide remained extracellular [129]. However, future studies have to prove the selectivity of the peptide for tumor cells only. Similar results were obtained by Kim *et al.* for another peptide [130]. They showed QD uptake and also transport of the QD-peptide-receptor complex into the endoplasmatic reticulum which was fluorescently labeled with Glibenclamide.

### 9.7 Other targets

The largest cell surface receptor family is represented by the G-protein coupled receptors (GPCRs) [131]. These receptors modulate various kinds of physiological processes and are involved in a number of diseases. Therefore, GPCRs represent the largest class of therapeutic targets [132]. As the localization of many of these receptors has been investigated intensively and as numerous ligands for these receptors are known, they might also be interesting for drug targeting. After binding of a ligand which can be a biogenic amine or a peptide, the ligand-receptor

complexes are usually internalized, mediated by clathrin. Therefore, this mechanism should also provide a gateway for selective uptake of particles tagged to ligands selective for certain GPCRs.

An early approach using ligand-conjugated QDs was presented by Rosenthal *et al.* [133]. In this publication, serotonin molecules were covalently bound to TOPO-coated CdSe QDs, referred to as serotonin-labeled CdSe nanocrystals (SNACs). The biogenic amine serotonin is recognized by serotonin transporter proteins (SERTs) which are responsible for the termination of neurotransmitter signal by clearing these molecules from extracellular spaces after release. The SNACs were able to label cell surface SERTs in transfected HEK cells but with reduced binding affinity, compared to free serotonin. However, electrophysiological experiments at *Xenopus* oocytes expressing the human serotonin receptor 5HT<sub>3</sub> suggest that the steric hindrance of the relatively large QDs can impair the biological activity of the small neurotransmitter. This point is subject to further improvements for specific substances binding to serotonin and dopamine transporters [134,135].

In a later approach by Mason *et al.* it was possible to label cell surface GPCRs, in this case for a peptidic ligand [136] offering a more favorable size ratio between the QDs and the ligand. Mercaptoacetic acid-coated QDs were covalently EDC-coupled with PEG and angiotensin II (ANG II), an octapeptide binding to angiotensin receptors (AT). These QD bioconjugates can bind to AT 1 receptors expressed in transfected CHO cells. Binding did not take place either when excess ANG II was applied or when AT 1-negative CHO cells were incubated. Similar results were presented by Young and Rozengurt for streptavidin-functionalized QDs conjugated to biotinylated ANG II. Agonist-induced internalization was observed with fluorescence microscopy which could be inhibited at 4° C, indicating uptake via endocytosis [137].

## 10. Intracellular delivery

As mentioned above, many targets of therapeutical relevance are located inside the cell, like the nucleus or the mitochondria, which requires intracellular delivery of nanoparticles [138]. Recent studies meet this requirement by the investigation of QD-based intracellular targeting strategies.

The nucleus, for example, plays a dominant role in gene therapy, since here most of the genetic information of a cell is located. In principle, nanoparticles are able to

enter the nucleus by diffusion through the nuclear pores. Since these pores are in most cases too small for most of the particles (up to 26 nm) [139], active transport via nuclear localization sequences (NLS) seems more promising for targeting this organelle. Similarly, mitochondria can be addressed with mitochondrial localization sequences (MLS). These organelles play a role in a number of pathophysiological dysfunctions, like neurodegenerative and cardiovascular diseases and cancer [140,141]. This fact renders mitochondria interesting targets for drug therapy.

Before QDs are able to find intracellular targets, the particles first have to enter the cell. Therefore, the complex problem of intracellular delivery has been divided into two parts. The first one, as described above, deals with the cellular uptake of colloids. CME is promising, due to its selective uptake of colloids, but also poses the problem that the particles remain sequestered in endosomal vesicles preventing intracellular tracking. Therefore, to study the intracellular targeting processes other delivery methods are used, usually non-specific ones, for direct delivery of the particles into the cytosol. A next step would be to combine specific uptake with intracellular delivery when both of these processes are better understood and when the colloids are further developed. The following approaches embark on this strategy in which first the QDs are delivered into the cytosol. Subsequently the QDs are able to address the respective organelles.

In order to facilitate further studies of intracellular targeting of organelles with QDs, Derfus *et al.* investigated several methods to find an appropriate method to deliver PEG-coated QDs into the cytosol of cells [12]. Quantification of cellular uptake using HeLa cells, determined by flow cytometry, revealed that cationic liposomes (Lipofectamine™) yielded the highest delivery efficiency, followed by dendrimers (Superfect™) and translocation peptides (Chariot™). To prove whether green-light-emitting QDs remain trapped in vesicles, which would disturb later organelle tracking, a second fraction of red-light-emitting QDs which were coupled to EGF was simultaneously incubated and analyzed by fluorescence microscopy. Since EGF-QDs were shown to enter cells via CME, they were used as an endosome marker. The approach showed only few colocalization of the both QD-fractions in vesicles after Lipofectamine-delivery, indicating that QDs can escape the endosomes (figure 7A). However, in this delivery method particles formed aggregates of several hundred nanometres. Electroporation showed similar effects (figure 7B), only microinjection prevented aggregation (figure 7C). Aggregation of the particles in the



cytosol has to be avoided since larger aggregates would prevent trafficking to the nucleus or mitochondria, e.g. when pores have to be passed. Additionally, nuclear localization sequences (NLS) -the SV40 T antigen- and mitochondrial localization sequences (MLS), consisting of the targeting presequence from human cytochrome oxidase subunit VIII (COX8), were adsorbed on the QD surface. These sequences are small peptides specific for transporter proteins at the respective organelle and should prove the possibility to address these organelles. After microinjection of the NLS- and MLS-conjugated QDs into the cytosol, the particles were delivered into the nuclei and the mitochondria, respectively. However, control experiments with random peptides would be needed to accredit this intracellular delivery to the activity of the localization sequences only.

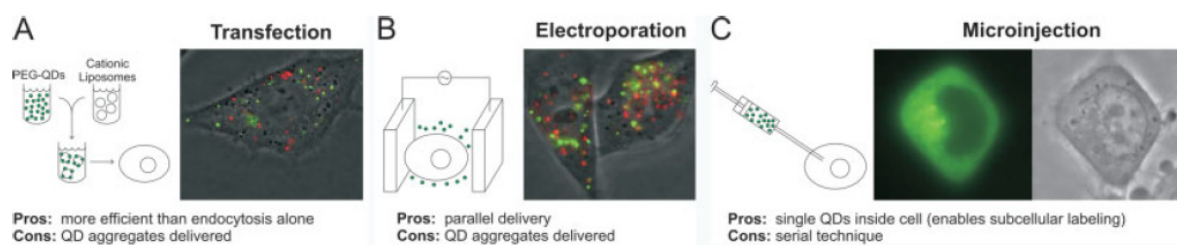


**Figure 7: Depiction of several delivery methods.** Transfection via cationic liposomes (A) and electroporation (B). Both methods allow for parallel delivery in the cells simultaneously but result in aggregation of the QDs (green spots). Microinjection into single cells (C) yields in an aggregate-free dispersion of the QDs inside the cell (reprinted from [12]).

Similar results were obtained by Chen *et al.* for silica-coated QDs connected to SV40 T antigen via streptavidin-biotin linkage [13]. Here, QDs were delivered into the cytosol of HeLa cells via electroporation. Subsequently, QDs were delivered into the nucleus, mediated by the NLS. Controls with random peptides were not localized inside the nucleus which indicates the uptake was dependent upon the NLS. Silica QDs were chosen as they are fairly non-cytotoxic and small enough (10-15 nm) for passing the nuclear pores. A colonogenic assay revealed no significant change of the surviving cell colony numbers after transfection compared to control. After 5 days and cell division, QDs were visible in the nuclei of the newly divided cells by fluorescence microscopy.

The peptide carrier Pep-1 was successfully connected to QDs in several studies and proved its potential for cellular delivery of QDs. Rozenhak *et al.* delivered streptavidin coated QDs non-covalently linked to Pep-1 into mammalian cells [104]. The QD-Pep-1 complexes were visible in the cytoplasm as aggregates. Besides nuclear targeting which was achieved via additional attachment of biotinylated SV-40 T-antigen, also mitochondrial targeting was possible. For this purpose, the GH3 domain of the Grim protein, an inducer of mitochondrial apoptosis, was coupled to the QDs before to Pep-1 was attached. After incubation of the cells, apoptosis was observed, as membrane blebbing and nuclear condensation in cells started to take place, an indirect sign of mitochondrial targeting.

In another study, an oligoarginine CPP, based on the HIV-1 Tat-protein, containing a terminal polyhistidine tag, was applied. By this sequence the peptide could be attached to QDs capped with dihydrolipoic acid (DHLLA) via metal-affinity interactions between the polyhistidine and the Zn atoms on the QD surface [142]. The colloid was able to be internalized into HEK293T/17 and COS-1 cells in a significantly higher manner than a control group without CPP. After uptake, colocalization with Alexa-labeled transferrin, an endocytic marker, showed localization of the QD-peptide conjugates in endosomes. Since uptake could be inhibited at 4° C, the group suggests endocytic uptake though the exact mechanism was not further characterized.

The Tat-protein coupled to QDs, coated with tiopronin (*N*-2-mercaptopropionylglycine) by EDC, mediated uptake into fibroblast and even nuclear targeting though in this approach no quantitative statement can be made [143]. Tat could also mediate brain targeting of QDs after injection into living mice [144]. The QDs were visible in the brain after its resection by the use of a handheld UV-lamp.

## **11. Conclusion and outlook**

Nanoparticles as colloidal drug carriers seem to be promising tools for targeting specific cells, tissues or organs. These drug carriers have not only to head for specific cell-types but should also address distinct cellular uptake processes to deliver their payload *into* cells. In order to investigate the pathways for nanoparticles into specific cells, model colloids of defined size and shape, which in addition have to be easy to detect, are a powerful tool.

As presented above, the use of QDs for the investigation of cellular uptake and intracellular delivery of nanoparticles offers new possibilities in order to study sub-cellular processes, due to the small, uniform size and due to the unique optical properties of the QDs. The approaches demonstrated that the pathway into the cell should be considered carefully since it also determines the intracellular fate of the colloid. CME was shown effective for targeting and uptake into cells but the endosomal release of the colloid after uptake can be a limiting factor for intracellular targeting.

Other promising pathways are the caveolae-mediated uptake [145] and uptake mediated by CPPs which circumvent the clathrin pathway. However, there is still need for more information on the distinct mechanisms for this uptake, as the examples of the SV40 virus (caveolae-dependent [80] and caveolae-independent [146]) and the Tat peptide (macropinocytosis [147] and caveolae [148]) show. A better understanding of such processes would obviously help to design colloids targeted nanoparticles for numerous applications.

Finally, new concepts can exploit specific pathophysiological situations, e.g. when an enzyme is upregulated, and activate particle delivery at the affected site on demand. A first promising approach was presented by Zhang *et al.* In this study, non-specific, transduction peptide-driven uptake of QDs was rendered cell-selective by linking a negatively charged, transduction-inhibiting peptide which was additionally substrate for matrix metalloproteases (MMPs). After cleavage of the negatively charged peptide by MMPs, the colloid could enter the target cells [149]. Since MMPs are upregulated in many tumors and in arthritic tissues this approach should be selective for these targets. This example shows that for the design of effective, cell-targeting colloids probably several targeting strategies have to be combined in one particle. Exploiting differently expressed enzymes or other forms of regulation specific for certain (patho)physiological events inside cells to 'switch on' colloids on the intracellular level could be an issue for the future development of advanced colloids. In the field of nanomedicine [150], QDs can make a worthy contribution to the development new diagnostic and delivery systems as they offer unique optical properties for highly sensitive detection, as well as they are well-defined in size and shape and as they can be modified with various targeting principles.

**References**

- [1] V.P. Torchilin, Drug targeting, *European Journal of Pharmaceutical Sciences* 11 (2000) S81-S91
- [2] D.A. Groneberg, M. Giersig, T. Welte, U. Pison, Nanoparticle-based diagnosis and therapy, *Current Drug Targets* 7 (2006) 643-648
- [3] D.E. Owens, N.A. Peppas, Opsonization, biodistribution, and pharmacokinetics of polymeric nanoparticles, *Int. J. Pharm.* 307 (2006) 93-102
- [4] H. Otsuka, Y. Nagasaki, K. Kataoka, PEGylated nanoparticles for biological and pharmaceutical applications, *Adv. Drug Deliv. Rev.* 55 (2003) 403-419
- [5] J. Vasir, M. Reddy, V. Labhassetwar, Nanosystems in Drug Targeting: Opportunities and Challenges, *Current Nanoscience* 1 (2005) 47-64
- [6] I.A. Khalil, K. Kogure, H. Akita, H. Harashima, Uptake Pathways and Subsequent Intracellular Trafficking in Nonviral Gene Delivery, *Pharmacol. Rev.* 58 (2006) 32-45
- [7] B. Rabinow, M.V. Chaubal, Injectable nanoparticles for efficient drug delivery, *Drugs and the Pharmaceutical Sciences* 159 (2006) 199-229
- [8] F. Osaki, T. Kanamori, S. Sando, T. Sera, Y. Aoyama, A Quantum Dot Conjugated Sugar Ball and Its Cellular Uptake. On the Size Effects of Endocytosis in the Subviral Region, *J. Am. Chem. Soc.* 126 (2004) 6520-6521
- [9] E. Chang, W.W. Yu, V.L. Colvin, R. Drezek, Quantifying the influence of surface coatings on quantum dot uptake in cells, *J. Biomed. Nanotechnol.* 1 (2005) 397-401
- [10] W.C.W. Chan, S. Nie, Quantum dot bioconjugates for ultrasensitive nonisotopic detection, *Science* 281 (1998) 2016-2018
- [11] D.S. Lidke, P. Nagy, R. Heintzmann, D.J. Arndt-Jovin, J.N. Post, H.E. Grecco, E.A. Jares-Erijman, T.M. Jovin, Quantum dot ligands provide new insights into erbB/HER receptor-mediated signal transduction, *Nat. Biotechnol.* 22 (2004) 198-203
- [12] A.M. Derfus, W.C.W. Chan, S.N. Bhatia, Intracellular delivery of quantum dots for live cell labeling and organelle tracking, *Adv. Mater.* 16 (2004) 961-966
- [13] F. Chen, D. Gerion, Fluorescent CdSe/ZnS Nanocrystal-Peptide Conjugates for Long-term, Nontoxic Imaging and Nuclear Targeting in Living Cells, *Nano Lett.* 4 (2004) 1827-1832

- 
- [14] P. Sharma, S. Brown, G. Walter, S. Santra, B. Moudgil, Nanoparticles for bioimaging, *Adv. Colloid Interface Sci.* 123-126 (2006) 471-485
- [15] L.J. Thorek Daniel, A.K. Chen, J. Czupryna, A. Tsourkas, Superparamagnetic iron oxide nanoparticle probes for molecular imaging, *Ann. Biomed. Eng.* 34 23-38
- [16] B. Bonnemain, Superparamagnetic agents in magnetic resonance imaging: physicochemical characteristics and clinical applications. A review, *J. Drug Target.* 6 (2004) 167-174
- [17] B. Ballou, B.C. Lagerholm, L.A. Ernst, M.P. Bruchez, A.S. Waggoner, Noninvasive imaging of quantum dots in mice, *Bioconjug. Chem.* 15 (2004) 79-86
- [18] B.D. Chithrani, A.A. Ghazani, W.C.W. Chan, Determining the Size and Shape Dependence of Gold Nanoparticle Uptake into Mammalian Cells, *Nano Letters* 6 (2006) 662-668
- [19] S. Gross, D. Piwnica-Worms, Molecular imaging strategies for drug discovery and development, *Curr. Opin. Chem. Biol.* 10 (2006) 334-342
- [20] M. Dahan, S. Levi, C. Luccardini, P. Rostaing, B. Riveau, A. Triller, Diffusion dynamics of glycine receptors revealed by single-quantum dot tracking, *Science* 302 (2003) 442-445
- [21] Z.A. Peng, X. Peng, Formation of high-quality CdTe, CdSe, and CdS nanocrystals using CdO as precursor, *J. Am. Chem. Soc.* 123 (2001) 183-184
- [22] A.M. Smith, S. Nie, Chemical analysis and cellular imaging with quantum dots, *Analyst* 129 (2004) 672-677
- [23] M. Bruchez, Jr., M. Moronne, P. Gin, S. Weiss, A.P. Alivisatos, Semiconductor nanocrystals as fluorescent biological labels, *Science* 281 (1998) 2013-2016
- [24] J.K. Jaiswal, H. Mattoussi, J.M. Mauro, S.M. Simon, Long-term multiple color imaging of live cells using quantum dot bioconjugates, *Nat. Biotechnol.* 21 (2003) 47-51
- [25] X. Gao, L. Yang, J.A. Petros, F.F. Marshall, J.W. Simons, S. Nie, In vivo molecular and cellular imaging with quantum dots, *Curr. Opin. Biotechnol.* 16 (2005) 63-72
- [26] M. Dahan, T. Laurence, F. Pinaud, D.S. Chemla, A.P. Alivisatos, M. Sauer, S. Weiss, Time-gated biological imaging by use of colloidal quantum dots, *Opt. Lett.* 26 (2001) 825-827
-

- [27] J.M. Costa-Fernandez, R. Pereiro, A. Sanz-Medel, The use of luminescent quantum dots for optical sensing, *Trends in Analytical Chemistry* 25 (2006) 207-218
- [28] C.B. Murray, D.J. Norris, M.G. Bawendi, Synthesis and characterization of nearly monodisperse CdE (E = sulfur, selenium, tellurium) semiconductor nanocrystallites, *J. Am. Chem. Soc.* 115 (1993) 8706-8715
- [29] M.A. Hines, P. Guyot-Sionnest, Synthesis and Characterization of Strongly Luminescing ZnS-Capped CdSe Nanocrystals, *J. Phys. Chem.* 100 (1996) 468-471
- [30] B.O. Dabbousi, J. Rodriguez-Viejo, F.V. Mikulec, J.R. Heine, H. Mattoussi, R. Ober, K.F. Jensen, M.G. Bawendi, (CdSe)ZnS Core-Shell Quantum Dots: Synthesis and Optical and Structural Characterization of a Size Series of Highly Luminescent Materials, *J. Phys. Chem. B* 101 (1997) 9463-9475
- [31] X. Michalet, F. Pinaud, T.D. Lacoste, M. Dahan, M.P. Bruchez, A.P. Alivisatos, S. Weiss, Properties of fluorescent semiconductor nanocrystals and their application to biological labeling, *Single Mol.* 2 (2001) 261-276
- [32] S. Kim, Y.T. Lim, E.G. Soltesz, A.M. De Grand, J. Lee, A. Nakayama, J.A. Parker, T. Mihaljevic, R.G. Laurence, D.M. Dor, L.H. Cohn, M.G. Bawendi, J.V. Frangioni, Near-infrared fluorescent type II quantum dots for sentinel lymph node mapping, *Nat. Biotechnol.* 22 (2004) 93-97
- [33] J. Frangioni, V, In vivo near-infrared fluorescence imaging, *Curr Opin Chem Biol* 7 (2003) 626-634
- [34] B. Ballou, Quantum dot surfaces for use in vivo and in vitro, *Curr Top Dev Biol* 70 (2005) 103-120
- [35] Y. Sahoo, P. Poddar, H. Srikanth, D.W. Lucey, P.N. Prasad, Chemically Fabricated Magnetic Quantum Dots of InP:Mn, *J. Phys. Chem. B* 109 (2005) 15221-15225
- [36] W.J.M. Mulder, R. Koole, R.J. Brandwijk, G. Storm, P.T.K. Chin, G.J. Strijkers, C. de Donega, K. Nicolay, A.W. Griffioen, Quantum Dots with a Paramagnetic Coating as a Bimodal Molecular Imaging Probe, *Nano Lett.* 6 (2006) 1-6
- [37] L. Prinzen, R.J. Miserus, A. Dirksen, T.M. Hackeng, N. Deckers, N.J. Bitsch, R.T.A. Megens, K. Douma, J.W. Heemskerk, M.E. Kooi, P.M. Frederik, D.W. Slaaf, M.A.M.J. van Zandvoort, C.P.M. Reutelingsperger, Optical and

- Magnetic Resonance Imaging of Cell Death and Platelet Activation Using Annexin A5-Functionalized Quantum Dots, *Nano Lett.* 7 (2007) 93-100
- [38] M.K. So, C. Xu, A.M. Loening, S.S. Gambhir, J. Rao, Self-illuminating quantum dot conjugates for in vivo imaging, *Nat. Biotechnol.* 24 (2006) 339-343
- [39] H. Mattoussi, J.M. Mauro, E.R. Goldman, G.P. Anderson, V.C. Sundar, F.V. Mikulec, M.G. Bawendi, Self-Assembly of CdSe-ZnS Quantum Dot Bioconjugates Using an Engineered Recombinant Protein, *J. Am. Chem. Soc.* 122 (2000) 12142-12150
- [40] S. Kim, M.G. Bawendi, Oligomeric Ligands for Luminescent and Stable Nanocrystal Quantum Dots, *J. Am. Chem. Soc.* 125 (2003) 14652-14653
- [41] W. Guo, J.J. Li, Y.A. Wang, X. Peng, Conjugation Chemistry and Bioapplications of Semiconductor Box Nanocrystals Prepared via Dendrimer Bridging, *Chem. Mater.* 15 (2003) 3125-3133
- [42] F. Pinaud, D. King, H.P. Moore, S. Weiss, Bioactivation and Cell Targeting of Semiconductor CdSe/ZnS Nanocrystals with Phytochelatin-Related Peptides, *J. Am. Chem. Soc.* 126 (2004) 6115-6123
- [43] H. Mattoussi, J.M. Mauro, E.R. Goldman, G.P. Anderson, V.C. Sundar, F.V. Mikulec, M.G. Bawendi, Self-Assembly of CdSe-ZnS Quantum Dot Bioconjugates Using an Engineered Recombinant Protein, *J. Am. Chem. Soc.* 122 (2000) 12142-12150
- [44] D. Gerion, F. Pinaud, S.C. Williams, W.J. Parak, D. Zanchet, S. Weiss, A.P. Alivisatos, Synthesis and Properties of Biocompatible Water-Soluble Silica-Coated CdSe/ZnS Semiconductor Quantum Dots, *J. Phys. Chem. B* 105 (2001) 8861-8871
- [45] T. Pellegrino, L. Manna, S. Kudera, T. Liedl, D. Koktysh, A.L. Rogach, S. Keller, J. Raedler, G. Natile, W.J. Parak, Hydrophobic Nanocrystals Coated with an Amphiphilic Polymer Shell: A General Route to Water Soluble Nanocrystals, *Nano Lett.* 4 (2004) 703-707
- [46] X. Gao, Y. Cui, R.M. Levenson, L.W.K. Chung, S. Nie, In vivo cancer targeting and imaging with semiconductor quantum dots, *Nat. Biotechnol.* 22 (2004) 969-976

- [47] B. Dubertret, P. Skourides, D.J. Norris, V. Noireaux, A.H. Brivanlou, A. Libchaber, In vivo imaging of quantum dots encapsulated in phospholipid micelles, *Science* 298 (2002) 1759-1762
- [48] A. Hezinger, J. Tessmar, A. Goepferich, Polymer coating of Quantum Dots - A powerful Tool toward Diagnostics and Sensorics, *Eur. J. Pharm. Biopharm.* in press (2007)
- [49] X. Wu, H. Liu, J. Liu, K.N. Haley, J.A. Treadway, J.P. Larson, N. Ge, F. Peale, M.P. Bruchez, Immunofluorescent labeling of cancer marker Her2 and other cellular targets with semiconductor quantum dots, *Nat. Biotechnol.* 21 (2003) 41-46
- [50] C. Zhang, H. Ma, Y. Ding, L. Jin, D. Chen, S. Nie, Quantum dot-labeled trichosanthin, *Analyst* 125 (2000) 1029-1031
- [51] C. Srinivasan, J. Lee, F. Papadimitrakopoulos, L.K. Silbart, M. Zhao, D.J. Burgess, Labeling and Intracellular Tracking of Functionally Active Plasmid DNA with Semiconductor Quantum Dots, *Mol. Ther.* 14 (2006) 192-201
- [52] W.J. Parak, D. Gerion, D. Zanchet, A.S. Woerz, T. Pellegrino, C. Micheel, S.C. Williams, M. Seitz, R.E. Bruehl, Z. Bryant, C. Bustamante, C.R. Bertozzi, A.P. Alivisatos, Conjugation of DNA to silanized colloidal semiconductor nanocrystalline quantum dots, *Chem. Mater.* 14 (2002) 2113-2119
- [53] M.E. Akerman, W.C.W. Chan, P. Laakkonen, S.N. Bhatia, E. Ruoslahti, Nanocrystal targeting in vivo, *Proc. Natl. Acad. Sci. U. S. A.* 99 (2002) 12617-12621
- [54] K.I. Hanaki, A. Momo, T. Oku, A. Komoto, S. Maenosono, Y. Yamaguchi, K. Yamamoto, Semiconductor quantum dot/albumin complex is a long-life and highly photostable endosome marker, *Biochem. Biophys. Res. Commun.* 302 (2003) 496-501
- [55] E.R. Goldman, G.P. Anderson, P.T. Tran, H. Mattoussi, P.T. Charles, J.M. Mauro, Conjugation of Luminescent Quantum Dots with Antibodies Using an Engineered Adaptor Protein To Provide New Reagents for Fluoroimmunoassays, *Anal. Chem.* 74 (2002) 841-847
- [56] W.J. Parak, T. Pellegrino, C. Plank, Labelling of cells with quantum dots, *Nanotechnology* 16 (2005) R9-R25



- 
- [57] X. Michalet, F.F. Pinaud, L.A. Bentolila, J.M. Tsay, S. Doose, J.J. Li, G. Sundaresan, A.M. Wu, S.S. Gambhir, S. Weiss, Quantum Dots for Live Cells, in Vivo Imaging, and Diagnostics, *Science* 307 (2005) 538-544
- [58] R. Shukla, V. Bansal, M. Chaudhary, A. Basu, R.R. Bhonde, M. Sastry, Biocompatibility of Gold Nanoparticles and Their Endocytotic Fate Inside the Cellular Compartment: A Microscopic Overview, *Langmuir* 21 (2005) 10644-10654
- [59] A.K. Gupta, M. Gupta, Synthesis and surface engineering of iron oxide nanoparticles for biomedical applications, *Biomaterials* 26 (2005) 3995-4021
- [60] A.M. Derfus, W.C.W. Chan, S.N. Bhatia, Probing the Cytotoxicity of Semiconductor Quantum Dots, *Nano Lett.* 4 (2004) 11-18
- [61] N. Pradhan, D. Goorskey, J. Thessing, X. Peng, An Alternative of CdSe Nanocrystal Emitters: Pure and Tunable Impurity Emissions in ZnSe Nanocrystals, *J. Am. Chem. Soc.* 127 (2005) 17586-17587
- [62] C. Kirchner, T. Liedl, S. Kudera, T. Pellegrino, A.M. Javier, H.E. Gaub, S. Stoelzle, N. Fertig, W.J. Parak, Cytotoxicity of Colloidal CdSe and CdSe/ZnS Nanoparticles, *Nano Lett.* 5 (2005) 331-338
- [63] A. Hoshino, K. Fujioka, T. Oku, M. Suga, Y.F. Sasaki, T. Ohta, M. Yasuhara, K. Suzuki, K. Yamamoto, Physicochemical Properties and Cellular Toxicity of Nanocrystal Quantum Dots Depend on Their Surface Modification, *Nano Lett.* 4 (2004) 2163-2169
- [64] J. Aldana, Y.A. Wang, X. Peng, Photochemical Instability of CdSe Nanocrystals Coated by Hydrophilic Thiols, *J. Am. Chem. Soc.* 123 (2001) 8844-8850
- [65] W.J. Parak, R. Boudreau, M. Le Gros, D. Gerion, D. Zanchet, C.M. Micheel, S.C. Williams, A.P. Alivisatos, C. Larabell, Cell motility and metastatic potential studies based on quantum dot imaging of phagokinetic tracks, *Adv. Mater.* 14 (2002) 882-885
- [66] A. Hoshino, K.I. Hanaki, K. Suzuki, K. Yamamoto, Applications of T-lymphoma labeled with fluorescent quantum dots to cell tracing markers in mouse body, *Biochem. Biophys. Res. Commun.* 314 (2004) 46-53
- [67] X. Gao, Y. Cui, R.M. Levenson, L.W.K. Chung, S. Nie, In vivo cancer targeting and imaging with semiconductor quantum dots, *Nat. Biotechnol.* 22 (2004) 969-976
-

- [68] E.B. Voura, J.K. Jaiswal, H. Mattoussi, S.M. Simon, Tracking metastatic tumor cell extravasation with quantum dot nanocrystals and fluorescence emission-scanning microscopy, *Nat. Med.* 10 (2004) 993-998
- [69] D.J. Bharali, D.W. Lucey, H. Jayakumar, H.E. Pudavar, P.N. Prasad, Folate-Receptor-Mediated Delivery of InP Quantum Dots for Bioimaging Using Confocal and Two-Photon Microscopy, *J. Am. Chem. Soc.* 127 (2005) 11364-11371
- [70] J. Lovric, S.J. Cho, F.M. Winnik, D. Maysinger, Unmodified Cadmium Telluride Quantum Dots Induce Reactive Oxygen Species Formation Leading to Multiple Organelle Damage and Cell Death, *Chem. Biol.* 12 (2005) 1227-1234
- [71] B.I. Ipe, M. Lehnig, C.M. Niemeyer, On the generation of free radical species from quantum dots, *Small* 1 (2005) 706-709
- [72] W.-H. Chan, N.-H. Shiao, P.-Z. Lu, CdSe quantum dots induce apoptosis in human neuroblastoma cells via mitochondrial-dependent pathways and inhibition of survival signals, *Toxicology Letters* In Press, Corrected Proof (2006)
- [73] M. Green, E. Howman, Semiconductor quantum dots and free radical induced DNA nicking, *Chemical communications (Cambridge, England)* (2004) 121-123
- [74] T. Zhang, J.L. Stilwell, D. Gerion, L. Ding, O. Elboudwarej, P.A. Cooke, J.W. Gray, A.P. Alivisatos, F.F. Chen, Cellular Effect of High Doses of Silica-Coated Quantum Dot Profiled with High Throughput Gene Expression Analysis and High Content Cellomics Measurements, *Nano Lett.* 6 (2006) 800-808
- [75] S.-W. Pang, H.-Y. Park, Y.-S. Jang, W. Kim, J.-H. Kim, Effects of charge density and particle size of poly(styrene/(dimethylamino)ethyl methacrylate) nanoparticle for gene delivery in 293 cells, *Colloids and surfaces. B, Biointerfaces* 26 (2002) 213-222
- [76] S.D. Conner, S.L. Schmid, Regulated portals of entry into the cell, *Nature* 422 (2003) 37-44
- [77] M. Marsh, H.T. McMahon, The Structural Era of Endocytosis, *Science* 285 (1999) 215-220
- [78] J.A. Swanson, C. Watts, Macropinocytosis, *Trends Cell Biol.* 5 (1995) 424-428
- [79] J.S. Shin, S.N. Abraham, CELL BIOLOGY: Caveolae--Not Just Craters in the Cellular Landscape, *Science* 293 (2001) 1447-1448

- 
- [80] R.G. Anderson, The caveolae membrane system, *Annu. Rev. Biochem.* 67 (1998) 199-225
- [81] L. Pelkmans, A. Helenius, Endocytosis via caveolae, *Traffic* 3 (2002) 311-320
- [82] Z.M. Qian, H. Li, H. Sun, K. Ho, Targeted Drug Delivery via the Transferrin Receptor-Mediated Endocytosis Pathway, *Pharmacol. Rev.* 54 (2002) 561-587
- [83] C. Sun, R. Sze, M. Zhang, Folic acid-PEG conjugated superparamagnetic nanoparticles for targeted cellular uptake and detection by MRI, *J. Biomed. Mater. Res. A* 78A (2006) 550-557
- [84] R. Sinha, G. Kim, S. Nie, D. Shin, Nanotechnology in cancer therapeutics: bioconjugated nanoparticles for drug delivery, *Mol. Cancer Ther.* 5 (2006) 1909-1917
- [85] M. Higgins, H. McMahon, Snap-shots of clathrin-mediated endocytosis, *Trends Biochem. Sci.* 27 (2002) 257-263
- [86] Y. Chan, V. Bulmus, M.H. Zareie, F.L. Byrne, L. Barner, M. Kavallaris, Acid-cleavable polymeric core-shell particles for delivery of hydrophobic drugs, *J. Control. Release* 115 (2006) 197-207
- [87] A. Potineni, D.M. Lynn, R. Langer, M.M. Amiji, Poly(ethylene oxide)-modified poly(b-amino ester) nanoparticles as a pH-sensitive biodegradable system for paclitaxel delivery, *J. Control. Release* 86 (2003) 223-234
- [88] Y. Bae, N. Nishiyama, S. Fukushima, H. Koyama, M. Yasuhiro, K. Kataoka, Preparation and Biological Characterization of Polymeric Micelle Drug Carriers with Intracellular pH-Triggered Drug Release Property: Tumor Permeability, Controlled Subcellular Drug Distribution, and Enhanced in Vivo Antitumor Efficacy, *Bioconjug. Chem.* 16 (2005) 122-130
- [89] J. Panyam, W.-Z. Zhou, S. Prabha, S.K. Sahoo, V. Labhasetwar, Rapid endo-lysosomal escape of poly(DL-lactide-co-glycolide) nanoparticles: implications for drug and gene delivery, *FASEB J.* 16 (2002) 1217-1226
- [90] M. Lindgren, M. Hallbrink, A. Prochiantz, U. Langel, Cell-penetrating peptides, *Trends Pharmacol. Sci.* 21 (2000) 99-103
- [91] Y.L. Tseng, J.J. Liu, R.L. Hong, Translocation of liposomes into cancer cells by cell-penetrating peptides penetratin and Tat: a kinetic and efficacy study, *Mol. Pharmacol.* 62 (2002) 864-872

- [92] T.S. Levchenko, R. Rammohan, N. Volodina, V.P. Torchilin, Tat peptide-mediated intracellular delivery of liposomes, *Methods in Enzymology* 372 (2003) 339-349
- [93] M. Lewin, N. Carlesso, C.H. Tung, X.W. Tang, D. Cory, D.T. Scadden, R. Weissleder, Tat peptide-derivatized magnetic nanoparticles allow in vivo tracking and recovery of progenitor cells, *Nat. Biotechnol.* 18 410-414
- [94] J.S. Suk, J. Suh, K. Choy, S.K. Lai, J. Fu, J. Hanes, Gene delivery to differentiated neurotypic cells with RGD and HIV Tat peptide functionalized polymeric nanoparticles, *Biomaterials* 27 (2006) 5143-5150
- [95] M.A. Bogoyevitch, T.S. Kendrick, D.C.H. Ng, R.K. Barr, Taking the cell by stealth or storm? Protein transduction domains (PTDs) as versatile vectors for delivery, *DNA Cell Biol.* 21 (2002) 879-894
- [96] M. Zorko, U. Langel, Cell-penetrating peptides: mechanism and kinetics of cargo delivery, *Adv. Drug Deliv. Rev.* 57 (2005) 529-545
- [97] H. Brooks, B. Lebleu, E. Vives, Tat peptide-mediated cellular delivery: back to basics, *Adv. Drug Deliv. Rev.* 57 (2005) 559-577
- [98] M.C. Morris, J. Depollier, J. Mery, F. Heitz, G. Divita, A peptide carrier for the delivery of biologically active proteins into mammalian cells, *Nat. Biotechnol.* 19 (2001) 1173-1176
- [99] T. Pellegrino, W.J. Parak, R. Boudreau, M.A. Le Gros, D. Gerion, A.P. Alivisatos, C.A. Larabell, Quantum dot-based cell motility assay, *Differentiation* 71 (2003) 542-548
- [100] A. Hoshino, K. Fujioka, Y.I. Kawamura, N. Toyama-Sorimachi, M. Yasuhara, T. Dohi, K. Yamamoto, Immune cells tracing using quantum dots, *Proc. of SPIE* 6096 (2006) 609613/1-609613/8
- [101] J. Silver, W. Ou, Photoactivation of quantum dot fluorescence following endocytosis, *Nano Lett.* 5 (2005) 1445-1449
- [102] B.C. Lagerholm, M. Wang, L.A. Ernst, D.H. Ly, H. Liu, M.P. Bruchez, A.S. Waggoner, Multicolor Coding of Cells with Cationic Peptide Coated Quantum Dots, *Nano Lett.* 4 (2004) 2019-2022
- [103] L.C. Mattheakis, J.M. Dias, Y.J. Choi, J. Gong, M.P. Bruchez, J. Liu, E. Wang, Optical coding of mammalian cells using semiconductor quantum dots, *Anal. Biochem.* 327 (2004) 200-208

- 
- [104] S.M. Rozenzhak, M.P. Kadakia, T.M. Caserta, T.R. Westbrook, M.O. Stone, R.R. Naik, Cellular internalization and targeting of semiconductor quantum dots, *Chem. Commun.* (2005) 2217-2219
- [105] E. Chang, W.W. Yu, V.L. Colvin, R. Drezek, Quantifying the influence of surface coatings on quantum dot uptake in cells, *J. Biomed. Nanotechnol.* 1 (2005) 397-401
- [106] E.L. Bentzen, I.D. Tomlinson, J. Mason, P. Gresch, M.R. Warnement, D. Wright, E. Sanders-Bush, R. Blakely, S.J. Rosenthal, Surface Modification To Reduce Nonspecific Binding of Quantum Dots in Live Cell Assays, *Bioconjug. Chem.* 16 (2005) 1488-1494
- [107] B. Ballou, B.C. Lagerholm, L.A. Ernst, M.P. Bruchez, A.S. Waggoner, Noninvasive imaging of quantum dots in mice, *Bioconjug. Chem.* 15 (2004) 79-86
- [108] W. Cai, D. Shin, K. Chen, O. Gheysens, Q. Cao, S. Wang, X, S.S. Gambhir, X. Chen, Peptide-labeled near-infrared quantum dots for imaging tumor vasculature in living subjects, *Nano Lett.* 6 (2006) 669-676
- [109] R.K. Jain, Transport of molecules across tumor vasculature, *Cancer Metastasis Rev.* 6 (1987) 559-593
- [110] J.O. Winter, T.Y. Liu, B.A. Korgel, C.E. Schmidt, Recognition molecule directed interfacing between semiconductor quantum dots and nerve cells, *Adv. Mater.* 13 (2001) 1673-1677
- [111] X. Wu, H. Liu, J. Liu, K.N. Haley, J.A. Treadway, J.P. Larson, N. Ge, F. Peale, M.P. Bruchez, Immunofluorescent labeling of cancer marker Her2 and other cellular targets with semiconductor quantum dots, *Nature Biotechnology* 21 (2002) 41-46
- [112] M. Howarth, K. Takao, Y. Hayashi, A.Y. Ting, Targeting quantum dots to surface proteins in living cells with biotin ligase, *Proc. Natl. Acad. Sci. U. S. A.* 102 (2005) 7583-7588
- [113] W. Jiang, S. Mardiyani, H. Fischer, W.C.W. Chan, Design and Characterization of Lysine Cross-Linked Mercapto-Acid Biocompatible Quantum Dots, *Chem. Mater.* 18 (2006) 872-878
- [114] Y. Pan, J. Cai, L. Qin, H. Wang, Atomic force microscopy-based cell nanostructure for ligand-conjugated quantum dot endocytosis, *Acta biochimica et biophysica Sinica* 38 (2006) 646-652
-

- [115] H.E. Grecco, K.A. Lidke, R. Heintzmann, D.S. Lidke, C. Spagnuolo, O.E. Martinez, E.A. Jares-Erijman, T.M. Jovin, Ensemble and single particle photophysical properties (two-photon excitation, anisotropy, FRET, lifetime, spectral conversion) of commercial quantum dots in solution and in live cells, *Microsc. Res. Tech.* 65 (2004) 169-179
- [116] J. Mendelsohn, J. Baselga, The EGF receptor family as targets for cancer therapy, *Oncogene* 19 (2000) 6550-6565
- [117] A. Kriete, E. Papazoglou, B. Edrissi, H. Pais, K. Pourrezaei, Automated quantification of quantum-dot-labelled epidermal growth factor receptor internalization via multiscale image segmentation, *Journal of microscopy* 222 (2005) 22-27
- [118] J. Wang, P.T. Vernier, Y. Sun, M.A. Gundersen, L. Marcu, A fluorescence microscopy study of quantum dots as fluorescent probes for brain tumor diagnosis, *Proc. of SPIE* 5703 (2005) 127-134
- [119] S.S. Rajan, T.Q. Vu, Quantum Dots Monitor TrkA Receptor Dynamics in the Interior of Neural PC12 Cells, *Nano Lett.* 6 (2006) 2049-2059
- [120] M.J. Humphries, Integrin structure, *Biochem. Soc. Trans.* 28 (2000) 311-340
- [121] E. Koivunen, B. Wang, E. Ruoslahti, Phage libraries displaying cyclic peptides with different ring sizes: ligand specificities of the RGD-directed integrins, *Biotechnology* 13 (1995) 265-270
- [122] R. Pasqualini, E. Koivunen, E. Ruoslahti, av Integrins as receptors for tumor targeting by circulating ligands, *Nat. Biotechnol.* 15 (1997) 542-546
- [123] C.P. Leamon, P.S. Low, Folate-mediated targeting: from diagnostics to drug and gene delivery, *Drug Discov. Today* 6 (2001) 44-51
- [124] J. Reddy, D. Dean, M. Kennedy, P. Low, Optimization of folate-conjugated liposomal vectors for folate receptor-mediated gene therapy, *J. Pharm. Sci.* 88 (2000) 1112-1118
- [125] A.R. Hilgenbrink, P.S. Low, Folate receptor-mediated drug targeting: From therapeutics to diagnostics, *J. Pharm. Sci.* 94 (2005) 2135-2146
- [126] W.C.W. Chan, D.J. Maxwell, X. Gao, R.E. Bailey, M. Han, S. Nie, Luminescent quantum dots for multiplexed biological detection and imaging, *Curr. Opin. Biotechnol.* 13 (2002) 40-46
- [127] E. Ruoslahti, Targeting tumor vasculature with homing peptides from phage display, *Semin. Cancer Biol.* 10 (2000) 435-442

- 
- [128] L.R.H. Krumpal, T. Mori, The use of phage-displayed peptide libraries to develop tumor-targeting drugs, *International Journal of Peptide Research and Therapeutics* 12 (2006) 79-91
- [129] T. Oyama, I.T. Rombel, K.N. Samli, X. Zhou, K.C. Brown, Isolation of multiple cell-binding ligands from different phage displayed-peptide libraries, *Biosensors & Bioelectronics* 21 (2006) 1867-1875
- [130] Y. Kim, A.M. Lillo, S.C.J. Steiniger, Y. Liu, C. Ballatore, A. Anichini, R. Mortarini, G.F. Kaufmann, B. Zhou, B. Felding-Habermann, K.D. Janda, Targeting Heat Shock Proteins on Cancer Cells: Selection, Characterization, and Cell-Penetrating Properties of a Peptidic GRP78 Ligand, *Biochemistry* 45 (2006) 9434-9444
- [131] S. Takeda, S. Kadowaki, T. Haga, H. Takaesu, S. Mitaku, Identification of G protein-coupled receptor genes from the human genome sequence, *FEBS Lett.* 520 (2002) 97-101
- [132] B.L. Cushing, V.L. Kolesnichenko, C.J. O'Connor, Recent Advances in the Liquid-Phase Syntheses of Inorganic Nanoparticles, *Chem. Rev.* 104 (2004) 3893-3946
- [133] S.J. Rosenthal, I. Tomlinson, E.M. Adkins, S. Schroeter, S. Adams, L. Swafford, J. McBride, Y. Wang, L.J. DeFelice, R.D. Blakely, Targeting Cell Surface Receptors with Ligand-Conjugated Nanocrystals, *J. Am. Chem. Soc.* 124 (2002) 4586-4594
- [134] I.D. Tomlinson, J.N. Mason, R.D. Blakely, S.J. Rosenthal, Inhibitors of the serotonin transporter protein (SERT): The design and synthesis of biotinylated derivatives of 3-(1,2,3,6-tetrahydropyridin-4-yl)-1H-indoles. High-affinity serotonergic ligands for conjugation with quantum dots, *Bioorg. Med. Chem. Lett.* 15 (2005) 5307-5310
- [135] I.D. Tomlinson, J.N. Mason, R.D. Blakely, S.J. Rosenthal, High affinity inhibitors of the dopamine transporter (DAT): Novel biotinylated ligands for conjugation to quantum dots, *Bioorg. Med. Chem. Lett.* 16 (2006) 4664-4667
- [136] J.N. Mason, H. Farmer, I.D. Tomlinson, J.W. Schwartz, V. Savchenko, L.J. DeFelice, S.J. Rosenthal, R.D. Blakely, Novel fluorescence-based approaches for the study of biogenic amine transporter localization, activity, and regulation, *J. Neurosci. Methods* 143 (2005) 3-25
-

- [137] S.H. Young, E. Rozengurt, Qdot nanocrystal conjugates conjugated to bombesin or ANG II label the cognate G protein-coupled receptor in living cells, *Am. J. Physiol.* 290 (2006) C728-C732
- [138] J. Panyam, V. Labhasetwar, Targeting Intracellular Targets, *Current Drug Delivery* 1 (2004) 235-247
- [139] B. Fahrenkrog, U. Aebi, The nuclear pore complex: Nucleocytoplasmic transport and beyond, *Nat. Rev. Mol. Cell Biol.* 4 (2003) 757-766
- [140] A. Szewczyk, L. Wojtczak, Mitochondria as a pharmacological target, *Pharmacol. Rev.* 54 (2002) 101-127
- [141] N. Dias, C. Bailly, Drugs targeting mitochondrial functions to control tumor cell growth, *Biochem. Pharmacol.* 70 (2005) 1-12
- [142] J.B. Delehanty, I.L. Medintz, T. Pons, F.M. Brunel, P.E. Dawson, H. Mattoussi, Self-Assembled Quantum Dot-Peptide Bioconjugates for Selective Intracellular Delivery, *Bioconjug. Chem.* 17 (2006) 920-927
- [143] J.M. de la Fuente, M. Fandel, C.C. Berry, M. Riehle, L. Cronin, G. Aitchison, A.S.G. Curtis, Quantum dots protected with tiopronin: A new fluorescence system for cell-biology studies, *ChemBioChem* 6 (2005) 989-991
- [144] S. Santra, H. Yang, J.T. Stanley, P.H. Holloway, B.M. Moudgil, G. Walter, R.A. Mericle, Rapid and effective labeling of brain tissue using TAT-conjugated CdS[Mn/ZnS] quantum dots, *Chem. Commun.* (2005) 3144-3146
- [145] M. Gumbleton, A.J. Hollins, Y. Omid, L. Campbell, G. Taylor, Targeting caveolae for vesicular drug transport, *J. Control. Release* 87 (2003) 139-151
- [146] E.M. Damm, L. Pelkmans, J. Kartenbeck, A. Mezzacasa, T. Kurzchalia, A. Helenius, Clathrin- and caveolin-1-independent endocytosis: Entry of simian virus 40 into cells devoid of caveolae, *J. Cell Biol.* 168 (2005) 477-488
- [147] I.M. Kaplan, J.S. Wadia, S.F. Dowdy, Cationic TAT peptide transduction domain enters cells by macropinocytosis, *J. Control. Release* 102 (2005) 247-253
- [148] A. Ferrari, V. Pellegrini, C. Arcangeli, A. Fittipaldi, M. Giacca, F. Beltram, Caveolae-Mediated internalization of extracellular HIV-1 tat fusion proteins visualized in real time, *Mol. Ther.* 8 (2003) 284-294
- [149] Y. Zhang, M.K. So, J. Rao, Protease-Modulated Cellular Uptake of Quantum Dots, *Nano Lett.* 6 (2006) 1988-1992



- [150] S.D. Caruthers, S.A. Wickline, G.M. Lanza, Nanotechnological applications in medicine, *Curr. Opin. Biotechnol.* 18 (2007) 26-30



# **Chapter 2**

## **Goals of the Thesis**

Considering the significant benefits that site-specific drug therapy offers, the goal of this thesis was to investigate the potential of G-protein-coupled receptors (GPCRs) as candidates for a new class of targets in the field of drug targeting. In order to evaluate this potential at the cellular level, nanoparticles were conjugated with specific ligands for the human neuropeptide Y (hNPY) Y<sub>1</sub> receptor and characterized according to their affinity to cells expressing this receptor. A second objective was to explore whether GPCRs provide a portal for nanoparticle delivery into cells, since GPCRs are known to internalize after agonist binding.

GPCRs represent the largest class of receptors in the human genome and have, therefore, been a key area of focus in drug research for several decades. Consequently, we know a number of specifically binding ligands as well as the organ distribution of many GPCRs. This makes GPCRs extremely interesting candidates for nanoparticle drug targeting. The human Y<sub>1</sub> receptor was chosen as model receptor to prove the principle of this new form of targeting. The peptidic ligands of this receptor were supposed to show more affinity towards their receptor after immobilization on a nanoparticle compared to small native ligands. Instead of using drug-loaded polymeric nanoparticles, a model colloid was chosen to provide optimal conditions for the investigation of the particle-cell-interactions. Quantum dots (QDs), semiconductor nanocrystals, offer a number of advantages over conventional nanoparticles, such as their increased detectability and their small and uniform size (**chapter 1**). While their small size is a prerequisite for entering distinct cellular uptake pathways, their strong fluorescence enables sensitive and highly resolved detection by fluorescence microscopy.

For the design of the QD-based model colloid, an initial aim was to synthesize QDs via traditional methods in organic solvents using safe, non-organometallic precursors. For this purpose, the conditions for the growth of the particles were optimized and the synthesis processes in coordinating as well as in non-coordinating solvents were compared (**chapter 3**).

Since these organic soluble nanoparticles are to be used in aqueous systems for the cellular investigations, different methods of modifying the nanoparticles were examined in order to render the particles water-soluble. Moreover, it was a goal to attach poly(ethylene glycol) (PEG) to the particles, since this modification is known to enhance the stability of the colloid and to reduce non-specific binding to cells – an important prerequisite for further studies of specific uptake (**chapter 4**).

Following this, the aqueous QDs were characterized according to their dispersity using different methods, such as transmission electron microscopy (TEM), dynamic light scattering (DLS) and asymmetric flow field-flow fractionation (AF4), since dispersity should strongly influence the cellular uptake pathway of nanoparticles. Furthermore, the cell-compatibility was evaluated (**chapter 5**).

Having optimized the preparation and the characterization of PEGylated QDs, their potential for use in cellular studies had to be evaluated. Therefore, their stability under cell-culture conditions and their detectability in fluorescence microscopy was investigated. Cytotoxicity, a major concern when dealing with QDs, was also analyzed. (**chapter 6**).

In establishing the conditions for the conjugation of the QDs with the peptidic ligands for the  $Y_1$  receptor, easily preparable micelles of PEGylated phospholipids, which were also used for the coating of the QDs, served as the surrogate for the PEGylated QDs. In addition to the ease of preparation, the absence of the QDs in this similar colloid facilitated the analytics of the bioconjugates by mass spectrometry and spectrometric methods. The micelles were additionally tested for their ligand-mediated delivery to  $Y_1$ -receptor positive MCF-7 cells (**chapter 7**).

The subsequent investigations focused on the biological activity of QDs conjugated with specific ligands of the  $Y_1$  receptor. Therefore, several peptidic analogs of the hNPY were bound to QDs and their binding and internalization at different human cancer cell lines (MCF-7, SK-N-MC) were investigated. Through confocal laser scanning microscopy, the specificity of binding and uptake was monitored and matched with different control groups and cells lacking the  $Y_1$  receptor (MDA). In order to evaluate whether a small non-peptidic  $Y_1$  receptor antagonist can be used for drug targeting as well, bioconjugates of QDs with an analog of BIBP3226 were examined using the same cell lines. The binding affinity of the agonistic and antagonistic QDs is a crucial parameter in estimating the potential of GPCR-targeted nanoparticles. Therefore, flow-cytometric binding and displacement studies were conducted to see whether the affinity and specificity towards the  $Y_1$ -receptor is acceptably high for such particles (**chapter 8**).

Finally, the way in which the particles are internalized into the target cells was explored. To compare the uptake of the QDs to non-specific uptake, QDs were coated with poly(ethylene imine) (PEI) and compared to NPY-QDs by confocal microscopy. An endosome marker and free NPY, labeled with a small fluorophore

were used to evaluate differences in uptake caused by the conjugation of the ligand to the QDs (**chapter 9**).

# **Chapter 3**

## **Synthesis of Quantum Dots – Comparison Between Non-coordinating and Coordinating Solvents**

W. Hild, K. Zenger, J. Teßmar, A. Göpferich

Department of Pharmaceutical Technology, University of Regensburg,  
Universitätsstraße 31, 93040 Regensburg, Germany

**Abstract**

Over the last decade, quantum dots (QDs) have attracted considerable attention in biomedical research, since these semiconductor nanocrystals are both extremely small and also exhibit unique optical properties, such as their bright and stable fluorescence in particular. These characteristics render QDs promising tools for discovering biological processes.

Up to now, a number of synthesis methods have been described to produce QDs for such purposes. However, the huge number of processes makes it hard to determine the most convenient method. In order to find a pragmatic method for the synthesis of CdSe/ZnS nanocrystals of favorable optical properties and narrow size distributions, protocols for the synthesis in organic solvents were established by comparing two common classes of synthesis routes. In this study, the preparation of quantum dots in non-coordinating solvent (octadecene) with those synthesized in non-coordinating solvents (trioctylphosphine oxide and hexadecylamine) was compared. Having optimized the synthesis routes, the preparation in coordinating solvents turned out to be more favorable. Narrower emission peaks and higher quantum yields of up to 80% were obtained.



## Introduction

Quantum dots (QDs), semiconductor nanocrystals in the size-range of approx. 1-10 nm, have become very important in various applications covering physical and chemical as well as biomedical sciences [1-4]. The major benefit of these nanocrystals lies in their small and very uniform size as well as in their remarkable optical properties, namely their bright photoluminescence obtained after excitation [5]. In contrast to organic fluorescent dyes, the emission peak of QDs is very sharp while their excitation spectra are very broad. Consequently, these characteristics provide large practical Stokes-shifts, the difference between the wavelengths of absorbed and emitted light. Moreover, QDs are very stable with regard to photobleaching, a phenomenon that has been a drawback for conventional dyes in long-term fluorescence imaging of cells and tissues [6,7]. Nanocrystals composed of cadmium selenide (CdSe) are advantageous for the application in cellular imaging, since this material exhibits photoluminescence in the visible range of the spectrum which can be detected by standard equipment of fluorescence microscopes and the detectors of flow cytometers [8]. To improve the optical properties of CdSe nanocrystals, layers of a semiconductor of higher bandgap are usually grown onto the particles [9] to provide an insulating effect for the exciton, the electron-hole-pair responsible for the fluorescence. Zinc sulfide (ZnS) [10] proved to be helpful, since this material on the one hand provides the mentioned prerequisite, and on the other hand shows only moderate lattice-mismatch with the CdSe crystals [11] when forming close coatings on the core particles.

Synthesis routes towards CdSe nanocrystals can be divided into methods using aqueous precursors yielding water-dispersable QDs [12,13], and into the vast majority of routes making use of organic solvents. The QDs synthesized using aqueous routes have the advantage that there is no additional surface-modification on the nanocrystals for solubilisation necessary. However, these nanocrystals cannot compete with the narrow size-distributions and high quantum yields of the ones obtained by using organic solvents. QDs synthesized in organic solvents usually exhibit narrower sizes and higher quantum yields [14]. Therefore, routes for QD synthesis in non-aqueous solvents at high temperatures are currently strongly preferred. Organic-soluble QDs were first produced by thermal decomposition of organo-metallic precursors, such as dimethylcadmium, which for the first time lead to

high-quality nanocrystals [15-17]. However in order to establish a QD synthesis route, safer reagents prove to be more favorable [18] by exchanging dimethylcadmium against cadmium oxide. Organic synthesis processes can be classified into ones making use of coordinating solvents, i.e. solvents forming complexes with metal ions, like trioctylphosphine oxide (TOPO) and hexadecylamine (HDA) [19], and ones based on non-coordinating ones, like octadecene (ODE) [20] or paraffin [21].

The objective of this study was to compare the synthesis of CdSe/ZnS nanocrystals in the coordinating solvents HDA/TOPO to the ones obtained in the non-coordinating solvent ODE. Therefore, both synthesis routes were optimized with respect to the main influence factors, such as temperature and precursor concentration. Methods for the purification of the particles were developed as well. After appropriate surface-modification, the particles obtained are intended for use in biological studies.

### **Materials and methods**

Cadmium oxide (CdO, 99.5%), hexadecylamine (HDA, tech. grade 90%), lauric acid (LA 98%), methanol (anhydr. 99.8%), octadecene (ODE, tech. grade 90%), oleic acid (OA, reagent grade 99%), sulfur (99.5%), toluene (anhydr. 99.8%), trioctylphosphine (TOP, tech. grade 90%), trioctylphosphine oxide (TOPO, tech. grade 90%) and zinc stearate (tech. grade) were obtained from Sigma-Aldrich (St. Louis, MO).

#### *Synthesis of CdSe/ZnS nanocrystals*

All reactions were carried-out under water-free conditions and under N<sub>2</sub> inert gas atmosphere. All reagents, unless obtained in water-free quality, were dried in vacuum at elevated temperatures.

#### *Synthesis using non-coordinating solvents (ODE)*

CdSe nanocrystals were synthesized with some modifications according to previously published methods [20,22]. In order to improve the reaction conditions, various parameters were changed. In the following, the synthesis is described by making use of the optimized conditions. The respective amount of CdO (0.4 mmol) was dissolved in OA (4.8 ml) at 200 °C. Afterwards, ODE (40 ml) was added and the solution was heated to 280 °C. At this temperature, the Se-precursor, which was kept

at room temperature, was injected quickly using a syringe. The Se-precursor was prepared by dissolving Se (0.2 mmol) in TOP (0.2 ml) and ODE (3.2 ml) under slight heating (60 °C). After injection, the nanocrystals were grown in the heating bath. Samples were taken at the respective time-points by a syringe. At the desired nanocrystal size, the reaction was stopped by injecting ODE (10 ml) at room temperature. For the set of different OA amounts, the following conditions were used: CdO: 0.1 mmol; OA: 0.3-2.0 ml (3-20%); T = 250 °C; Se: 0.07 mmol. For the set of different total precursor concentrations: CdO: 0.05/0.1/0.2/0.3/0.4 mmol; OA: 0.06/1.2/2.4/3.6/4.8 ml; ODE: 10 ml; T = 250 °C; Se: 0.0125/0.025/0.05/0.1/0.2 mmol. For the set of different reaction temperatures: T = 220/235/250/265/280 °C.

After preparation, the nanocrystals were precipitated by adding acetone of the same volume. After centrifugation at 20.000 g, the precipitated QDs were redispersed in 500 µl of toluene. For coating with ZnS, the CdSe nanocrystals in toluene were added to 20 ml of ODE and heated to the respective coating temperature (100/150/200 °C). For ZnS-coating, the exact amounts of zinc stearate and S were calculated in correlation to the amount and diameter of the CdSe cores which were determined by UV-absorption using estimations for the extinction coefficients and nanocrystal diameter [23]. By calculating the volume for a ZnS-shell of 4 monolayers, the theoretical amount of Z and S for all particles was determined (density of ZnS  $4.1 \times 10^{-21}$  g/nm<sup>3</sup>, thickness of ZnS monolayer 0.31 nm). Zinc stearate and S were dissolved in 6 ml of TOP under heating to 100 °C. After cooling to room temperature, the precursor was added dropwise to the CdSe cores over 30 or 60 minutes each at 100/150/200 °C. The CdSe/ZnS nanocrystals were precipitated and redispersed as described above.

#### *Synthesis using coordinating solvents (TOPO/HDA)*

The cadmium precursor was prepared by dissolving CdO (0.2 mmol) in lauric acid (1.6 mmol) at 200 °C. TOPO (10 mmol, 3.88 mg) and HDA (16 mmol, 3.88 mg) were added and the mixture was heated to 285 °C. At this temperature, the heating bath was removed and Se (2 mmol) dissolved in 3.5 ml of TOP (room temperature) was injected. At the desired nanocrystal size, the reaction was stopped by adding 20 ml of toluene. The CdSe cores were precipitated with an equal volume of methanol and centrifuged and redispersed as described above. ZnS-coating was conducted after

dispersing the CdSe cores in the same amount of TOPO and HDA as for the core synthesis at the respective temperature (100/150/200 °C) over 30 or 60 min. The amounts for the ZnS precursor were calculated as described above. After shell-growth, the nanocrystals were purified by precipitation as described above.

#### *Spectrophotometric measurements*

UV absorbance spectra were recorded using an Uvikon 941 (Kontron Instruments, UK) and 10 cm quartz cuvettes. Fluorescence was determined in 10 cm quartz cuvettes using a RF-1501 spectrometer (Shimadzu Deutschland GmbH, Duisburg, Germany) in order to follow the growth of the CdSe QDs in ODE. For all other fluorescence measurements (including all determinations of quantum yields), an LS 55 fluorescence spectrometer from PerkinElmer (Waltham, MA) was used. Fluorescence quantum yields were determined in correlation to a fluorescein standard in 0.1 N NaOH (quantum yield 90%). Samples were excited at 450 nm.

#### *Size determination*

The size (solvodynamic diameter) of the QDs was determined by dynamic light scattering (DLS) using a ZetaSizer 3000 HSA (Malvern, Worcestershire, UK) at 20 °C and an angle of 90° in toluene. Data was processed using the NNLS algorithm.

## **Results and discussion**

### *Synthesis of CdSe nanocrystals*

Two chemically different routes towards CdSe/ZnS quantum dots have been established in order to compare them with each other concerning the reproducibility and the optical properties of the resulting nanocrystals. Both processes are based upon the thermal decomposition of the respective precursors for CdSe and ZnS (see fig. 1A). For both reactions the cadmium precursor was based on CdO to avoid hazardous and dangerous organometallic precursors. In both cases, trioctylphosphine selenide (TOPSe) was used as the selenium precursor. The approaches varied with the solvents used: non-coordinating (ODE) or coordinating (TOPO), both exhibiting commonly-used systems. As shown in the reaction scheme (fig. 1A), CdSe nanocrystals are formed by reacting the cadmium precursors

(cadmium oleate or cadmium laurate) with TOPSe in either a non-coordinating (ODE) or a coordinating solvent (TOPO/HDA). The setup for the reactions comprising standard Schlenk methods is depicted in fig. 1B.

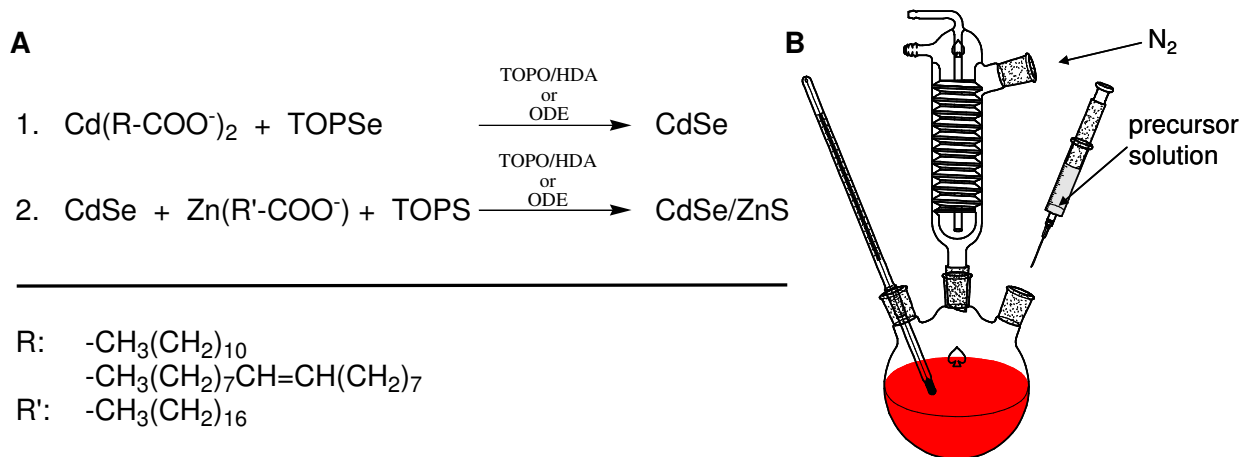


**Figure 1: Preparation of CdSe/ZnS nanocrystals.** (A) Synthesis scheme, starting from two different Cd-salts (laurate or oleate). CdSe nanocrystals were either formed in the coordinating solvent mixture TOPO/HDA or ODE by reaction with the selenium precursor (TOPSe) (1). The coating with ZnS was subsequently achieved by using zinc stearate and the sulfur precursor (TOPS) under the same solvent conditions (2). (B) Setup of the reaction. The reactions were carried out under inert gas atmosphere. For CdSe-formation, the Se-precursor was injected quickly. For the coating, the ZnS-precursor was added dropwise via a syringe.

#### CdSe-growth in non-coordinating solvents

In order to optimize this reaction in the non-coordinating solvent ODE towards high emission wavelengths and narrow emission peaks, beneficial features for probes in biological investigations, the optimal reaction conditions concerning the amount of oleic acid were determined. Oleic acid serves as a complexing stabilizer for the Cd-precursor and depending on the concentration it influences, the reaction kinetics of the crystal growth. In the growth curve (fig. 2A), the fluorescence emission maxima are plotted against the growth time. Since the emission maxima grow with increasing particle size, the curves are representative of the corresponding particle sizes. Each curve follows typical growth characteristics. After a short nucleation phase, during which small CdSe nanocrystals are generated, the crystals grow and as a result rapidly increasing emission maxima were observed. Nucleation decreases due to the

loss of temperature resulting from the injection of the cold Se-precursor and due to the decrease of the monomer concentration. During the growth phase, small crystals are dissolved in favor of larger ones (focusing of the size distribution) [24]. This phase continues until the curves finally level off, when equilibrium between growth and decomposition is reached. Finally, decomposition begins to dominate and hence reactions are then stopped before this point by rapidly reducing the temperature. This behavior can also be seen when regarding the full width at half maximum (FWHM) values of the corresponding emission peaks of the growth curves (fig. 1B). These values are correlated with the particle size-distribution: the broader the size distribution, the higher the FWHM values. After initial higher values, the FWHM decreases during the growth phase until the point of the maximum size is reached and decomposition processes start. The optimum OA concentration was found to be 12%, relative to the total volume. Here, the growth is controllable over about 400 seconds. High emission maxima can be reached while lower OA concentrations yielded lower maxima and shorter time spans of controllable growth. The FWHM values are the lowest and, therefore, the best when applying the 12% OA concentration. Thus, OA was kept at this concentration for further studies.

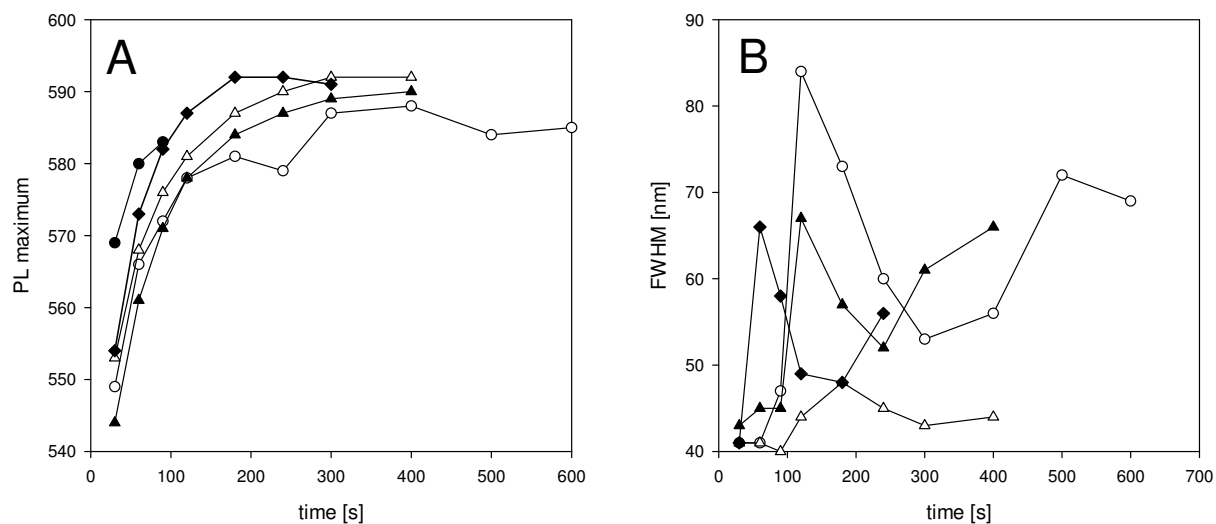


**Figure 2: Influence of OA concentration on growth and size distribution (FWHM).** Higher OA concentrations yield more controllable growth to higher emission wavelengths and therefore higher nanocrystal sizes (A). The FWHM values and, therefore, the size-distributions of the nanocrystals decrease during the reaction. The lowest and thus the best values were obtained at 12% of OA (B). (OA concentration: ● 3%; ○ 6%; ▲ 9%; △ 12 %; ◆ 20%).

In order to produce larger amounts of nanocrystals, it was investigated whether an increase in the total amounts of the precursors exerts an influence on the nanocrystal growth. Therefore, the total volume of the reaction solution was kept constant while an x-fold amount of all precursors was used. Fig. 3A shows the effect of the total concentration of the precursors by maintaining the ratio Cd : Se : OA. For the sake of clarity, only the concentration of Cd is depicted. An increase in the total concentration of all precursors causes a decrease in emission maxima. Under the chosen conditions, the FWHM decrease for higher precursor concentrations (fig. 3B). This proves that the growth reaction is related to the amount of precursors, even when their ratio is unchanged. A possible reason for this behavior might be the hindered diffusion from the precursor solution to the nanocrystals. For the Cd-concentrations of 7.5 and 10 mM, the reaction is well controllable and yields higher amounts than for lower concentrations. Therefore, these concentrations are considered favorable.

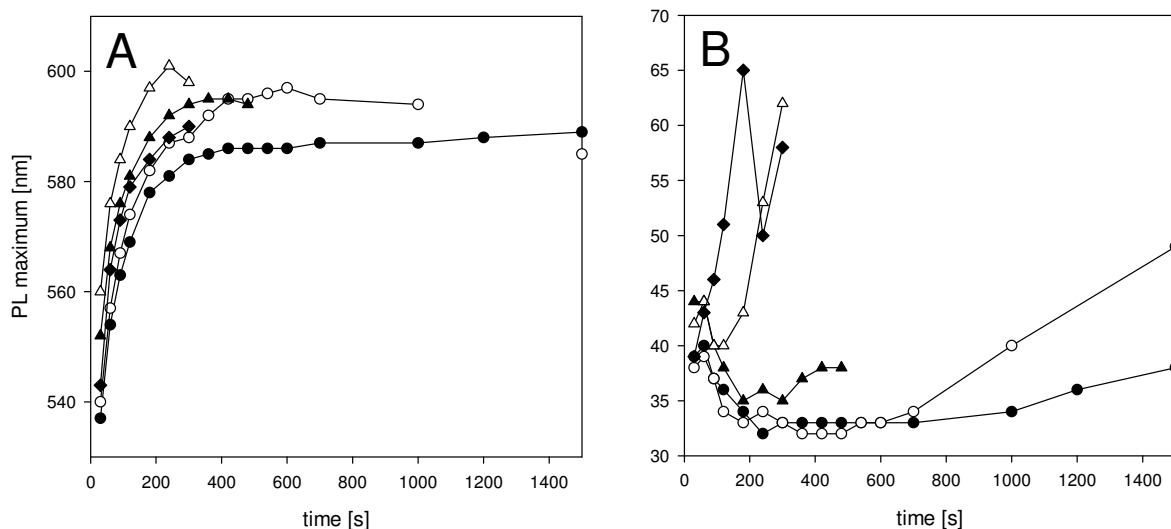


**Figure 3: Influence of the total precursor concentration on growth and size distribution (FWHM).** Keeping the ratio of the precursors constant the influence of the total precursor concentration showed an optimum for the threefold batch-size. Here, relatively high amounts of QDs can be produced and growth continues up to high emission maxima (A). The FWHM values are optimal for this batch size (B). (Values calculated in correlation to Cd concentration: ● 1.25 mM; ○ 2.5 mM; ▲ 5.0 mM; △ 7.5 mM; ◆ 10 mM).

The largest influence on the growth characteristics of the CdSe nanocrystals is related to the process temperature. In a series from 220 to 280 °C, the final particle increases in correlation with the emission maxima (fig. 4A). Therefore, for the optimization of the reaction conditions later on, the temperature was set to 280 °C. This provided the highest flexibility for the preparation of a broad spectrum of differently emitting QDs. Moreover, at this growth temperature, the size distribution and, therefore, the FWHM value of the resulting CdSe QDs is the lowest which emphasizes that the optimum growth temperature is at 280 °C (fig. 4B).

As shown in fig. 5, the nanocrystal growth under the optimized conditions is well-controllable, since deviations in the growth curve as well as in the FWHM values are on an acceptably low level. The data show that during the growth reaction, the FWHM values are narrow and therefore the size-distributions are focussing.

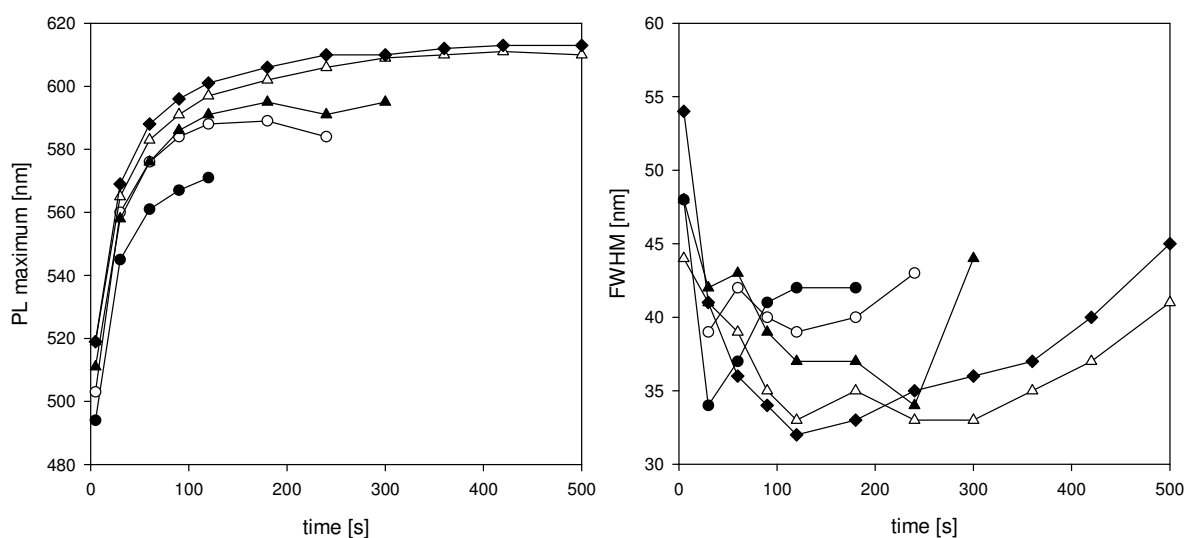


**Figure 4: Influence of the growth temperature on growth and size distribution (FWHM).** Increasing the growth temperature of the nanocrystals leads to longer growth times and higher emission maxima, with an optimum at 280 °C (A). For this temperature, the FWHM values corresponding to the broadness of the size distribution are lowest (B). (Growth temperatures: ● 220 °C; ○ 235 °C; ▲ 250 °C; △ 265 °C; ◆ 280 °C).



An overview of the optical properties of the CdSe nanocrystals prepared under the optimized conditions in the non-coordinating solvent ODE is given in fig. 6. Here, five collectives of CdSe QDs of distinguishable fluorescence spectra are depicted together with the absorbance spectrum of the QDs exhibiting an emission maximum of 606 nm. Typical fluorescence quantum yields obtained under these conditions are around 5%.

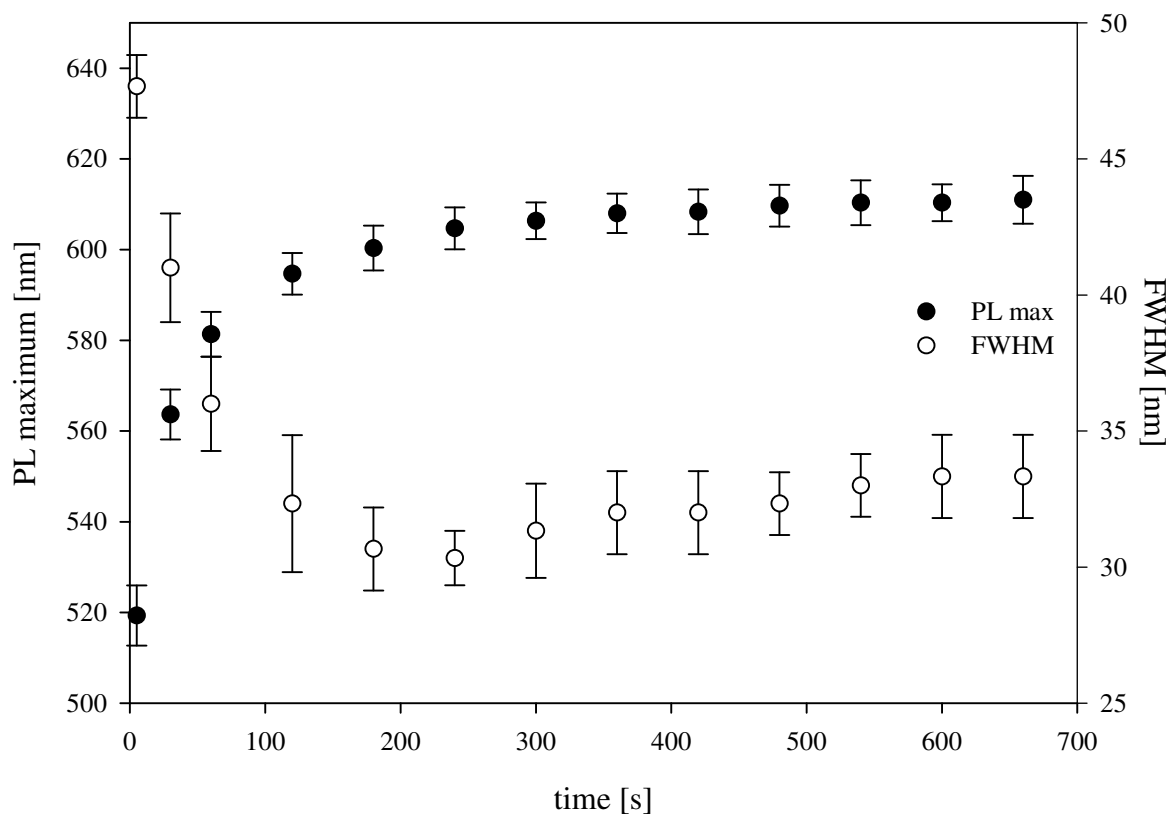
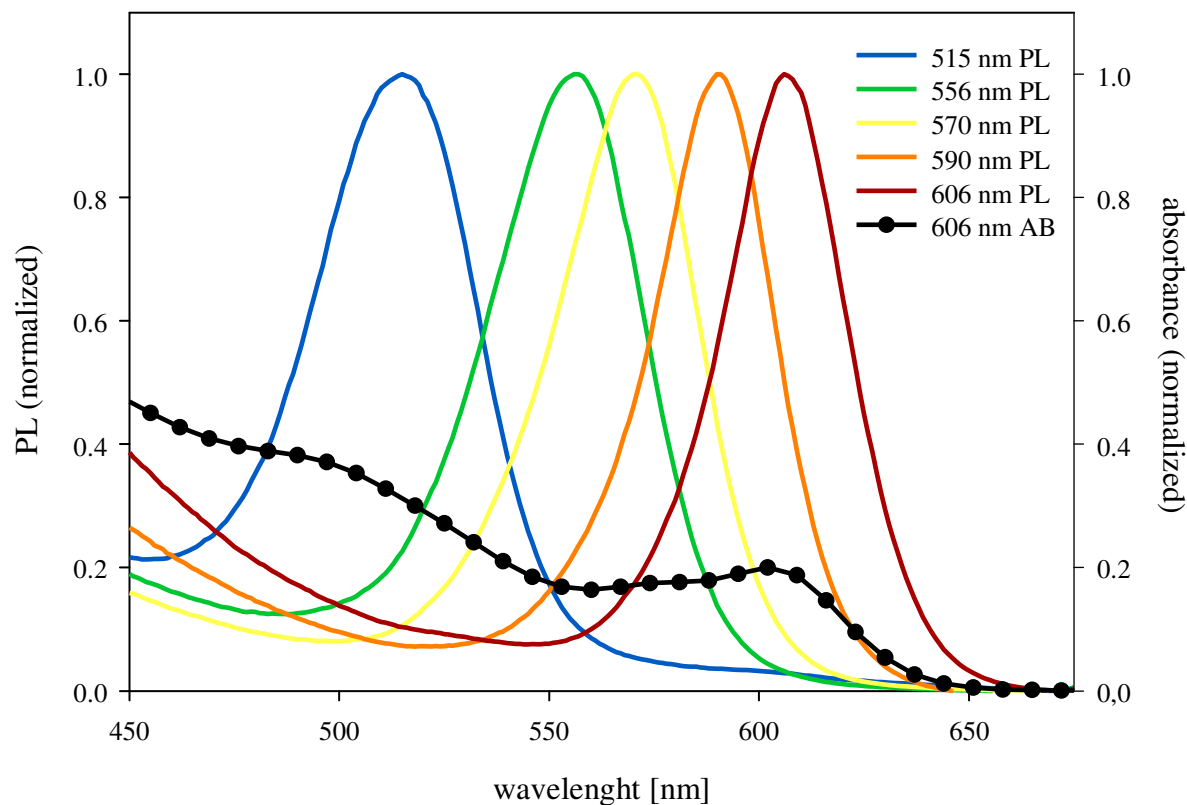


Figure 5: Growth kinetics of CdSe nanocrystals in the non-coordinating solvent ODE (●), represented by the emission maxima plotted against the growth time. After rapid nucleation, growth goes on for about 200 s and finally levels off. Together with growth, a focussing of the crystal size-distribution takes place, represented by the time course of the FWHM values (○).



**Figure 6: Emission spectra (colored lines) of different-sized CdSe nanocrystals grown in the non-coordinating solvent ODE.** The crystal samples were taken at different time-points during growth and exhibit five distinguishable colors. The corresponding absorbance spectrum of the sample exhibiting an emission maximum of 606 nm is represented by the circle-marked curve.

#### *CdSe-growth in coordinating solvents*

In order to compare the results obtained by the synthesis of CdSe QDs in non-coordinating solvents with the ones obtained in coordinating solvents, and then identify the most convenient synthesis method, the nanocrystal growth was conducted in a 1:1 mixture of TOPO and HDA.

In these experiments, the reaction conditions published in literature were converted [25,26], since the TOPO/HDA system is quite common. The resulting overview of the growth reaction is given in fig. 7. Under the chosen conditions, QDs emitting light in the green to orange range of the spectrum were obtained. These QDs are optimal for modification with PEG phospholipids (see chapter 4). Like the synthesis in ODE, here the growth which was initiated at 280 °C and maintained at approx. 250 °C quickly takes place after the nucleation. Further growth was stopped by quickly reducing the

temperature by injecting toluene. Moreover, addition of solvent prevented the TOPO/HDA mixture from solidification.

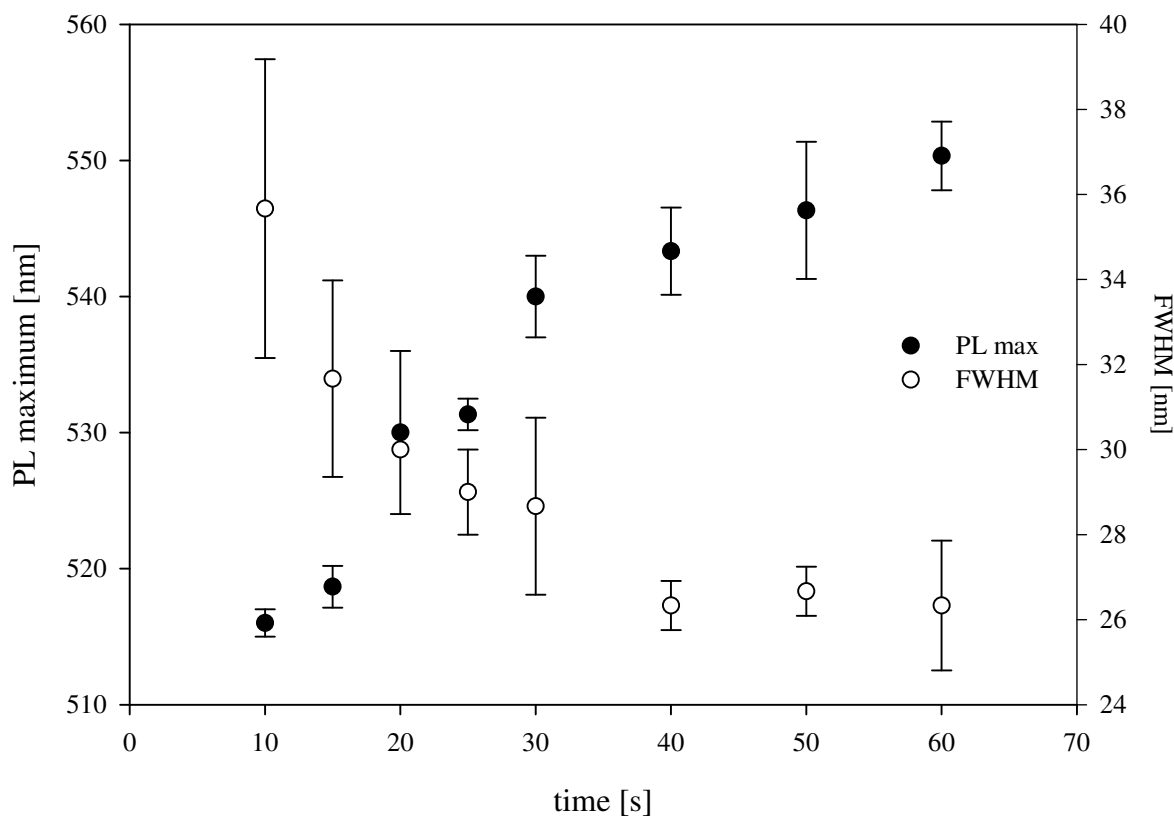


**Figure 7: Overview of the growth kinetics of the QDs obtained by synthesis in the coordinating solvents TOPO/HDA.** Growth was stopped after 60 seconds. Again, the size distributions are focusing during the reaction, yielding low FWHM values around 30nm.

Likewise, during crystal growth, the size distribution of the particle fractions, correlating with the FWHM, narrows. However, the final FWHM values were significantly lower than compared to the QDs obtained in OA, about 26 nm. The range of the fluorescent quantum yields was around 10-30 %. Their reproducibility was comparable to the synthesis in the non-coordinating solvent.

An overview of the emission and absorbance properties of the CdSe nanocrystals obtained in the coordinating solvent mixture is given in fig. 8. Here, the emission peaks exhibit a favorable, very sharp form.

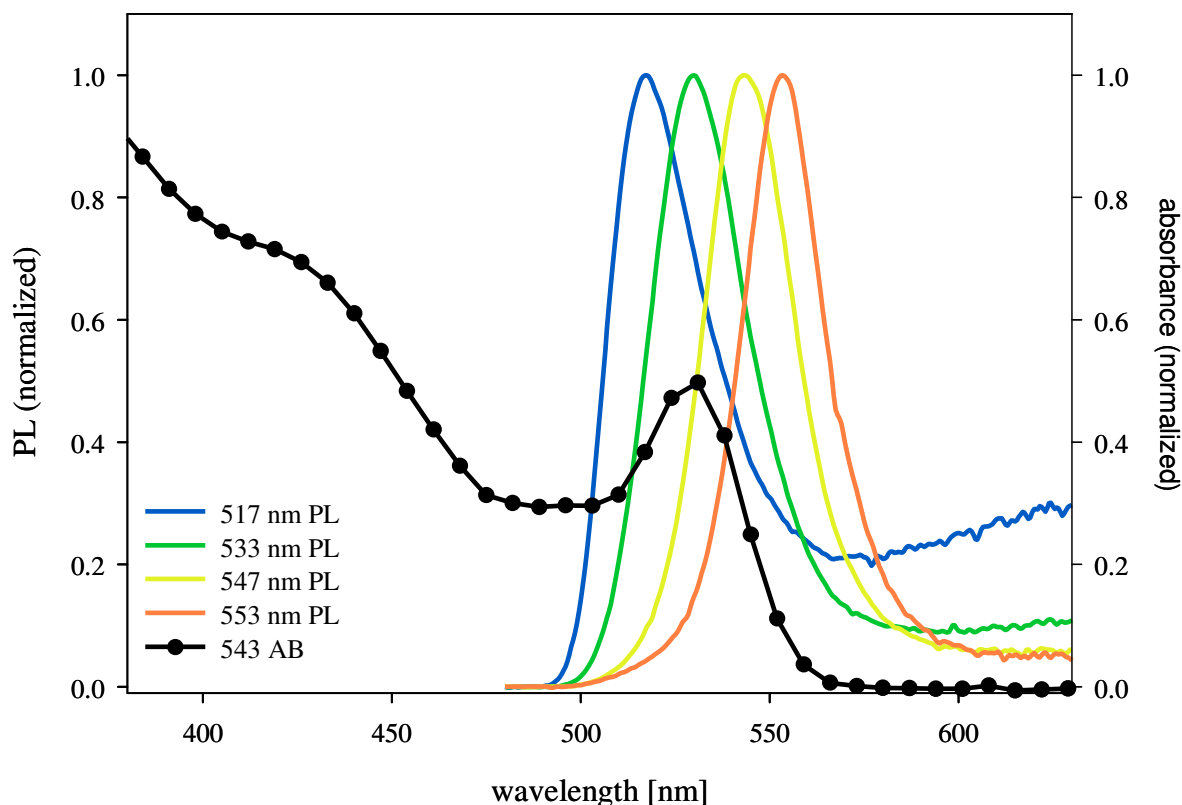


**Figure 8: Overview of the emission and absorbance properties of the CdSe nanocrystals obtained in the coordinating solvent mixture.** The emission peaks which show maxima between 517 and 553 nm exhibit a sharp appearance. The absorbance spectrum of the highest emitting QDs is represented by the optical circle-marked curve.

To sum up the synthesis of CdSe nanocrystals in non-coordinating and coordinating solvents, the latter exhibits several advantages. The size distribution of the particles is significantly lower and the reaction produces nanocrystals of higher quantum yields. In addition to this, the purification of the particles obtained in the non-coordinating solvent mixture was easier, since solvent residues could be easily removed by centrifugation as they are solids at room temperature.

#### *Coating of CdSe nanocrystals with ZnS*

Both species of CdSe nanocrystals were further coated with a ZnS shell in order to increase the quantum yields. Fig. 1A shows the scheme of the coating reaction after the synthesis of the CdSe QDs. Similar solvent mixtures to the growth of the CdSe cores were used while the ZnS precursors consisted of zinc stearate and trioctylphosphine sulfide (TOPS).

In an ideal case, a significant increase in the quantum yields as well as a red-shift of the emission maximum of the CdSe nanocrystals indicates a successful coating process [11]. Changes in the CdSe cores, like broadening of the size distribution, are undesired and have to be avoided, e.g. by adjusting the temperature. The growth temperature should allow for the growth of ZnS onto CdSe, but should avoid the formation of ZnS nanocrystals as well as changes in the core nanocrystals. Therefore, the optimum temperature as well as the growth reaction time for both kinds of solvents was investigated.

#### *ZnS shell-growth in non-coordinating solvent*

In fig. 9, the conditions investigated for the ZnS growth in the non-coordinating solvent ODE are compared. Temperatures from 100 to 200 °C over 30 and 60 minutes of reaction time were compared. For all conditions, no increase in the emission maximum was observed. Moreover, the FWHM values increased after the coating process, indicating that the CdSe cores were not stable under these conditions. Both facts suggest insufficient ZnS coating of the particles. However, for all coating reaction conditions, an increase of the quantum yields was registered.

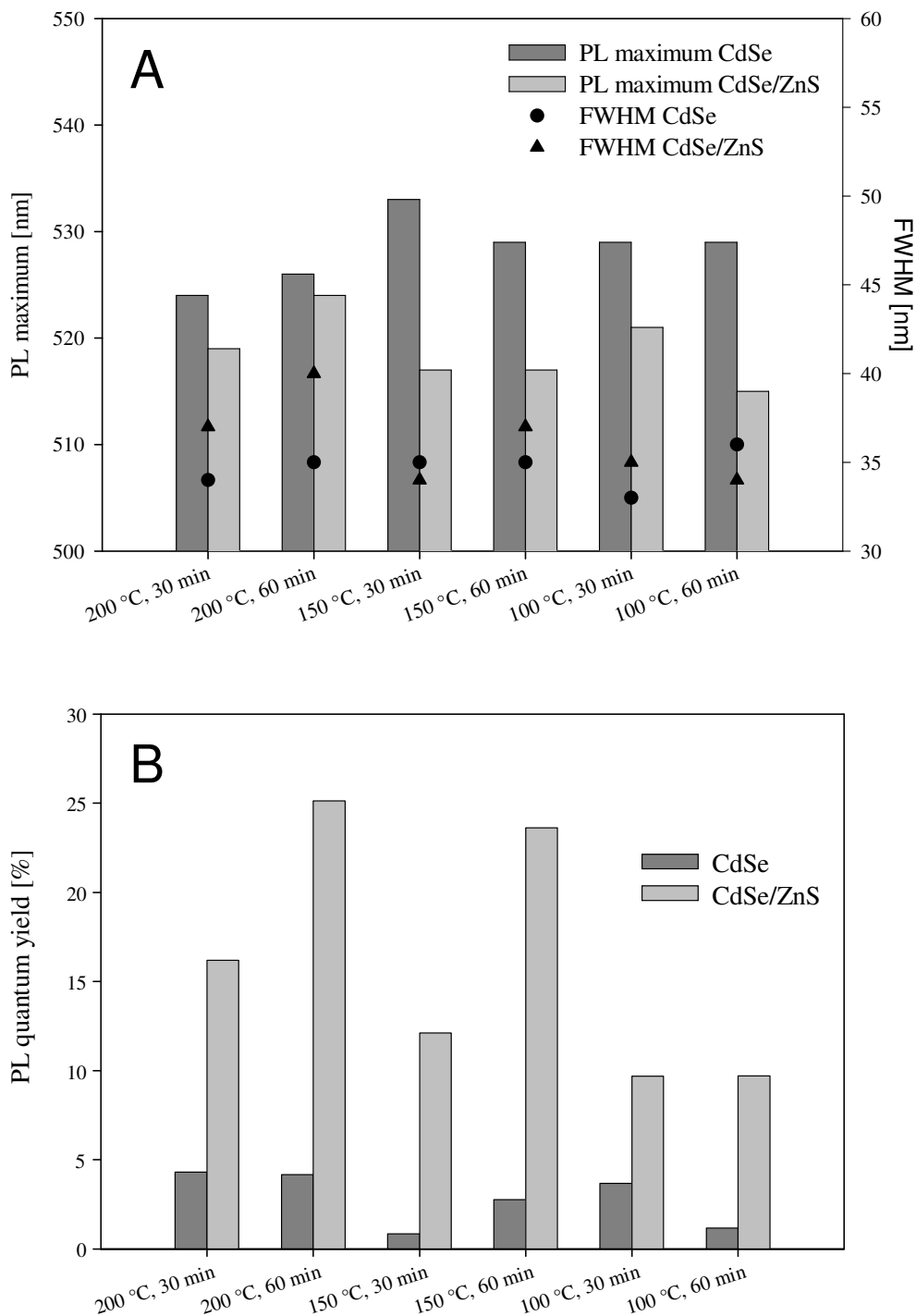


**Figure 9: Coating of CdSe nanocrystals with ZnS in the non-coordinating solvent ODE. (A)** Comparison of emission maxima and FWHM values before and after coating with ZnS for 30 and 60 minutes reaction time at temperatures between 100 and 200 °C. **(B)** The corresponding quantum yields obtained for CdSe/ZnS nanocrystals under these conditions show an increase compared to the CdSe nanocrystals.

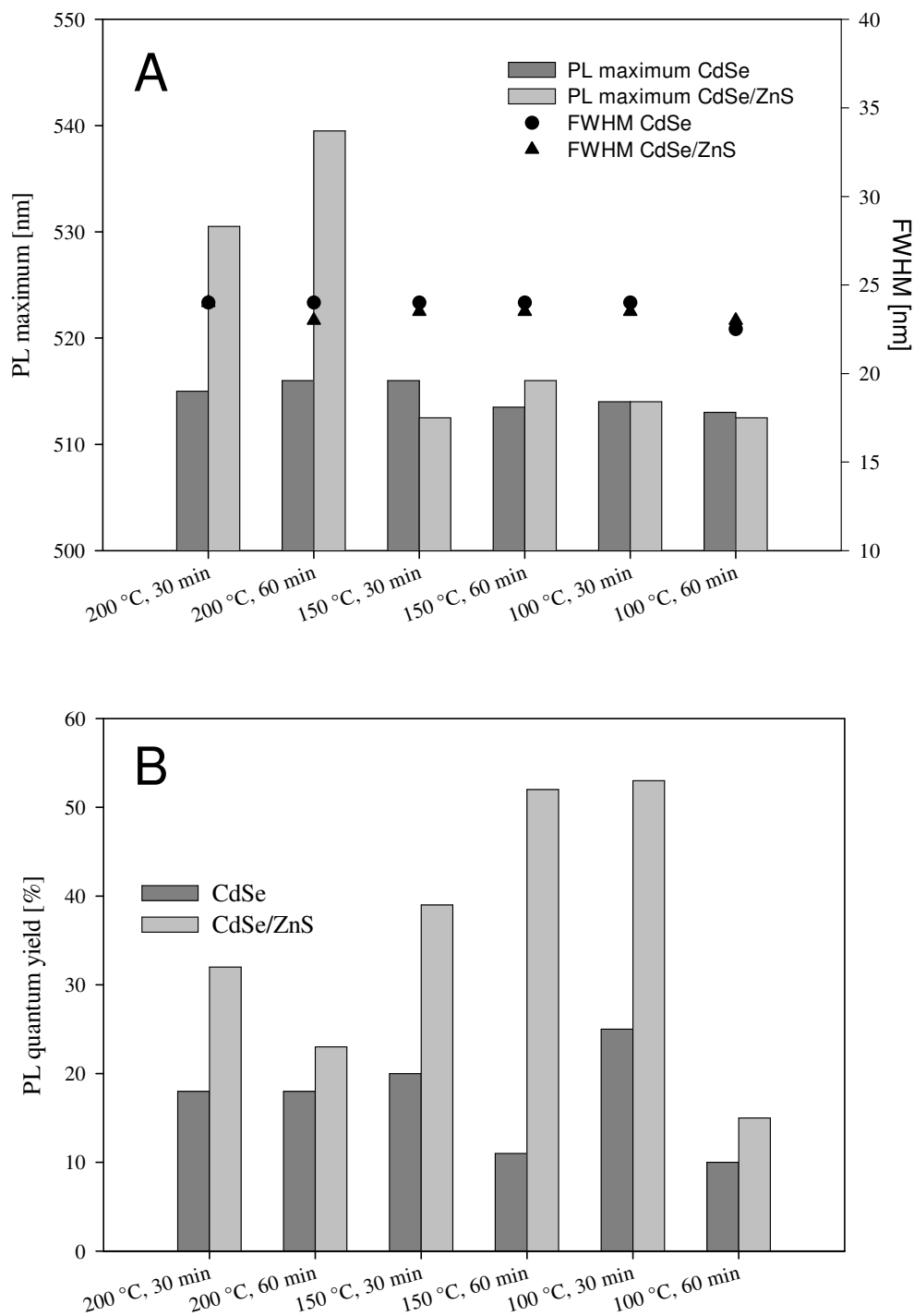


**Figure 10: Coating of CdSe nanocrystals with ZnS in the coordinating solvent mixture TOPO/HDA. (A)** A significant increase in the emission maxima of the nanocrystals was obtained for the reaction conducted at 200 °C while lower temperatures did not yield a red-shift of the emission maxima. **(B)** Under these conditions the FWHM values remain constant. For all reactions an increase in the quantum yields was observed.

*ZnS shell-growth in coordinating solvent*

In contrast, the ZnS coating under similar conditions using the coordinating solvent mixture was successful (fig. 10A). However, for the modification, only a reaction temperature of 200 °C yielded a significant red-shift of the emission maxima, indicating successful shell growth. Despite the high temperatures, the FWHM before and after coating remained nearly constant which shows the CdSe cores were not affected. The quantum yields increased after modification with ZnS under these conditions (fig. 10B). Since only in the coordinating solvent mixture a successful ZnS coating could be achieved, further investigations were carried out only using this solvent. To find out whether thicker ZnS shells can additionally improve optical properties, increasing amounts of ZnS precursors were reacted with the CdSe cores. In order to do this, the amount of ZnS was calculated based on the theoretical amount which is needed for one or more monolayers. As shown in fig. 11, the increasing amounts of ZnS yielded an increase in the absorbance and emission maxima as well as in an increase in the fluorescence quantum yields. The FWHM values were constant under these conditions. The results clearly show that shell growth needs more precursors and thus becomes more complete.

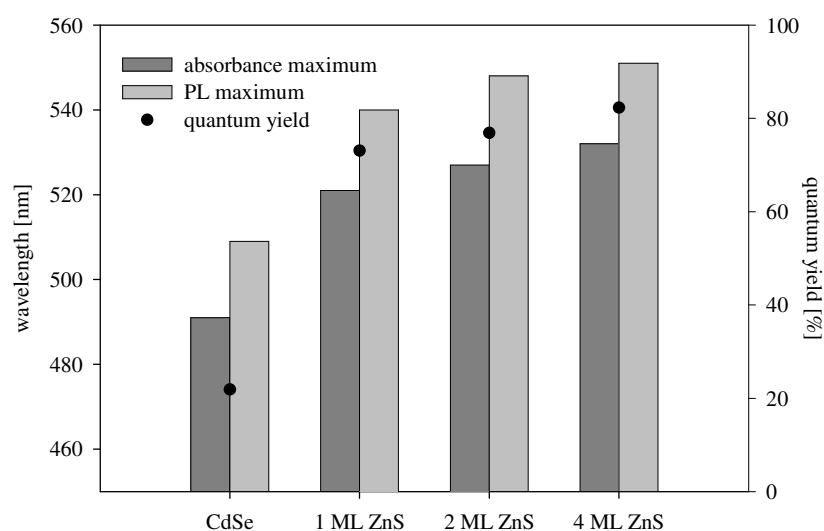


**Figure 11: Influence of the amount of ZnS-precursors on optical properties of CdSe nanocrystals.** The properties were investigated for unmodified CdSe and an increasing amount of ZnS, calculated for 1-4 theoretical monolayers. Photoluminescence (PL) and absorbance maxima increase as well as the quantum yields.



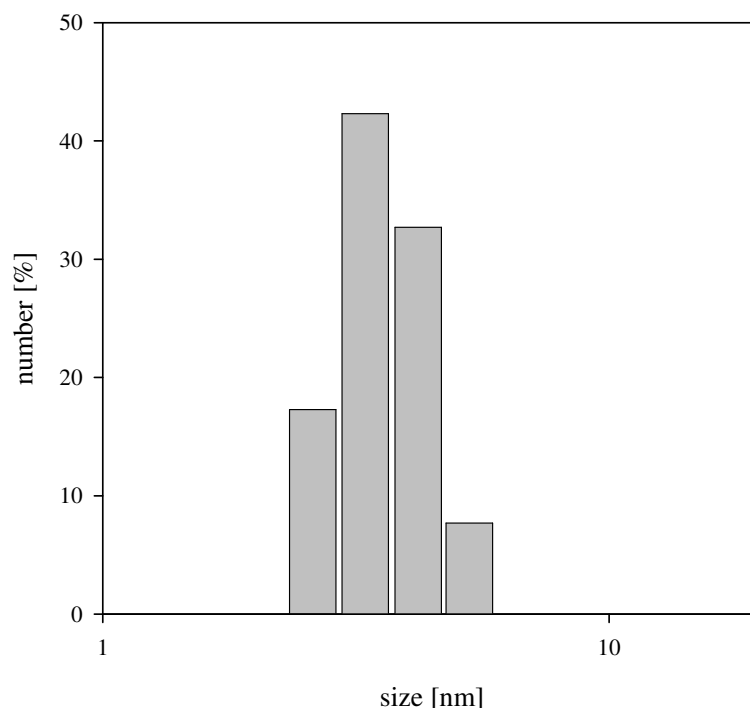


**Figure 10: Size distribution of the CdSe/ZnS nanocrystals optimized for growth in the coordinating solvent TOPO.** The small size (3.6nm) and narrow size-distribution ( $PI = 0.076$ ) render the crystals suitable for surface modifications such as embedding in polymeric micelles.

Finally, DLS measurements were conducted in order to determine the size of the obtained CdSe/ZnS QDs. Fig. 11 shows the size distribution of the CdSe/ZnS nanocrystals after repeated precipitation and redispersion in toluene. The particles exhibit a size of 3.6 nm and very low polydispersity (polydispersity index 0.076). This shows that even after the coating with ZnS, the crystal diameter remains low which is desirable for its incorporation in phospholipid micelles (see chapter 4). The low polydispersity shows that after precipitation, particulate impurities are effectively removed.

### Summary and conclusion

In order to establish a facile and reproducible method for the synthesis of CdSe/ZnS QDs, two commonly used synthesis routes were optimized and compared, one in the non-coordinating solvent ODE, and the other in the coordinating solvent mixture TOPO/HDA. Both methods led to CdSe nanocrystals emitting over a wide range of

the spectrum. However, for the preparation of high-quality CdSe/ZnS nanocrystals, the route using the coordinating solvent mixture proved to be more favorable. In this route, the particles exhibited narrower size-distributions and higher fluorescence quantum yields. The coating with ZnS also yielded significantly brighter QDs. By increasing the amount of ZnS, this effect could even be amplified. In summary, a convenient method for the preparation of CdSe/ZnS nanocrystals was established using the TOPO/HDA route and the CdO precursor.

---

**References**

- [1] P. Alivisatos, The use of nanocrystals in biological detection, *Nat. Biotechnol.*, 22 (2004) 47-52.
- [2] X. Michalet, F. F. Pinaud, L. A. Bentolila, J. M. Tsay, S. Doose, J. J. Li, G. Sundaresan, A. M. Wu, S. S. Gambhir, and S. Weiss, Quantum Dots for Live Cells, in Vivo Imaging, and Diagnostics, *Science*, 307 (2005) 538-544.
- [3] X. Gao, L. Yang, J. A. Petros, F. F. Marshall, J. W. Simons, and S. Nie, In vivo molecular and cellular imaging with quantum dots, *Curr. Opin. Biotechnol.*, 16 (2005) 63-72.
- [4] B. Dubertret, P. Skourides, D. J. Norris, V. Noireaux, A. H. Brivanlou, and A. Libchaber, In vivo imaging of quantum dots encapsulated in phospholipid micelles, *Science*, 298 (2002) 1759-1762.
- [5] I. L. Medintz, H. T. Uyeda, E. R. Goldman, and H. Mattoussi, Quantum dot bioconjugates for imaging, labelling and sensing, *Nat. Mater.*, 4 (2005) 435-446.
- [6] J. K. Jaiswal, H. Mattoussi, J. M. Mauro, and S. M. Simon, Long-term multiple color imaging of live cells using quantum dot bioconjugates, *Nat. Biotechnol.*, 21 (2003) 47-51.
- [7] S. S. Rajan, H. Y. Liu, and T. Q. Vu, Ligand-Bound Quantum Dot Probes for Studying the Molecular Scale Dynamics of Receptor Endocytic Trafficking in Live Cells, *ACS Nano*, 2 (2008) 1153-1166.
- [8] F. Pinaud, X. Michalet, L. A. Bentolila, J. M. Tsay, S. Doose, J. J. Li, G. Iyer, and S. Weiss, Advances in fluorescence imaging with quantum dot bio-probes, *Biomaterials*, 27 (2006) 1679-1687.
- [9] B. O. Dabbousi, J. Rodriguez-Viejo, F. V. Mikulec, J. R. Heine, H. Mattoussi, R. Ober, K. F. Jensen, and M. G. Bawendi, (CdSe)ZnS Core-Shell Quantum Dots: Synthesis and Optical and Structural Characterization of a Size Series of Highly Luminescent Materials, *J. Phys. Chem. B*, 101 (1997) 9463-9475.
- [10] A. R. Kortan, R. Hull, R. L. Opila, M. G. Bawendi, M. L. Steigerwald, P. J. Carroll, and L. E. Brus, Nucleation and growth of cadmium selenide on zinc sulfide quantum crystallite seeds, and vice versa, in inverse micelle media, *J. Am. Chem. Soc.*, 112 (1990) 1327-1332.
- [11] B. O. Dabbousi, J. Rodriguez-Viejo, F. V. Mikulec, J. R. Heine, H. Mattoussi, R. Ober, K. F. Jensen, and M. G. Bawendi, (CdSe)ZnS Core-Shell Quantum Dots: Synthesis and Characterization of a Size Series of Highly Luminescent Nanocrystallites, *The Journal of Physical Chemistry B*, 101 (1997) 9463-9475.
- [12] A. L. Rogach, A. Kornowski, M. Gao, A. Eychmueller, and H. Weller, Synthesis and Characterization of a Size Series of Extremely Small Thiol-Stabilized CdSe Nanocrystals, *J. Phys. Chem. B*, 103 (1999) 3065-3069.

- [13] F. Teng, A. w. Tang, Y. h. Gao, C. j. Liang, Z. Xu, and Y. s. Wang, Study of water-sol core-shell CdSe/CdS quantum dots, *Guangpuxue Yu Guangpu Fenxi*, 25 (2005) 651-654.
- [14] A. M. Smith, H. Duan, A. M. Mohs, and S. Nie, Bioconjugated quantum dots for in vivo molecular and cellular imaging, *Adv. Drug Delivery Rev.*, 60 (2008) 1226-1240.
- [15] M. L. Steigerwald and L. E. Brus, Semiconductor crystallites: a class of large molecules, *Acc. Chem. Res.*, 23 (1990) 183-188.
- [16] C. B. Murray, D. J. Norris, and M. G. Bawendi, Synthesis and characterization of nearly monodisperse CdE (E = sulfur, selenium, tellurium) semiconductor nanocrystallites, *J. Am. Chem. Soc.*, 115 (1993) 8706-8715.
- [17] M. A. Hines and P. Guyot-Sionnest, Synthesis and Characterization of Strongly Luminescing ZnS-Capped CdSe Nanocrystals, *J. Phys. Chem.*, 100 (1996) 468-471.
- [18] X. Peng, Green chemical approaches toward high-quality semiconductor nanocrystals, *Chemistry--A European Journal*, 8 (2002) 334-339.
- [19] D. V. Talapin, A. L. Rogach, A. Kornowski, M. Haase, and H. Weller, Highly Luminescent Monodisperse CdSe and CdSe/ZnS Nanocrystals Synthesized in a Hexadecylamine-Trioctylphosphine Oxide-Trioctylphosphine Mixture, *Nano Lett.*, 1 (2001) 207-211.
- [20] J. J. Li, Y. A. Wang, W. Guo, J. C. Keay, T. D. Mishima, M. B. Johnson, and X. Peng, Large-Scale Synthesis of Nearly Monodisperse CdSe/CdS Core/Shell Nanocrystals Using Air-Stable Reagents via Successive Ion Layer Adsorption and Reaction, *J. Am. Chem. Soc.*, 125 (2003) 12567-12575.
- [21] D. Yang, Q. Chen, and S. Xu, Synthesis of CdSe/CdS with a simple non-TOP-based route, *Journal of Luminescence*, 126 (2007) 853-858.
- [22] E. M. Boatman, G. C. Lisensky, and K. J. Nordell, A safer, easier, faster synthesis for CdSe quantum dot nanocrystals, *Journal of Chemical Education*, 82 (2005) 1697-1699.
- [23] W. W. Yu, L. Qu, W. Guo, and X. Peng, Experimental Determination of the Extinction Coefficient of CdTe, CdSe, and CdS Nanocrystals, *Chem. Mater.*, 15 (2003) 2854-2860.
- [24] X. Peng, J. Wickham, and A. P. Alivisatos, Kinetics of II-VI and III-V Colloidal Semiconductor Nanocrystal Growth: "Focusing" of Size Distributions, *J. Am. Chem. Soc.*, 120 (1998) 5343-5344.
- [25] D. Wang, J. He, N. Rosenzweig, and Z. Rosenzweig, Superparamagnetic Fe<sub>2</sub>O<sub>3</sub> Beads-CdSe/ZnS Quantum Dots Core-Shell Nanocomposite Particles for Cell Separation, *Nano Lett.*, 4 (2004) 409-413.

- [26] G. W. Huang, C. Y. Chen, K. C. Wu, M. O. Ahmed, and P. T. Chou, One-pot synthesis and characterization of high-quality CdSe/ZnX (X, Se) nanocrystals via the CdO precursor, *J. Cryst. Growth*, 265 (2004) 250-259.



# Chapter 4

## **Solubilization and Characterization of Quantum Dots for Biological Applications**

W. Hild, J. Teßmar, A. Göpferich

Department of Pharmaceutical Technology, University of Regensburg,  
Universitätsstraße 31, 93040 Regensburg, Germany

**Abstract**

With the introduction of quantum dots (QDs) in modern bioanalytics and biosensorics, a quantum leap with regard to sensitivity and traceability was taken. Meanwhile, the protocols for the synthesis of such nanocrystals have become highly developed. The vast majority of these protocols have their organic synthesis medium in common. Consequently, the as-prepared QDs are extremely hydrophobic. Therefore, powerful methods for the solubilization of QDs in aqueous media are needed. With respect to the various applications, an appropriate surface coating must keep the particles as small as possible, and must also prevent aggregation and provide defined sites for chemical modifications, such as the attachment of biomolecules. In this study, different strategies for the surface modification of QDs were compared. Exchange of the surface bound hydrophobic stabilizing ligands by mercaptoundecanoic acid was compared with a more complex approach using phosphine oxide-modified poly(ethylene glycol) (PEG). Finally, the coating of QDs by PEGylated phospholipids was investigated in detail, concentrating on the fabrication, low polydispersity and functionalization with reactive groups. Taking into account all the investigated methods, the last one is the most favorable concerning the optical as well as the colloidal properties of the solubilized QDs.



## Introduction

Quantum dots (QDs), small semiconductor nanocrystals (2-10 nm), exhibit outstanding optical properties which have rendered them extremely attractive labels in biological applications [1-4]. In contrast to conventional organic fluorescent dyes, QDs do not suffer from photobleaching [5] and exhibit a very sharp emission range, which can be tuned precisely by adjusting the particle size during synthesis. Moreover, QDs have been used in numerous studies as templates for small nanoparticles and could be traced easily. Therefore, over the past decade, routes for the synthesis of high-quality QDs with optimized optical properties have been elaborated and further enhanced. Thus, QDs have been prepared in organic solvents, like trialkylphosphine oxide and aliphatic amines [6] or alkylphosphonic acids [7]. These solvents not only provide a reaction medium for the growth of the nanocrystals, but they also coordinate with the metal atoms on the surface of the QDs to prevent excessive growth of the nanocrystals which would yield larger crystals -bulk semiconductors- lacking the optical properties of QDs. As a consequence, the QD surfaces are capped with hydrophobic ligands after synthesis and the particles cannot be dispersed in aqueous media. However, biological studies, such as cell culture experiments [8,9] or *in vivo* investigations [10,11], are usually conducted in aqueous environments. Therefore, the surfaces of the QDs have to be modified in order to render them hydrophilic and to be able to make use of the particles and their unique optical properties in biological studies. Several studies show that the properties of the nanoparticle surface significantly influence the reaction of the biological system towards the particles, such as non-specific binding [12] and cell-uptake [13].

In order to gain control over these processes, a first step is to modify the particle surface with coatings that reduce adsorption to proteins and cells. One solution is the introduction of poly(ethylene glycol) (PEG) on the particle surface. This surface modification proved to be a powerful tool for stabilization and could even prolong the circulation half-life of QDs in mice [14]. The interactions of the particles with the target cells or the organism can then be influenced by attaching bioactive substances to the QDs, like peptides [15], proteins [1] or antibodies [16]. To enable this bioconjugation, the surface coating of the QDs has to carry functional groups. From

all reactive groups, amine groups are preferable in most of the studies since they are versatile and stable by forming covalent amide bonds with carboxylic acids.

In this study, three different methods for the surface modification of QDs were investigated. The first two approaches are based on a ligand-exchange strategy where the hydrophobic surface-bound stabilizing ligands were exchanged with more hydrophilic ones. In this scenario, the exchange with mercaptoundecanoic acid (MUA) was compared to ligand-exchange with a custom-synthesized phosphine oxide-modified PEG. In a second approach, the hydrophobic QDs were surface-coated with amphiphilic PEGylated phospholipids. The last method was explored in depth in order to check whether it fulfils the above requirements regarding a coating of QDs that can be used in biological studies.

### **Materials and methods**

1,2-bis(dichlorophosphino)ethane, cadmium oxide (CdO, 99.5%), *N,N'*-dicyclohexylcarbodiimide (DCC, 99%), DL-lysine (98%), hexadecylamine (HDA, tech. grade 90%), lauric acid (98%), methanol (anhydr. 99.8%), sulfur (99.5%), poly(ethylene glycol) (PEG, MW 600 Da), toluene (anhydr. 99.8%), trioctylphosphine (TOP, tech. grade 90%), trioctylphosphine oxide (TOPO, tech. grade 90%) and zinc stearate (tech. grade) were obtained from Sigma-Aldrich (St. Louis, MO). 1,2-distearoyl-sn-glycero-3-phosphatidylethanolamine covalently linked to methoxy-PEG (PEG-PE) and linked to amino-PEG (amino-PEG-PE), both PEGs having an average molecular weight of 2000 Da, were obtained from Lipoid (Ludwigshafen, Germany) and from Avanti Polar Lipids (Alabaster, AL), respectively.

#### *Synthesis of CdSe/ZnS nanocrystals*

CdSe/ZnS QDs were synthesized by thermal decomposition of the corresponding precursors as described in chapter 3. In brief, CdO (0.2 mmol) was dissolved in lauric acid (1.6 mmol) at 200 °C. TOPO (10 mmol, 3.88 mg) and HDA (16 mmol, 3.88 mg) were added and the mixture was heated to 285 °C. After removing the heating bath, Se (2 mmol) dissolved in 3.5 ml of TOP was injected. At the desired nanocrystal size (5-30 sec of crystal growth), the growth was stopped by injection of 20 ml of toluene. The CdSe cores were precipitated with an equal volume of methanol and centrifuged at 6000 x g for 5 min and redispersed as described above. ZnS-coating was

conducted after dispersing the CdSe cores in the same amount of TOPO and HDA as for the core synthesis at 200 °C over 60 min. The amounts for the ZnS precursor were calculated for four theoretical monolayers per QD. After shell-growth, the nanocrystals were purified by precipitation as described above and redissolved in toluene.

#### *Synthesis of phosphine oxide modified PEG (PO-PEG)*

Phosphine oxide modified poly(ethylene glycol) (PO-PEG) was synthesized according to the method published by Kim *et al.* [17]. Therefore, PEG of an average molecular weight of 600 Da (12.9 mmol) was dried under heat and vacuum, rinsed with Ar and transferred into a glovebox. The polymer was dissolved in 20 ml of DMF. To this solution, 1,2-Bis(dichlorophosphino)ethane (4.3 mmol) was added dropwise over 1 h. After stirring over a period of 1 d, the solution was neutralized with approx. 3 g of K<sub>2</sub>CO<sub>3</sub> and stirred for 2 d. After this, the salts were removed by filtration and the polymer was precipitated in cold ether and finally redissolved in dichloromethane. The precipitation was repeated twice. The polymer was analyzed in CDCl<sub>3</sub> by <sup>1</sup>H-NMR using an Avance 300 NMR spectrometer (Bruker BioSpin, Rheinstetten, Germany).

#### *Hydrophilization of QDs with mercaptoundecanoic acid*

Ligand-exchange by mercaptoundecanoic acid (MUA) and subsequent cross-linking by lysine was conducted as described by Jiang *et al.* [18]. In brief, 1 g of MUA was molten at 65 °C under Ar-atmosphere and 0.33 μmol of QDs dissolved in chloroform were added. After 2h of stirring at 80 °C, 25 ml of DMSO was added and the solution was stirred for another 2h. The QDs were precipitated by addition of 80 ml of chloroform, isolated by centrifugation at 600 x g for 5 min and redissolved in DMSO (MUA-QDs). For cross-linking, lysine (9.6 mmol) was dissolved in 10 ml of 10 mM PBS and DCC (48 mmol) was dissolved in 25 ml of DMSO. Both solutions were added to the MUA-QDs and the mixture was stirred for 2h. The precipitated LM-QDs were then isolated by centrifugation, washed with THF and redissolved in water. The LM-QDs were subsequently purified by dialysis using a 5000 MWCO membrane.

*Hydrophilization of QDs with PO-PEG*

600 mg of the PO-PEG and 0.04  $\mu\text{mol}$  of CdSe/ZnS QDs were dissolved in 2 ml of chloroform and stirred overnight under reflux. After removing the solvent under reduced pressure, the particles were dissolved in 2 ml of water and ultrasonicated for 5 min. After this, the colloid was centrifuged and the supernatant was filtered using a 0.22 mm pore-size syringe filter.

*Hydrophilization of QDs with PEG-PE*

0.1  $\mu\text{mol}$  of QDs in toluene were precipitated with the same amount of methanol and isolated by centrifugation at 6000 x g for 5 min. The pellet was dissolved in 500  $\mu\text{l}$  of DCM and transferred into a 10 ml flask. 2.5  $\mu\text{mol}$  of PEG-PE was dissolved in 500  $\mu\text{l}$  dichloromethane and added to the QD-solution. The solvent was removed under reduced pressure to form a QD-PEG-PE film. After removing solvent residues under vacuum overnight, the film was heated to 80  $^{\circ}\text{C}$  in a water bath and water of the same temperature was added. The samples were vortexed for 30 sec and cooled to room temperature. Thereafter, non-coated QDs were removed by centrifugation at 16000 x g and the pellet was removed. To remove excess PEG-PE, the samples were purified by ultracentrifugation at 47000 x g for 2 h. The supernatant was discarded, the QDs were redissolved in water and the purification was repeated twice. Samples were stored at 4  $^{\circ}\text{C}$ .

*Spectrophotometric measurements*

UV absorbance spectra were recorded using an Uvikon 941 (Kontron Instruments, UK) and 10 cm quartz cuvettes. Fluorescence was determined in 10 cm quartz cuvettes using a RF-1501 spectrometer (Shimadzu Deutschland GmbH, Duisburg, Germany) for the spectra of the MUA-QDs and the PO-PEG-QDs. For all other fluorescence measurements (including all determinations of quantum yields), an LS 55 fluorescence spectrometer from PerkinElmer (Waltham, MA) was used. Fluorescence quantum yields were determined in correlation to a fluorescein standard in 0.1 N NaOH (quantum yield 90%). Samples were excited at 450 nm. Fluorescence decay was determined using a Fluorolog F112A fluorimeter (Horiba

Jobin Yvon, Bensheim, Germany), with excitation at 375 nm and emission at 540 nm at 25 °C.

#### *Dynamic light scattering*

The hydrodynamic diameter of the PEG-PE-QDs was determined by dynamic light scattering (DLS) using a ZetaSizer 3000 HSA (Malvern, Worcestershire, UK) at 20 °C and an angle of 90° in toluene or water. Therefore, samples were purified by centrifugation at 16000 x g for 15 min and subsequently syringe-filtered (0.22 µm pore diameter). Data was processed using the CONTIN algorithm [19].

#### *Cryo-transmission electron microscopy (cryo-TEM)*

For imaging of the QDs using cryo-TEM, a few microlitres of the dilute aqueous samples were transferred onto a 600 mesh copper grid (Plano, Wetzlar, Germany) and spare sample was removed by suction. Thereafter, the samples were immediately frozen by submerging them in liquid ethane in a cryo-box. After mounting the sample on a cryo-transfer holder (CT 3500, Gatan, Munich), images were obtained by a Zeiss EM 922 EFTEM (ZeissNTS, Oberkochen, Germany) at 200 kV and a temperature of 90 K.

#### *Determination of amines*

Before the determination of the amines per QD, different ratios of amino-PEG-PE to unreactive PEG-PE were used for the hydrophilization of the QDs (0%/25%/50%/100%). After hydrophilization and purification as described above, the concentration of the QDs was determined using a plate reader (Shimadzu, Duisburg, Germany) and the absorbance maximum at 518 nm and the common approximation for the absorbance coefficient [20]. The same batch of QDs was used for all experiments. To determine the number of amines per QD, 5 µl of the PEG-PE QDs were transferred into a 96 well-plate, 135 µl of borate buffer (50 mM, pH 8.5) and 60 µl of a 1 mM solution of fluorescamine in acetone were added. Immediately after the addition of fluorescamine, fluorescence was measured by a LS 55 fluorescence spectrometer from PerkinElmer (Waltham, MA) equipped with a plate reader unit (excitation at 390 nm, emission at 475 nm). Amino-PEG-PE was the calibration standard. In order to reduce the inner-filter effect of the QDs towards the

fluorescence of the amine-activated fluorescamine, QDs were kept at low optical densities below 0.1, according to literature [21].

#### *Determination of hydrophilization capacity*

Different-sized QD-samples were hydrophilized with PEG-PE and purified as described above using the same amounts of PEG-PE and QDs for each batch. After preparation, non-coated QDs were removed by centrifugation at 16000 x g for 10 min. The diameter of the QDs before coating with PEG-PE was determined using the correlation between the highest maximum of the absorbance spectrum and the size of the nanocrystals as published by Yu *et al.* [20]. The concentration after the hydrophilization procedure was calculated using the common approximation of the absorbance coefficient and the optical density of the sample [20].

### **Results and discussion**

In this investigation, three different strategies for the surface modification of QDs were compared to each other in order to find out the most appropriate one to be used for subsequent biological investigations. While the first method represents a simple exchange of the surface-bound stabilizing ligands of the organic-soluble QDs by MUA, in a second approach, PEG is used to replace these ligands and to bind to the QDs (fig. 1).

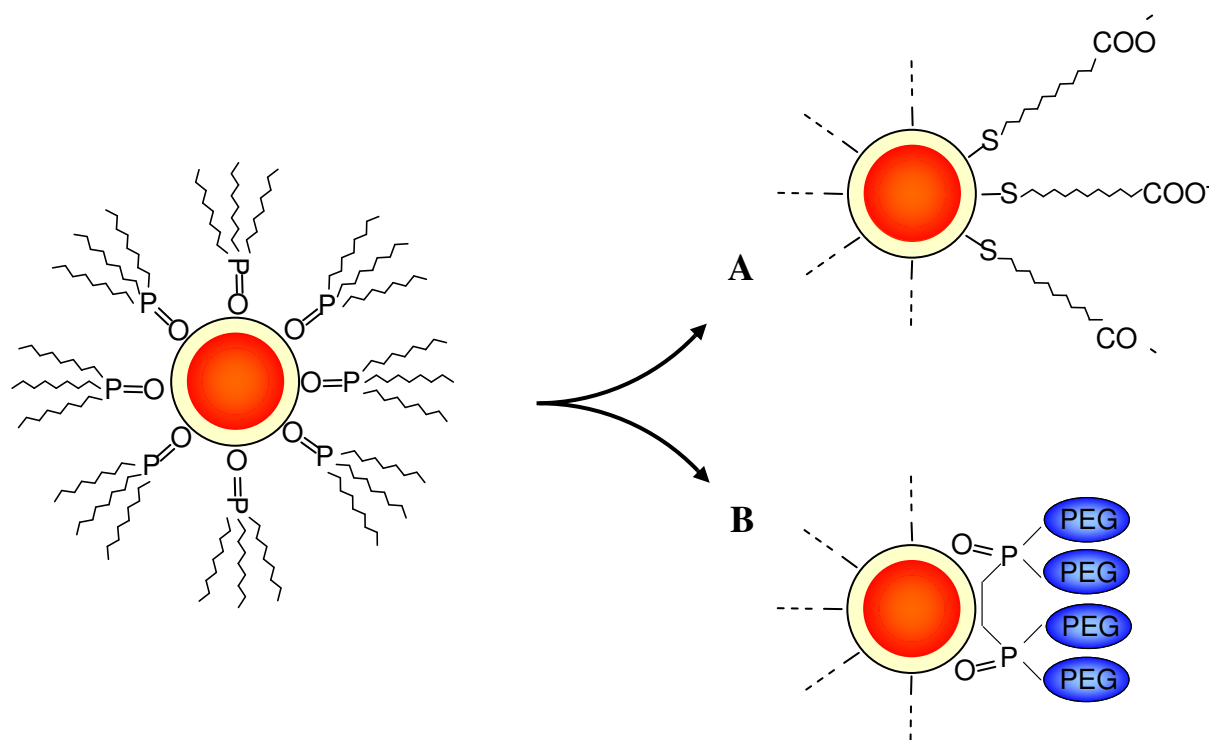


**Figure 1: Hydrophilization of organic-soluble QDs by ligand exchange.** The organic-soluble QDs are coated with a hydrophobic monolayer of stabilizing ligands (here shown for TOPO). For hydrophilization, the ligands are removed either by MUA or by PO-PEG.

The exchange of the surface bound stabilizing ligands by the small molecule MUA was easy to conduct (fig. 1A). The particles obtained were dispersible in water and showed hardly any change in their absorbance behavior (fig. 2).

As shown in fig. 3, the QDs exhibit small hydrodynamic radii (approx. 4 nm) after coating with MUA. However, due to photooxidation of the thiols and aggregation [22], the size distribution broadened. Therefore, the coating was stabilized by cross-linking with lysine. The obtained particles (CL-MUA-QDs) are slightly larger due to an increasing coating layer. However, a lack of colloidal stability is visible as the DLS measurements show an increase in the mean diameter even after the cross-linking procedure and purification by dialysis, together with an increasing polydispersity index (fig. 3). This aggregation can also be attributed to the lack of a PEG-layer on the particle surfaces which efficiently serves as a steric stabilizer. A second drawback is the drastic loss of quantum efficiency after changing the surface

environment of the particles by the ligand exchange. The quantum yields for the obtained particles were far below 1%.

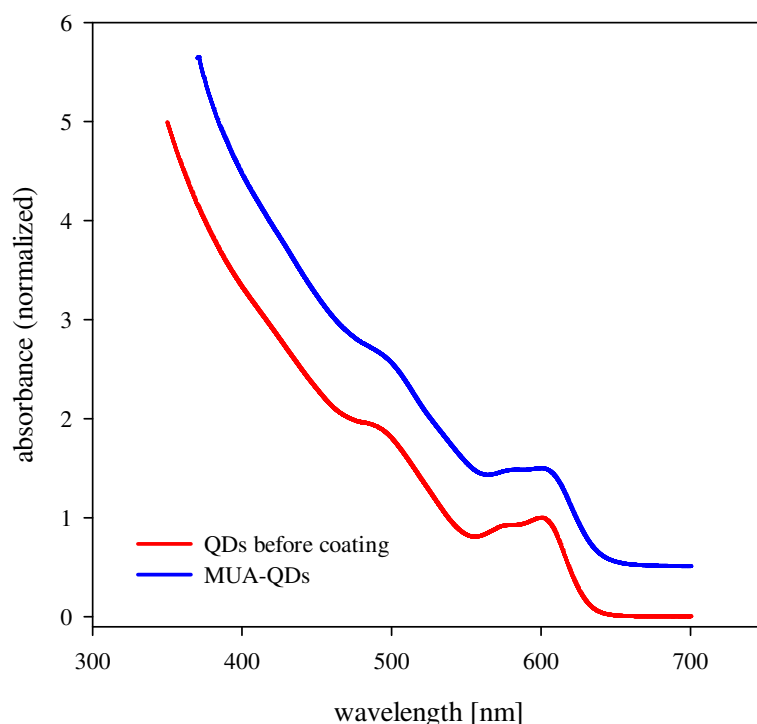


**Figure 2: Absorbance spectra before and after coating with MUA.** Both curves show similar characteristics in organic and in aqueous media which proves the successful transfer from the organic to aqueous phase.

In order to overcome the lack of stability, a strategy for introducing PEG on the particle surface had to be developed. Since the processes on the particle surface always represent equilibria between association and dissociation of surface-bound stabilizing ligands, multidentate PEG-ligands were developed to increase the affinity of the ligands to the particle surface [17,23].

It was investigated whether multidentate phosphine oxide modified PEGs could sufficiently maintain the optical properties of the QDs and moreover prevent aggregation. Since the phosphine oxide groups of this polymer are similar to those of TOPO, a stabilizing ligand for the synthesis of the QDs, it was expected to be able to replace these ligands and thus introduce PEG on the surface of the QDs (fig. 1B).



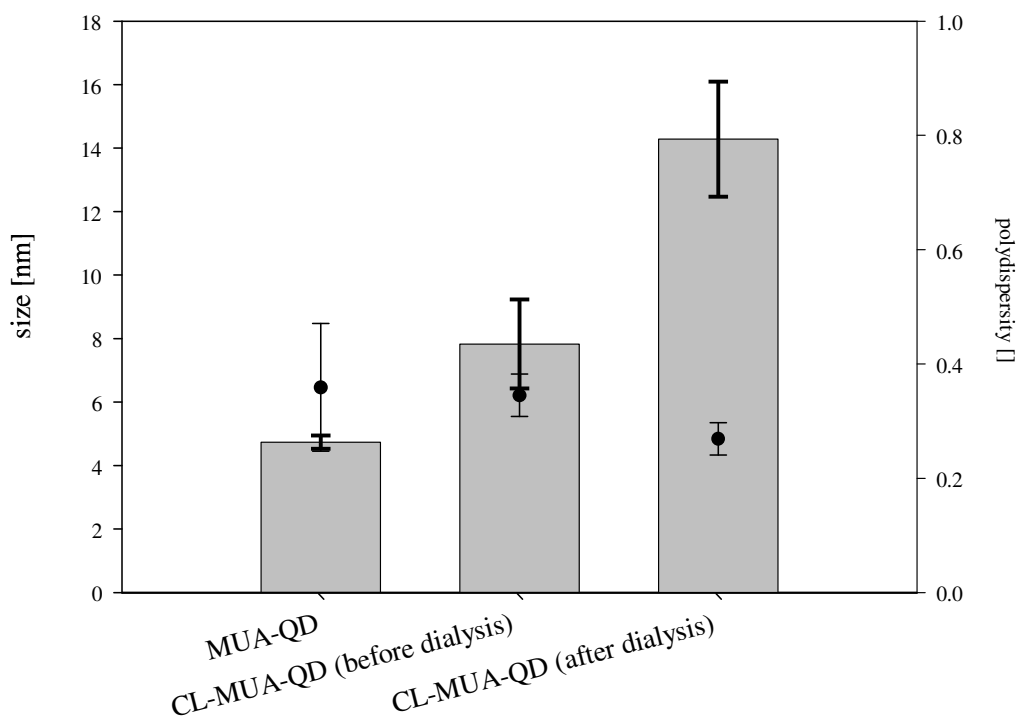


**Figure 3: Size analysis of MUA-QDs and MUA-QDs crosslinked with lysine.** After surface-modification, the MUA-QDs exhibit small sizes (bars) of approx. 4 nm and increased polydispersity (•). Crosslinked with lysine (CL-MUA-QD), the diameter increases up to 14 nm (after 1 day of dialysis).

As described by Kim *et al.*, the reaction between PEG and the chlorides of the phosphinic acid derivatives yields covalent networks (fig. 4). PEG (B) is reacted with 1,2-bis(dichlorophosphino)ethane (A) under water-free conditions to form random networks of esters of PEG and the phosphonous acid derivative (C) which are subsequently oxidized to the phosphonic acid derivative resulting in PO-PEG (D). The success of the reaction was examined using  $^1\text{H}$  NMR (fig. 5). The spectrum is characterized by the signal of the protons of the PEG methylene groups at -3.6 ppm and the multiplet of the terminal methylene groups at -4.2 ppm which couple with the phosphine oxide groups.

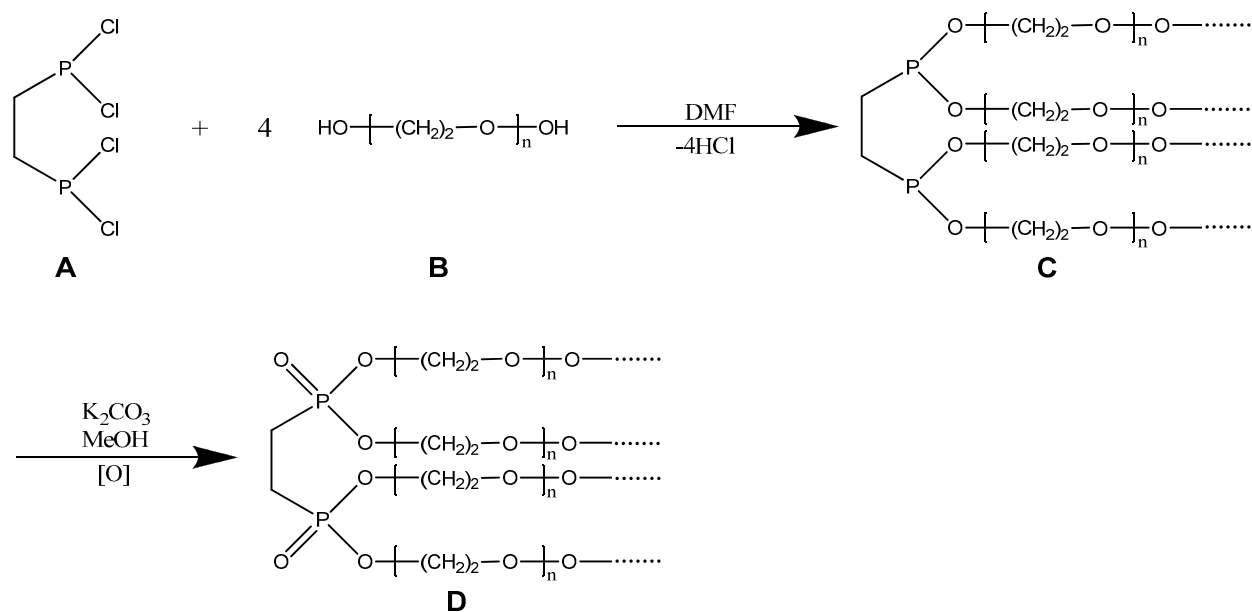


**Figure 4: Synthesis scheme for the modification of PEG with phosphine oxide groups.** PEG (B) is esterified with 1,2-bis(dichlorophosphino)ethane (A) forming covalent random-networks (C) which are subsequently oxidized to PO-PEG (D).

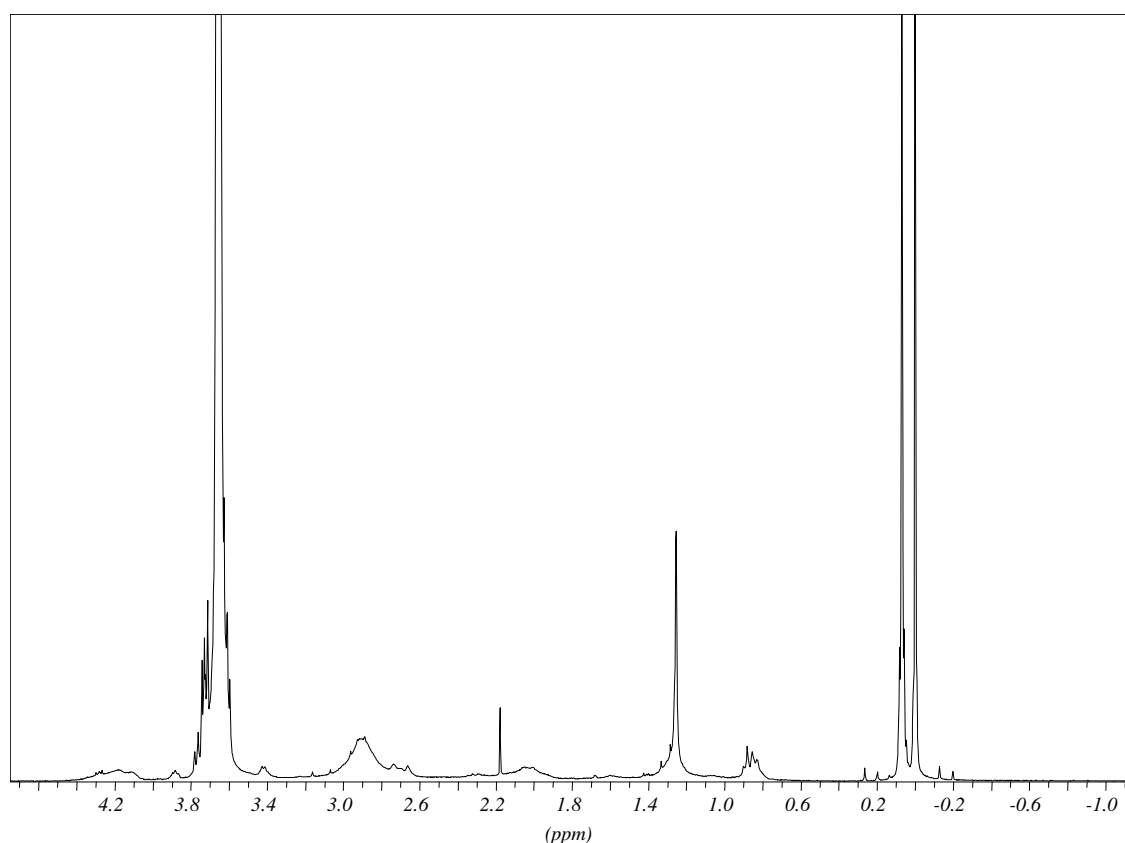


**Figure 5: <sup>1</sup>H NMR of PO-PEG.** The methylene groups at -3.6 ppm refer to the PEG. The multiplet at -4.2 ppm represents the outer methylene groups which are chemically shifted into the deep field due to its proximity to the phosphine oxide groups.

The polymer is able to bind to the QDs and to render the initially organic soluble nanocrystals water soluble. Thus, the quality of the optical properties of the QDs remains unchanged. As depicted in fig. 6, the appearance of both the absorbance and the emission spectra of the unmodified QDs in chloroform as well as after modification with PO-PEG in aqueous the medium, is very similar. The successful transfer into aqueous medium as well as the retention of the optical properties shows the effective coupling of the modified PEG to the QDs. Due to PEG, the polymer modified QDs reveal good colloidal stability in the aqueous medium.

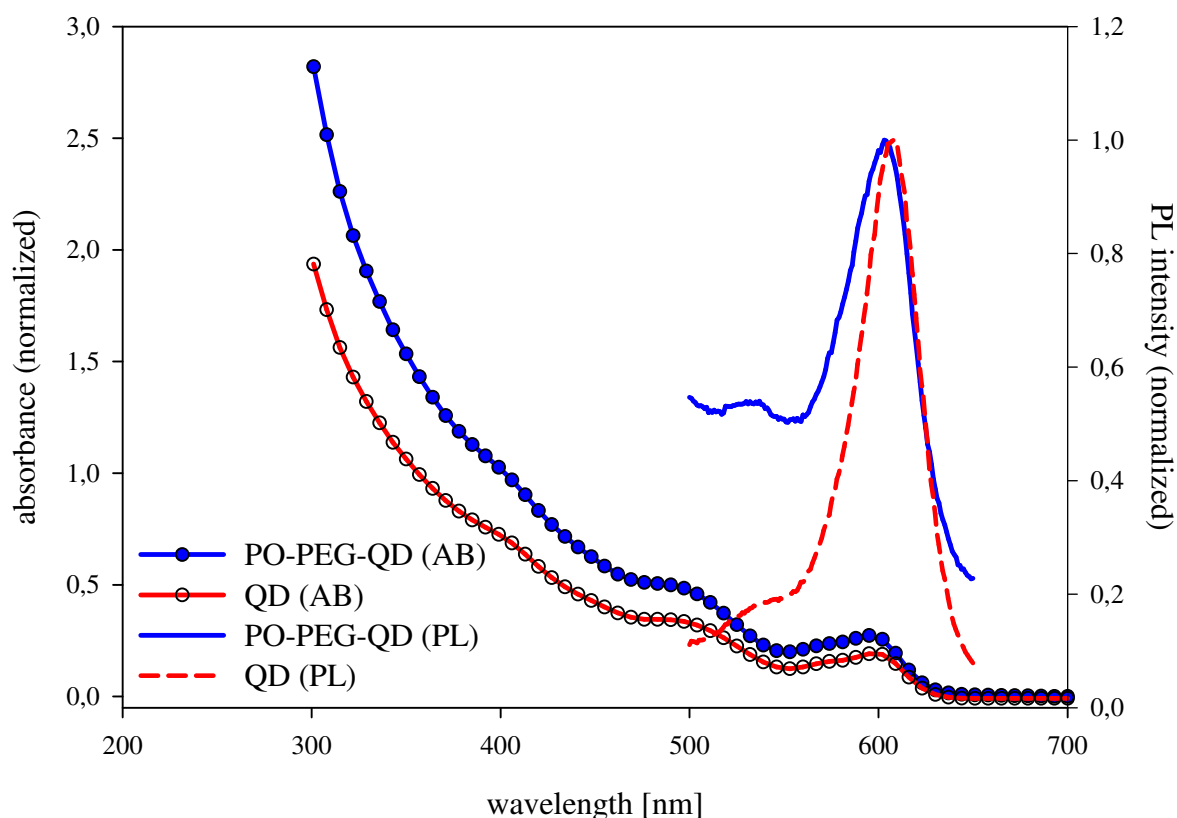


**Figure 6: Absorbance and emission spectrum of QDs before and after solubilization with PO-PEG.** The absorbance spectra (marked with circles) before (red) and after (blue) transfer of the QDs into the aqueous medium using the PO-PEG are nearly unchanged. The position of the emission peak in the aqueous medium also shows almost no difference compared to the organic soluble QDs.

Fig. 7 shows the size distribution of the PO-PEG-QDs determined by DLS. Whereas the free modified PEG forms loose networks of high sizes and broad size-

distributions, the system becomes more ordered when bound to the QDs. As a consequence, the hydrodynamic diameter of the PEGylated particles as well as the polydispersity index decreases after modification with the QDs, an effect which is also described in literature [17]. The colloid is well-stabilized by the polymer; no sign of aggregation was visible for the aqueous colloid after two years of storage at room temperature.

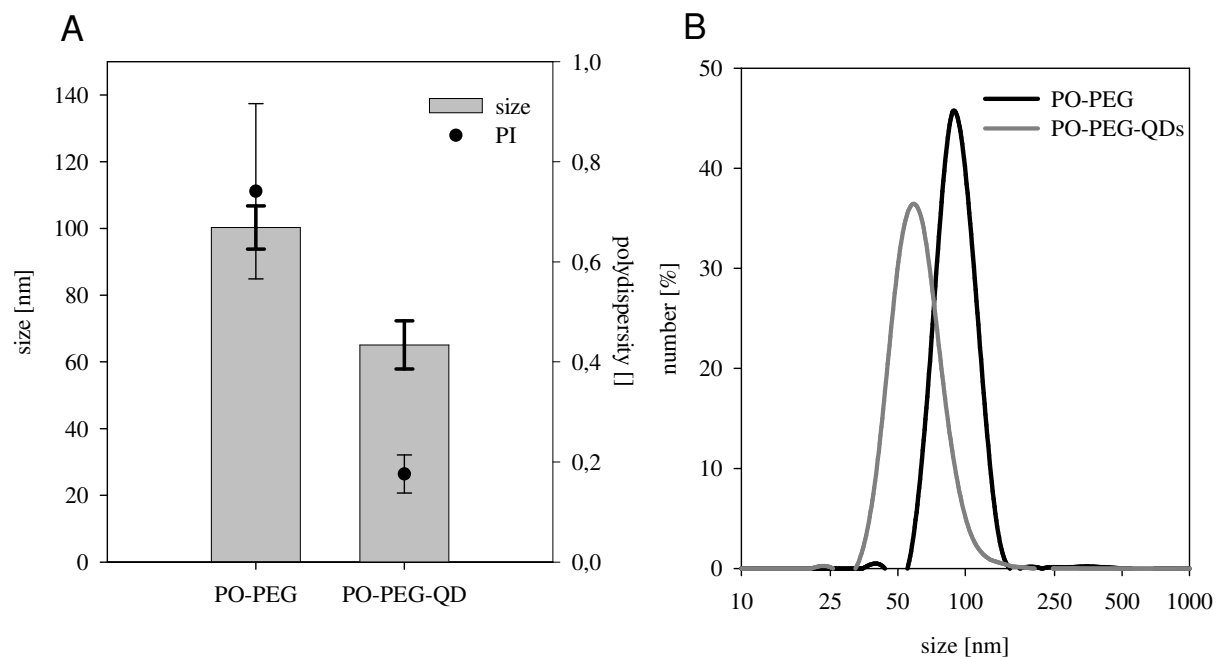


**Figure 7: Size analysis and distribution of PO-PEG-modified water soluble QDs and of the pure polymer obtained by DLS. (A)** The loose and disordered polymer network (PO-PEG) shows higher sizes and higher polydispersity than when bound to the QDs (PO-PEG-QDs) (left panel). The PEGylated particles exhibit a size of approx. 60 nm and a polydispersity index below 0.2. **(B)** Size distribution of both species.

Though the modification of the QDs with PEG using the PO-PEG polymer yields quite stable and water soluble particles, there were still some drawbacks. Firstly, the optical properties again were too low for the use of the QDs in biological applications (below 1%). Moreover, the phosphine oxide modified PEG increases the hydrodynamic diameter of the particles drastically (over 50 nm) which might be a disadvantage when investigating size-dependent uptake processes in cells [24].

Finally, the PEG-networks created exhibit no defined site for the chemical attachment of biologically active compounds, like peptides, proteins or antibodies.

To meet these requirements, an approach was chosen that was not based on exchanging the stabilizing surface ligands. By leveraging van-der-Waals interactions, it is possible to build a coating of amphiphilic molecules around the QDs that show aliphatic chains on their surface. In this context, PEGylated phosphatidylethanolamines (PEG-PE) prove to be favorable [10]. The coating of QDs with PEG-PE was achieved in two simple steps (fig. 8). After forming a film consisting of QDs and PEG-PE, it was then hydrated by warm water. During this procedure, the polymer arranges itself spontaneously around the QDs. Since excess PEG-PE is used, PEG-PE micelles form as well. To remove empty PEG-PE micelles, the PEG-PE-QDs were purified by ultracentrifugation.

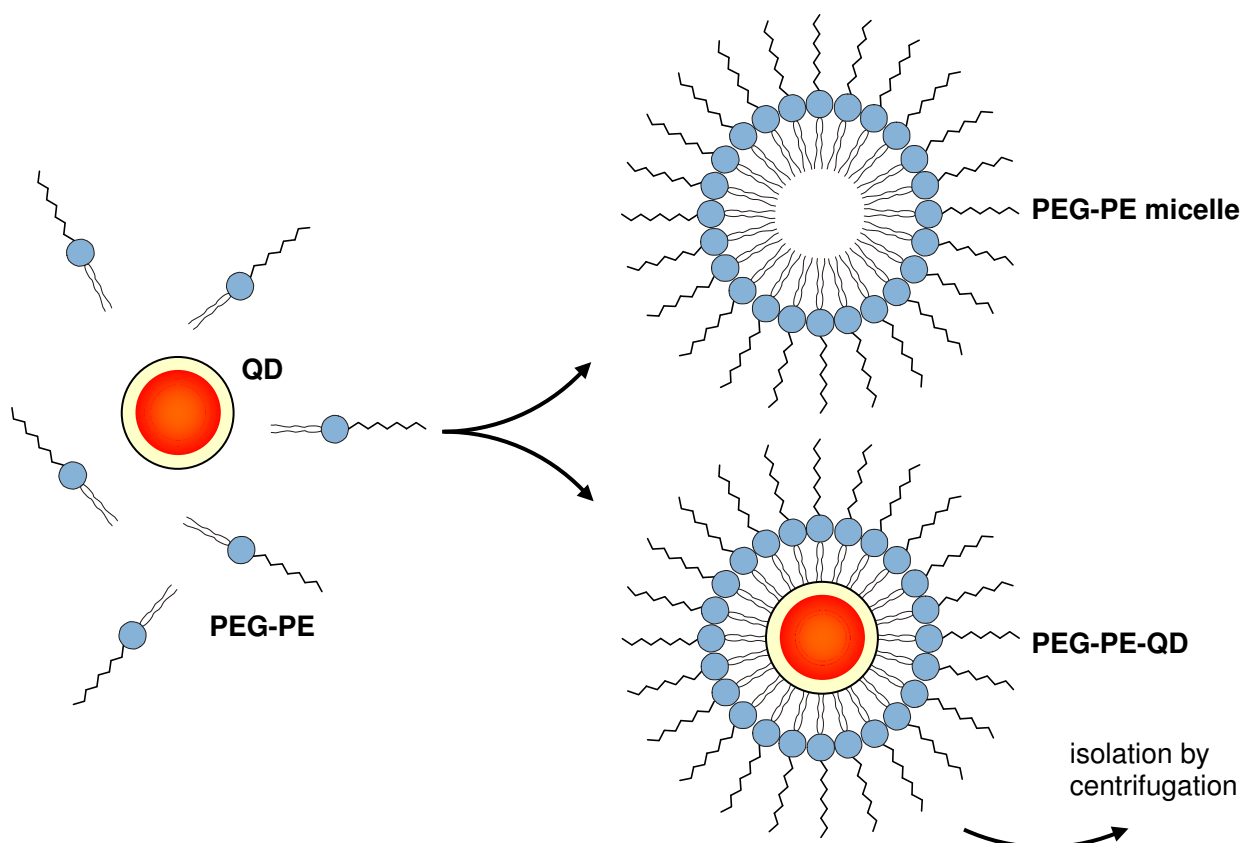


**Figure 8: Coating of organic soluble QDs with PEG-PE.** After dissolving a film of PEG-PE and QDs (left side) with water, the polymer spontaneously arranges itself around the nanocrystals (PEG-PE-QD). PEG-PE forms micelles which were separated by centrifugation.

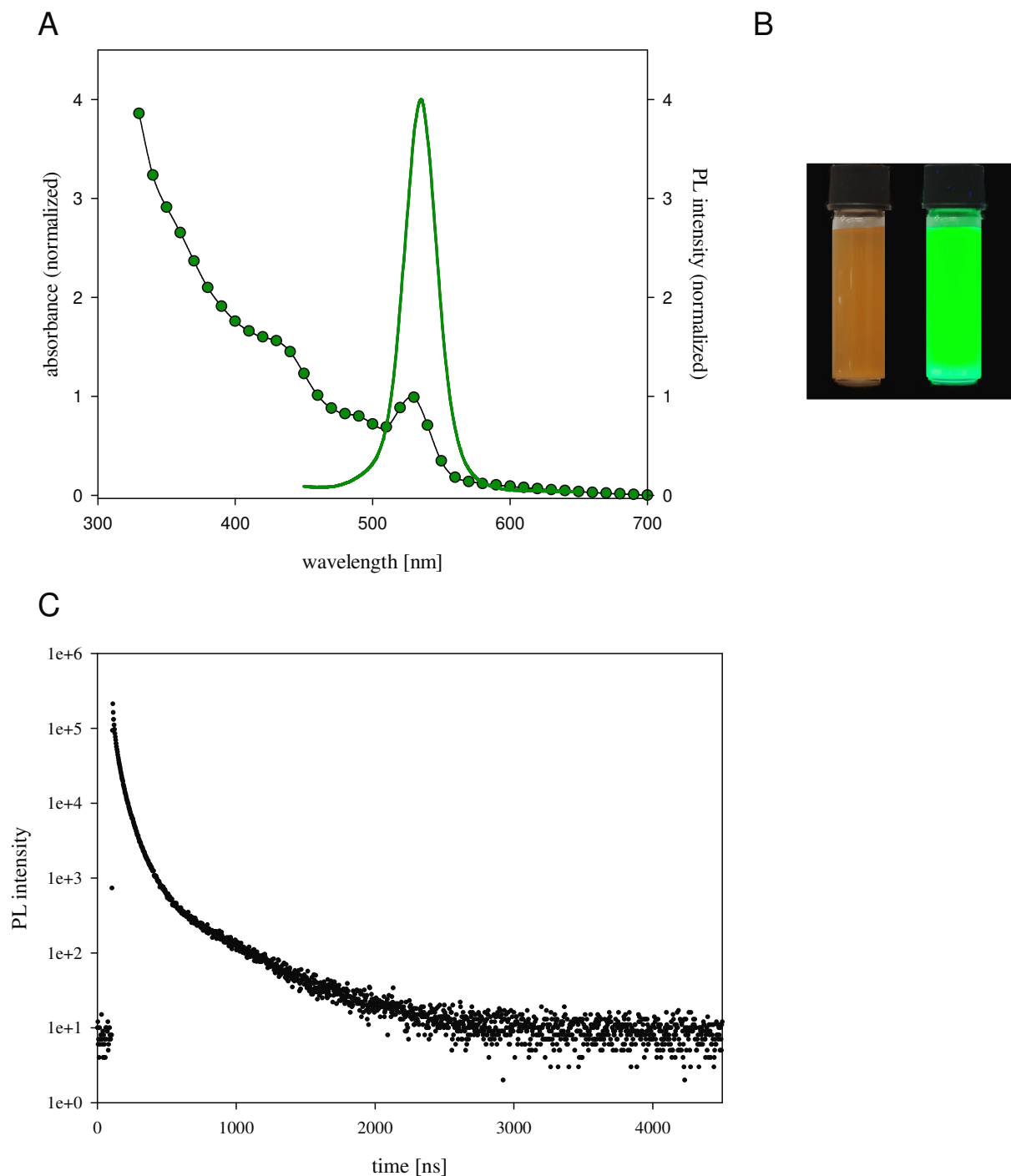


**Figure 9: Optical properties of PEG-PE-QDs. (A)** Absorbance (marked with circles) and emission spectrum of PEG-PE-QDs. The particles maintain their optical properties when coated with the polymer. Quantum yields typically range between 3 and 10%. **(B)** Photographs of PEG-PE-QDs under visible light (left) and under UV light (right) showing the bright fluorescence. **(C)** Fluorescence decay curve exhibiting a fluorescence half-life of approx. 20 ns.

The resulting PEG-PE-QDs have favorable optical properties similar to those of organic soluble QDs. The absorbance and emission spectra have a similar appearance to the ones obtained for unmodified QDs (fig. 9A). The PEG-PE-QDs exhibited quantum yields of 3-10% which were the highest values of all the investigated methods for solubilization. The photograph in fig. 9B depicts the PEG-PE-QDs under ambient light as well as upon excitation by UV light showing the bright fluorescence of the QDs in aqueous medium. A fluorescence decay-curve is given in fig. 9C. The fluorescence half-life is approx. 20 ns. Though not extremely high, this decay characteristic allows for signal separation from fast-decaying biological samples and increases the signal-to-background ratio after termination of autofluorescence. In comparison to a lysate of murine kidney cells, the QDs showed prolonged fluorescence and could be detected after the disappearance of the cell fluorescence (data published elsewhere).

Size analysis of the PEG-PE-QDs revealed a uniform size (PI approx. 0.2) and an acceptable low hydrodynamic diameter, around 20-25 nm, determined by DLS (fig. 10A). Compared to the unmodified PEG-PE micelles, the PEG-PE-QDs exhibit larger sizes due to the encapsulation of one or several QDs. Fig. 10B shows the corresponding size distributions of both the PEG-PE micelles and the PEG-PE-QDs. The graph shows that after encapsulating the QDs inside the PEG-PE, the initial uniformity of the PEG-PE micelles is widely maintained.

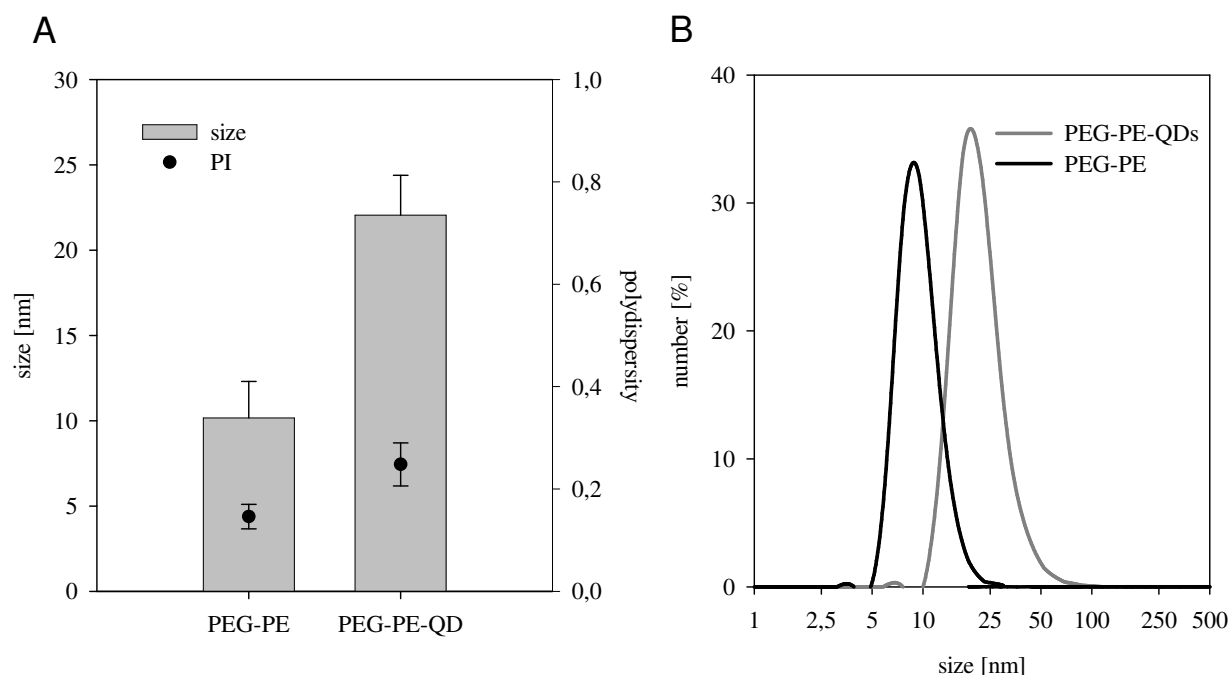


**Figure 10: Size analysis and distribution of PEG-PE-QDs in comparison to micelles of PEG-PE. (A)** Size analysis by DLS. Compared to the PEG-PE micelles, the PEG-PE-QDs exhibit an increased hydrodynamic radius (below 25 nm) due to the loading of PEG-PE with QDs. For both species polydispersity is low. **(B)** The size distribution of both species is narrow. The shift in sizes is caused by the loading of the PEG-PE with the QDs.

In order to examine which size of QDs fits optimally inside the PEG-PE micelles, a series of QD batches with increasing diameters were encapsulated in PEG-PE. Thereafter, the concentration of the solubilized QDs was determined by UV spectroscopy. During preparation, aggregates were removed and therefore only the encapsulated QDs were measured. As shown in fig. 11, the amount of QDs solubilized by the same amount of PEG-PE is decreases by the diameter of the QDs. The higher the size of the QDs, the more difficult it is for the nanoparticles to fit into PEG-PE micelles. In this study, QDs of a diameter of 3.8 nm could successfully be encapsulated whereas larger QDs of up to 7 nm in diameter showed significantly lower concentrations in the aqueous medium. The reason for this behavior is due to the properties of the PEG-PE micelles. Since the PEG-PE molecules have a fixed size and geometry, they consequently always arrange themselves around micelles of a fixed size. This proves that there has to be an optimum for the size of a particle to be encapsulated inside such a micelle. As a consequence of this size-dependence,



QDs emitting around the green range (around 500-550 nm) of the spectrum can be encapsulated favorably, since the photoluminescence maximum and the particle diameter are strongly correlated [20].

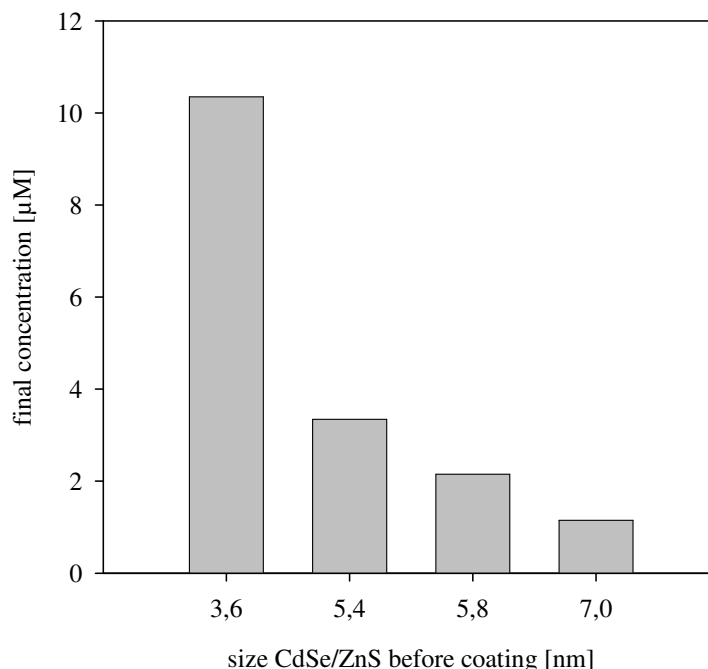


**Figure 11: Size-dependence of the solubilization behavior of QDs in PEG-PE-micelles.** Small QDs (3.8 nm) are encapsulated more efficiently than larger particles (up to 7 nm) since the absorbance of the QDs after solubilization drastically decreases by size.

These findings were confirmed by cryo-TEM. QDs of 3.8 nm in diameter were quite homogeneously distributed (fig. 12A, left panel). Only a few aggregates of several QDs can be found. The majority of the nanocrystals was separated inside the PEG-PE, resulting in quite uniform PEG-PE coated particles (right panel). In all pictures, the QDs are represented by the small dark spots which result from the high contrast of the semiconductor nanocrystals. In contrast, when solubilizing particles of 7.0 nm in diameter, the particles tend to aggregate and form large clusters (fig. 12B). The reason for this behavior is the already mentioned unfavorable size of this species of QDs that does not fit properly inside the micelles.

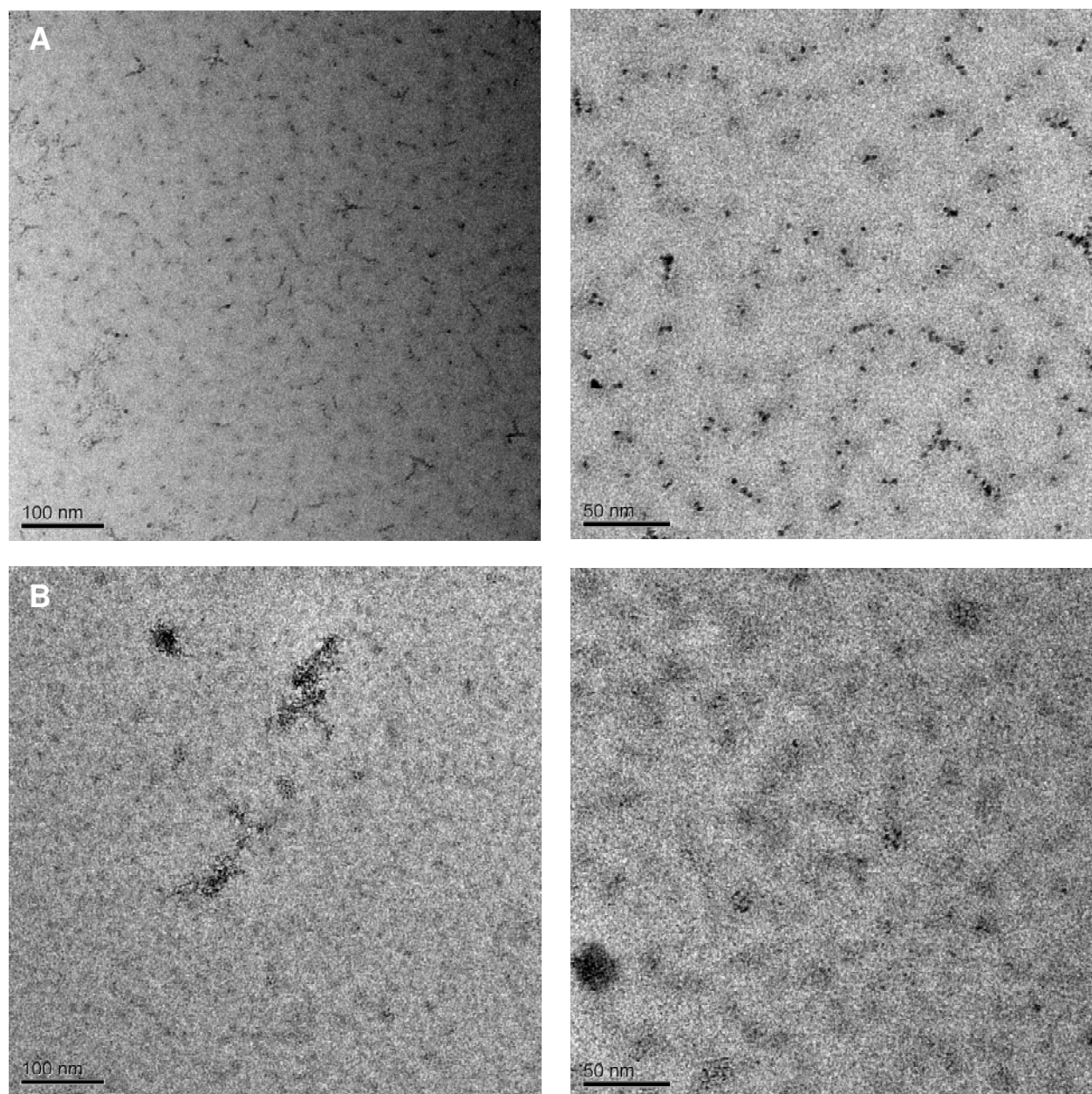


**Figure 12: Cryo-TEM micrographs of PEG-PE-QDs.** (A) QDs of 3.8 nm encapsulated in PEG-PE micelles. The nanocrystals are evenly distributed throughout the sample (left panel). The majority of the nanocrystals are separated and only a few aggregates can be found (right panel). (B) QDs of 7.0 nm solubilized by PEG-PE. The particles tend to form aggregates and are located in large clusters (left and right panel). The dark spots in the pictures represent the semiconductor nanocrystals that exhibit high contrast under TEM. The light grey spherical structures are caused by PEG-PE.

Having optimized the conditions to obtain PEGylated QDs of narrow size-distribution and small size, it is crucial to ensure that the particles exhibit a sufficient number of reactive sites on the colloid surface in order to connect the particles to biologically active substances. For the attachment of a number of biomolecules, amines proved to be useful [15]. Through direct coupling to the biomolecules or by using crosslinkers [25], amine groups form stable covalent conjugates via amide bonds. Since PEG-PE is available with a number of functional groups, it is easy to introduce such functional groups, like amines, into the colloid.

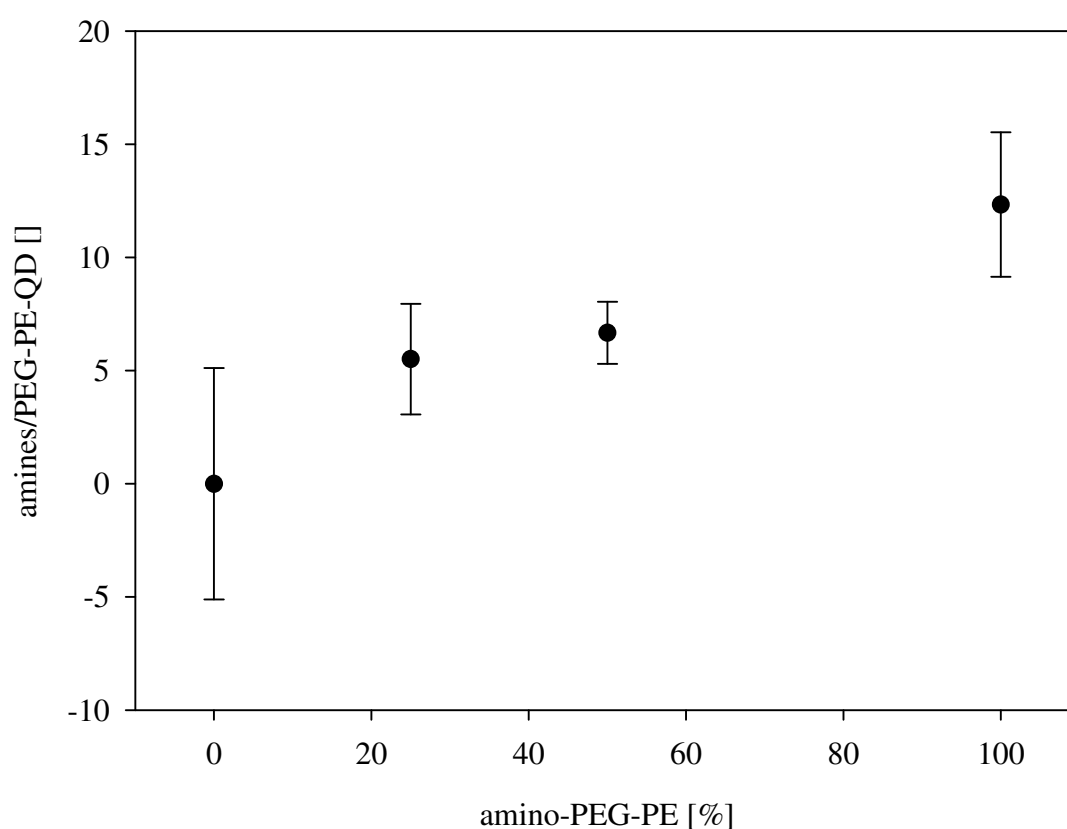


**Figure 13: Determination of the content of primary amines per QD when using different amounts of amino-PEG-PE.** Increasing amounts of amino-PEG-PE for the coating of the hydrophobic QDs yields PEG-PE-QDs of increasing amine content. The maximum number of amines per QD was approx. 12.

It was investigated how many amine groups per PEG-PE-QD are available when coating the QDs with different amounts of amino-PEG-PE. The fluorescamine reaction with primary amines yields a fluorescent product with fluorescence intensity proportional to the concentration of free amines. As expected, when using increasing amounts of amino-PEG-PE for the coating of the QDs, the resulting PEG-PE-QDs carry increasing amounts of amines on the colloid surface as well (fig. 13). The maximum number of amines per PEG-PE-QD was hereby found to be around 12 when using 100% of amino-PEG-PE for the coating. Therefore, a maximum of 12 biomolecules per particle can be conjugated to the PEG-PE-QDs which should be sufficient for most of the applications. It was also possible to tune the number of amines per QD to lower amounts by adjusting the ratio between non-functionalized PEG-PE and amino-PEG-PE. The results show that coating with PEG-PE, besides providing a powerful method for the solubilization of QDs, represents a versatile strategy for the functionalization of QD surfaces.

### **Summary and conclusion**

Several different strategies for the hydrophilization of QD-surfaces were explored. The exchange of the surface-bound organic ligands allows for the creation of both small, but not highly stable, hydrophilic QDs when using thiol-containing carboxylic acids, as well as more stable PEGylated QDs. However, the latter are characterized by a large hydrodynamic diameter. For both routes the quantum yields in aqueous medium were low. The coating of QDs with PEG-PE overcomes the restrictions of the above mentioned strategies. The resulting PEG-PE-QDs are stable in aqueous media, exhibit small sizes around of 20 nm and good quantum yields. When encapsulating QDs of diameters of up to 4 nm, the PEG-PE-QDs are characterized by low polydispersity. Additionally, when applying functionalized PEG-PEs, like amino-PEG-PE, the QDs can be capped with a customized number of functional groups, which enable the attachment of various molecules, such as peptides, proteins or antibodies.

Therefore, PEG-PE-QDs are versatile candidates for bioprobes after chemical modification with biologically active substances.

---

**References**

- [1] W. C. W. Chan and S. Nie, Quantum dot bioconjugates for ultrasensitive nonisotopic detection, *Science* (Washington, D. C. ), 281 (1998) 2016-2018.
- [2] X. Michalet, F. F. Pinaud, L. A. Bentolila, J. M. Tsay, S. Doose, J. J. Li, G. Sundaresan, A. M. Wu, S. S. Gambhir, and S. Weiss, Quantum Dots for Live Cells, in Vivo Imaging, and Diagnostics, *Science*, 307 (2005) 538-544.
- [3] W. J. Parak, D. Gerion, T. Pellegrino, D. Zanchet, C. Micheel, S. C. Williams, R. Boudreau, M. A. Le Gros, C. A. Larabell, and A. P. Alivisatos, Biological applications of colloidal nanocrystals, *Nanotechnology*, 14 (2003) R15-R27.
- [4] J. K. Jaiswal, H. Mattoussi, J. M. Mauro, and S. M. Simon, Long-term multiple color imaging of live cells using quantum dot bioconjugates, *Nat. Biotechnol.*, 21 (2003) 47-51.
- [5] A. M. Smith, H. Duan, A. M. Mohs, and S. Nie, Bioconjugated quantum dots for in vivo molecular and cellular imaging, *Adv. Drug Delivery Rev.*, 60 (2008) 1226-1240.
- [6] D. V. Talapin, A. L. Rogach, A. Kornowski, M. Haase, and H. Weller, Highly Luminescent Monodisperse CdSe and CdSe/ZnS Nanocrystals Synthesized in a Hexadecylamine-Trioctylphosphine Oxide-Trioctylphosphine Mixture, *Nano Lett.*, 1 (2001) 207-211.
- [7] K. Yu, B. Zaman, R. Taal, and J. A. Ripmeester, Colloidal CdSe nanocrystals from tri-n-octylphosphine with various Cd sources: control of a slow growth for high-quality and large-scale production, *J. Cryst. Growth*, 283 (2005) 115-123.
- [8] A. M. Derfus, W. C. W. Chan, and S. N. Bhatia, Intracellular delivery of quantum dots for live cell labeling and organelle tracking, *Adv. Mater.*, 16 (2004) 961-966.
- [9] I. D. Tomlinson, D. W. Wright, T. D. Giorgio, R. D. Blakely, S. J. Pennycook, D. Hercules, L. Bentzen, R. A. Smith, J. McBride, M. J. Vergne, and S. Rosenthal, The quantum dot nanoconjugate toolbox, *Proc. of SPIE*, 5705 (2005) 199-209.
- [10] B. Dubertret, P. Skourides, D. J. Norris, V. Noireaux, A. H. Brivanlou, and A. Libchaber, In vivo imaging of quantum dots encapsulated in phospholipid micelles, *Science*, 298 (2002) 1759-1762.
- [11] X. Gao, Y. Cui, R. M. Levenson, L. W. K. Chung, and S. Nie, In vivo cancer targeting and imaging with semiconductor quantum dots, *Nat. Biotechnol.*, 22 (2004) 969-976.
- [12] E. L. Bentzen, I. D. Tomlinson, J. Mason, P. Gresch, M. R. Warnement, D. Wright, E. Sanders-Bush, R. Blakely, and S. J. Rosenthal, Surface Modification To Reduce Nonspecific Binding of Quantum Dots in Live Cell Assays, *Bioconjug. Chem.*, 16 (2005) 1488-1494.

- [13] E. Chang, W. W. Yu, V. L. Colvin, and R. Drezek, Quantifying the influence of surface coatings on quantum dot uptake in cells, *J. Biomed. Nanotechnol.*, 1 (2005) 397-401.
- [14] B. Ballou, B. C. Lagerholm, L. A. Ernst, M. P. Bruchez, and A. S. Waggoner, Noninvasive imaging of quantum dots in mice, *Bioconjug. Chem.*, 15 (2004) 79-86.
- [15] W. Cai, D. Shin, K. Chen, O. Gheysens, Q. Cao, S. Wang, X. S. S. Gambhir, and X. Chen, Peptide-labeled near-infrared quantum dots for imaging tumor vasculature in living subjects, *Nano Lett.*, 6 (2006) 669-676.
- [16] X. Wu, H. Liu, J. Liu, K. N. Haley, J. A. Treadway, J. P. Larson, N. Ge, F. Peale, and M. P. Bruchez, Immunofluorescent labeling of cancer marker Her2 and other cellular targets with semiconductor quantum dots, *Nat. Biotechnol.*, 21 (2002) 41-46.
- [17] S. W. Kim, S. Kim, J. B. Tracy, A. Jasanoff, and M. G. Bawendi, Phosphine Oxide Polymer for Water-Soluble Nanoparticles, *J. Am. Chem. Soc.*, 127 (2005) 4556-4557.
- [18] W. Jiang, S. Mardiyani, H. Fischer, and W. C. W. Chan, Design and Characterization of Lysine Cross-Linked Mercapto-Acid Biocompatible Quantum Dots, *Chem. Mater.*, 18 (2006) 872-878.
- [19] S. W. Provencher, CONTIN: A general purpose constrained regularization program for inverting noisy linear algebraic and integral equations, *Computer Physics Communications*, 27 (1982) 229-242.
- [20] W. W. Yu, L. Qu, W. Guo, and X. Peng, Experimental Determination of the Extinction Coefficient of CdTe, CdSe, and CdS Nanocrystals, *Chem. Mater.*, 15 (2003) 2854-2860.
- [21] W. Liu, M. Howarth, A. B. Greytak, Y. Zheng, D. G. Nocera, A. Y. Ting, and M. G. Bawendi, Compact Biocompatible Quantum Dots Functionalized for Cellular Imaging, *J. Am. Chem. Soc.*, 130 (2008) 1274-1284.
- [22] J. Aldana, Y. A. Wang, and X. Peng, Photochemical Instability of CdSe Nanocrystals Coated by Hydrophilic Thiols, *J. Am. Chem. Soc.*, 123 (2001) 8844-8850.
- [23] H. T. Uyeda, I. L. Medintz, J. K. Jaiswal, S. M. Simon, and H. Mattoussi, Synthesis of Compact Multidentate Ligands to Prepare Stable Hydrophilic Quantum Dot Fluorophores, *J. Am. Chem. Soc.*, 127 (2005) 3870-3878.
- [24] W. Jiang, B. Y. S. Kim, J. T. Rutka, and W. C. W. Chan, Nanoparticle-mediated cellular response is size-dependent, *Nat. Nanotechnol.*, 3 (2008) 145-150.
- [25] W. J. M. Mulder, R. Koole, R. J. Brandwijk, G. Storm, P. T. K. Chin, G. J. Strijkers, C. de Donega, K. Nicolay, and A. W. Griffioen, Quantum Dots with a

Paramagnetic Coating as a Bimodal Molecular Imaging Probe, Nano Lett., 6 (2006) 1-6.





# Chapter 5

## **Characterization of Aqueous Quantum Dot Dispersions using Asymmetrical Flow Field-flow Fractionation (AF4)**

W. Hild<sup>1</sup>, R. Lang<sup>2</sup>, J. Teßmar<sup>1</sup>, A. Göpferich<sup>1</sup>

<sup>1</sup>Department of Pharmaceutical Technology, University of Regensburg,  
Universitätsstraße 31, 93040 Regensburg, Germany

<sup>2</sup>Pharmaceutical Technology and Biopharmaceutics, Ludwig-Maximilians-  
University, Center for Drug Research, Butenandtstraße 5, 81377 Munich,  
Germany

**Abstract**

Quantum dots (QDs) emerged as a powerful tool in biomedical investigations due to their well-characterized optical properties, emitting strong and stable fluorescence. QDs are usually covered by hydrophilic coatings, preferably consisting of poly(ethylene glycol) (PEG) to minimize non-specific interactions, such as adsorption and aggregation, and to render them accessible for use in biological systems. Together with the rising demand for high-quality QDs of defined size and narrow size-distribution, the need for powerful analytics increased as well. Unfortunately, standard methods, like dynamic light scattering (DLS) and transmission electron microscopy (TEM), have various drawbacks. Dynamic light scattering suffers from missing separation of nanoparticles of different sizes and transmission electron microscopy requires extremely high experimental effort. Asymmetrical flow field-flow fractionation (AF4), in contrast, seems to be a promising alternative due to its high-resolving separation. Coupling to multiple angle light scattering (MALS) detection allows for obtaining even molecular masses of single fractions. In this study, the feasibility of using AF4 for the analysis of PEGylated QDs was investigated and a method for the reliable separation and analysis of QDs by AF4 coupled with MALS detection was developed. The method was then used for the analysis of QDs of different dispersity and the comparison with commercially available QDs.

## Introduction

Quantum dots, semiconductor nanocrystals, have emerged as ideal model colloids for biomedical investigations, since they exhibit unique optical properties, such as bright fluorescence that is resistant to photobleaching, sharp and tuneable emissions as well as a large Stokes shift [1-4]. QDs have been used for approaches in labeling cancerous tissues [5], unveiling transport mechanisms into cells [6] and as labels of cellular structures in the discovery of distinct mechanisms, like receptor trafficking [7-9].

Along with the tremendous progress that has been made since the introduction of their first colloidal syntheses [10] and the development of powerful surface coatings to render QDs more biocompatible [11], the need for powerful analytics of the dispersity of QDs has grown. Recent approaches emphasize the enormous influence of particle size on interactions with biological systems, such as cellular uptake and other cellular responses [12] and even toxicity [13]. In order to obtain highly monodisperse collectives of QDs with hydrophilic surface coatings, like PEGylated surfaces [14], a powerful separation technique is needed for highly specific biological investigations. Up to now, the standard analytics for the determination of the size of hydrophilic QDs comprise mainly of microscopic methods or dynamic light scattering (DLS). These microscopic methods consist of transmission electron microscopy (TEM) and atomic force microscopy (AFM) in particular. Even though both techniques provide an unmatched resolution, they are highly-demanding in terms of the equipment used and the time needed for obtaining a statistically relevant number of pictures for their analysis. Therefore, these methods cannot serve for standard analytics for the quality assurance of QDs. In contrast, DLS represents a valuable method for characterizing batches in a short period of time. However, the results are only based on averaged values of the sample dispersity. Moreover, there is no possibility to characterize polydispers samples or even to fractionate them for all the above mentioned methods.

Asymmetrical flow field-flow fractionation would be a method to overcome these drawbacks by offering a powerful method for the separation of samples of various compositions according to the particle size. When coupled with a multiple angle light scattering detector (MALS), it is also possible to obtain detailed information on the size as well as the molar mass of the single fractions [15-17].

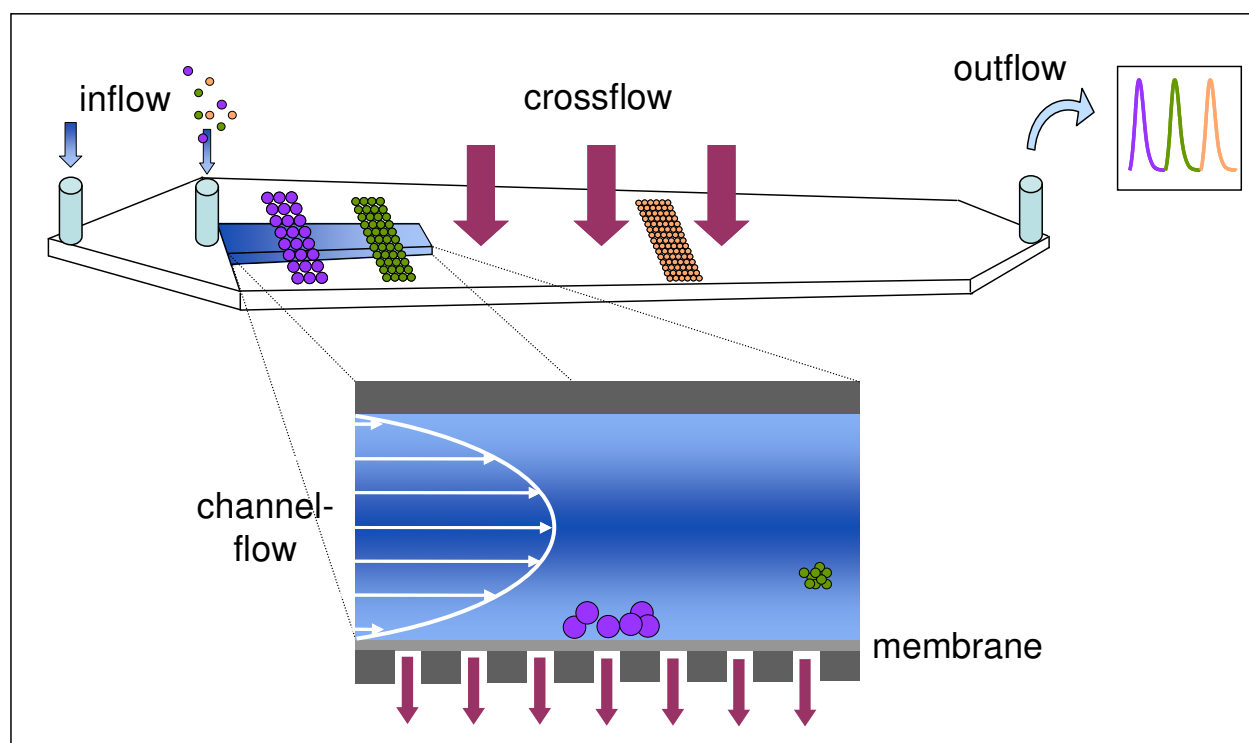


**Figure 1: Schematic depiction of the functionality of AF4.** The sample is introduced into the flow channel and focused. Then, separation takes place along the channel due to the influence of a flow perpendicular to the laminar channel flow (cross flow). Because of this cross flow and the size-dependent diffusion of the particles, the particles are localized in regions of higher (small particles) or lower (larger particles) flow speed. Smaller particles are eluted before larger ones.

Fig. 1 shows the principle of the separation obtained by AF4. After injection and focussing at the beginning of the flow channel, the sample is carried by a controllable laminar flow along the flow channel. Separation is caused by a cross flow perpendicular to the channel flow which passes through a membrane of defined molecular weight cut-off (MWCO) on the bottom of the flow chamber. After this, the analyte leaves the regions of faster flow and moves towards the bottom region of the flow cell which exhibits slower flow. According to the sample size and thus the diffusion coefficient, smaller particles diffuse back into regions of higher flow speed faster than larger particles. Therefore, smaller particles are eluted before larger particles. Subsequently, molar masses can be obtained by analysis using MALS detection [18].

In this approach, this advanced technique was introduced for the analysis of PEGylated QDs concerning the dispersity as well as approximations of their molar

mass. The objective of this study was to prove the feasibility of using AF4 for the characterization of QDs, since at the time of the investigations only one report was available [19].

### **Materials and methods**

Cadmium oxide (CdO, 99.5%), hexadecylamine (HDA, tech. grade 90%), lauric acid (LA 98%), methanol (anhydr. 99.8%), sulfur (99.5%), toluene (anhydr. 99.8%), trioctylphosphine (TOP, tech. grade 90%), trioctylphosphine oxide (TOPO, tech. grade 90%) and zinc stearate (tech. grade) were obtained from Sigma-Aldrich (St. Louis, MO). 1,2-distearoyl-sn-glycero-3-phosphatidylethanolamine covalently linked to methoxy-PEG (PEG-PE) of an average molecular weight of 2000 Da was obtained from Lipoid (Ludwigshafen, Germany). EviTags were obtained from Evident Technologies (Troy, NY).

#### *Synthesis of CdSe/ZnS nanocrystals and PEG-PE coating*

CdSe/ZnS QDs were synthesized by thermal decomposition of the corresponding precursors as described in chapter 3. In brief, CdO (0.2 mmol) was dissolved in lauric acid (1.6 mmol) at 200 °C. TOPO (10 mmol, 3.88 mg) and HDA (16 mmol, 3.88 mg) were added and the mixture was heated to 285 °C. After removing the heating bath, Se (2 mmol) dissolved in 3.5 ml of TOP was injected. At the desired nanocrystal size (5-30 sec of crystal growth), the growth was stopped by injection of 20 ml of toluene. The CdSe cores were precipitated with an equal volume of methanol and centrifuged at 6000 x g for 5 min and redispersed as described above. ZnS-coating was conducted after dispersing the CdSe cores in the same amount of TOPO and HDA as for the core synthesis at 200 °C over 60 min. The amounts for the ZnS precursor were calculated for four theoretical monolayers per QD. After shell-growth, the nanocrystals were purified by precipitation as described above and redissolved in toluene. For the coating with PEG-PE, the nanocrystals were precipitated with methanol and redispersed in dichloromethane together with the phospholipids as described in chapter 3. Thereafter, dichloromethane was evaporated and the obtained film was hydrated at 80 °C. The solution was vortexed and centrifuged to remove aggregates. Then, the PEG-PE-QDs were collected as pellet after ultracentrifugation (for details, see chapter 4). Three samples were prepared. Sample

A represents a rather monodisperse sample (compare to fig 12A and 10, chapter 4, core size 3.8 nm) while sample C was a sample rich in aggregates (compare to fig 12B, chapter 4, core size 7.0 nm). Sample B was an intermediate between both (core size 5.4 nm). For all measurements sample A was used, unless stated differently.

#### *Asymmetric flow field-flow fractionation and molar mass determination*

For the particle separation, an Eclipse2 separation system (Wyatt Technology, Dernbach, Germany) was used. The separation channel was equipped with a 5000 Da MWCO membrane consisting of regenerated cellulose. The system was coupled to a Dawn EOS multiple angle light scattering (MALS) detector (Wyatt Technologies) and a multiple wavelength detector (Agilent, Santa Clara, CA) operating at 280 nm. As eluent 10 mM sodium phosphate buffer pH 6.8 was used. The following flow profile was used: channel flow: 1.5 ml/min; focus flow: 3.0 ml/min (0-8 min); cross flow: 2.0 ml/min (8-23 min), 2.0-0.15 ml/min (23-28 min), 0.15-0.00 ml/min (28-29 min), 0 ml/min (29-49 min). An overview of the flow profile is depicted in fig. 2. For the determination of the molecular mass, the absolute absorption coefficient of the PEG-PE-QD samples was determined by freeze-drying a sample of known molar concentration inside a microcentrifuge cup (Eppendorff, Hamburg, Germany). The molar concentration of the sample was determined by UV-measurement before drying, using an Uvikon 941 (Kontron Instruments, UK) and 10 cm quartz cuvettes. The concentrations were calculated using commonly used approximations of the absorbance coefficient for QDs [20] and Lambert-Beer's law. After this, the weight of the dried QDs was determined. For the PEG-PE-QDs the absolute absorbance coefficient obtained at 280 nm was 2.089 ml/mg\*cm. Because the EviTags used exhibit a similar absorbance maximum to a lipid-based, PEG 2000-containing coating, and since high amounts of QDs are needed for an accurate determination, the absorbance coefficient obtained was used for the EviTags as well.

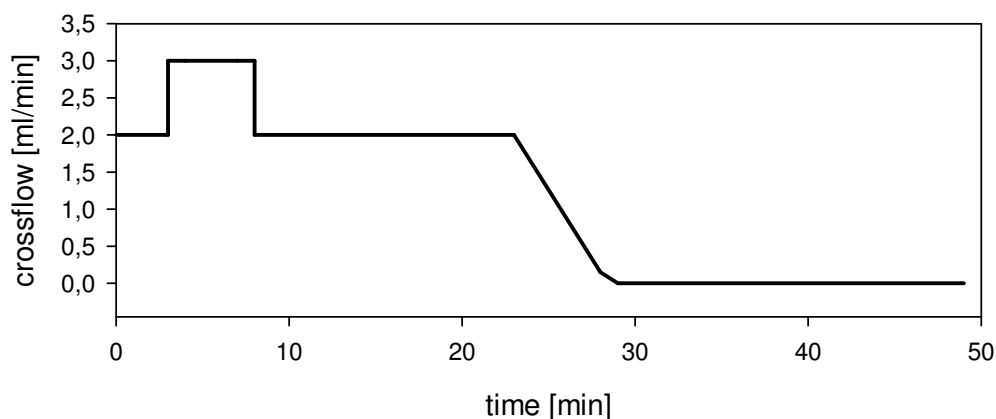


**Figure 2: Flow profile for AF4 separation.** The channel flow was kept constant at 1.5 ml/min.

### Results and discussion

The described flow profile was applied to separate QDs which were coated with PEGylated phospholipids (PEG-PE). In order to obtain a reproducible method for the analysis of water-soluble QDs, several cross flow profiles were tested (data not shown) and the one yielding the best separation was chosen. In order to identify the QD-fraction, UV detection was applied at two wavelengths. While at 280 nm most of the sample content could be detected, at 530 nm only the QDs could be detected. As shown in fig. 3A, for both channels, the chromatogram exhibits a main peak at approx. 15 min, which corresponds to the colloid. At 280 nm, a signal from the QD-cores as well as from other material, such as the coating, can be obtained. In contrast, at 530 nm, only the absorbance of the QDs can be detected. This ensures that the main peak indeed is due to the presence of the QDs and it also ensures that the sample is free from excess coating material, as far as possible, since other peaks in the chromatogram are weak. The UV spectrum of the PEG-PE-QDs is presented in fig. 3B and shows that the QDs are able to absorb over a wide range, enabling detection at various wavelengths.

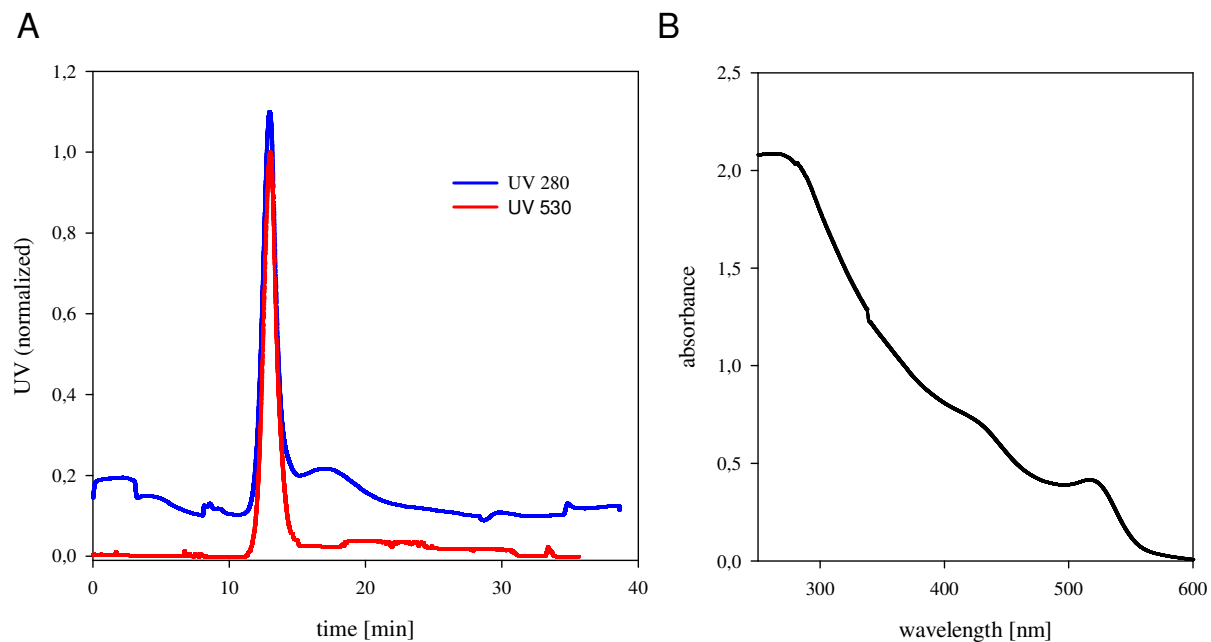


**Figure 3: AF4 measurement of PEG-PE-QDs at different UV/VIS wavelengths.** (A) The chromatogram shows a main peak at approx. 15 min representing the PEG-PE-QDs. While the signal obtained by UV 280 (before normalization) is more intense, the signal at 530 nm is weaker and only correlated to the absorbance of the QD-cores. (B) Absorbance spectrum of PEG-PE-QDs.

In order to investigate whether the approach is sound and yields reproducible results, different amounts of QDs were injected repeatedly. By doing this, it was ensured that the recovery of the main peak was constant when reproducing the measurements and using different amounts of PEG-PD-QDs. Only when reproducibility is granted, reliable results covering the whole sample can be obtained. As depicted in fig. 4, the injection of increasing amounts of PEG-PE-QDs does not result in changes in the appearance and retention time of the main peak. Only the peak area is enlarged due to the increasing amounts of PEG-PE-QDs injected. The results are summarized in tab. 1 and prove that the ratio of the mass of the PEG-PE-QD main peak to the total mass remains under the chosen conditions for increasing injected amounts constant and is reproducible for the same injected amounts. Therefore, adsorption of the sample to the membrane through which the cross flow leaves the flow channel can be excluded, as well as washing-out of the sample through the pores of the membrane.



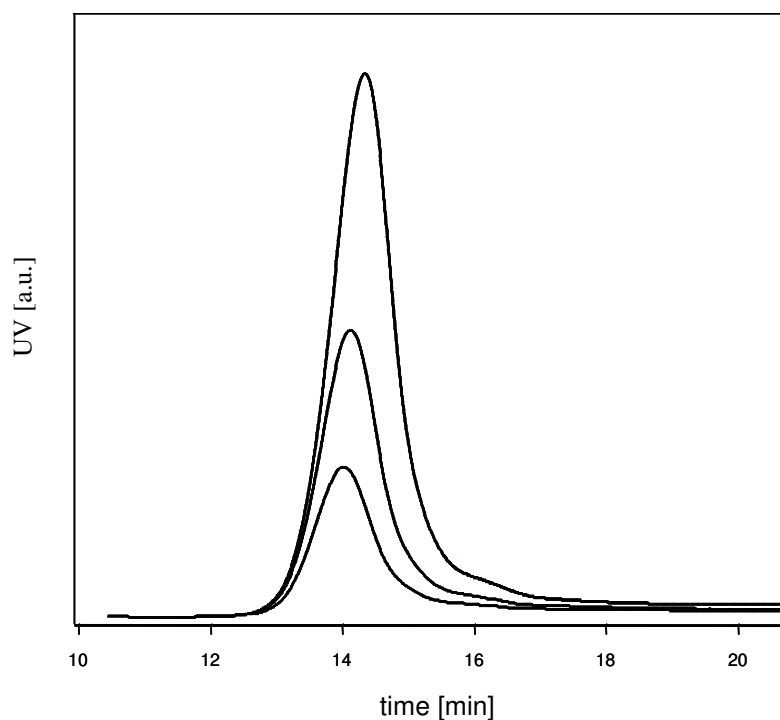


**Figure 4: Reproducibility of the AF4 method for the determination of PEG-PE-QDs.** Increasing amounts of PEG-PE-QDs were applied and no change in the peak position and shape of the PEG-PE-QD fraction was detected. For quantitative evaluation, see tab. 1.

injected mass [mg]	mass 1 <sup>st</sup> peak [%]
5µg (1)	69.0
5µg (2)	71.7
10µg (1)	75.4
10µg (2)	73.7
20µg (1)	77.3
20µg (2)	74.6

**Table 1: Quantitative analysis of the peak area of the samples (and repetition) in fig. 4.** The three different PEG-PE-QD amounts were measured repeatedly and the peak area of the main fraction was correlated with the injected amount. Values for the ratio of the first peak to the whole sample are stable and remain quite constant proving reproducibility of the method.

In the next step, the established method was used to characterize different batches of PEG-PE-QDs. For this purpose, three samples (A-C) of different composition and dispersity were analyzed. As shown in fig. 5A, the three batches exhibit significant differences in their chromatograms regarding the UV-signal which was used for determining the concentration. While the first peak (15 min) for all three of the batches is decreasing, corresponding to the intact and dispersed PEG-PE-QDs, a peak also forms at 17 min as well as at the fraction of large aggregates (around 30 min). This leads to the conclusion that sample A is rather monodisperse, while in sample B the first signs of aggregation are emerging. Sample C, finally, has a high amount of large aggregates. These findings are supported when analyzing the molar masses of the samples and their fractions. While the first fraction exhibits a mass of more than 100 kDa, the mass of the second fraction is higher, about twice the amount, indicating small aggregates. The third fraction, however, contains aggregates beyond 1 MDa. This shows that the composition of hydrophilic QDs can be characterized precisely using AF4 coupled to UV- and MALS-detection. The extent of these fractions was determined by calculating the area under the curve for all fractions. An overview is depicted in fig 5B. While sample A is dominated by the first fraction, the second fraction and the aggregates grow larger for fraction B and C. The method therefore represents a valuable technique for the quality control monitoring of the preparation of hydrophilic QDs. While under PCS sample B and C will appear polydisperse, the separation using AF4 allows for analysis of the product and consequently for optimizations of the colloid preparation.

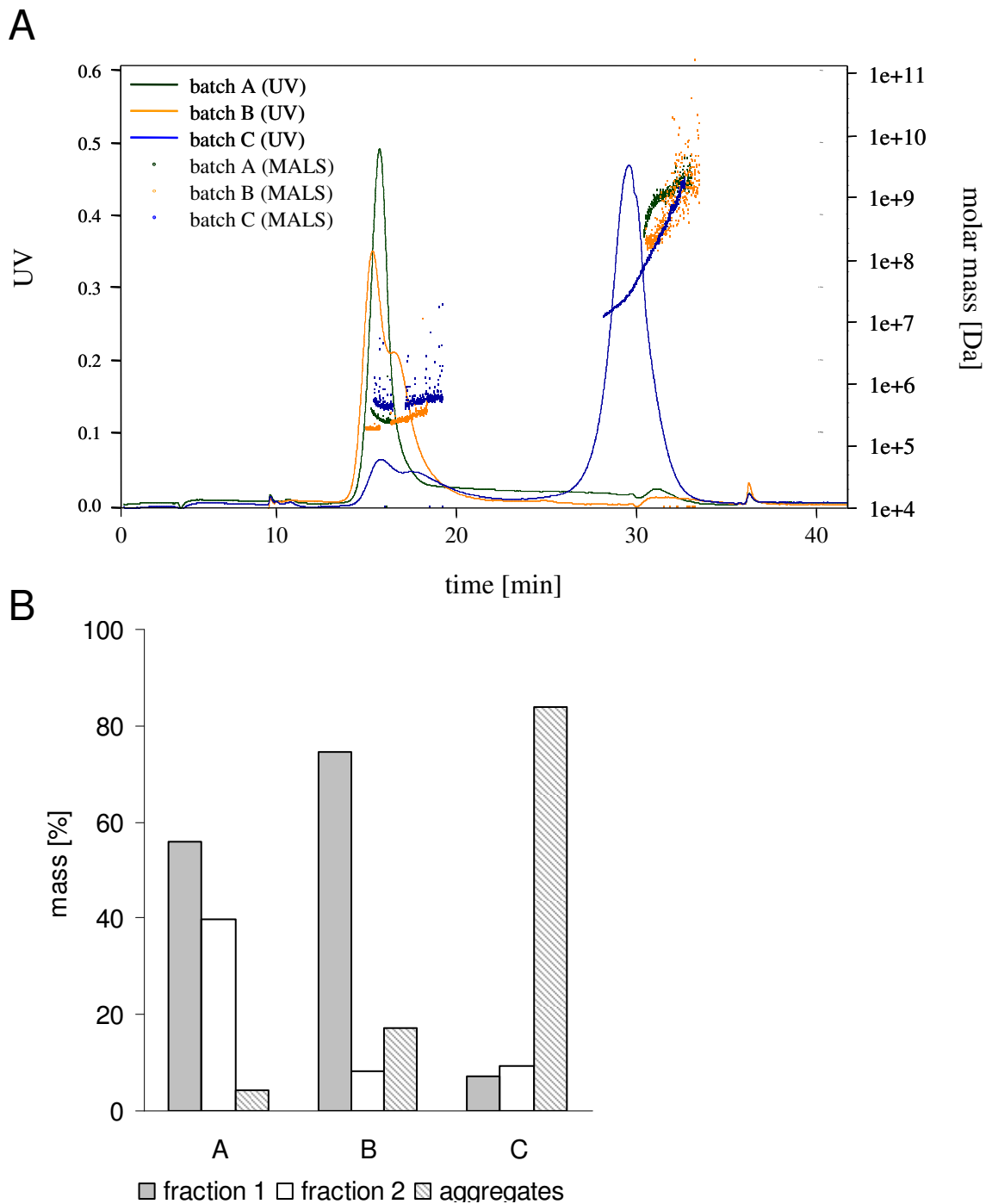


**Figure 5: AF4-analysis of three different batches of PEG-PE-QDs.**

**(A)** Chromatogram of three different batches of PEG-PE-QDs. All batches are characterized by three typical fractions: 15 min (QDs of low dispersity), 17 min (small aggregates of QDs), 30 min (large aggregates). The lines represent the signal obtained from UV-detection; the spots represent the MALS-signal. The first and second fractions exhibit molar masses of 300 kDa and higher; the third fraction exhibits aggregates over 1 MDa. **(B)** Quantitative classification of the three different fractions of each batch.

Finally, the PEG-PE-QDs were compared to commercially available PEGylated QDs (EviTags). According to the information from the manufacturer, the QDs were coated by polar lipids which were conjugated to PEG of a molecular weight of 2000 Da, like the PEG-PE. Therefore, the PEG-PE-QDs exhibit similar properties to the EviTags concerning their AF4 chromatogram. The hypothesis is supported by the results presented in figure 6. Both species exhibit a main peak around 15 min in the UV-signal in the AF4 chromatogram. The molar masses obtained by the MALS detector are resident in the same range of around 300 kDa. For both kinds of hydrophilic QDs, the aggregate fraction is low, almost on the background level obtained by a blank run (not shown). This is a valuable indication that the developed PEG-PE-QDs are comparable to the quality of commercially available QDs concerning their dispersity.

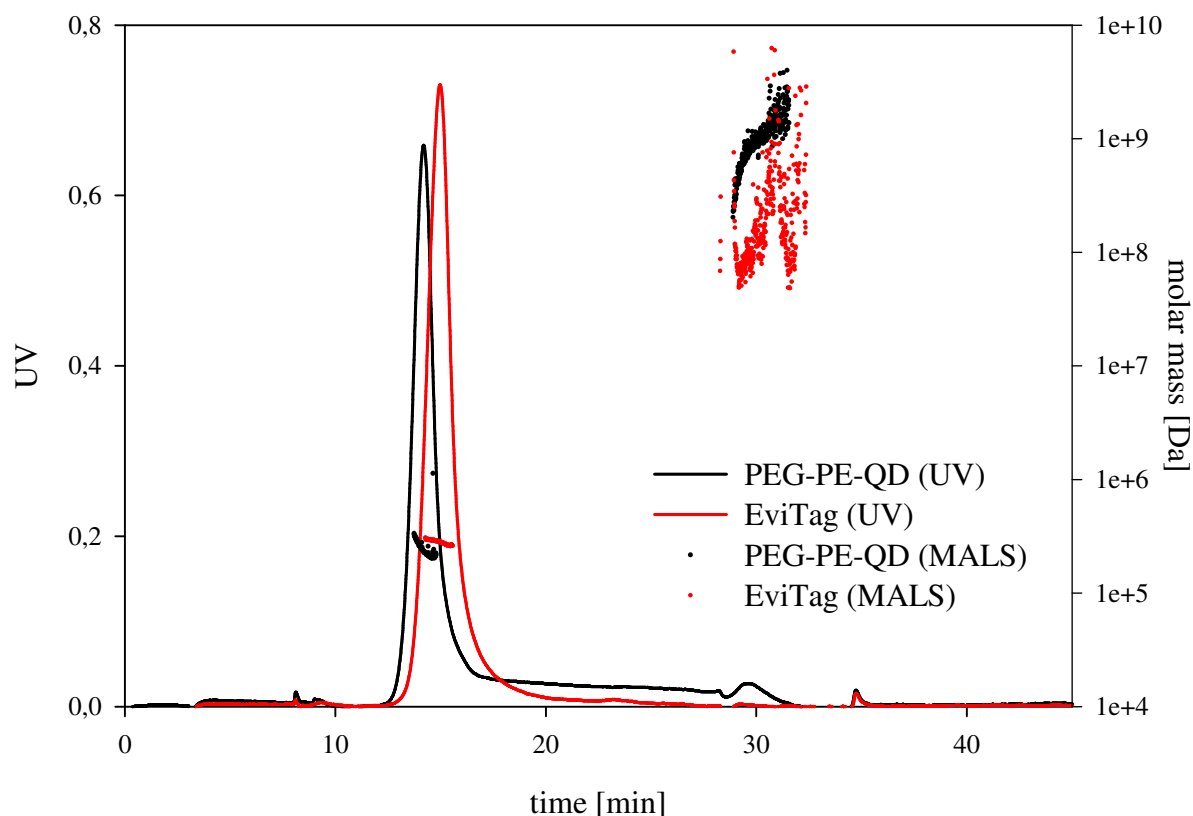


**Figure 6: Comparison between PEG-PE-QDs and commercially available PEGylated QDs (EviTag).** Both species exhibit a main peak at approx. 15 min (obtained by UV) and masses of around 300 kDa (obtained by MALS).

**Summary and conclusion**

An AF4 method for the separation of a collective of hydrophilic QDs containing different-sized fractions has been established. Besides the use of this fractionation for the preparation of hydrophilic QDs of lower dispersity, the method also allows for the quantification of the fractions. Using the MALS detector, molar masses of QDs were calculated. Taking into account the powerful separation obtained by AF4, this method has great potential for the quality assurance of QDs and as a tool for the optimization of preparation techniques.

**References**

- [1] P. Alivisatos, The use of nanocrystals in biological detection, *Nat. Biotechnol.*, 22 (2004) 47-52.
- [2] W. J. Parak, T. Pellegrino, and C. Plank, Labelling of cells with quantum dots, *Nanotechnology*, 16 (2005) R9-R25.
- [3] X. Michalet, F. F. Pinaud, L. A. Bentolila, J. M. Tsay, S. Doose, J. J. Li, G. Sundaresan, A. M. Wu, S. S. Gambhir, and S. Weiss, Quantum dots for live cells, in vivo imaging, and diagnostics, *Science*, 307 538-544.
- [4] W. A. Hild, M. Breunig, and A. Goepferich, Quantum dots - Nano-sized probes for the exploration of cellular and intracellular targeting, *Eur. J. Pharm. Biopharm.*, 68 (2008) 153-168.
- [5] W. Cai, D. Shin, K. Chen, O. Gheysens, Q. Cao, S. Wang, X, S. S. Gambhir, and X. Chen, Peptide-labeled near-infrared quantum dots for imaging tumor vasculature in living subjects, *Nano Lett.*, 6 (2006) 669-676.
- [6] J. K. Jaiswal, H. Mattoussi, J. M. Mauro, and S. M. Simon, Long-term multiple color imaging of live cells using quantum dot bioconjugates, *Nat. Biotechnol.*, 21 (2003) 47-51.
- [7] S. Courty, C. Luccardini, Y. Bellaiche, G. Cappello, and M. Dahan, Tracking Individual Kinesin Motors in Living Cells Using Single Quantum-Dot Imaging, *Nano Lett.*, 6 (2006) 1491-1495.
- [8] M. Dahan, S. Levi, C. Luccardini, P. Rostaing, B. Riveau, and A. Triller, Diffusion dynamics of glycine receptors revealed by single-quantum dot tracking, *Science*, 302 (2003) 442-445.
- [9] D. S. Lidke, P. Nagy, R. Heintzmann, D. J. Arndt-Jovin, J. N. Post, H. E. Grecco, E. A. Jares-Erijman, and T. M. Jovin, Quantum dot ligands provide new insights into erbB/HER receptor-mediated signal transduction, *Nat. Biotechnol.*, 22 (2004) 198-203.
- [10] M. A. Hines and P. Guyot-Sionnest, Synthesis and Characterization of Strongly Luminescing ZnS-Capped CdSe Nanocrystals, *J. Phys. Chem.*, 100 (1996) 468-471.
- [11] M. Dahan, S. Levi, C. Luccardini, P. Rostaing, B. Riveau, and A. Triller, Diffusion dynamics of glycine receptors revealed by single-quantum dot tracking, *Science*, 302 (2003) 442-445.
- [12] W. Jiang, B. Y. S. Kim, J. T. Rutka, and W. C. W. Chan, Nanoparticle-mediated cellular response is size-dependent, *Nat. Nanotechnol.*, 3 (2008) 145-150.
- [13] R. Hardman, A toxicologic review of quantum dots: toxicity depends on physicochemical and environmental factors, *Environ Health Perspect.*, 114 (2009) 165-172.

- 
- [14] A. Hezinger, J. Tessmar, and A. Goeperich, Polymer coating of Quantum Dots - A powerful Tool toward Diagnostics and Sensorics, *Eur. J. Pharm. Biopharm.*, in press (2007).
- [15] W. Fraunhofer, G. Winter, and C. Coester, Asymmetrical Flow Field-Flow Fractionation and Multiangle Light Scattering for Analysis of Gelatin Nanoparticle Drug Carrier Systems, *Analytical Chemistry*, 76 (2004) 1909-1920.
- [16] M. Bouby, H. Geckeis, and F. Geyer, Application of asymmetric flow field-flow fractionation (AsFIFFF) coupled to inductively coupled plasma mass spectrometry (ICPMS) to the quantitative characterization of natural colloids and synthetic nanoparticles, *Analytical and Bioanalytical Chemistry*, 392 (2008) 1447-1457.
- [17] B. Roda, A. Zattoni, P. Reschiglian, M. H. Moon, M. Mirasoli, E. Michelini, and A. Roda, Field-flow fractionation in bioanalysis: A review of recent trends, *Analytica Chimica Acta*, 635 (2009) 132-143.
- [18] B. H. Zimm, Apparatus and Methods for Measurement and Interpretation of the Angular Variation of Light Scattering; Preliminary Results on Polystyrene Solutions, *The Journal of Chemical Physics*, 16 (1948) 1099-1116.
- [19] T. Rameshwar, S. Samal, S. Lee, S. Kim, J. Cho, and I. S. Kim, Determination of the size of water-soluble nanoparticles and quantum dots by field-flow fractionation, *Journal of Nanoscience and Nanotechnology*, 6 (2006) 2461-2467.
- [20] W. W. Yu, L. Qu, W. Guo, and X. Peng, Experimental Determination of the Extinction Coefficient of CdTe, CdSe, and CdS Nanocrystals, *Chem. Mater.*, 15 (2003) 2854-2860.





# Chapter 6

## Cell-culture Characterization of Quantum Dots

W. Hild, J. Teßmar, M. Breunig, A. Göpferich

<sup>1</sup>Department of Pharmaceutical Technology, University of Regensburg,  
Universitätsstraße 31, 93040 Regensburg, Germany

**Abstract**

Quantum dots (QDs), semiconductor nanocrystals, offer outstanding fluorescence properties which render them ideal tools for studying interactions of nanoparticles with cells, such as specific binding or endocytosis. As the QDs have to be surface-modified in order to render them water-soluble and thus accessible for biological studies, a number of strategies for their hydrophilization have been developed. A promising solution for the hydrophilic coating of QDs is represented by poly(ethylene glycol)-modified phospholipids (PEG-PE). After reliable coating steps, this material forms dense layers of PEG on the QDs and offers a multitude of different functional groups that can be introduced on the surface of the QDs by choice. These groups enable versatile attachment of different biomolecules, like nanoparticle targeting to specific cells. To ensure that PEG-PE-QDs can be used for such purposes, we investigated their behavior under cell-culture conditions. Besides the colloidal stability, non-specific binding to cells as well as cytotoxicity was explored. While PEG-PE-QDs are stable during the investigations, toxicity remains a concern. However, PEG-PE-QDs can be used within a comfortable range of concentration without impairing cells (up to 500 nM). The results confirmed that PEG-PE-QDs are promising candidates for cellular investigations.

## Introduction

Quantum dots (QDs), semiconductor nanocrystals, have contributed essentially over the past several years in that we have been able to follow cellular processes with high resolution and high sensitivity over much longer periods of observation than when using conventional organic fluorophores [1-4]. This is possible through the paramount optical properties these nanocrystals exhibit. QDs provide us with strong fluorescence which is not extinguished by photobleaching over long spans of time [5], a disadvantage that organic fluorescent dyes suffer from. Moreover, QDs exhibit rather small sizes and thus are favorable to enter small pathways in cellular and intracellular targeting as well as organelle tracking [6-8].

Besides the favorable narrow size distributions and adequate optical properties *in vitro*, there are several requirements a QD-based colloid has to fulfil in order to be successfully used in biological investigations as a biomarker or model nanoparticle. Therefore, it is a logical prerequisite that the QDs are not only detectable *in vitro* but also in biological environments. The colloid has to exhibit sufficient stability under the conditions necessary for such investigations, i.e. in the presence of a cell culture medium containing high salt concentrations and proteins. In a huge number of experiments where QDs are used as a model particle of high detectability, cellular processes mediated by biomolecules are investigated. Such investigations include specific labeling and targeting of cell-surface structures with QDs decorated with peptides and proteins [9-11] or antibodies [12,13]. Of course, in these cases, non-specific interactions of the QDs with the target cells have to be excluded. Otherwise, the non-specific binding will dominate the specific one and thus undermine the initial idea of specific targeting. The introduction of poly(ethylene glycol) (PEG) onto the surface of QDs has been shown to be an effective tool for the reduction of such non-specific interactions [3,14,15]. Therefore, the QDs tested in this study have been coated with PEGylated phosphatidylethanolamines (PEG-PE). A final, but very important aspect is the biocompatibility of QDs [16-19]. Since these materials are usually composed of heavy metals, consideration must be given to whether these nanoparticles influence the viability of the cells to be investigated. Therefore, a range of concentration was determined, inside which QDs can be applied to cells safely. By measuring the differences in metabolic activity of CHO and MCF-7 cells after

exposition to PEG-PE-modified QDs using a MTT-assay, the concentration-dependent cytotoxicity of QDs was determined.

### **Materials and methods**

Cadmium oxide (CdO, 99.5% purity), hexadecylamine (HDA, tech. grade 90%), lauric acid (LA 98%), methanol (anhydr. 99.8%), sulfur (99.5%), toluene (anhydr. 99.8%), trioctylphosphine (TOP, tech. grade 90%), trioctylphosphine oxide (TOPO, tech. grade 90%) and zinc stearate (tech. grade) were obtained from Sigma-Aldrich (St. Louis, MO). 1,2-distearoyl-*sn*-glycero-3-phosphatidylethanolamine-*N*-[methoxy-(polyethylene glycol)-2000] (PEG-PE) of an average molecular weight of 2000 Da was obtained from Lipoid (Ludwigshafen, Germany). All cell-culture media and trypsin EDTA as well as fetal calf serum (FCS) were obtained from Sigma-Aldrich (St. Louis, MO). Phosphate buffered saline (PBS) was obtained by Invitrogen (Karlsruhe, Germany).

#### *Synthesis of CdSe/ZnS nanocrystals and PEG-PE coating*

CdSe/ZnS QDs were synthesized according to the methods described in chapter 3 of this thesis. Coating with PEG-PE was conducted as described in chapter 4. In brief, CdSe cores were grown in a mixture of TOPO and HDA (each 3.88 g) by quickly injecting the selenium precursor (2 mmol Se dissolved in 3.5 ml TOP) into the dissolved cadmium precursor consisting of 0.2 mmol CdO and 1.6 mmol lauric acid. After approx. 15 sec, the growth was stopped with toluene. The CdSe cores were isolated by precipitation with methanol and redissolved in the TOPO / HDA mixture. Shell growth was obtained by dropping a solution of 0.14 mmol sulfur in 3 ml of TOP together with 0.16 mmol zinc stearate over 1 h. After this, QDs were isolated as described above and redissolved in dichloromethane. To this solution, an excess of PEG-PE in dichloromethane was added and a film was formed after removing the solvent at reduced pressure, as described in chapter 4. The film was subsequently dissolved in water at 80 °C leading to PEG-PE-QDs. The QDs were finally purified using ultracentrifugation. The PEG-PE-QDs exhibited a fluorescence maximum at 533 nm which was ideal for the detection channels of the flow cytometer (see below).

*Size analysis of PEG-PE-QDs*

The size of the QDs was analysed by dynamic light scattering (DLS) in cell culture medium (HAM F-15), supplemented with 5 % FCS. For the measurement, a ZetaSizer 3000 HSA (Malvern, Worcestershire, UK), operating at 20 °C and at an angle of 90°, was used. Data was processed using the CONTIN algorithm [20] regarding number distributions.

*Cell culture*

Cell lines were cultivated in 75 cm<sup>2</sup> bottles at 37 °C, 5 % CO<sub>2</sub> and saturated humidity. Chinese hamster ovary (CHO) cells were grown in HAM F-15 medium supplemented with 10 % of FCS. MCF-7 cells were maintained in Minimum Essential Medium containing Earl's salts (EMEM).

*Observation of PEG-PE-QDs inside living cells*

PEG-PE-QDs in a concentration of 0.33 μM were injected into living CHO cells using a microcapillary and an injection unit consisting of InjectMan NI2 and FemtoJet (Eppendorf, Hamburg, Germany). The injection pressure was approx. 30-60 hPa and injection took up to 1 sec. 24 h after microinjection, cells were observed using a Zeiss Axiovert 200M inverted epifluorescence microscope coupled with a LSM 510 laser scanning device using the Axiovert software (Zeiss, Oberkochen, Germany). The PEG-PE-QDs were imaged upon excitation at 458 nm using a 505 nm longpass optical filter. Approx. 30 cells were treated while only few cells could be analyzed after the procedure.

*Flow-cytometric binding and uptake*

Cells were seeded into 24-well plates one day before the experiments and reached approx. 80 % confluence (approx. 80000 cells). Then, the medium was removed and cells were washed with PBS and the respective substances were added to the cells in the corresponding serum-free medium. The cells were incubated for 10 h, the substances were removed by suction and cells were washed with PBS. Then, the cells were detached using trypsin for 5 min. After this, the reaction was stopped with serum-containing medium and the cells were isolated by centrifugation for 5 min at

200 x g. After washing with PBS (4 °C) twice, the cells were resuspended in cold PBS (200 µl) and 0.5 µl of an aqueous solution of propidium iodide (1 mg/ml) was added. The cells were measured using a FACSCalibur flow cytometer (BD Biosciences, San Jose, CA). The QD signal was obtained by excitation with an Ar laser at 488 nm and detection in channel FL1-H (530 / 30 nm). Propidium iodide was detected upon excitation at 635 nm in the channel FL3-H (670 nm longpass). The results were analyzed using WinMDI 2.8. For the diagrams describing the toxicity as well as the binding and uptake, the population containing the whole cells was gated and a threshold slightly above the background signal (obtained by recording cells without dye or QDs for each channel) was set. All cells above the threshold were counted and correlated to the total number of gated cells.

#### *Cytotoxicity assay*

For the determination of the cytotoxicity, two cell lines (CHO, MCF-7) were used. Cells were grown in 96-well plates to 80 % confluence. For the experiments, the medium was removed and the serum-free medium for the respective cell type containing the sample was added. After 4 h of incubation time under the conditions described above, a solution of MTT (0.5 mg/ml) was added. Cells were incubated for another 2 h. Then, the medium was removed carefully and the cells were lysed using a 10 % solution of sodium dodecyl sulfate (SDS) in 0.1 N HCl. After gentle shaking, the samples were measured by a plate reader (Shimadzu, Duisburg, Germany) at 570 nm.

### **Results and discussion**

To ensure that the PEG-PE-QDs exhibited sufficient colloidal stability under the conditions applied for cellular studies, the QDs were incubated for 24 h in cell culture medium rich in serum proteins. Under these conditions, poorly stabilized nanoparticles usually tended towards aggregation due to electrostatic and van-der-Wals interactions. As shown in fig. 1, the particles maintained their size after incubation for 24 h in the serum-containing medium, as the size which was obtained before incubation and without serum (around 20 nm in hydrodynamic diameter), did not significantly change. The high stability of the QDs can be attributed to the steric stabilization caused by the PEG chains in the coating of the nanocrystals. Therefore,

the as prepared PEG-PE-QDs exhibited sufficient stability, at least for investigations over 24 h under cell culture conditions.

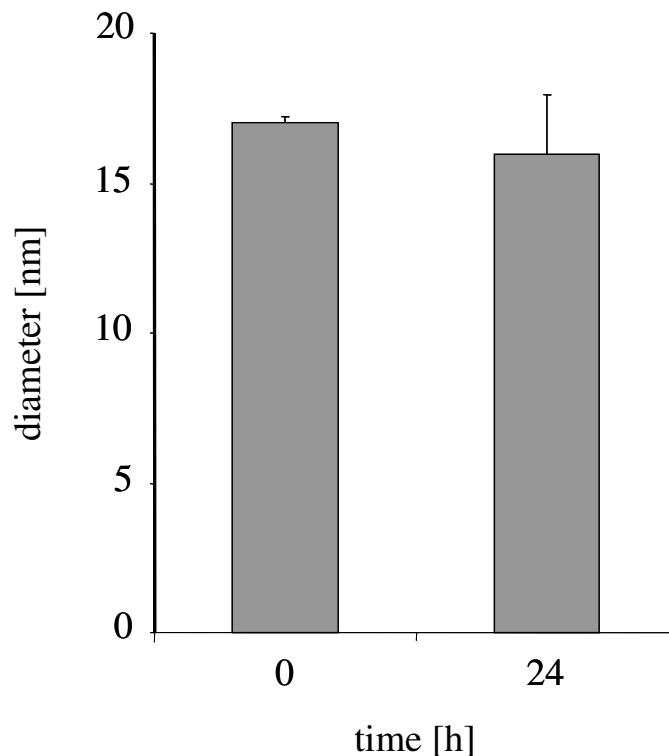


**Figure 1: Stability of PEG-PE-QDs under cell-culture conditions.** The QDs were investigated by DLS in cell culture medium before and after incubation for 24 h with 5% of serum. After 24 h, the colloid size shows no significant change. QDs remain stable under these conditions.

For many studies, QDs are used to follow the nanoparticle-uptake by cells. In the specific targeting of nanoparticles to distinct cell-types or even organs, the nanoparticles are connected with specific targeting molecules, such as peptides, proteins or antibodies [21]. *In order to investigate the detectability of the nanocrystals inside living cells*, the PEG-PE-QDs were microinjected into CHO cells. As depicted in fig. 2, the QDs are clearly visible inside the cytoplasm of the living CHO cells. Moreover, after 24 h of recovery time, which is necessary for the cells to overcome the harmful procedure of microinjection, the cells seem intact.

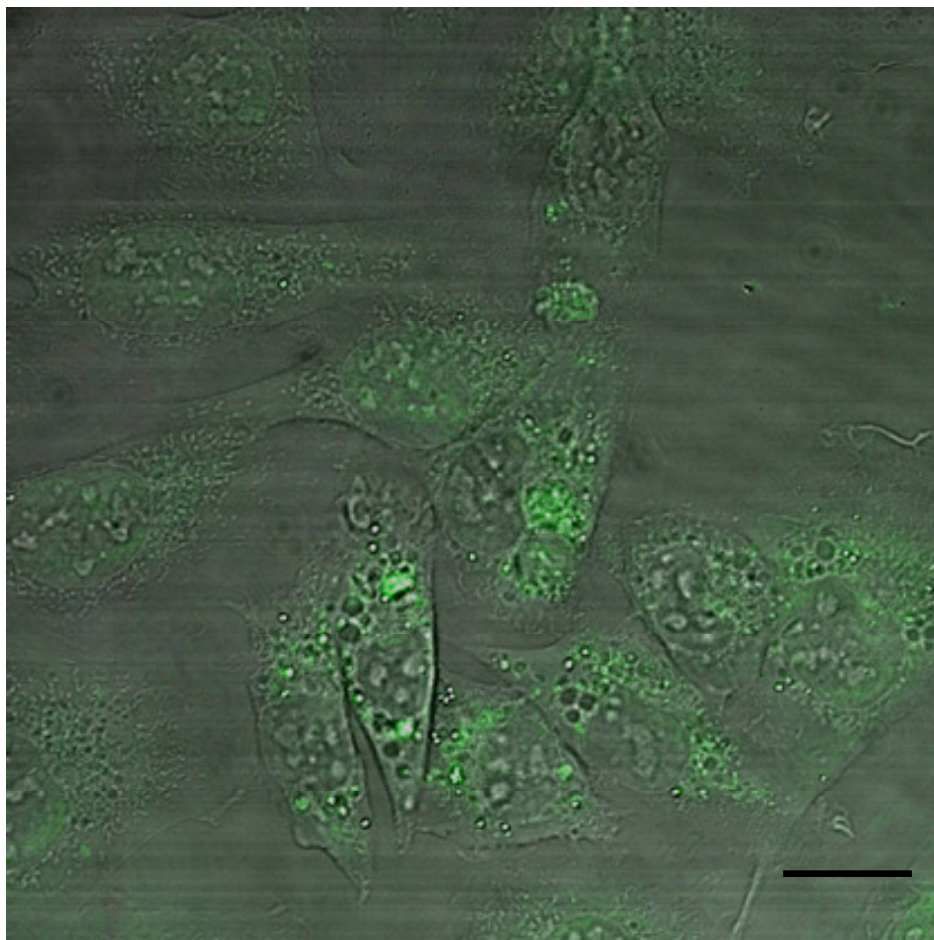


**Figure 2: Fluorescence micrograph of CHO cells after microinjection with PEG-PE-QDs.** After microinjection and 24 h of recovery time, the QDs are clearly visible inside the cytosol of the cells. This shows that the prepared QDs are detectable inside living cells and do not lead to extensive cell damage after 24 h. (Scale bar = 20  $\mu\text{m}$ ).

To investigate the extent of non-specific binding and uptake of the PEG-PE-QDs by the cells as well as eventual toxic effects of the QDs on the cells, CHO cells were incubated with increasing concentrations of PEG-PE-QDs (up to 10  $\mu\text{M}$ ) and were subsequently analyzed by flow cytometry. In order to make the eventual toxic effects of the QDs visible, the cells were stained with propidium iodide. This dye is able to penetrate the membranes of damaged cells and starts fluorescing when intercalating with DNA. Therefore, each cell exhibiting an increased dye signal was regarded as dead. Fig 3A compares the histograms of the fluorescence of control cells and the fluorescence of cells incubated with 1  $\mu\text{M}$  PEG-PE-QDs. Almost no shift in the



histogram is visible for the cells incubated with the QDs, indicating almost no non-specific binding and uptake. Fig 3B confirms this result as the ratio of the cells exhibiting increased QD-fluorescence in relation to all cells is very low, almost on the level of the control cells. It can be seen that increasing amounts of QDs lead to increased cytotoxicity as the cell viability of the regarded cell population is decreasing for higher concentrations. However, compared to the entire collective of the regarded whole cells, the viability of the cells remains high.

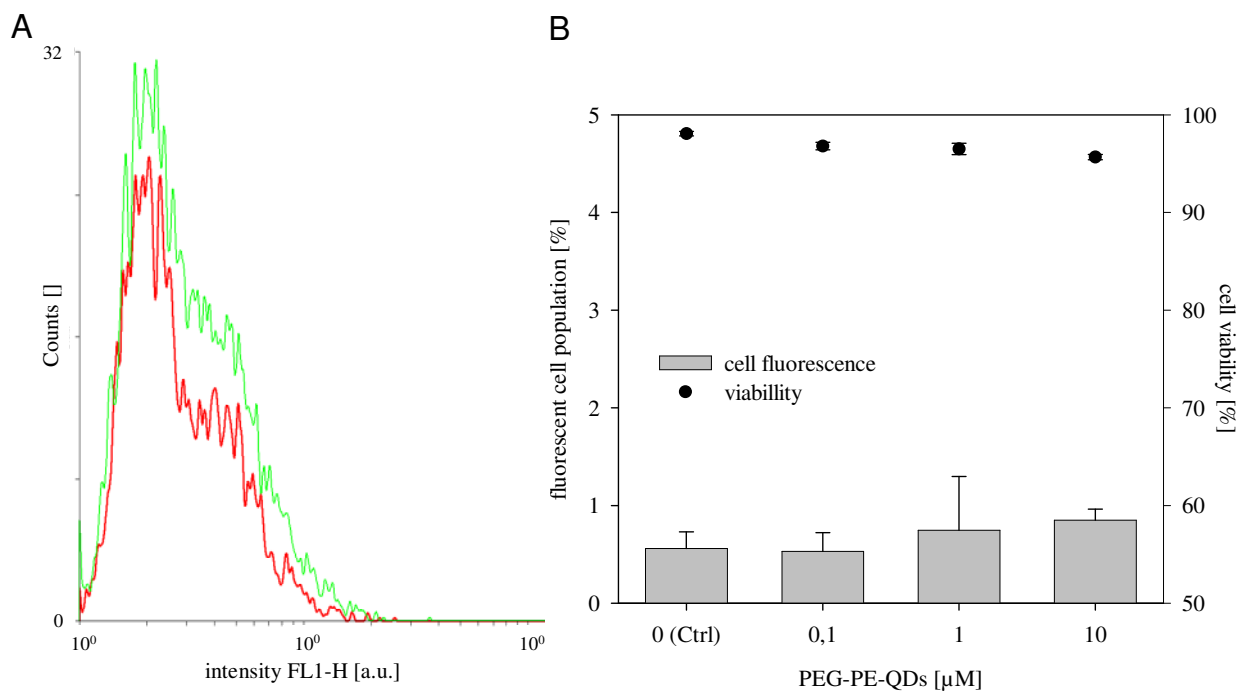


**Figure 3: Flow-cytometric analysis of non-specific binding and uptake of PEG-PE-QDs. (A)** Histogram of fluorescence intensity before (red) and after (green) incubation with 1  $\mu$ M PEG-PE-QDs. **(B)** Gated living cell population investigated with regard to QD-fluorescence and cell viability by staining with propidium iodide. Even high concentrations (10  $\mu$ M) show no significant non-specific binding or uptake as well as almost no loss of cell viability.

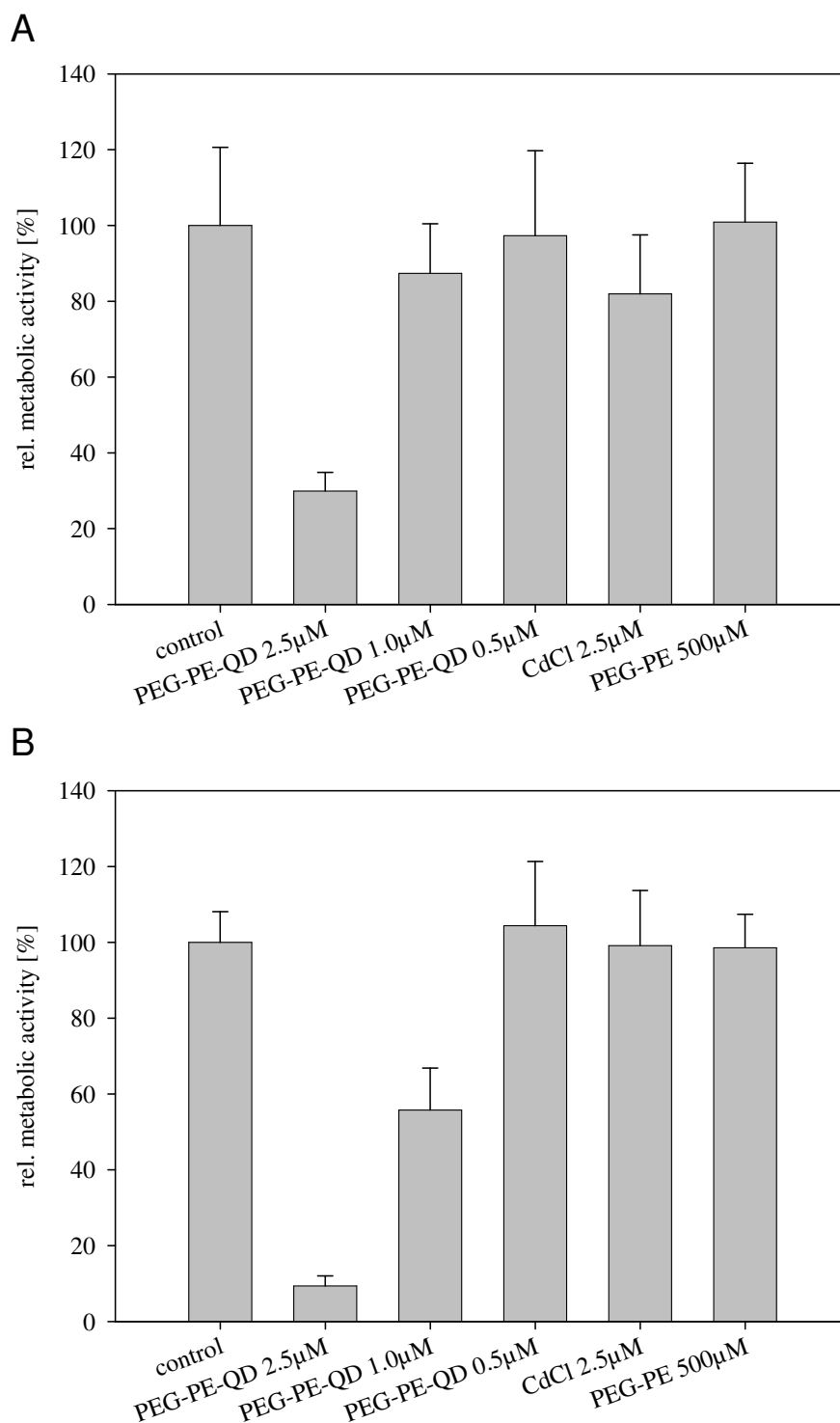


**Figure 4: Investigation of metabolic activity of cells after incubation with PEG-PE-QDs. (A)** CHO cells show reduced metabolic activity for higher PEG-PE concentrations (2.5 and 1.0  $\mu\text{M}$ ) but no significant decrease for 0.5  $\mu\text{M}$ . Interestingly, the control with 2.5  $\mu\text{M}$   $\text{CdCl}_2$  exhibits no significant stress on metabolic activity as well as excess of coating material (PEG-PE). **(B)** Similar results were obtained when using the MCF-7 cell line.

Besides the toxic effects which go along with the damage of cell membranes, the impairment of cells can also be recognized when looking at the metabolic activity. Measuring the metabolic activity is very sensitive in the determination of impairments of cells, as a decrease already occurs when the cells are morphologically not damaged and even when the cell membranes are still intact. When exploring nanoparticle targeting and controlled delivery into cells, it is important that the particles do not influence the physiology of the cells. To visualize the metabolic state of cells after the application of substances of eventual toxic properties, the MTT assay became state of the art [22,23]. In this assay, MTT is metabolized by the cells to a coloured formazan dependence of the metabolic activity of the cells. Fig. 4 shows the metabolic activity of CHO (A) and MCF-7 cells (B) after the application of increasing amounts of PEG-PE-QDs. While lower concentrations (0.5  $\mu\text{M}$ ) do not impair the metabolic activity of both cell-types compared to control cells, higher concentrations lead to a reduction. This concentration-dependent effect is not due to the surface coating of the nanocrystals, which is the layer of the particles that the cells have contact with, since excess of PEG-PE does not reduce the metabolic activity of both cell-types. Since CdSe/ZnS QDs consist of toxic elements, it has been suggested that the toxicity of QDs is to a large extent caused by the heavy metal they may release [24,25]. To investigate this, a control group consisting of 2.5 mM cadmium chloride was tested. Intriguingly, here the metabolic activity of the cells was not impaired during the time of the investigations. This result shows that there might be a toxic effect of the QDs themselves and not only of the materials they consist of. However, for cellular investigations, QDs are usually applied in concentrations below 100 nM [12,26,27]. Therefore, the range of concentration where PEG-PE-QDs can be used for such investigations is comfortable.

### **Summary and conclusion**

The results show that PEG-PE-QDs are very well suited for cellular investigations in cellular environments as they fulfil the major requirements of nanoparticles for such purposes. The QDs exhibit high stability under cell culture conditions and are almost free of non-specific interactions with cells, which renders them interesting model nanoparticles for drug targeting. Moreover, PEG-PE-QDs exhibit tolerable toxic effects and can be used in a wide range (below 500  $\mu\text{M}$ ) that is sufficient for the vast

majority of cellular assays. Together with the unique optical properties QDs offer, PEG-PE-QDs are a promising tool for the discovery of cellular uptake and targeting processes.

---

**References**

- [1] F. Pinaud, X. Michalet, L. A. Bentolila, J. M. Tsay, S. Doose, J. J. Li, G. Iyer, and S. Weiss, *Advances in fluorescence imaging with quantum dot bio-probes*, *Biomaterials*, 27 (2006) 1679-1687.
- [2] X. Michalet, F. F. Pinaud, L. A. Bentolila, J. M. Tsay, S. Doose, J. J. Li, G. Sundaresan, A. M. Wu, S. S. Gambhir, and S. Weiss, *Quantum Dots for Live Cells, in Vivo Imaging, and Diagnostics*, *Science*, 307 (2005) 538-544.
- [3] X. Gao, L. Yang, J. A. Petros, F. F. Marshall, J. W. Simons, and S. Nie, *In vivo molecular and cellular imaging with quantum dots*, *Curr. Opin. Biotechnol.*, 16 (2005) 63-72.
- [4] P. Alivisatos, *The use of nanocrystals in biological detection*, *Nat. Biotechnol.*, 22 (2004) 47-52.
- [5] I. L. Medintz, H. T. Uyeda, E. R. Goldman, and H. Mattoussi, *Quantum dot bioconjugates for imaging, labelling and sensing*, *Nat. Mater.*, 4 (2005) 435-446.
- [6] A. M. Derfus, A. A. Chen, D. H. Min, E. Ruoslahti, and S. N. Bhatia, *Targeted Quantum Dot Conjugates for siRNA Delivery*, *Bioconjugate Chemistry*, 18 (2007) 1391-1396.
- [7] A. M. Derfus, W. C. W. Chan, and S. N. Bhatia, *Intracellular delivery of quantum dots for live cell labeling and organelle tracking*, *Adv. Mater.*, 16 (2004) 961-966.
- [8] A. Hoshino, K. Fujioka, T. Oku, S. Nakamura, M. Suga, Y. Yamaguchi, K. Suzuki, M. Yasuhara, and K. Yamamoto, *Quantum dots targeted to the assigned organelle in living cells*, *Microbiol. Immunol.*, 48 (2004) 985-994.
- [9] M. Zhou, E. Nakatani, L. S. Gronenberg, T. Tokimoto, M. J. Wirth, V. J. Hruby, A. Roberts, R. M. Lynch, and I. Ghosh, *Peptide-Labeled Quantum Dots for Imaging GPCRs in Whole Cells and as Single Molecules*, *Bioconjugate Chemistry*, 18 (2007) 323-332.
- [10] M. Bruchez, Jr., M. Moronne, P. Gin, S. Weiss, and A. P. Alivisatos, *Semiconductor nanocrystals as fluorescent biological labels*, *Science*, 281 (1998) 2013-2016.
- [11] Y. Kim, A. M. Lillo, S. C. J. Steiniger, Y. Liu, C. Ballatore, A. Anichini, R. Mortarini, G. F. Kaufmann, B. Zhou, B. Felding-Habermann, and K. D. Janda, *Targeting Heat Shock Proteins on Cancer Cells: Selection, Characterization, and Cell-Penetrating Properties of a Peptidic GRP78 Ligand*, *Biochemistry*, 45 (2006) 9434-9444.
- [12] J. K. Jaiswal, H. Mattoussi, J. M. Mauro, and S. M. Simon, *Long-term multiple color imaging of live cells using quantum dot bioconjugates*, *Nat. Biotechnol.*, 21 (2003) 47-51.

- [13] D. S. Lidke, P. Nagy, R. Heintzmann, D. J. Arndt-Jovin, J. N. Post, H. E. Grecco, E. A. Jares-Erijman, and T. M. Jovin, Quantum dot ligands provide new insights into erbB/HER receptor-mediated signal transduction, *Nat. Biotechnol.*, 22 (2004) 198-203.
- [14] E. Chang, W. W. Yu, V. L. Colvin, and R. Drezek, Quantifying the influence of surface coatings on quantum dot uptake in cells, *J. Biomed. Nanotechnol.*, 1 (2005) 397-401.
- [15] E. L. Bentzen, I. D. Tomlinson, J. Mason, P. Gresch, M. R. Warnement, D. Wright, E. Sanders-Bush, R. Blakely, and S. J. Rosenthal, Surface Modification To Reduce Nonspecific Binding of Quantum Dots in Live Cell Assays, *Bioconjug. Chem.*, 16 (2005) 1488-1494.
- [16] R. Hardman, A Toxicologic Review of Quantum Dots: Toxicity Depends on Physicochemical and Environmental Factors, *Environ Health Perspect.*, 114 (2006) 165-172.
- [17] W. h. Chan and N. h. Shiao, Cytotoxic effect of CdSe quantum dots on mouse embryonic development, *Acta Pharmacol Sin*, 29 (2008) 259-266.
- [18] A. M. Derfus, W. C. W. Chan, and S. N. Bhatia, Probing the Cytotoxicity of Semiconductor Quantum Dots, *Nano Lett.*, 4 (2004) 11-18.
- [19] A. Hoshino, K. Fujioka, T. Oku, M. Suga, Y. F. Sasaki, T. Ohta, M. Yasuhara, K. Suzuki, and K. Yamamoto, Physicochemical Properties and Cellular Toxicity of Nanocrystal Quantum Dots Depend on Their Surface Modification, *Nano Lett.*, 4 (2004) 2163-2169.
- [20] S. W. Provencher, CONTIN: A general purpose constrained regularization program for inverting noisy linear algebraic and integral equations, *Computer Physics Communications*, 27 (1982) 229-242.
- [21] W. A. Hild, M. Breunig, and A. Goepferich, Quantum dots - Nano-sized probes for the exploration of cellular and intracellular targeting, *Eur. J. Pharm. Biopharm.*, 68 (2008) 153-168.
- [22] A. Cory, T. Owen, J. Barltrop, and J. Cory, Use of an aqueous soluble tetrazolium/formazan assay for cell growth assays in culture, *Cancer Commun.*, 3 (1991) 207-212.
- [23] L. Wang, D. Nagesha, S. Selvarasah, M. Dokmeci, and R. Carrier, Toxicity of CdSe Nanoparticles in Caco-2 Cell Cultures, *Journal of Nanobiotechnology*, 6 (2008) 11.
- [24] K. G. Li, J. T. Chen, S. S. Bai, X. Wen, S. Y. Song, Q. Yu, J. Li, and Y. Q. Wang, Intracellular oxidative stress and cadmium ions release induce cytotoxicity of unmodified cadmium sulfide quantum dots, *Toxicology in Vitro*, 23 (2009) 1007-1013.
- [25] J. M. Tsay and X. Michalet, New Light on Quantum Dot Cytotoxicity, *Chemistry & Biology*, 12 (2005) 1159-1161.

- [26] W. J. Parak, R. Boudreau, M. Le Gros, D. Gerion, D. Zanchet, C. M. Micheel, S. C. Williams, A. P. Alivisatos, and C. Larabell, Cell motility and metastatic potential studies based on quantum dot imaging of phagokinetic tracks, *Adv. Mater.*, 14 (2002) 882-885.
- [27] S. H. Young and E. Rozengurt, Qdot nanocrystal conjugates conjugated to bombesin or ANG II label the cognate G protein-coupled receptor in living cells, *Am. J. Physiol.*, 290 (2006) C728-C732.





# Chapter 7

## G-Protein Coupled Receptor Targeted Micelles

W. Hild<sup>1</sup>, A. Caporale<sup>2</sup>, C. Cabrele<sup>2</sup>, E. Hochmuth<sup>3</sup>, J. Teßmar<sup>1</sup>, M. Breunig<sup>1</sup>,  
A. Göpferich<sup>1</sup>

<sup>1</sup>Department of Pharmaceutical Technology, University of Regensburg,  
Universitätsstraße 31, 93040 Regensburg, Germany

<sup>2</sup>Department of Pharmaceutical and Medicinal Chemistry, University of  
Regensburg, Universitätsstrasse 31, 93040 Regensburg, Germany

<sup>3</sup>Institute of Biochemistry, Microbiology and Genetics, Universitätsstraße 31,  
93040 Regensburg, Germany

**Abstract**

Targeted nanoparticle delivery to specific cells bears a high potential in diagnostics and drug therapy and has been in the focus of biomedical research for the past decade. However, for further progress in this field of research, establishing new targeting-strategies is necessary, since the number of relevant cell-surface targets that have proven useful so far is still highly limited. Up to now, G-protein coupled receptors (GPCRs), the largest class of receptors in humans, have hardly been investigated for nanoparticle targeting, though they do play a predominant role in modern drug therapy. For these receptors, numerous specific ligand-receptor combinations are known which could be exploited for cellular drug targeting.

To gain access to this class of receptors, we investigated whether the human neuropeptide Y (NPY) Y<sub>1</sub> receptor can serve as a model receptor for the active targeting of polymeric micelles to cells. Therefore, an analog of the porcine NPY was immobilized on micelles consisting of poly(ethylene glycol)-modified phospholipids (PEG-PE) as a model delivery system. The targeted micelles were finally tested in cell culture using the human breast cancer cell-line MCF-7 which expresses the corresponding NPY Y<sub>1</sub> receptor, to see whether GPCRs serve as a portal for micelle-based cellular delivery. The results show that highly specific delivery of the peptide-targeted micelles into cells is possible. By virtue of this targeting strategy it is obvious that these and similar constructs could be used to transport therapeutically relevant molecules into cells comprising of the respective GPCR of interest.

## Introduction

Targeted delivery of nanoparticles and other colloids to specific cells and tissues is of key interest in biomedical research [1-3]. Strategies in this field comprise of passive and active targeting principles. Though colloids can passively be accumulated in cancerous tissues due to their favored size, an effect also known as enhanced permeability and retention (EPR) [4], active targeting remains the more specific form of targeting. Here, cell-specific ligands mediate the binding of the nanoparticles to their target cells, preferably to cell-surface receptors, while binding to other cells that lack such receptors is ideally avoided [5,6]. Regarding such cell-surface receptors, only a few promising targets have been discussed so far, like the folic acid- [7], the transferrin- [8] or growth factor receptors [9]. However, all of these receptors are expressed in a variety of different tissues. Recent research has shown that G-protein coupled receptors (GPCRs) have high potential in mediating specific cellular uptake of nanoparticles [10]. Since knowledge about the distribution of these receptors in the body is broad, this largest class of receptors with approx. 800 different members represents a highly interesting class of cell surface target [11]. Unfortunately, these studies were carried out using quantum dots that do not allow for incorporation of a drug substance. Therefore, we were looking for an alternate model carrier consequently we identified micellar systems [12,13]. They offer several advantages: their preparation is quite facile, their surface chemistry can easily be modified by their monomer composition and they exhibit small sizes, which is important for reaching the target tissues *in vivo*. Moreover, diagnostic as well as therapeutic active entities [14] can be incorporated into micelles, which allows for the handling of otherwise poorly deliverable drugs of unfavorable physico-chemical or toxic properties [15,16]. To prove the concept of intracellular delivery of polymeric micelles mediated by GPCRs, we conjugated an analog of the porcine neuropeptide Y (pNPY) to PEGylated phospholipid (PEG-phosphatidylethanolamine, PEG-PE) micelles. The corresponding GPCR – the human NPY Y<sub>1</sub>-receptor – exhibits an incidence of 85% in breast carcinoma and 100% of their lymph node metastases [17]. Therefore, a micelle-based delivery system targeting these receptors also exhibits a high therapeutic potential since micelles have already successfully been used for the incorporation of anti-tumor agents and showed a promising therapeutic profile [16,18]. In order to design targeted PEG-PE micelles, we established an effective

protocol for the attachment of the peptidic ligand using specific conjugation chemistry based on the reaction of thiols with maleimides. Finally, we investigated whether labeled PEG-PE micelles were specifically delivered into human breast cancer cells expressing the NPY Y<sub>1</sub>-receptor by confocal laser scanning microscopy to examine the potential of such targeted micelles as a potential drug delivery system.

## Materials and Methods

### *Materials*

The phospholipids used in this study consisted of 1,2-distearoyl-sn-glycero-3-phosphatidylethanolamine which was covalently linked to poly(ethylene glycol) (PEG) of 2000 Da, and are referred to as PEG-PE. Two different kinds of PEG-PE were used, the first exhibited non-reactive methoxy-groups at the end of the PEG chain and was obtained from Lipoid (Ludwigshafen, Germany); the second class of PEG-PE contained reactive amino-PEG and was purchased from Avanti Polar Lipids (Alabaster, AL) and is referred to as amino-PEG-PE. Acetone, 5(6)-carboxytetramethylrhodamine *N*-succinimidyl ester (TAMRA-NHS), fluorescamine, cysteine, sulfosuccinimidyl-4-(*N*-maleimidomethyl)-cyclohexane-1-carboxylate (sulfo-SMCC) and trifluoroacetic acid (TFA) were purchased from Sigma-Aldrich (St. Louis, MO). Acetonitrile (ACN) in HPLC grade was obtained from Merck (Darmstadt, Germany). For all reactions, water purified by a Millipore system was used.

### *Peptide synthesis*

The peptide [Lys<sup>4</sup>(<sup>α</sup>N-Acetyl-Cys), Arg<sup>6</sup>, Pro<sup>34</sup>]-pNPY (Cys-NPY) was synthesized by standard automated solid phase synthesis and exhibited the sequence of the porcine neuropeptide Y (pNPY), with two amino acid exchanges in position 6 and 34 by Arg and Pro [19]. In position 4, an additional cysteine side-chain was introduced for the bioconjugation with the PEG-PE micelles. The sequence of the peptide was *H*-YPSK(Ac-*N*-C)PRNPGEDAPAEDLARYYSALRHYINLITRPRY-*NH*<sub>2</sub>. The mass was confirmed by MALDI-Tof using an  $\alpha$ -cyano-4-hydroxycinnamic acid (HCA) matrix (calculated mass: 4409 Da; found mass: 4412 Da). For a detailed synthesis protocol, see [10].

*Micelle preparation*

The micelles used in all of the studies were prepared by dissolving 6 parts of PEG-PE and 1 part of amino-PEG-PE in the corresponding medium. All reactions were carried out in 1.5 ml standard reaction vessels (Eppendorf, Hamburg, Germany). For the establishment of the bioconjugation reaction, 2.3 mg of the lipid mixture (corresponding to 0.12  $\mu\text{mol}$  amino-PEG-PE) and 0.15 mg of sulfo-SMCC (0.34  $\mu\text{mol}$ ) were each dissolved in 50  $\mu\text{l}$  of water and transferred into 100  $\mu\text{l}$  of 50 mM phosphate buffered saline (PBS) at pH 7.2, 7.5 and 8.0, respectively, to yield a final buffer capacity of 50 mM. After 30 min of shaking, the reaction mixture was purified by gel filtration chromatography (GFC) as described below. The fraction containing the micelles was then collected and immediately frozen by submerging it into liquid nitrogen to avoid hydrolysis of the maleimides. Subsequently, the samples were freeze-dried using a Beta 2-16 lab-scale freeze-drier from Christ (Osterode am Harz, Germany) operating at  $-20\text{ }^{\circ}\text{C}$  and 0.12 mbar overnight. After this, 1 mg of the samples (approx. 5.2  $\mu\text{M}$ ) was dissolved in 50 mM PBS, and a 3-fold molar excess of lysine (2.3  $\mu\text{mol}$ , calculated for the theoretical number of maleimides) in the same buffer was added and reacted for 12h to investigate the reactivity of the maleimide-modified micelles since the amino group of lysine is accessible for an amine group assay (see below). The final products were again purified by GFC and freeze-dried, as described above.

For the conjugation of the micelles with the Cys-NPY, to yield NPY-PEG-PE, mixed PEG-PE micelles were reacted with sulfo-SMCC at pH 7.2 and purified as described above. Thereafter, the activated PEG-PEs were dissolved in 300  $\mu\text{l}$  of PBS pH 7.2 containing 30% acetonitrile to a concentration of 1 mg/ml, and an equimolar amount of the Cys-NPY dissolved in a small amount of the same buffer was added, followed by shaking of the mixture for 12 h. After incubation, the final product (Cys-NPY-PEG-PE) was obtained after GFC and freeze-drying (see above).

Dye-labeled PEG-PE (TAMRA-PEG-PE) was prepared by reacting 7 mg of mixed micelles (corresponding to 0.56  $\mu\text{mol}$  amino-PEG-PE) in 500  $\mu\text{l}$  PBS pH 7.4 with 0.5 mg (0.95  $\mu\text{mol}$ ) TAMRA-NHS for 30 min. After this, the micelles were purified by GFC and freeze-dried as described above.

*Gel filtration chromatography (GFC)*

Gel filtration was conducted using a Sephacryl S-100 resin packed into a Tricorn 10/300 column (GE Healthcare, Chalfont St. Giles, UK). The column was coupled to standard HPLC equipment (Shimadzu, Duisburg, Germany) operating in the isocratic mode at a flow rate of 0.5 ml/min. The mobile phase consisted of 30% acetonitrile in water with the addition of 0.1% trifluoroacetic acid. A SPD-10 AV UV-detector (Shimadzu, Duisburg, Germany) recorded the absorbance at a wavelength of 220 nm.

*Size determination*

PEG-PE micelles were imaged by cryo-transmission electron microscopy (cryo-TEM). For sample preparation, a few microliters of a dilute solution of PEG-PE were transferred onto a 600 mesh copper grid (Plano, Wetzlar, Germany). After the removal of excess liquid by suction, the sample was quickly frozen in liquid ethane in a cryo-box. The sample was mounted on a cryo-transfer holder (CT 3500, Gatan, Munich) and measured using a Zeiss EM 922 EFTEM (ZeissNTS, Oberkochen, Germany), operated at 200 kV and around 90 K.

The hydrodynamic diameter of the mixed PEG-PE micelles was determined by dynamic light scattering (DLS) using a ZetaSizer 3000 HSA (Malvern, Worcestershire, UK) at 20 °C and an angle of 90°. Data was processed using the CONTIN algorithm [20].

*Determination of amines*

The mixed PEG-PE micelles containing free primary amines were analyzed after preparation and went through the same GFC purification route like as the products. The colloid was also analyzed after the reaction with sulfo-SMCC and the coupling with lysine as well, in order to investigate the conversion. Therefore, the corresponding lipids, modified or unmodified, were dissolved at a concentration of approx. 7 mg/ml in water. 5 µl of the sample was added to 135 µl of 50 mM borate buffer pH 8.5 and 60 µl of a 1 mM solution of fluorescamine in acetone. Fluorescence was determined in 96 well-plates directly after the addition of the fluorescamine using a LS 55 fluorescence spectrometer from PerkinElmer (Waltham, MA) equipped with a

plate reader unit (excitation at 390nm, emission at 475nm). The fluorescence intensity was correlated to the theoretical mass of the lipids.

#### *Matrix assisted laser desorption ionization (MALDI)*

For the determination of the mass, equal volumes of the Cys-NPY-PEG-PE samples in a concentration of 4 mg/ml and a saturated matrix solution were cocrystallized. A matrix consisting of  $\alpha$ -cyano-4-hydroxycinnamic acid (CHCA) in 50% acetonitrile with the addition of 0.1% TFA was used. The mass spectra were obtained using a 4700 proteomics Analyzer MALDI-ToF/ToF mass spectrometer (Applied Biosystems, Foster City, CA), operating in the linear mode.

#### *Cell culture and cellular uptake studies*

The human breast cancer cell line MCF-7 was cultivated in Minimum Essential Medium containing Earl's salts (EMEM) supplemented with 5% of foetal bovine serum (FBS) at 37 °C in an atmosphere of 95% humidity and 5% CO<sub>2</sub>.

Before the observations by confocal laser scanning microscopy (CLSM), MCF-7 cells were seeded into 8-well  $\mu$ -slides (Ibidi, Munich, Germany) in a density of 5000 cells / chamber and incubated for 48 h with the addition of 1 nM estradiol to increase the amount of Y<sub>1</sub>-receptors on the cells [21]. For the investigation of specific micelle uptake by the cells, TAMRA-labeled micelles were prepared by dissolving PEG-PE (1 mg/ml) and TAMRA-PEG-PE (0.05 mg/ml) in water. Labeled micelles containing Cys-NPY were prepared by adding 0.1 mg/ml of NPY-PEG-PE to the labeled micelles. 10  $\mu$ l of both kinds of labeled micelles was added to 150  $\mu$ l of incubation medium containing EMEM medium supplemented with 1% BSA and 0.01% of bacitracin and incubated at 37 °C for 30 min. The cells were washed with PBS and again exposed to a sample-free incubation medium. The living cells were imaged at 37 °C using an Axiovert 200M inverted epifluorescence microscope coupled with a LSM 510 laser scanning device using Axiovert Software (Zeiss, Oberkochen, Germany), using a Plan-Apochromat X40 water-immersion objective with a numerical aperture of 1.2. The labeled micelles were excited at 543 nm and dye-emission was measured using a 560-615 nm band-pass filter. The thickness of the optical sections was below 1  $\mu$ m. Image data was processed using ImageJ 1.42q [22].

## Results and discussion

In order to be used as an adequate delivery system for the delivery into specific cells, small sizes and uniform size-distributions are a crucial prerequisite [23]. To investigate this, the PEG-PE micelles were analyzed by TEM and DLS. The data suggests that PEG-PE micelles represent an almost ideal colloid due to their outstanding uniformity. As depicted in fig. 1A, the micelles display a very uniform shape in TEM images. The micelles exhibit a diameter of approx. 13 nm which supports the results obtained by DLS which revealed an average size of  $13.7 \pm 0.6$  nm and a polydispersity index of  $0.15 \pm 0.03$  (fig. 1B). This shows that the colloid should be small enough for entering cellular uptake pathways, like receptor-mediated endocytosis [24,25].

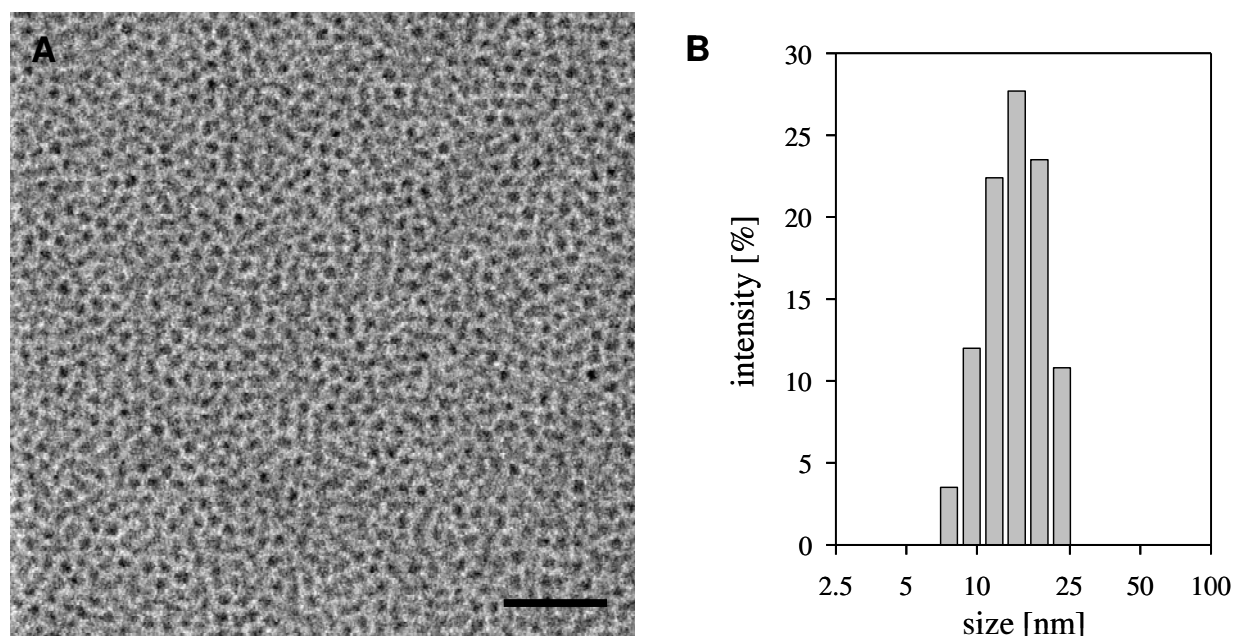


**Figure 1: Size analysis of PEG-PE micelles.** (A) Cryo-TEM micrograph of PEG-PE in water showing uniform, spherical micelles. (B) Size distribution, determined by DLS (average size:  $13.7 \pm 0.6$  nm; polydispersity: index  $0.146 \pm 0.024$ ).

Since the micelles are not only in pure water but also in various solvent mixtures as well as cell culture media for their preparation and their later biological testing, respectively, it was investigated whether the micelles show sufficient stability in various environments. Therefore, the micelles were exposed to aqueous solutions of ACN with and without addition of TFA, to PBS buffer (needed for the bioconjugation reaction later on), as well as to culture media lacking and containing serum proteins



and were analyzed by DLS (fig. 2). The results show sizes similar to the ones obtained in water and a moderate increase in polydispersity. Interestingly, when using ACN, the addition of TFA was necessary to keep the micellar structures needed for the GFC purification later on. The high stability in these different media, especially in the serum-containing medium, can be attributed to the PEG-shielding of the PEG-PE micelles which minimized the adsorption of proteins. Therefore, the colloid is suitable for modification under various conditions as well for the cellular drug targeting studies.

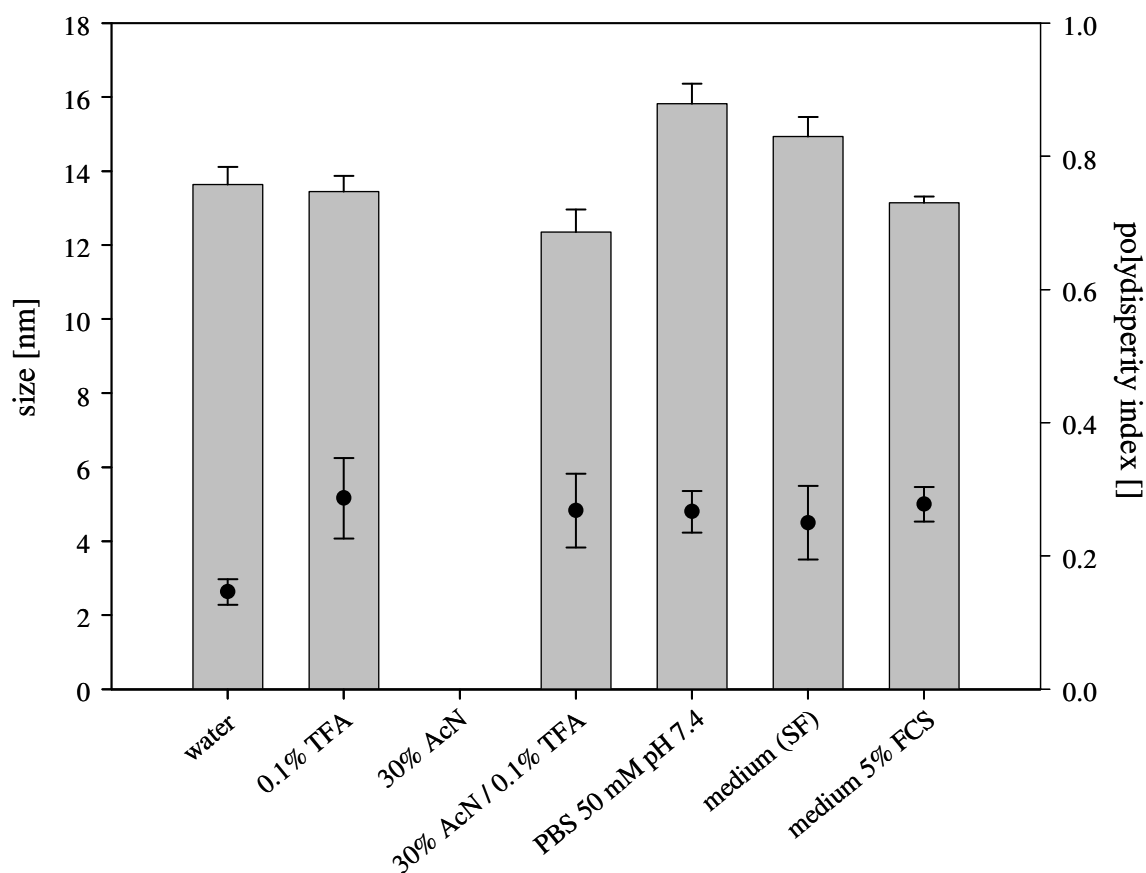


**Figure 2: Formation of PEG-PE micelles in different media.** The micelles show good stability under various conditions, like aqueous TFA / acetonitrile solutions, PBS buffer and also cell-culture medium. The colloid size (bars) remains constant. The polydispersity index (●) decreases in solvents different from pure water but remains low.

In the following approaches we investigated, how the PEG-PE micelles can be coupled effectively with a peptidic agonist of the  $Y_1$ -receptor (Cys-NPY). The conjugation using maleimide-thiol couplings is especially favorable, since maleimides

react very selectively with thiols. Therefore, Cys-NPY could selectively be attached to the micelles at a position in the peptide sequence where modifications are well-tolerated which was the lysine side-chain [10,26] that was acylated by an additional cysteine. Another advantage is the low size of the small-molecular thiol-reactive linkers, compared to bulky streptavidin molecules (over 60 kDa [27]). Fig. 3 shows the reaction scheme of the conjugation of PEG-PE micelles (fig. 3, 1) to thiol-containing molecules by using the hetero-bifunctional crosslinker sulfo-SMCC. In this two-step reaction, first the amine-containing micelles are activated by the crosslinker forming a stable amide bond. After purification by gel filtration to remove excess crosslinker and subsequent freeze drying, the activated PEG-PE (fig. 3, 2) is then reactive towards thiol groups yielding stable covalent conjugates (fig. 3, 3).

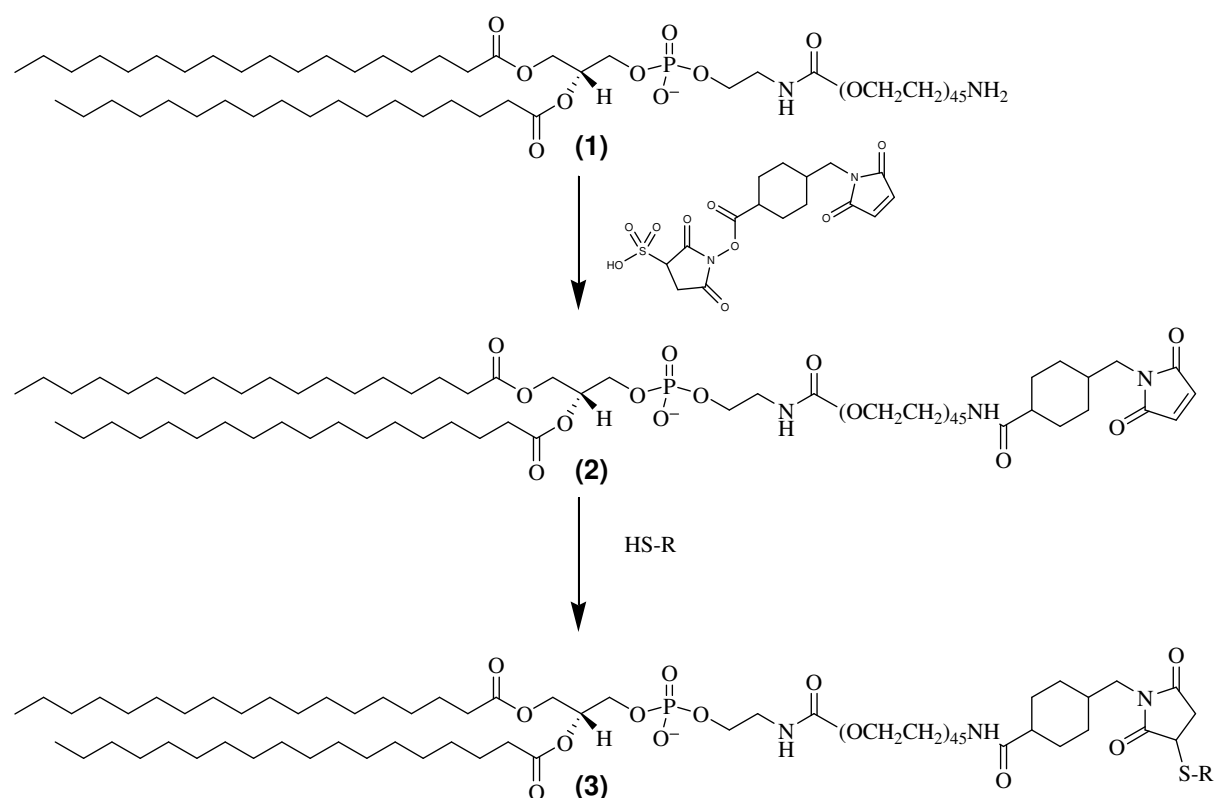


**Figure 3: Reaction scheme of the bioconjugation of PEG-PE micelles with amino acids or peptides.** The activation of the micelles containing amino-PEG with the crosslinker sulfo-SMCC renders the colloid thiol-reactive (1). The activated PEG-PE then is reacted with thiol-containing molecules (cysteine or Cys-NPY) to form a stable covalent conjugate (2).

To obtain conditions that allow for an effective coupling, the conversion of each step of the reaction was analyzed by an amino-group assay. For this purpose, the micelles were activated by sulfo-SMCC at mild basic conditions (pH 7.2, 7.5, 8.0). Then the remaining amines of the micelles that had not reacted with the crosslinker were analyzed by the amino group assay using fluorescamine and by detecting the fluorescence of the product during GFC (fig. 4). As expected, the more basic the reaction medium the lower the amount of unreacted amines was. To investigate at which pH the maleimide of the thus activated micelles is kept most reactive, these micelles subsequently were reacted with cysteine and again assayed using fluorescamine and GFC. All of the three differently activated micelles had reacted with the thiol-containing amino acid as the fluorescence due to fluorescamine increased significantly. However, when the activation step was carried out at pH 7.2, the highest yields were obtained, though the yield of the first step was the lowest. The reason for this is the hydrolysis of the maleimide that increases at increasing pH. Thus, the optimal pH for the activation reaction was 7.2.

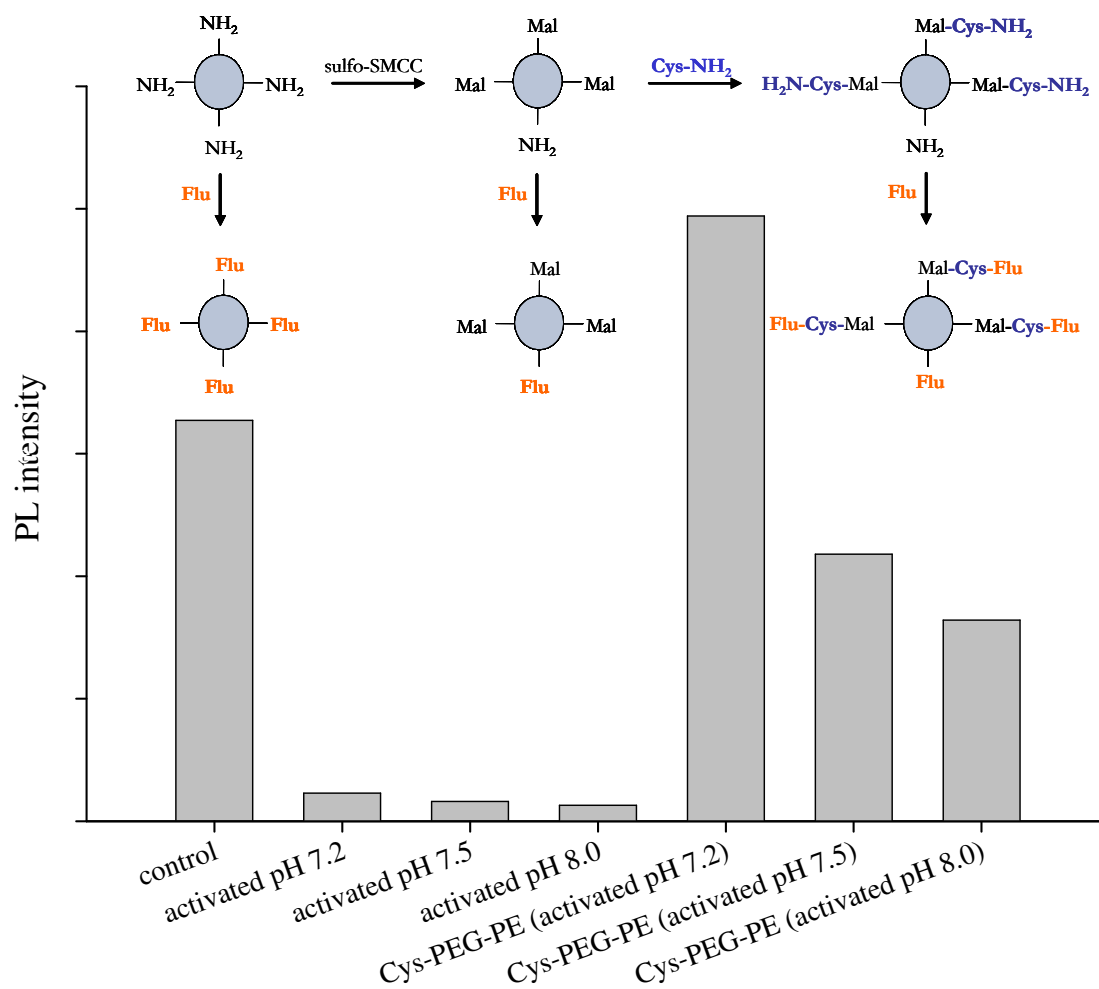


**Figure 4: Observation of the efficacy of the bioconjugation at different pH values.** The above reaction scheme shows how the amino-PEG containing PEG-PE micelles are activated using sulfo-SMCC and how the activated colloid then is conjugated to cysteine. Each species is converted with fluorescamine to determine the free amines. The graph shows the fluorescence intensity per mg of PEG-PE after conversion of the free amines with fluorescamine. After a decrease of the amines due to the conversion with sulfo-SMCC (more efficient at higher pH) the amines increase due to the reaction of the activated colloid with cysteine at pH 7.2. The highest overall conversion can be found when the colloid was activated at pH 7.2.

Subsequently, we investigated the conjugation of Cys-NPY under the optimized conjugation conditions. To this end, the PEG-PE micelles were activated with sulfo-SMCC at pH 7.2 and the colloid was then purified by GFC. The corresponding chromatogram is shown in fig. 5. A very weak signal was recorded for the activated PEG-PE micelles. However, after the reaction with Cys-NPY, the corresponding GFC chromatogram shows a clear increase in absorbance at the first peak which represents the colloid (fig. 5). This clearly shows that the peptide was conjugated successfully to the PEG-PE micelles.

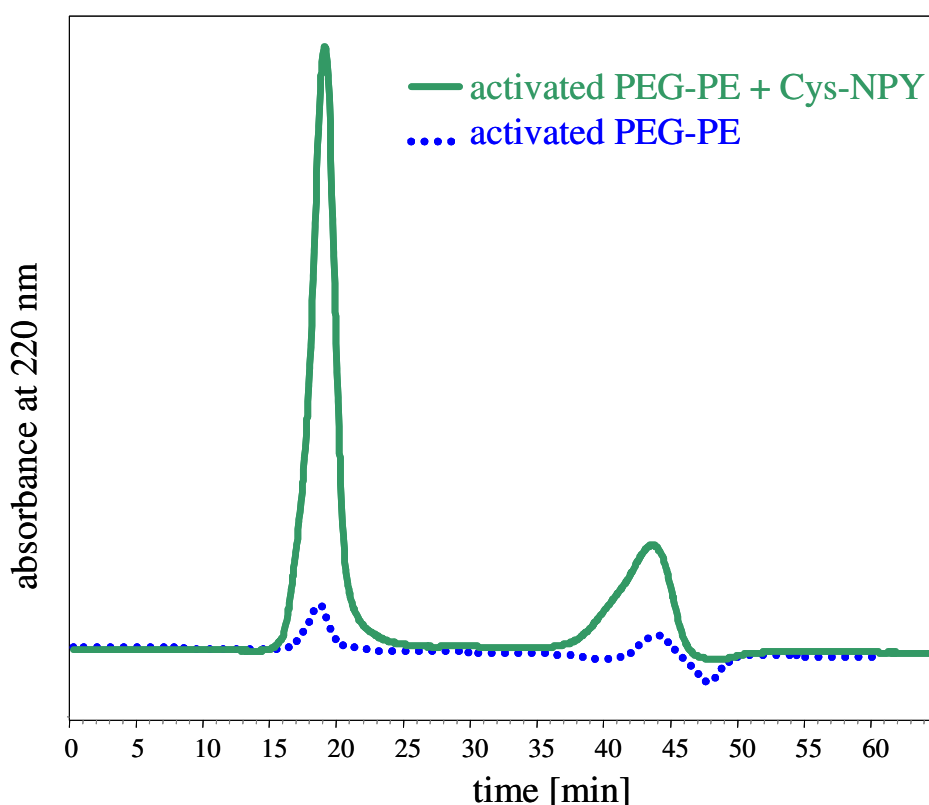


**Figure 5: Gel filtration chromatograms of PEG-PE micelles before and after bioconjugation.** The first chromatogram (....) shows the PEG-PE micelles gained by UV-detection at 220 nm after activation with sulfo-SMCC (1<sup>st</sup> peak) and excess of the crosslinker (2<sup>nd</sup> peak). The second chromatogram (—) represents the micelles after conjugation with the peptide. The signal of the 1<sup>st</sup> peak is clearly increased indicating a successful bioconjugation, while the second peak shows non-reacted peptide.

In order to investigate whether the association of the peptide with the PEG-PE is based on a covalent linkage and not only due to adsorption of the peptide to the micelles, mass analysis of the peak corresponding to the PEG-PE-peptide conjugate was performed. Mass analysis using MALDI-ToF was possible for the PEG-PE micelles, since the phospholipids form non-covalent micelles in aqueous environments. The mass spectrum in fig. 6 shows the unmodified PEG-PE (left) exhibiting a molar mass of around 2600. The broad peak corresponds to the mass distribution caused by the different molecular mass distribution of the PEG chains. The same pattern can be found for the conjugate. Here, the mass corresponding to the sum of PEG-PE, the linker part and the peptide was found to be around 7400 Da. Therefore, it is evident that the bioconjugation reaction between the colloid and the peptide yielded a covalent product.

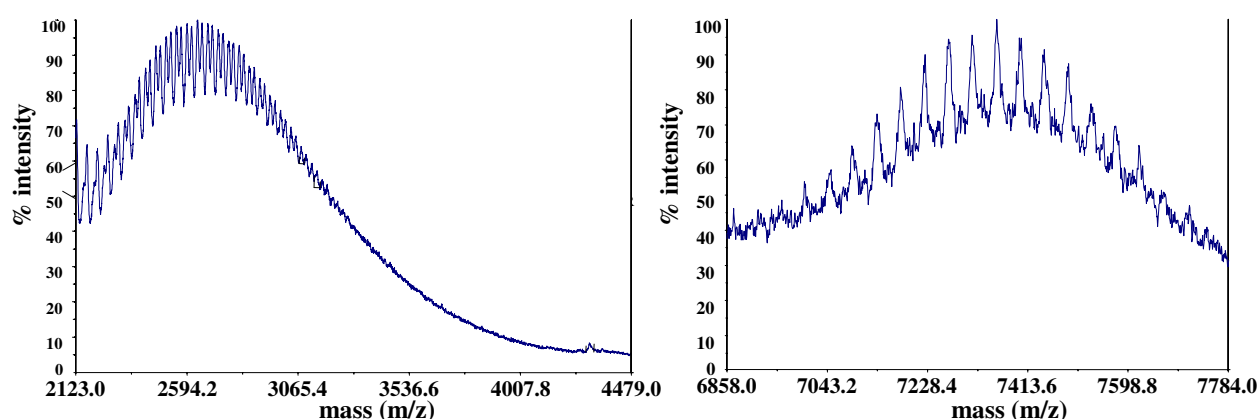


**Figure 6: Mass spectrogram of the PEG-PE micelles conjugated to the Cys-NPY.** The lower masses at 2600 Da represent the non-functionalized part of the micelles (left) while the higher masses at a mean of approx 7400 Da are due to the bioconjugate (right).

In order to investigate the specific uptake of the NPY-PEG-PE micelles by cells expressing the NPY  $Y_1$ -receptor, the NPY-PEG-PE micelles were labeled by integrating TAMRA-labeled PEG-PE molecules into the micelles. To follow cellular uptake, the  $Y_1$ -receptor positive human breast cancer cell line MCF-7 was imaged after incubation with the labeled micelles. The TAMRA-labeled micelles without the targeting ligand Cys-NPY showed no affinity towards the target cells under the confocal fluorescence microscope. Non-specific uptake was effectively reduced, due to the PEG-shielding of the micelles (fig. 7A). In contrast, when the micelles

contained NPY-PEG-PE, delivery into the target cells took place. As can be seen in fig. 7B, the cells then showed fluorescence due to the uptake of the fluorescent micelles. As expected, fluorescence is concentrated in vesicular structures, typical for receptor-mediated endocytosis [24,25]. However, except for the cell nuclei, fluorescence was also located throughout the cells indicating that escape from the endosomal structures into the cytoplasm may take place (fig. 7B).

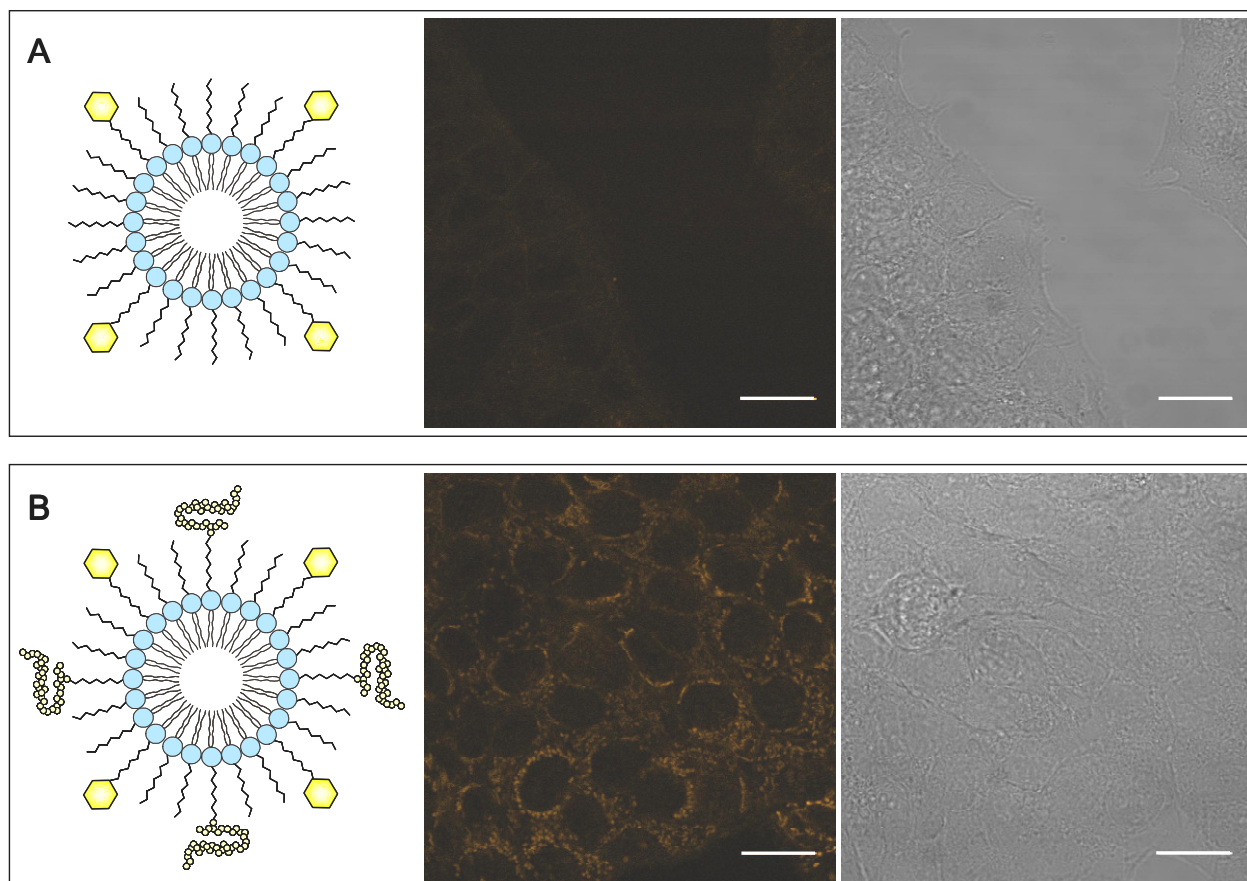


**Figure 7: Specific cellular uptake of PEG-PE micelles at  $Y_1$ -receptor positive MCF-7 breast cancer cells investigated by CLSM. (A) Non-targeted TAMRA-labeled (represented by the orange hexagons in the scheme) PEG-PE micelles are not taken-up as no signal appears in the confocal micrograph. (B) In contrast, the TAMRA-PEG-PE micelles modified by the ligand Cys-NPY (represented by the ball-chain) are taken up by the cells. The micelles are accumulated in vesicular structures as well as they are distributed into the cytosol. Dark circles correspond to the cell nuclei where the colloid was not delivered to. (Scale bar = 20  $\mu\text{m}$ )**

Since the endosomal escape is a crucial prerequisite for intracellular targeting, the delivery of micelles for cellular targeting may be favorable compared to solid nanoparticles. The data demonstrates that the introduction of Cys-NPY as a targeting ligand for  $Y_1$ -receptors effectively renders the colloid affine to cells expressing the receptor. Moreover, the micelles or seem to be delivered into the cytoplasm of the target cells. These findings make GPCR-targeted micelles interesting for further diagnostic and therapeutic purposes.

### **Summary and conclusion**

In conclusion, we showed that polymeric PEG-PE micelles are potent candidates for a GPCR-targeted drug delivery system. After precisely modifying these micelles with specific ligands for GPCRs using site-specific peptide-attachment by thiol-maleimide-interaction, the micelles are effectively delivered into human breast cancer cells expressing the NPY  $Y_1$ -receptor, whereas in the absence of the targeting peptide, no delivery takes place. Moreover, the micelles are not only internalized, they also seem to be delivered into the cytoplasm after endosomal escape, a decisive step in intracellular drug targeting. Therefore, the combination of PEG-PE micelles as drug carrier and GPCRs as selective portal into cells is a promising candidate for future targeted drug delivery.



---

**References**

- [1] D. Peer, J. M. Karp, S. Hong, O. C. Farokhzad, R. Margalit, and R. Langer, Nanocarriers as an emerging platform for cancer therapy, *Nat Nano*, 2 (2007) 751-760.
- [2] S. M. Moghimi, A. C. Hunter, and J. C. Murray, Long-Circulating and Target-Specific Nanoparticles: Theory to Practice, *Pharmacol Rev*, 53 (2001) 283-318.
- [3] A. H. Faraji and P. Wipf, Nanoparticles in cellular drug delivery, *Bioorganic & Medicinal Chemistry*, 17 (2009) 2950-2962.
- [4] H. Maeda, J. Wu, T. Sawa, Y. Matsumura, and K. Hori, Tumor vascular permeability and the EPR effect in macromolecular therapeutics: a review, *Journal of Controlled Release*, 65 (2000) 271-284.
- [5] J. D. Byrne, T. Betancourt, and L. Brannon-Peppas, Active targeting schemes for nanoparticle systems in cancer therapeutics, *Advanced Drug Delivery Reviews*, 60 (2008) 1615-1626.
- [6] K. F. Pirollo and E. H. Chang, Does a targeting ligand influence nanoparticle tumor localization or uptake?, *Trends in Biotechnology*, 26 (2008) 552-558.
- [7] H. S. Yoo and T. G. Park, Folate receptor targeted biodegradable polymeric doxorubicin micelles, *Journal of Controlled Release*, 96 (2004) 273-283.
- [8] S. Vinogradov, E. Batrakova, S. Li, and A. Kabanov, Polyion Complex Micelles with Protein-Modified Corona for Receptor-Mediated Delivery of Oligonucleotides into Cells, *Bioconjug. Chem.*, 10 (1999) 851-860.
- [9] H. Lee, M. Hu, R. M. Reilly, and C. Allen, Apoptotic Epidermal Growth Factor (EGF)-Conjugated Block Copolymer Micelles as a Nanotechnology Platform for Targeted Combination Therapy, *Molecular Pharmaceutics*, 4 (2007) 769-781.
- [10] see chapter 8 of this thesis
- [11] M. C. Lagerstroem and H. B. Schioeth, Structural diversity of G protein-coupled receptors and significance for drug discovery, *Nature Reviews Drug Discovery*, 7 (2008) 339-357.
- [12] A. N. Lukyanov, Z. Gao, and V. P. Torchilin, Micelles from polyethylene glycol/phosphatidylethanolamine conjugates for tumor drug delivery, *J. Controlled Release*, 91 (2003) 97-102.
- [13] V. P. Torchilin, Micellar Nanocarriers: Pharmaceutical Perspectives, *Pharm. Res.*, 24 (2007) 1-16.
- [14] N. Nasongkla, E. Bey, J. Ren, H. Ai, C. Khemtong, J. S. Guthi, S. F. Chin, A. D. Sherry, D. A. Boothman, and J. Gao, Multifunctional Polymeric Micelles as

- Cancer-Targeted, MRI-Ultrasensitive Drug Delivery Systems, *Nano Lett.*, 6 (2006) 2427-2430.
- [15] H. S. Yoo, E. A. Lee, and T. G. Park, Doxorubicin-conjugated biodegradable polymeric micelles having acid-cleavable linkages, *Journal of Controlled Release*, 82 (2002) 17-27.
- [16] V. P. Torchilin, Targeted polymeric micelles for delivery of poorly soluble drugs, *Cellular and Molecular Life Sciences (CMLS)*, 61 (2004) 2549-2559.
- [17] J. C. Reubi, M. Gugger, B. Waser, and J. C. Schaer, Y1-mediated effect of neuropeptide Y in cancer: breast carcinomas as targets, *Cancer Res.*, 61 (2001) 4636-4641.
- [18] T. Musacchio, V. Laquintana, A. Latrofa, G. Trapani, and V. P. Torchilin, PEG-PE Micelles Loaded with Paclitaxel and Surface-Modified by a PBR-Ligand: Synergistic Anticancer Effect, *Molecular Pharmaceutics*, 6 (2009) 468-479.
- [19] R. M. Soll, M. C. Dinger, I. Lundell, D. Larhammer, and A. G. Beck-Sickinger, Novel analogues of neuropeptide Y with a preference for the Y1-receptor, *Eur. J. Biochem.*, 268 (2001) 2828-2837.
- [20] S. W. Provencher, CONTIN: A general purpose constrained regularization program for inverting noisy linear algebraic and integral equations, *Computer Physics Communications*, 27 (1982) 229-242.
- [21] H. Amlal, S. Faroqui, A. Balasubramaniam, and S. Sheriff, Estrogen up-regulates neuropeptide Y Y1 receptor expression in a human breast cancer cell line, *Cancer Research*, 66 (2006) 3706-3714.
- [22] M. D. Abramoff, P. J. Magelhaes, and S. J. Ram, Image Processing with ImageJ, *Biophotonics International*, 11 (2004) 36-42.
- [23] S. D. Perrault, C. Walkey, T. Jennings, H. C. Fischer, and W. C. W. Chan, Mediating Tumor Targeting Efficiency of Nanoparticles Through Design, *Nano Lett.*, 9 (2009) 1909-1915.
- [24] S. D. Conner and S. L. Schmid, Regulated portals of entry into the cell, *Nature*, 422 (2003) 37-44.
- [25] M. Marsh and H. T. McMahon, Cell biology: The structural era of endocytosis, *Science*, 285 (1999) 215-220.
- [26] E. Schneider, M. Mayer, R. Ziemek, L. Li, C. Hutzler, G. Bernhardt, and A. Buschauer, A simple and powerful flow cytometric method for the simultaneous determination of multiple parameters at G protein-coupled receptor subtypes, *ChemBioChem*, 7 (2006) 1400-1409.
- [27] E. P. Diamandis and T. K. Christopoulos, The biotin-(strept)avidin system: principles and applications in biotechnology, *Clin Chem*, 37 625-636.

# Chapter 8

## **G-protein Coupled Receptor Targeted Nanoparticles Allow for Choosing between Membrane Binding and Cellular Uptake**

W. Hild<sup>1</sup>, K. Pollinger<sup>1</sup>, A. Caporale<sup>2</sup>, C. Cabrele<sup>3</sup>, M. Keller<sup>2</sup>, N. Pluym<sup>2</sup>,  
A. Buschauer<sup>2</sup>, R. Rachel<sup>4</sup>, J. Teßmar<sup>1</sup>, M. Breunig<sup>1</sup>, A. Göpferich<sup>1</sup>

<sup>1</sup> Department of Pharmaceutical Technology, University of Regensburg, Universitätsstraße 31, 93040 Regensburg, Germany

<sup>2</sup> Department of Pharmaceutical and Medicinal Chemistry, University of Regensburg, Universitätsstraße 31, 93053 Regensburg, Germany

<sup>3</sup> Department of Organic Chemistry, Ruhr-University Bochum, Universitätsstraße 150, 44801 Bochum, Germany

<sup>4</sup> Center for Electron Microscopy at the Institute for Anatomy, University of Regensburg, Universitätsstraße 31, 93053 Regensburg, Germany

**Abstract**

Improving the selectivity of interactions between nanoparticles and cells would substantially increase the potential for nanoparticle diagnostic and therapeutic applications. Thus it is desirable not only that nanoparticles be targeted to any cell with high specificity and affinity, but also that one be able to unequivocally determine whether they rest immobilized on the cell surface (as a diagnostic tag) or are internalized (to serve as a drug delivery vehicle). To date no class of targets is known that would allow one to direct nanoparticle interactions with cells alternatively into one of these mutually exclusive events. Using MCF-7 breast cancer cells expressing the human  $Y_1$ -receptor we demonstrate that G-protein coupled receptors (GPCRs) provide us with this ability. We show that quantum dots carrying a surface-immobilized antagonist remain with nanomolar affinity on the cell surface, while particles carrying an agonist are internalized upon receptor binding. We found that agonist- and antagonist-modified nanoparticles bind to several receptor molecules simultaneously. This multiligand binding leads to an increase of 5 orders of magnitude in the receptor affinities (compared to free ligand). The fact that there are more than 800 GPCRs in humans provides us with the possibility of targeting of a plethora of cells. This work demonstrates that switching from cell recognition to cell uptake is simply a matter of modifying the nanoparticle surface with the appropriate choice of ligand type.

## Introduction

A major goal of biomedical targeting is the selective delivery of nanoparticles to a specific mammalian tissue for diagnostic or therapeutic purposes [1-3]. Current strategies for guiding nanoparticles to their target have focused mainly on immobilizing either antibodies against cell surface proteins [4-6] or natural ligands for cell surface receptors [7] on particle surfaces. The substantial molecular mass and size added to the nanoparticles decreases the utility of attached antibodies, and receptor ligands have not provided us with the necessary versatility to date. Only a few receptors, such as the transferrin receptor or the epidermal growth factor receptor, have emerged as targeting sites [4,7]; these are unfortunately expressed in a multitude of tissues and are therefore rather unspecific.

In addition to these severe limitations, a problem of paramount significance is the loss of control over such particles' fate once they bind to their target. To date no mechanism is known that would allow one to design particles destined for a single target structure such that they are addressed exclusively to the cell surface or to the cell interior. The former would allow the use of particles for diagnostic purposes without interfering with intracellular processes, while the latter would allow one to elicit a cellular response in cells identified by nanoparticles. Despite the tremendous progress towards a better understanding of factors having an impact on particle uptake by cells, such as size and surface charge [8-10], a fundamentally new strategy to control nanoparticle trafficking has yet to be developed.

To develop this strategy, it was necessary to utilize a new family of targets for which ligands are available that are highly tissue-type specific and allow 'sorting' of particles after binding. The family of G-protein coupled receptors (GPCRs), which exhibit high tissue-specificity and represent the largest class of receptors in the human genome [11], appeared to be a promising choice. High affinity ligands for GPCRs of moderate molecular mass exist, and early reports have indicated that ligand-decorated nanoparticles still interact with the receptor [12,13]. Most importantly, however, two classes of GPCR ligands exist: agonists that lead to receptor internalization upon binding and antagonists that do not [14].

Having identified this potential 'molecular switch' for controlling the gateway into cells, we hypothesized that the immobilization of an agonist on a nanoparticle surface would cause cellular uptake, while the immobilization of an antagonist to a particle

would result in arrest on the cell surface. Furthermore, we believed that such nanoparticles would preserve their high cell affinity and target specificity by attaching to cell surface receptors via a multi-ligand binding mode.

To investigate the validity of both hypotheses, we selected the human neuropeptide Y (NPY) Y<sub>1</sub>-receptor as a model receptor. This receptor has an incidence of 85% in breast carcinoma and 100% in lymph node metastases [15]. We used quantum dots (QDs) [16] to which peptidic agonists of a few kDa in molecular mass or a small-molecule antagonist were attached to examine if GPCR trafficking upon ligand binding [17] can be exploited as a selective nanoparticle gateway into cells.

## **Materials and Methods**

### *Buffers and reagents*

All chemicals were obtained from Sigma (St. Louis, MO) in the highest purity available, unless stated differently. Activation buffer consisted of 50 mM sodium tetraborate buffer, pH 7.2. Purification buffer I consisted of activation buffer, supplemented with 150 mM sodium chloride and 10 mM ethylenediaminetetraacetic acid (EDTA) disodium salt. Conjugation buffer contained two parts of purification buffer I and one part of dimethylformamide (DMF), whereas purification buffer II contained dimethylsulfoxide (DMSO) instead of DMF and 0.01% sodium azide. The ultrafiltration units had a 100 kDa cut-off membrane (Amicon Ultra-4, Millipore, Billerica, MA). Incubation medium consisted of phenol red-free Leibovitz F-15 medium (Invitrogen, Carlsbad, CA), 1% of bovine serum albumin and 0.01% of Bacitracin (Invitrogen).

### *Synthesis of pNPY analogs*

Three analogs of the porcine neuropeptide Y (pNPY) were synthesized by standard automated solid phase synthesis. Lysine in position 4 was modified by side chain attachment of an additional cysteine residue for the bioconjugation with the QDs. The sequences of the peptides are given in tab. 1. The mass was confirmed by matrix-assisted laser desorption/ionization time-of-flight mass spectrometry (MALDI-ToF-MS) using  $\alpha$ -cyano-4-hydroxycinnamic acid (HCA) matrix (for details see SI methods).

*Synthesis of BIBP3226 and SH-BIBP*

BIBP3226 and (*R*)-*N*<sup>α</sup>-(2,2-diphenylacetyl)-*N*-(4-hydroxybenzyl)-*N*ω-(6-sulfanylhexanoyl)-argininamide, in this article referred to as SH-BIPB, were synthesized based on a procedure which was published previously for other NG-substituted derivatives of BIBP3226 [21] (for details see SI methods and SI fig. 1).

*Conjugation of Y<sub>1</sub>-receptor ligands to QDs*

1 nmol of Qdot 655 IT amino (PEG) quantum dot (Invitrogen) was transferred into 200 μl of activation buffer by buffer exchange using ultrafiltration (Amicon Ultra-4, 100K MWCO, GE Healthcare, Chalfont St. Giles, UK). The QDs were subsequently activated by a 500-fold molar excess of sulfosuccinimidyl-4-(*N*-maleimidomethyl)-cyclohexane-1-carboxylate (sulfo-SMCC) dissolved in activation buffer to yield a final volume of 250 μl. After 30 min of gentle shaking at room temperature, the activated QDs were purified by gel filtration chromatography (GFC) using purification buffer I as mobile phase (for details see SI methods and SI fig. 2). After buffer exchange to conjugation buffer, removal of the excess conjugation buffer by ultrafiltration and concentration to a volume of 100 μl, QDs were incubated with a 30-fold excess of the respective NPY-analog or a 100-fold excess of SH-BIPB for 12 h at 4 °C. Thereafter, a 100-fold molar excess of 2-mercaptoethanol was added to quench unreacted maleimides. After 30 min, the obtained bioconjugate was purified again by GFC using purification buffer II. Subsequently, the conjugate was concentrated by ultrafiltration to a final concentration of 3 μM that was used for the biological studies.

*Cell culture*

The human breast cancer cell line MCF-7 and the human neuroblastoma cell line SK-N-MC were maintained in Minimum Essential Medium containing Earl's salts (EMEM) supplemented with 5% fetal bovine serum (FBS). 48 h before the experiments MCF-7 cells were seeded in the same medium supplemented with 1 nM estradiol (Sigma). SK-N-MC cells were cultured in the absence of estradiol. MDA cells were kept in McCoy's medium supplemented with 5% FBS and seeded 24 h before the experiments.

*Imaging: Confocal laser scanning microscopy (CLSM)*

Two days before the experiments, cells were seeded in 8-well  $\mu$ -slides (Ibidi, Munich, Germany). All experiments were conducted in incubation medium at 37 °C. Cells were observed using a Zeiss Axiovert 200M inverted epifluorescence microscope coupled with a LSM 510 laser scanning device, using a 40x Plan-Apochromat water-immersion objective (NA 1.2). QDs and QD/ligand-conjugates were excited using the 488 nm line of an Ar-laser. Emission was measured using a 650 nm long pass filter. For the investigation of agonist- and antagonist-modified QDs interactions with MCF-7 cells by z-stack images we used as slice thickness of 1.1  $\mu$ m for agonist-modified QDs, and 1.8  $\mu$ m for antagonist-modified QDs.

*Binding and displacement studies*

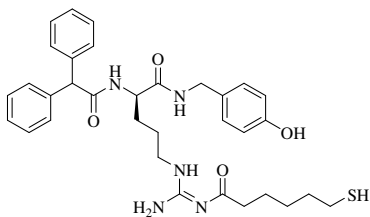
Cells were seeded in 24-well plates at a density of 130,000 (MCF-7) and 80,000 (MDA) cells per well. For the studies, the medium was removed, cells were washed with phosphate buffered saline (PBS) and incubated with the QD dilutions for 2 h at 23 °C. After incubation, the QDs were removed, and the cells were washed with PBS and trypsinized. After centrifugation at 200 RCF at 4 °C, the cells were washed twice with cold PBS and used for FACS analysis. For association curves, the respective amount of the testing substance was diluted in incubation medium. For displacement studies, all ligand-modified QDs were used at a concentration of 1 nM. The incubation medium contained the respective amount of BIBP3226 and 7.5% DMSO to increase the solubility of the antagonist. Cells were analyzed on a FACSCalibur (BD Biosciences, San Jose, CA). QDs were excited at 633 nm via a diode laser and emission was measured using a 661/16 nm bandpass filter. Data was analyzed by using the WinMDI 2.8 software. The population representing whole cells (on average 20,000 cells) was gated and the fluorescence was plotted in a histogram. All values were corrected for the background signal obtained in absence of QDs. For binding studies, the intensities of the geometric mean of the histogram were plotted. For displacement studies, the intensity of the geometric mean obtained for 1 nM of the respective QD sample without antagonist was set to 100%, and all other samples were calculated proportional to this value. Each data point represents the mean of 3 independent measurements ( $\pm$  SEM). All data to be fitted were processed with SigmaPlot 8.0. Data from binding experiments were evaluated by one-site saturation



fits. Data from displacement experiments were analyzed by four-parameter sigmoidal fits.

## Results and discussion

Different peptidic agonists of the  $Y_1$ -receptor, analogs of porcine NPY (pNPY) exhibiting different receptor affinities and molecular masses (tab. 1A-C), were synthesized (for details see Supporting Information (SI)). The introduction of a cysteine residue by side-chain modification of a lysine found in the selected agonists [18-20] provided a specific reaction site for the stable covalent linkage to the QDs.

	Name (abbreviation)	Sequence / structure	Ligand type	Lit*
a	[Lys <sup>4</sup> (N <sup>α</sup> -Acetyl-Cys)]-pNPY	H-YPSK(Ac-N-C)PDNPGEDAPAEDLA RYYSALRHYINLITRQRY-NH <sub>2</sub>	peptidic agonist	18
b	[Lys <sup>4</sup> (N <sup>α</sup> -Acetyl-Cys), Arg <sup>6</sup> , Pro <sup>34</sup> ]-pNPY	H-YPSK(Ac-N-C)PRNPGEDAPAEDLA RYYSALRHYINLITRPRY-NH <sub>2</sub>	peptidic agonist	19
c	[Lys <sup>4</sup> (N <sup>α</sup> -Acetyl-Cys), Ahx <sup>9-17</sup> ]-pNPY [Ahx = 6-aminohexanoyl]	H-YPSK(Ac-N-C)PDNP-Ahx- ARYYSALRHYINLITRQRY-NH <sub>2</sub>	peptidic agonist	20
d	SH-BIBP		non-peptidic antagonist	21

**Table 1: Overview of ligands used in the study.** Structures and names of the NPY-analogs (**A-C**) and non-peptidic  $Y_1$ -receptor antagonist (**D**) used for bioconjugation with the QDs. (\*Literature refers to the cysteine-free peptide and the non-acylated BIBP3226.)

As shown in fig. 1A, amino-PEG coated QDs were rendered thiol-reactive upon treatment with sulfosuccinimidyl-4-(*N*-maleimidomethyl)-cyclohexane-1-carboxylate (sulfo-SMCC), subsequently reacted with the peptides and purified by gel filtration chromatography (details of the conjugation and purification procedure can be found in SI). Transmission electron microscopy images confirmed that this strategy yielded monodisperse (see SI methods and SI fig. 1), peptide-modified (see SI fig. 2) QDs, a schematic illustration of which is shown in fig. 1B. Similarly, QDs decorated with a low molecular mass, non-peptidic antagonist were prepared. For the attachment to the QDs, a thiol was introduced into the antagonist BIBP3226 by acylation with 6-mercaptohexanoic acid to obtain (*R*)-*N*<sup>α</sup>-(2,2-diphenylacetyl)-*N*-(4-hydroxybenzyl)-*N*<sup>ω</sup>-(6-sulfanylhexanoyl)-argininamide, referred to as SH-BIPB (tab. 1D) (for details of BIBP and SH-BIPB synthesis see SI and SI fig. 3).

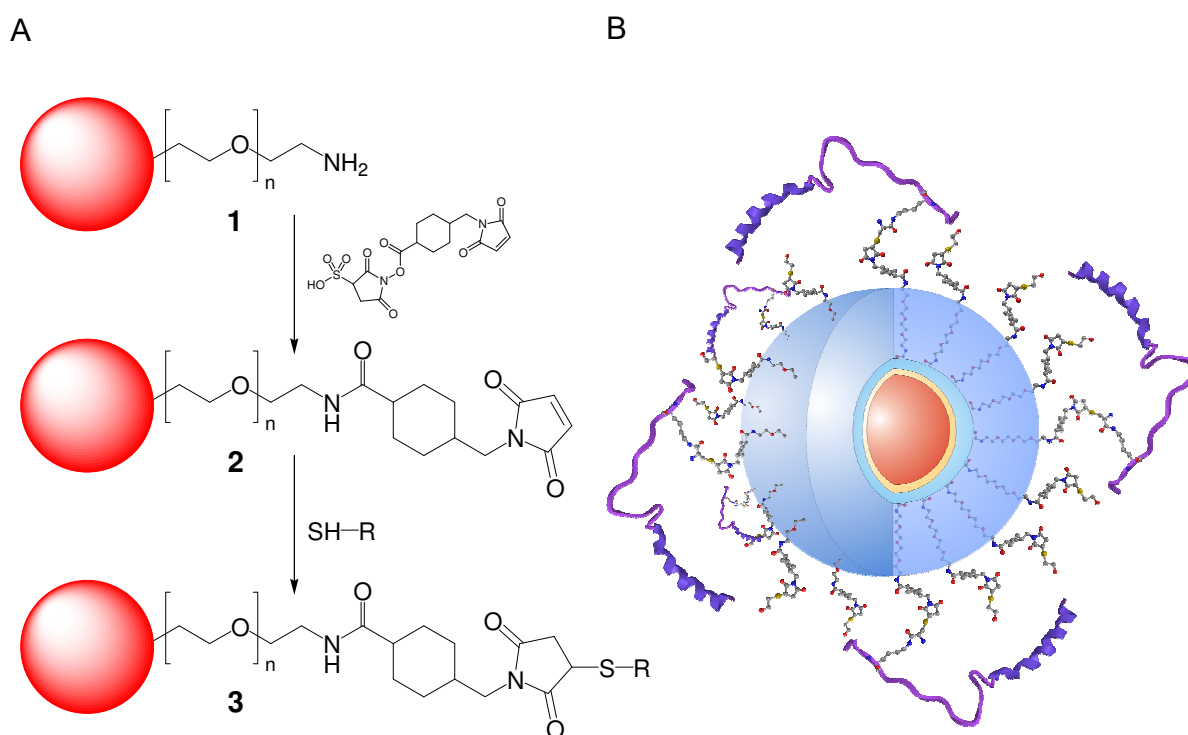


**Figure 1: Method of Y1-receptor ligand conjugation to QDs. (A)** Scheme of the bioconjugation reaction. After activation of the amino-PEG QDs (1) with sulfo-SMCC, the resulting thiol-reactive nanoparticles (2) were connected with either the peptidic agonistic analogs of pNPY or the non-peptidic antagonist SH-BIPB to yield the ligand-modified QDs (3). R-SH refers to the structures A-D depicted in tab. 1.

**(B)** Schematic illustration of NPY-modified QDs. The nanoparticles consist of polymer-coated CdSe/ZnS QDs, decorated with amine PEGs and the attached NPY analog.

Both agonist- and antagonist-modified QDs were investigated by confocal laser scanning microscopy (CLSM) to observe binding to the human breast cancer cell-line MCF-7, which expresses the  $Y_1$ -receptor (cell culture conditions and details of CLSM investigations are provided in SI methods). Both QD types exhibited highly specific binding (fig. 2 and 3). To assure that ligand-free QDs are not internalized by any unspecific uptake mechanism, NPY  $Y_1$ -receptor positive MCF-7 cells were incubated under the conditions described for ligand-modified nanoparticles. Fig. 4 shows that there is no significant uptake of the particles.

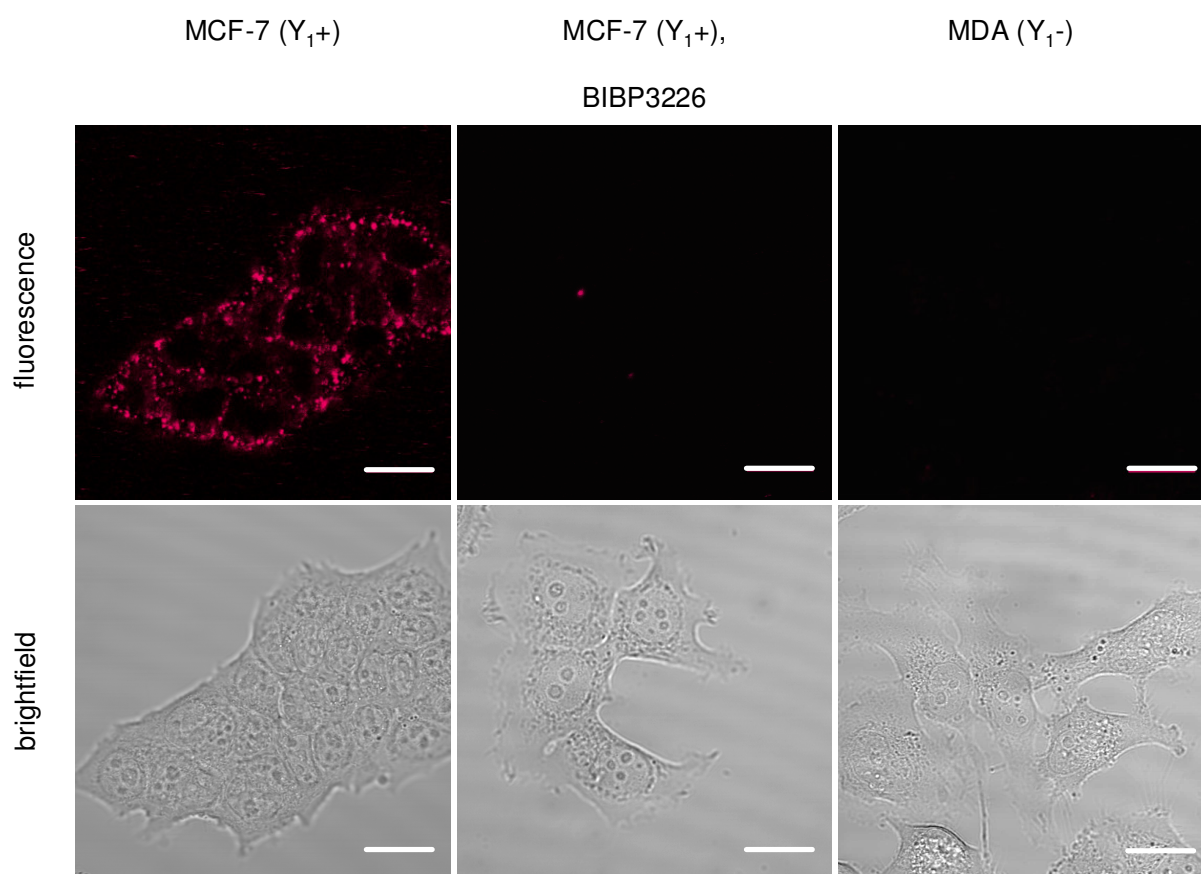


**Figure 2: Specific binding and uptake of agonist-modified QDs.** Confocal fluorescence micrographs and corresponding brightfield images of cell clusters after incubation with  $[Lys^4(N^\alpha\text{-Acetyl-Cys}), Arg^6, Pro^{34}]$ -pNPY-QDs (10 nM). The nanoparticles are delivered into living MCF-7 cells in vesicular structures. Except for the cell nuclei, the particles are located throughout the cellbodies. After blocking receptors with the soluble antagonist BIBP3226 (10 mM) or when using MDA cells ( $Y_1-$ ), no internalization can be observed (scale bars = 20  $\mu$ m).

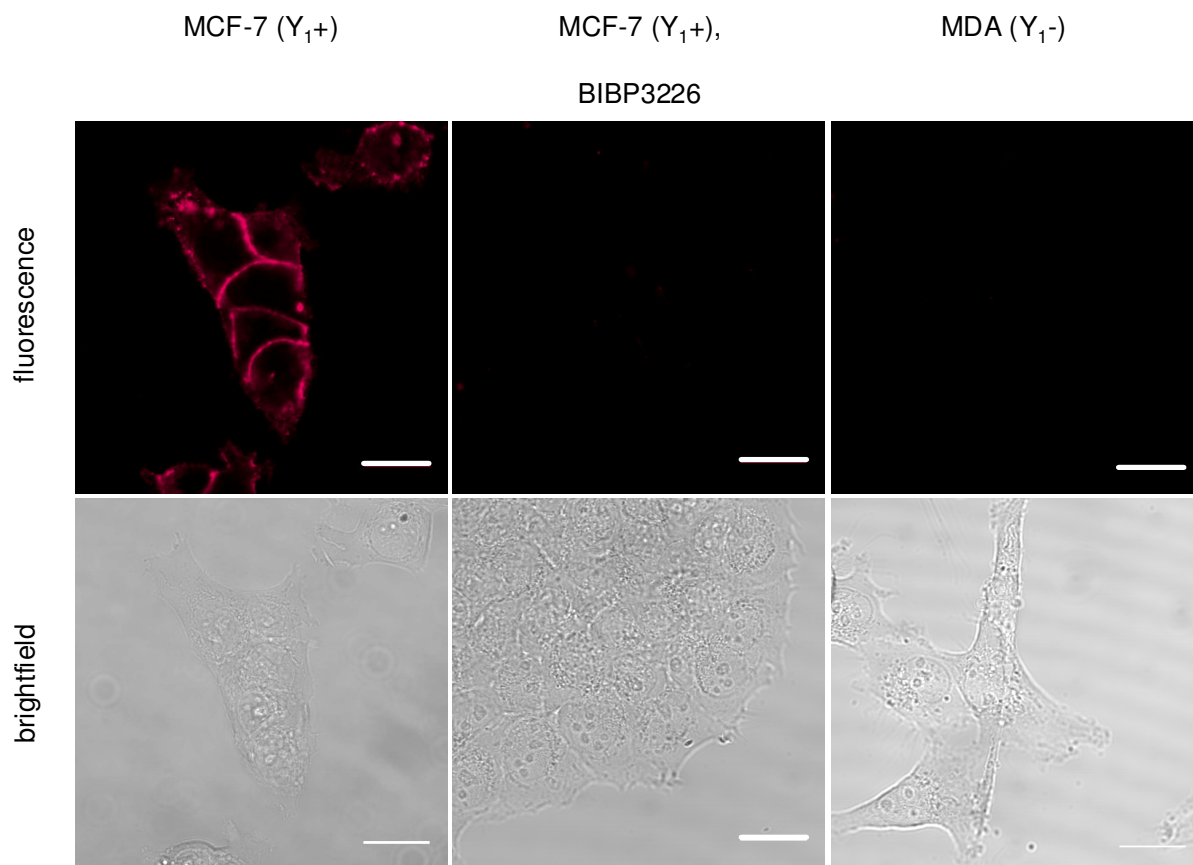


**Figure 3: Cell-binding of antagonist-modified QDs.** Confocal fluorescence micrographs and corresponding brightfield images of cells incubated with 10 nM of SH-BIBP-QDs. The particles exhibit binding to the cell surfaces of living MCF-7 cells, whereas upon displacement with 10 mM of the antagonist BIBP3226 or for MDA cells ( $Y_{1-}$ ) no binding occurs (scale bars = 20  $\mu\text{m}$ ).

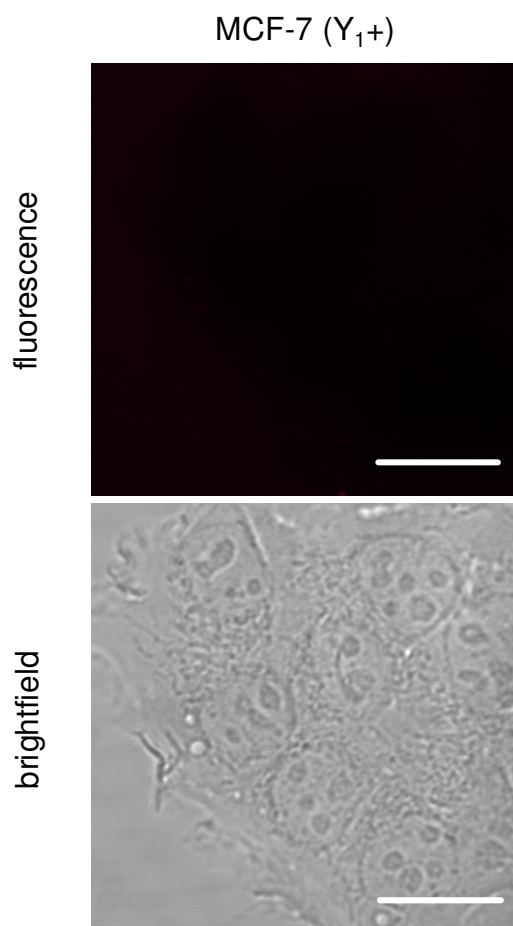


**Figure 4: Cell binding of ligand-free QDs.** 100 nM of QDs lacking ligands show no binding and uptake after incubation with MCF-7 cells (scale bars = 20  $\mu\text{m}$ ).

The control experiments (fig. 2 and 3) showed that binding is specific to the  $Y_1$ -receptor since no binding was observed either to MCF-7 cells in the presence of free antagonist BIBP3226 or when conducting the experiment with MDA cells lacking the receptor. Both agonist- and antagonist-modified QDs exhibited specific cell binding, but there was a tremendous difference with respect to cellular uptake. Only agonist-modified QDs were internalized. The cells formed vesicular structures containing agonist-modified QDs which indicate that the nanoparticles had been transported into the cells (fig. 2). The internalization of these particles was corroborated by confocal z-stack images. To further elucidate the location of agonist-modified particles after their interaction with cells, images representing optical sections through the cells were taken from MCF-7 cells after incubation with [Lys<sup>4</sup>( $N^\alpha$ -Acetyl-Cys), Arg<sup>6</sup>, Pro<sup>34</sup>]-pNPY-QDs. As depicted in fig. 5, strong fluorescence due to the QDs can be found throughout the cells, except for the cell nuclei. This supports the concept that the

particles were effectively delivered into the target cells. The cells show spots in the cytoplasm that are typical of endocytotic vesicles formed upon receptor-mediated endocytosis.

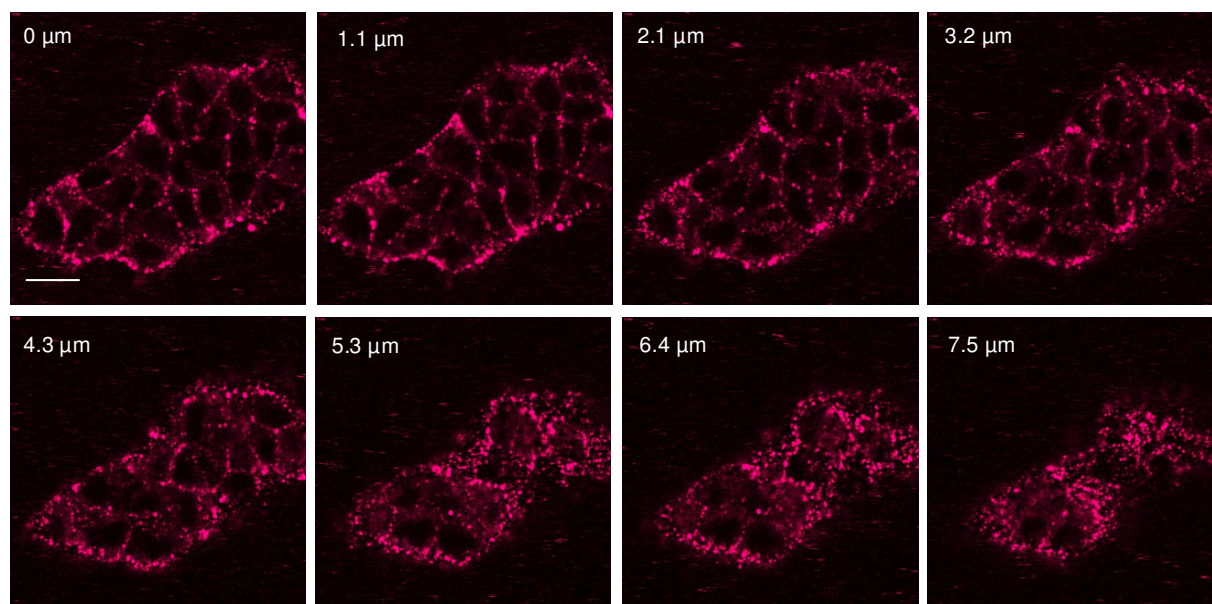


**Figure 5:** CLSM investigation of agonist-modified QDs' interactions with cells. The z-stack images shows MCF-7 cells incubated with 10 nM of [Lys<sup>4</sup>(N<sup>α</sup>-Acetyl-Cys), Arg<sup>6</sup>, Pro<sup>34</sup>]-pNPY-QDs. In every optical section, QD-fluorescence is located throughout the cells, except for the nuclei (scale bar = 20 μm). The numbers in μm indicate the distance of the focal plane to the surface of the cell culture plate.

In the case of antagonist-modified particles, the fluorescence was strictly limited to the cell membrane, indicating that particles were located on the cell surfaces only (fig. 6).

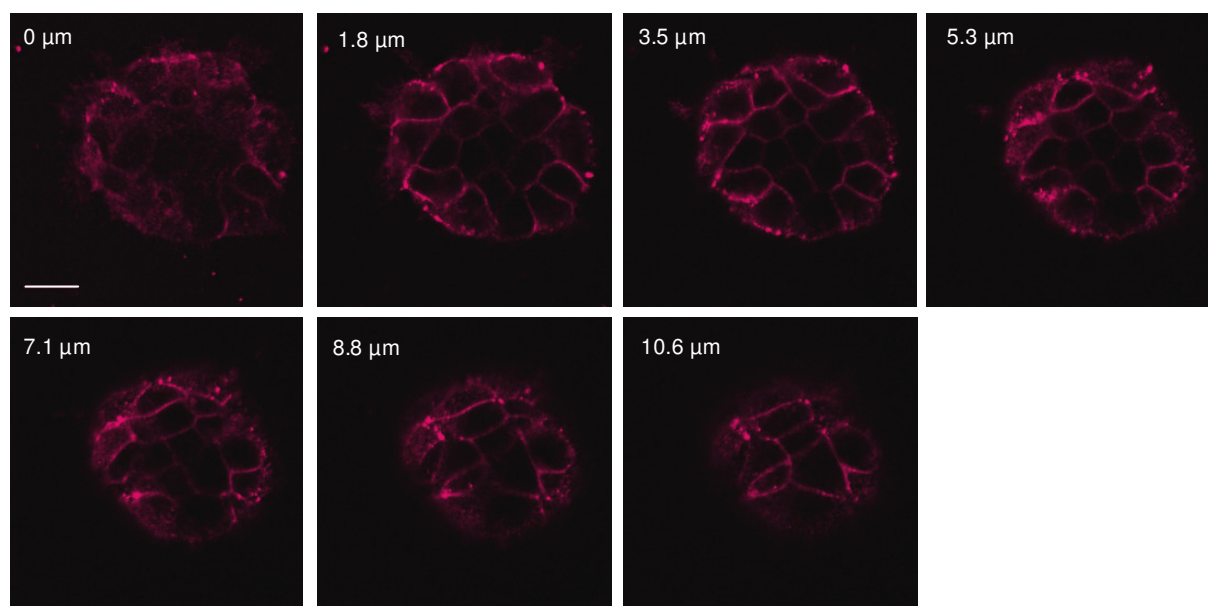


**Figure 6: CLSM investigation of antagonist-modified QDs' interactions with cells.** The stack of images shows MCF-7 cells incubated with 10 nM of SH-BIBP-QDs. In every optical section, QD-fluorescence is located on the cell surface only (scale bar = 20  $\mu\text{m}$ ). The numbers in  $\mu\text{m}$  indicate the distance of the focal plane to the surface of the cell culture plate.

Similar results concerning binding and internalization were obtained when repeating the experiment with SK-N-MC cells, another  $Y_1$ -receptor positive cell line derived from the central nervous system (SI fig. 4). This clearly demonstrates that the findings are neither dependent upon the cell type nor the receptor density (SK-N-MC cells – approx. 60,000 receptors/cell [21]; MCF-7 cells – approx. 300,000 receptors/cell [21]). In summary, our results show that GPCRs can be used to target nanoparticles specifically either to the target cell's surface or to its intracellular compartment by simply attaching an antagonist or an agonist, respectively, to the particle surface.

After demonstrating that GPCRs can function as selective gateways, we investigated if tagged nanoparticles still exhibited a sufficiently high affinity towards their receptor. This is of concern for future in vivo applications, which demand that particles accumulate reliably at the target site in the presence of competing unspecific binding sites that may exist. Binding curves of QDs modified with the agonist [Lys<sup>4</sup>(N <sup>$\alpha$</sup> -Acetyl-Cys), Arg<sup>6</sup>, Pro<sup>34</sup>]-pNPY (fig. 7A) and the antagonist SH-BIBP respectively (fig. 7B) were recorded for  $Y_1$ -receptor positive MCF-7 cells using MDA cells as a negative

control (for details of binding and displacement studies see SI methods). The resulting saturation of binding sites and the low non-specific binding indicate that the particles bind specifically to the receptor. Similar results were obtained for the other two agonistic peptides (SI fig. 5). When we calculated the concentrations at which 50% of the binding sites are occupied (the dissociation constant,  $K_d$ ), the values were approximately 21 nM for agonist-modified and approx. 30 nM for antagonist-modified QDs (SI tab. 1). These values reflect that the nanoparticles, even though their ligands were chemically altered, still possess a superb affinity for the receptor. To further confirm the specificity of the interaction with cells, we investigated the binding behavior of particles in a competitive binding assay with unbound  $Y_1$ -receptor antagonist BIBP3226. As expected, both agonist- and antagonist-modified QDs can be displaced from the receptors almost completely (fig. 7C and D). However, we found that very high amounts of BIBP3226 were needed to displace the nanoparticles from the receptor. For 1 nM agonist-modified particles, the inhibitory constant ( $IC_{50}$ , reflecting the concentration at which BIBP3226 displaces 50% of the particles) ranged from 640 to 1550  $\mu$ M (SI, fig. 5 and tab. 1). This is approx. 5 orders of magnitude higher than values usually obtained for the free agonist according to the literature [22]. The results were similarly striking for the antagonist-modified QDs. For the half-maximum displacement of 1 nM of antagonist-modified (i.e. BIBP3226-modified) QDs, again a 5 order of magnitude excess of free BIBP3226 was needed.



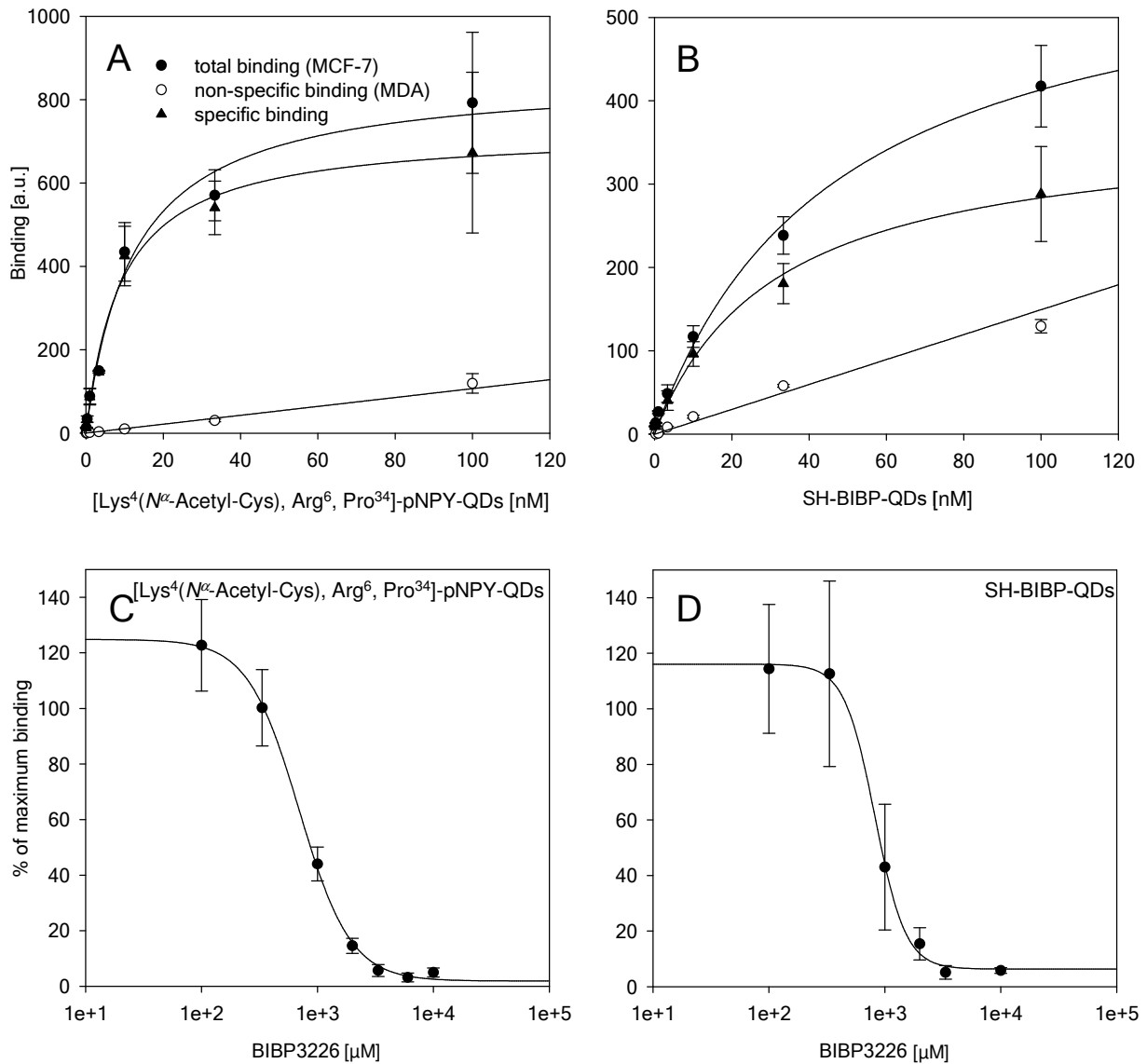


**Figure 7: Cell-binding and displacement curves for agonist- and antagonist modified QDs. (A, B).** Binding curves of ‘agonistic’ [Lys<sup>4</sup>(N<sup>α</sup>-Acetyl-Cys), Arg<sup>6</sup>, Pro<sup>34</sup>]-pNPY-QDs and ‘antagonistic’ SH-BIBP-QDs. For the determination of the total binding MCF-7 cells (Y1+) were used (filled circles) while MDA cells (Y1-) served as a control to assess non-specific binding (open circles). The resulting specific binding curve is indicative of receptor saturation beyond 100 nM for both species. **(C, D)** Displacement of [Lys<sup>4</sup>(N<sup>α</sup>-Acetyl-Cys), Arg<sup>6</sup>, Pro<sup>34</sup>]-pNPY-QDs and SH-BIBP-QDs from MCF-7 cells by the Y<sub>1</sub>-receptor antagonist BIBP3226, determined by flow cytometry. At high concentrations of the competitive antagonist, both types of particles can be displaced from the receptor almost completely. Error bars, ± SEM (n = 3).

We hypothesize that such a tremendously high affinity of the agonist- and antagonist-modified particles compared to the free antagonist is attributed to the fact that nanoparticles can bind to several receptors at a time, a phenomenon that is referred to as 'multiligand binding' [23-25]. This is strongly supported by other examples in the literature in which monovalent ligands were found to poorly displace multivalent particles or molecules subject to multiligand binding [25,26].

The results that we obtained have a number of significant implications for the delivery of nanoparticles to cells. GPCRs provide us with a tool that allows us to target a multitude of cells in an organism with exceptionally high specificity. Currently there are more than 800 receptors known for humans and approx. 1800 in rats and mice [27]. This suggests that, if we want to direct nanoparticles to a certain tissue, we only have to pick the appropriate GPCR for the respective tissue from a database [28], choose the appropriate ligand for this GPCR and tether it to the nanoparticles surface as an 'address label' - a "building block" strategy. In addition to high target specificity, a significant advantage of GPCR-targeting is that we can control the particles' fate after binding to the cell surface: by choosing an agonist for the interaction with the receptor we open the gate into cells or by selecting an antagonistic ligand we leave it closed. This strategy improves upon other sophisticated approaches with antibodies that also demonstrate highly specific binding [29], but are associated with accepting the subsequent fate of the particle as it is. In the future our technique could lead to applications in which antagonistic nanoparticles first identify cells inside a tissue or an organism and then agonistic particles are used for therapeutic purposes to deliver nanoparticles via the same target structure into the same cell type.

In addition, our results have implications beyond the fact that we can reproducibly target particles either to the cytosol or the cell surface. The findings reported here may represent the first step to granting us access to a toolbox currently only employed by viruses that allows them to achieve outstanding target cell specificity. By binding to several different cell surface proteins at the same time, viruses unequivocally identify their target cell and make use of a single additional interaction to trigger cell internalization [30,31]. If we would like to mimic this strategy using nanoparticles, we would have to design multiligand binding particles that allow for target identification by tagging the cell surface in a first step followed by triggering cell entry. Our results have shown that GPCRs would be ideal target candidates. GPCR binding nanoparticles can thus be used as a tool to optimize targeting and trafficking

of particles *in vivo*. Simultaneously they provide us with a mechanism for a multitude of biotechnological applications, such as receptor mediated siRNA delivery into cells (for which we recently developed a new type of carrier [32]). While more research is necessary to further tailor the targeting and uptake events for specific tissues, the remarkable biological and pharmaceutical implications of such “dual-action” nanoparticles indicates this is an exciting line of future inquiry with broad-ranging applications.

**References**

- [1] M. E. Davis, Z. Chen, and D. M. Shin, Nanoparticle therapeutics: an emerging treatment modality for cancer, *Nat. Rev. Drug Discovery*, 7 (2008) 771-782.
- [2] M. V. Yezhelyev, X. Gao, Y. Xing, A. Al Hajj, S. Nie, and R. M. O'Regan, Emerging use of nanoparticles in diagnosis and treatment of breast cancer, *Lancet Oncol.*, 7 (2006) 657-667.
- [3] K. Cho, X. Wang, S. Nie, Z. Chen, and D. M. Shin, Therapeutic Nanoparticles for Drug Delivery in Cancer, *Clinical Cancer Research*, 14 (2008) 1310-1316.
- [4] Z. Zhu, Targeted cancer therapies based on antibodies directed against epidermal growth factor receptor: status and perspectives, *Acta Pharmacol. Sin.*, 28 (2007) 1476-1493.
- [5] N. Ferrara, H. P. Gerber, and J. LeCouter, The biology of VEGF and its receptors, *Nat. Med. (N. Y. , NY, U. S. )*, 9 (2003) 669-676.
- [6] T. M. Allen, Ligand-targeted therapeutics in anticancer therapy, *Nat. Rev. Cancer*, 2 (2002) 750-763.
- [7] Z. M. Qian, H. Li, H. Sun, and K. Ho, Targeted Drug Delivery via the Transferrin Receptor-Mediated Endocytosis Pathway, *Pharmacol. Rev.*, 54 (2002) 561-587.
- [8] W. Jiang, B. Y. S. Kim, J. T. Rutka, and W. C. W. Chan, Nanoparticle-mediated cellular response is size-dependent, *Nat. Nanotechnol.*, 3 (2008) 145-150.
- [9] R. Minchin, Sizing up targets with nanoparticles, *Nat. Nanotechnol.*, 3 (2008) 12-13.
- [10] B. D. Chithrani and W. C. W. Chan, Elucidating the Mechanism of Cellular Uptake and Removal of Protein-Coated Gold Nanoparticles of Different Sizes and Shapes, *Nano Lett.*, 7 (2007) 1542-1550.
- [11] M. C. Lagerstroem and H. B. Schioeth, Structural diversity of G protein-coupled receptors and significance for drug discovery, *Nature Reviews Drug Discovery*, 7 (2008) 339-357.
- [12] S. H. Young and E. Rozengurt, Qdot nanocrystal conjugates conjugated to bombesin or ANG II label the cognate G protein-coupled receptor in living cells, *Am. J. Physiol.*, 290 (2006) C728-C732.
- [13] N. Chanda, R. Shukla, K. V. Katti and R. Kannan, Gastrin Releasing Protein Receptor Specific Gold Nanorods: Breast and Prostate Tumor Avid Nanovectors for Molecular Imaging, *Nano Lett.* 9 (2009) 1798–1805.
- [14] A. C. Hanyaloglu and M. von Zastrow, Regulation of GPCRs by endocytic membrane trafficking and its potential implications., *Annu. Rev. Pharmacol. Toxicol.* 48 (2008) 537-568.

- 
- [15] J. C. Reubi, M. Gugger, B. Waser, and J. C. Schaer, Y1-mediated effect of neuropeptide Y in cancer: breast carcinomas as targets, *Cancer Res.*, 61 (2001) 4636-4641.
- [16] W. A. Hild, M. Breunig, and A. Goepferich, Quantum dots - Nano-sized probes for the exploration of cellular and intracellular targeting, *Eur. J. Pharm. Biopharm.*, 68 (2008) 153-168.
- [17] B. L. Wolfe and J. Trejo, Clathrin-dependent mechanisms of G protein-coupled receptor endocytosis, *Traffic (Oxford, U. K.)*, 8 (2007) 462-470.
- [18] K. Tatemoto, Neuropeptide Y: complete amino acid sequence of the brain peptide, *Proc. Natl. Acad. Sci. U. S. A.*, 79 (1982) 5485-5489.
- [19] R. M. Soll, M. C. Dinger, I. Lundell, D. Larhammer, and A. G. Beck-Sickinger, Novel analogues of neuropeptide Y with a preference for the Y1-receptor, *Eur. J. Biochem.*, 268 (2001) 2828-2837.
- [20] B. Rist, H. A. Wieland, K. D. Willim, and A. G. Beck-Sickinger, A rational approach for the development of reduced-size analogues of neuropeptide Y with high affinity to the Y1 receptor, *J Pept Sci*, 1(1995) 341-348.
- [21] M. Keller, N. Pop, C. Hutzler, A. G. Beck-Sickinger, G. Bernhardt, and A. Buschauer, Guanidine-Acylguanidine Bioisosteric Approach in the Design of Radioligands: Synthesis of a Tritium-Labeled NG-Propionylargininamide ([<sup>3</sup>H]-UR-MK114) as a Highly Potent and Selective Neuropeptide Y Y1 Receptor Antagonist, *J. Med. Chem.*, 51 (2008) 8168-8172.
- [22] K. Rudolf, W. Eberlein, W. Engel, H. A. Wieland, K. D. Willim, M. Entzeroth, W. Wienen, A. G. Beck-Sickinger, and H. N. Doods, The first highly potent and selective non-peptide neuropeptide Y Y1 receptor antagonist: BIBP3226, *European Journal of Pharmacology*, 271 (1994) R11-R13.
- [23] S. Hong, P. R. Leroueil, I. J. Majoros, B. G. Orr, J. R. Baker, and M. M. Banaszak Holl, The Binding Avidity of a Nanoparticle-Based Multivalent Targeted Drug Delivery Platform, *Chem. Biol. (Cambridge, MA, U. S.)*, 14 (2007) 107-115.
- [24] C. B. Carlson, P. Mowery, R. M. Owen, E. C. Dykhuizen, and L. L. Kiessling, Selective Tumor Cell Targeting Using Low-Affinity, Multivalent Interactions, *ACS Chem. Biol.*, 2 (2007) 119-127.
- [25] X. Montet, M. Funovics, K. Montet-Abou, R. Weissleder, and L. Josephson, Multivalent Effects of RGD Peptides Obtained by Nanoparticle Display, *J. Med. Chem.*, 49 (2006) 6087-6093.
- [26] R. H. Kramer and J. W. Karpen, Spanning binding sites on allosteric proteins with polymerlinked ligand dimers, *Nature* 395 (1998) 710-713.
- [27] D. E. Gloriam, R. Fredriksson and H. B. Schioth, The G protein-coupled receptor subset of the rat genome, *BMC Genomics* 8 (2007).
-

- [28] Y. Okuno, J. Yang, K. Taneishi, H. Yabuuchi, and G. Tsujimoto, GLIDA: GPCR-ligand database for chemical genomic drug discovery, *Nucleic Acids Res.*, 34 (2006) D673-D677.
- [29] N. Dinauer, S. Balthasar, C. Weber, J. Kreuter, K. Langer and H. von Briesen, Selective targeting of antibody-conjugated nanoparticles to leukemic cells and primary T-lymphocytes, *Biomaterials* 26 (2005) 5898-5906.
- [30] T. Pietschmann, Virology: Final entry key for hepatitis C, *Nature* 457 (2009) 797-798.
- [31] A. Ploss, M. J. Evans, V. A. Gaysinskaya, M. Panis, H. You, Y. P. de Jong and C. M. Rice, Human occludin is a hepatitis C virus entry factor required for infection of mouse cells, *Nature* 457 (2009) 882-886.
- [32] A. Elbakry, A. Zaky, R. Liebl, R. Rachel, A. Goepferich and M. Breunig, Layer-by-Layer Assembled Gold Nanoparticles for siRNA Delivery, *Nano Lett.* 9 (2009) 2059-2064.

# Supporting information

## **G-protein Coupled Receptor Targeted Nanoparticles Allow for Choosing between Membrane Binding and Cellular Uptake**

W. Hild<sup>1</sup>, K. Pollinger<sup>1</sup>, A. Caporale<sup>2</sup>, C. Cabrele<sup>3</sup>, M. Keller<sup>2</sup>, N. Pluym<sup>2</sup>,  
A. Buschauer<sup>2</sup>, R. Rachel<sup>4</sup>, J. Teßmar<sup>1</sup>, M. Breunig<sup>1</sup>, A. Göpferich<sup>1</sup>

<sup>1</sup> Department of Pharmaceutical Technology, University of Regensburg,  
Universitätsstraße 31, 93040 Regensburg, Germany

<sup>2</sup> Department of Pharmaceutical and Medicinal Chemistry, University of  
Regensburg, Universitätsstraße 31, 93053 Regensburg, Germany

<sup>3</sup> Department of Organic Chemistry, Ruhr-University Bochum,  
Universitätsstraße 150, 44801 Bochum, Germany

<sup>4</sup> Center for Electron Microscopy at the Institute for Anatomy, University of  
Regensburg, Universitätsstraße 31, 93053 Regensburg, Germany

*Transmission electron microscopy (TEM) investigation of ligand-conjugated QDs*

The QD-bioconjugates were imaged using a Philips CM12 transmission electron microscope (FEI Co., Eindhoven, The Netherlands). Therefore, 5  $\mu$ l of a 30 nM aqueous dilution of the sample were transferred onto a carbon-coated, glow-discharged copper grid. Excess liquid was removed by blotting with filter paper. A typical micrograph is shown in Supplementary Information (SI) fig. 1.

*Synthesis of [Lys<sup>4</sup>(N <sup>$\alpha$</sup> -Acetyl-Cys)]- (1), [Lys<sup>4</sup>(N <sup>$\alpha$</sup> -Acetyl-Cys), Arg<sup>6</sup>, Pro<sup>34</sup>]- (2) and [Lys<sup>4</sup>(N <sup>$\alpha$</sup> -Acetyl-Cys), Ahx<sup>9-17</sup>]-pNPY (3)*

Solid-phase peptide-chain assembly was performed on the synthesizer Syro-1 (MultiSynTech, Witten, Germany) by using the Rink amide 4-methylbenzhydrylamine resin (loading: 0.6 mmol·g<sup>-1</sup>). All amino acids were N <sup>$\alpha$</sup> -(9-fluorenylmethoxycarbonyl, Fmoc)-protected, with the exception of Tyr1 that was introduced as N <sup>$\alpha$</sup> -(*tert*-butyloxycarbonyl, Boc)-amino acid. The following side-chain protecting groups were used: 4-methyltrityl (Mtt) for Lys; *tert*-butyl for Asp, Glu, Ser, Thr and Tyr; trityl for Asn, Gln, Cys and His; 2,2,4,6,7-pentamethyldihydrobenzofuran-5-sulfonyl for Arg. Double couplings (2 x 40 min) were performed with amino acids (5 equivalents) activated *in situ* with O-(1-benzotriazolyl)-1,1,3,3-tetramethyluronium hexafluorophosphate (HBTU, 5 equiv.), 1-hydroxybenzotriazole (HOBt, 5 equiv.) and N,N-diisopropylethylamine (DIPEA, 10 equiv.). Fmoc cleavage was accomplished by first treating with 40% piperidine in N,N-dimethylformamide (DMF)/N-methylpyrrolidone (NMP) (4:1 vol./vol.) for 3 min, followed by a second treatment with 20% piperidine for 10 min. After coupling of Boc-Tyr1(*tert*-butyl) the Mtt group was selectively removed by washing (30 x 1 min) the peptidyl-resins with trifluoroacetic acid (TFA) / triisopropylsilane (TIS) / dichloromethane (DCM) (1:1:98 vol./vol.), followed by washings with DCM, DIPEA (1.2 equiv. in NMP), and DMF. The free Lys<sup>4</sup> side chain was acylated by performing a first coupling overnight with Fmoc-Cys(trityl)-OH / N,N-dicyclohexylcarbodiimide / HOBt/DIPEA (6:6:6:3 equiv.), followed by a second coupling with Fmoc-Cys(trityl)-OH / HBTU / HOBt / DIPEA (5:5:5:10 equiv.) for two hours. After removal of the Fmoc group with 20% piperidine in DMF (2 x 25 min) the free  $\alpha$ -amino group of Cys(trityl) was acetylated by using acetic anhydride / DIPEA (10:0.1 equiv.) for one hour. The completed peptides were cleaved from the resin with simultaneous side-chain deprotection by a three-hour treatment with the mixture TFA / TIS /



ethanedithiol / water (90:4:3:3 *vol./vol.*). The crude peptides were recovered by precipitation from ice-cold diethylether and centrifugation at 3 °C for 8 min. After several ether-washing / centrifugation cycles, the crude peptides were purified by preparative RP-HPLC (Agilent equipment) using the Phenomenex (Aschaffenburg, Germany) C18(2) column Luna (10 µm, 100 Å, 21.2 mm x 250 mm) and the following binary elution system: (A) 0.004% (*vol./vol.*) TFA in water and (B) acetonitrile. The peptide purity was > 90%, as determined by analytical RP-HPLC (L-6200A Intelligent Pump from Merck, HP detector Series 1050 from Agilent) with the Phenomenex C18(2) column Luna (3 µm, 100 Å, 4.60 mm x 150 mm) and the following elution system: (A) 0.012% (*vol./vol.*) TFA in water and (B) 0.01% (*vol./vol.*) TFA in acetonitrile. Analytical RPHPLC:  $t_R$  of 17 min. for **1**, 17.5 min. for **2**, and 15 min. for **3** (gradient: 10% B for 3 min., 10-70% B over 40 min.; UV-detection at 220 nm; flow of 1 ml/min). MALDI-TOF-MS (Future GSG spectrometer, Bruchsal, Germany): MW<sub>calcd.</sub>/MW<sub>found</sub> (Da): 4398.92/4400 for **1**, 4409.01 / 4410 for **2**, and 3614.18 / 3614 for **3**.

#### *Purification of nanoparticles after ligand coupling by gel filtration chromatography*

Gel filtration was conducted using a Sephacryl S-100 resin packed into a Tricorn 10/300 column (GE Healthcare, Chalfont St. Giles, UK). The column was coupled to standard HPLC equipment (Shimadzu, Duisburg, Germany) operating in the isocratic mode with the respective eluent and a flow rate of 0.5 ml/min. A UV-detector (SPD-10 AV, Shimadzu) operating at 635 nm was used for the determination of the QD concentrations. The peptides were detected by a fluorescence detector (RF-551) with excitation at 275 nm and emission at 310 nm. All QD concentrations were determined using the UV-detector signal together with a standard curve obtained from the areas under the curve for different QD concentrations. A typical chromatogram is shown in SI Figure 2. The fluorescence (area under curve) of the peptides occurring at 18 minutes, which corresponds to the conjugated fraction, was obtained after reaction and compared to the background measured for the activated QDs, normalized respective to the QD-concentrations obtained by UV-detection. The strong increase in the peak area of the fluorescence signal after bioconjugation to the particles indicated the successful linkage.

*Synthesis of BIBP3226 and SH-BIBP*

BIBP3226 and SH-BIBP were obtained by conversion of the  $N^G$ -Boc-*O*-*tert*-butyl protected analog of BIBP3226 (SI fig. 3) as published by Keller et al. (*J. Med. Chem.* **51**, 8168-81724 (2008)). BIBP3226 was obtained by deprotection in DCM / TFA (1:1) at room temperature for 3 h. SH-BIBP was synthesized under Ar atmosphere at room temperature using degassed solvents. Mass analysis results were obtained by electrospray ionization mass spectrometry (ESI-MS). First, 0.310 mmol of 6-acetylthiohexanoic acid was activated with 0.357 mmol carbonyldiimidazole in 3 ml DCM for 30 min. Then, 0.238 mmol of **1** and 0.119 mmol of triethylamine were added to the solution and left to react for 12 h. After solvent reduction under reduced pressure, **2** was purified by column chromatography using a preparative silica column and DCM / EE (5-3:1) as eluent. After solvent reduction, **2** was deprotected in 5 ml of DCM / TFA (2:3) with addition of 50  $\mu$ l of water for 2 h. After removing DCM and TFA under reduced pressure and re-suspension in 25 ml water, **3** was obtained after freeze-drying ( $MH^+=646.3$ ). The acetyl group of **3** was hydrolyzed by 1 N aqueous NaOH for 30 min at room temperature. After purification by preparative HPLC and the removal of the eluent under reduced pressure, Thiol-BIBP (**4**) was obtained. The product was lyophilized after resuspension in water ( $MH_+=604.3$ ). For more detailed information on the HPLC method see Keller et al. (*J. Med. Chem.* **51**, 8168-8172 (2008)).

*Binding and uptake of ligand-modified nanoparticles using NPY  $Y_1$ -receptor positive SK-N-MC neuroblastoma cells*

The results of the confocal fluorescence microscopy studies using the human neuroblastoma cell line SK-N-MC were similar to those for the MCF-7 cells. As shown in SI fig. 4, the [Lys<sup>4</sup>( $N^\alpha$ -Acetyl-Cys), Arg<sup>6</sup>, Pro<sup>34</sup>]-pNPY-QDs strongly associate with the cells (SI fig. 4A). The QDs can be found on the cell surfaces as well as internalized inside vesicular structures. Since the number of  $Y_1$ -receptors on SK-N-MC cells is lower as compared to MCF-7 cells, the internalized particles are even more clearly visible, since the fluorescence signal here is less dominated by the particles located near the cell surface. In contrast, the SH-BIBP-QDs can mainly be found on the cell surface and no internalization is visible (SI fig. 4B). The pictures (SI fig. 4C) and (SI fig. 4D) show the corresponding brightfield images.

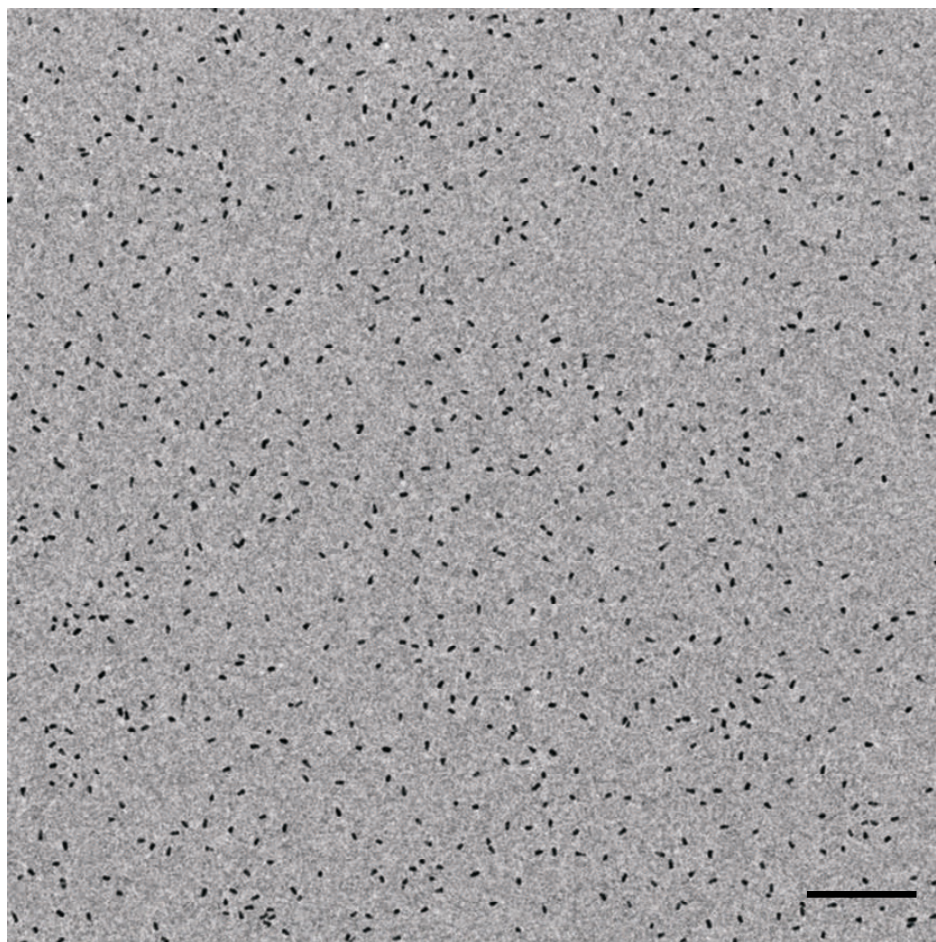


**Figure 1: TEM micrograph of peptide-modified QDs.** QDs were conjugated with  $[Lys^4(N^\alpha\text{-Acetyl-Cys}), Arg^6, Pro^{34}]$ -pNPY and imaged after purification. The particles are monodisperse, evenly distributed and show no sign of aggregation. The QD-cores are visible by TEM, due to their inherent contrast, while the polymer coating and the peptide show no contrast.

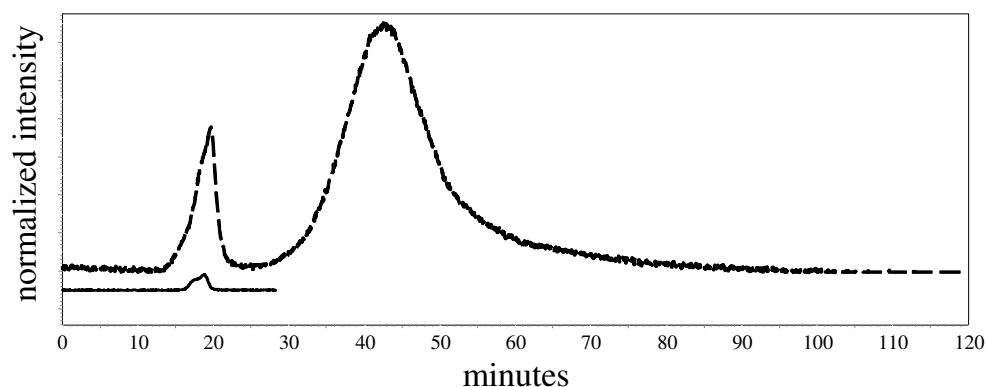


**Figure 2: Chromatogram recorded during quantum dot purification after bioconjugation.** Chromatogram, showing the peptide fluorescence signal, of QDs after activation with sulfo-SMCC (solid line) and after incubation with [Lys<sup>4</sup>(N<sup>α</sup>-Acetyl-Cys), Arg<sup>6</sup>, Pro<sup>34</sup>]-pNPY (dashed line), normalized to the QD-concentration obtained by the UV-signal (not shown). The first peak corresponds to the size-excluded fraction (QDs), the second peak is due to the excess of non-bound peptide. The strong increase of the fluorescence signal after bioconjugation shows the success of the reaction.

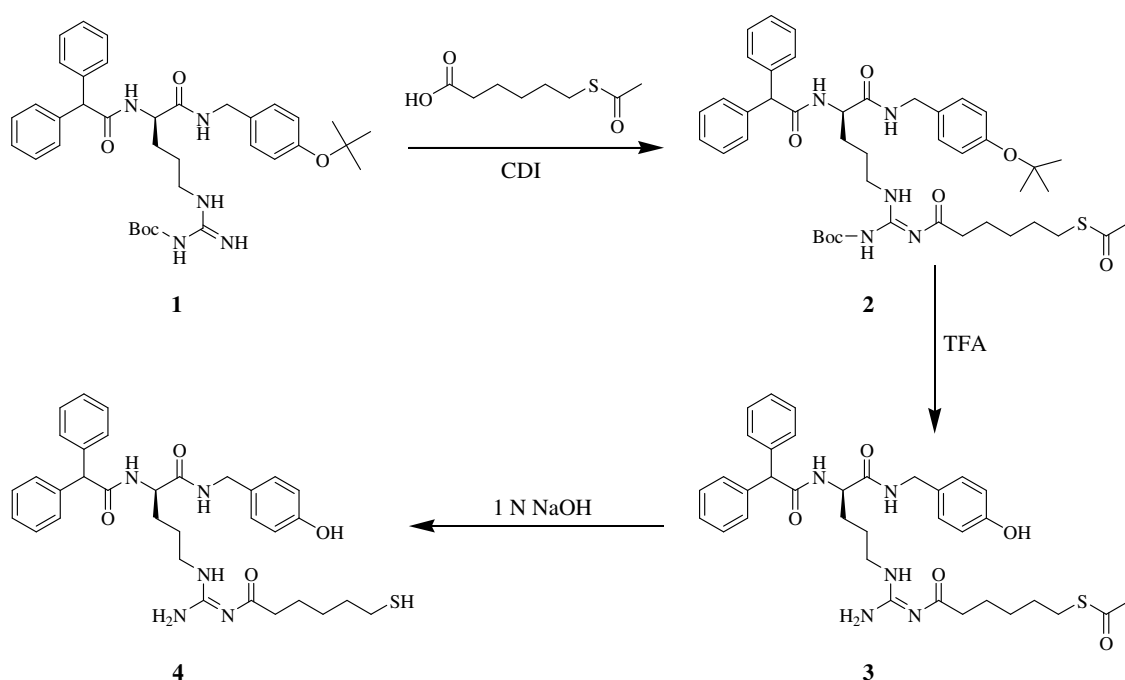


**Figure 3: Synthesis scheme of thiolated-BIBP (4).** Starting from the N<sup>G</sup>-Boc-O-tert-butyl protected analog of BIBP3226 (1), the guanidino group was acylated with 6-acetylthiohexanoic acid after activation of the carboxylic acid group using carbodiimidazole (CDI). After complete deprotection by TFA and NaOH, 4 was obtained.

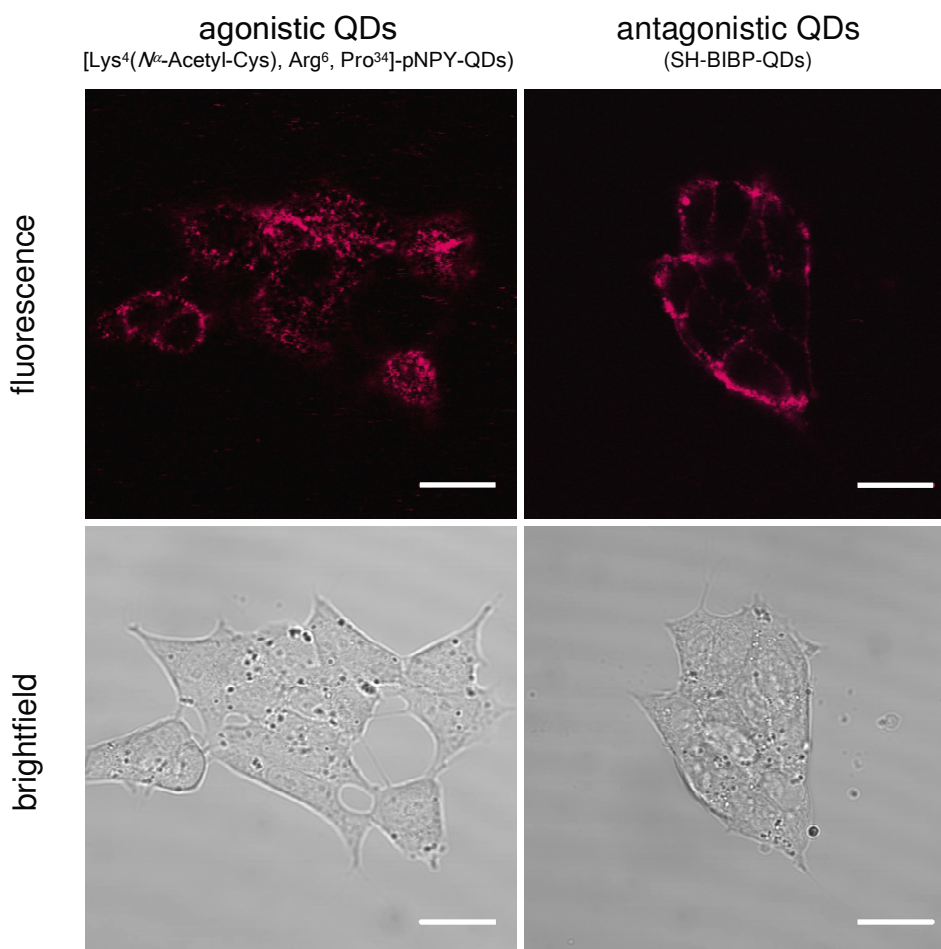


**Figure 4: Selective binding and uptake of QDs by SK-N-MC cells.** Confocal fluorescence micrographs showing the interaction of  $Y_1$ -receptor positive SK-N-MC cells with 10 nM of agonist-modified [Lys<sup>4</sup>(N<sup>α</sup>-Acetyl-Cys), Arg<sup>6</sup>, Pro<sup>34</sup>]-pNPY-QDs and antagonist-modified SH-BIBP-QDs. Both species associate with the cells. The fluorescence images (upper row) confirm that antagonist-modified QDs are only visible on the cell surfaces, whereas the agonist-modified particles are internalized into the cells in vesicular structures (scale bars = 20  $\mu$ m).

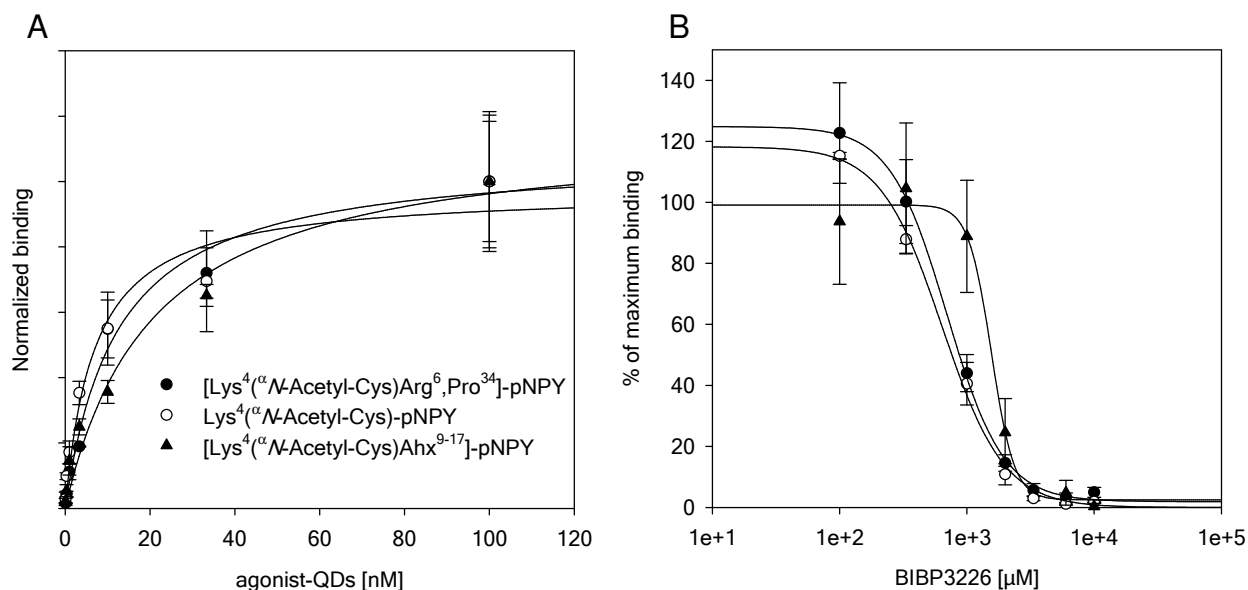


**Figure 5: Overview over the binding and displacement curves for the three different types of agonist-modified QDs. (A)** Specific binding curves normalized to the respective maximum binding. The binding behavior of the three peptides conjugated to the QDs is similar, each reaching saturation at approx. 100 nM. **(B)** Displacement curves were obtained by displacement of the QDs (1 nM) from MCF-7 cells by BIBP3226. All particles could be displaced from the receptors almost completely by millimolar amounts of the antagonist. (error bars represent SEM for  $n = 3$ ).

	$K_d \pm SD$ [nM]	$IC_{50} \pm SD$ [ $\mu$ M]
[Lys <sup>4</sup> (N <sup><math>\alpha</math></sup> -Acetyl-Cys)]-pNPY-QDs	6.92 $\pm$ 2.10	641 $\pm$ 61.1
[Lys <sup>4</sup> (N <sup><math>\alpha</math></sup> -Acetyl-Cys), Arg <sup>6</sup> , Pro <sup>34</sup> ]-pNPY-QDs	12.3 $\pm$ 2.60	696 $\pm$ 34.6
[Lys <sup>4</sup> (N <sup><math>\alpha</math></sup> -Acetyl-Cys), Ahx <sup>9-17</sup> ]-pNPY-QDs	20.7 $\pm$ 6.49	1555 $\pm$ 127
SH-BIBP-QDs	31.3 $\pm$ 5.66	822 $\pm$ 53.8

**Table 1: Comparison of binding- and inhibitory constants of different multiligand QDs and the monovalent antagonist BIBP3226.** Dissociation constants ( $K_d$ ) of the three agonist-modified QDs and SH-BIBP antagonist-modified QDs obtained from the binding curves and half maximal inhibitory concentrations ( $IC_{50}$ ) of BIBP3226 (using MCF-7 cells) determined in displacement studies.





# Chapter 9

## **Towards the Characterization of the Mechanism of Internalization of QDs Targeted to NPY Y<sub>1</sub>-receptors**

W. Hild, F. Schlenk, A. Göpferich

Department of Pharmaceutical Technology, University of Regensburg,  
Universitätsstraße 31, 93040 Regensburg, Germany

**Abstract**

The targeting of G-protein coupled receptors (GPCRs) represents a promising strategy for addressing nanoparticles to most types of cells in the human organism, since this receptor family is the largest, with over 800 different specific receptor subtypes. Being able to access these receptors for the delivery of nanoparticles carrying active substances directly to as well as into the target cells would substantially increase diagnostic and therapeutic possibilities.

It has been shown that the neuropeptide Y (NPY)  $Y_1$ -receptor can be selectively and very effectively targeted with nanoparticles that bind to the receptor-positive cells in high affinity. Moreover, the receptor mediated uptake of nanoparticles carries agonists for the receptor on the surface. However, there is almost no knowledge about the mechanism of this internalization of nanoparticles today. In this study, the uptake of quantum dots (QDs) modified with a peptidic  $Y_1$ -receptor agonist was analyzed using endosome markers and was compared to the uptake of the natural dye-labeled ligand. In addition, the specific uptake was compared to non-specific uptake of QDs modified with poly(ethyleneimine).

## Introduction

G-protein coupled receptors are the largest class of receptors in humans, with approx. 800 different subtypes and represent the most important class of targets in pharmacotherapy [1-3]. Besides their physiological function, i.e. signal transduction and mediation of sensoric impressions [4], these receptors also mediate specific interactions with nanoparticles. [5].

Neuropeptide Y (NPY)  $Y_1$ -receptors play an important role in signal transduction in the central nervous system and mediate effects like vasoconstriction and anxiolysis [6]. Moreover, these receptors are overexpressed in cancerous tissues, such as breast carcinoma and neuroblastoma [7-10], which renders these receptors interesting candidates for drug targeting.  $Y_1$ -receptors have been shown to rapidly internalize after agonist binding [11,12]. However, besides the internalization of natural ligands, these receptors have also been proven to mediate strong and very specific interactions between cells expressing the receptor and nanoparticles, more precisely quantum dots (QDs), which carry ligands for the receptor on their surface. Via these GPCRs, selective uptake of the QDs was observed (see chapter 8). However, the mechanism of internalization of the nanoparticles by these receptors has not been elucidated so far. Thus, it is not clear whether the particles are internalized by the route commonly taken by GPCRs after activation by their natural ligands, clathrin-mediated endocytosis [13,14]. It is possible that although this binding is highly receptor-specific, the appearance of the uptake could be via a route other than receptor-mediated endocytosis. To make a step towards the mechanism of the particle uptake by GPCRs, in this study the internalization of QDs modified with an agonistic peptide-ligand for the  $Y_1$ -receptor was investigated using dye-labeled transferrin, a marker for clathrin-mediated endocytosis [15]. The uptake of the peptide-modified agonistic QDs also was compared to the uptake of dye-labeled free ligand and QDs modified with a custom-designed poly(ethyleneimine) (PEI). While the former allows for comparison with the physiological uptake, the latter is typically bound and internalized non-specifically and thus is frequently used for nucleic acid delivery [16-18]. Thus, QDs modified with PEI represent a model for non-specific particle uptake. Using these tools, we were hopeful that new insights into the cellular delivery of nanoparticles mediated by GPCRs could be obtained.

**Materials and methods**

6-acetylthiohexanoic acid (97%), 4-(4,6-Dimethoxy-1,3,5-triazin-2-yl)-4-methylmorpholinium chloride (DMTMM) (purum,  $\geq 96\%$ ), 5,5'-dithiobis(2-nitrobenzoic acid) (DTNB) (99%), 2-mercaptoethanol ( $\geq 99\%$ ), 3-mercaptopropionic acid ( $\geq 99\%$ ), ninhydrin reagent (2% solution), poly(ethyleneimine) 50% solution (average molecular weight 1200 Da) (PEI) and sulfosuccinimidyl-4-(N-maleimidomethyl)-cyclohexane-1-carboxylate (sulfo-SMCC) were obtained from Sigma-Aldrich (St. Louis, MO). S0536-NPY was synthesized as published before [19] and was a generous gift of Prof. Buschauer, Department of Medicinal Chemistry, University of Regensburg. QDs (Qdot 655 IT amino (PEG) quantum dot), SYTO 13 and Alexa fluor 488 conjugated with human transferrin (Alexa488-Tf) were obtained from Invitrogen (Karlsruhe, Germany). Activation buffer consisted of 50 mM sodium tetraborate buffer, pH 7.2. Purification buffer I consisted of activation buffer, supplemented with 150 mM sodium chloride and 10 mM ethylenediaminetetraacetic acid (EDTA) disodium salt. Conjugation buffer contained two parts of purification buffer I and one part of dimethylformamide (DMF), whereas purification buffer II contained dimethylsulfoxide (DMSO) instead of DMF and 0.01% sodium azide. The ultrafiltration units had a 100 kDa cut-off membrane (Amicon Ultra-4, Millipore, Billerica, MA). Incubation medium consisted of phenol red-free Leibovitz F-15 Medium (Invitrogen), 1% of bovine serum albumin and 0.01% of Bacitracin (Invitrogen). All other cell-culture media as well as fetal calf serum (FCS) were obtained from Sigma-Aldrich.

*Peptide synthesis*

The peptidic  $Y_1$ -receptor agonist [Lys<sup>4</sup>( $\alpha$ -N-Acetyl-Cys), Arg<sup>6</sup>, Pro<sup>34</sup>]-pNPY was synthesized by standard automated solid phase synthesis and exhibited the sequence of the porcine neuropeptide Y (pNPY), with two amino acid exchanges in position 6 and 34 by Arg and Pro [20] and an additional cysteine side-chain in position 4 for the bioconjugation with the QDs. The sequence of the peptide was *H*-YPSK(Ac-N-C)PRNPGEDAPAEDLARYYSALRHYINLITRPRY-NH<sub>2</sub>. The mass was confirmed by MALDI-Tof using  $\alpha$ -cyano-4-hydroxycinnamic acid (HCA) matrix (calculated mass: 4409 Da; found mass: 4412 Da). For a detailed synthesis protocol see [21].

*Synthesis of thiol-modified poly(ethylene imine) (SH-PEI)*

The water of the PEI solution was removed by distillation with ethanol. For the reaction, 0.8 mmol of polymer dissolved in ethanol was reacted with 1.6 mmol of 6-acetylthiohexanoic acid and 6.4 mmol of DMTMM for 24 h at 40 °C. The solvent was removed under reduced pressure and the residue was dissolved in 0.1 N NaOH. After 1 h of stirring, the polymer was purified by a gravity PD-10 desalting column containing Sephadex G-25 (GE Healthcare, Chalfont St. Giles, UK), using 50 mM phosphate buffer at pH 7.0 as mobile phase. At every 0.5 ml, fractions were collected and analyzed for PEI and thiol content. The amount of PEI was determined by using the ninhydrin reaction [22]. The colored product was determined spectrophotometrically by measuring the absorbance at 570 nm and using unmodified PEI as the standard substance. Samples and the standard curve were prepared together by heating to 60 °C for 1h before measurement. The thiols were determined by means of the Ellman reagent. The reagent consisted of 50 mM sodium acetate and 2 mM DTNB. For the measurement, 50 µl of this solution and 100 µl of Tris buffer pH 8 were diluted with 849 µl of water. 10 µl of the sample was added and the sample was measured spectro-photometrically detecting the emerging thionitrobenzoic acid at 417 nm. A standard curve was obtained using mercaptopropionic acid. All UV absorbance measurements were recorded using an Uvikon 941 (Kontron Instruments, UK) and 10 cm polystyrol cuvettes.

*Conjugation of SH-PEI and [Lys<sup>4</sup>(<sup>α</sup>N-Acetyl-Cys)]- pNPY to quantum dots*

1 nmol of the QDs was transferred into 200 µl of activation buffer by buffer exchange using ultrafiltration. The QDs were subsequently activated using a 500-fold molar excess of sulfo-SMCC dissolved in activation buffer to yield a final volume of 250 µl. After 30 mins of gentle shaking at room temperature, the activated QDs were purified by gel filtration chromatography (see below) using purification buffer I as eluent. After buffer exchange by conjugation, buffer by ultrafiltration and concentration to a volume of 100 µl, the QDs were incubated with a 30 fold excess of [Lys<sup>4</sup>(<sup>α</sup>N-Acetyl-Cys), Arg<sup>6</sup>, Pro<sup>34</sup>]-pNPY or of the SH-PEI for 12 h at 4° C. Thereafter, a 100-fold molar excess of 2-mercaptoethanol was added to quench unreacted maleimides and after 30 mins the bioconjugate was purified by GFC using purification buffer II. Subsequently, the bioconjugate was concentrated by ultrafiltration to a final

concentration of 3  $\mu\text{M}$  and used for the biological studies. QDs covalently linked to [Lys<sup>4</sup>( $\alpha$ N-Acetyl-Cys), Arg<sup>6</sup>, Pro<sup>34</sup>]-pNPY or to SH-PEI are denoted NPY-QDs and PEI-QDs, respectively.

#### *Gel filtration chromatography*

Gel filtration of the QDs was conducted using a Sephacryl S-100 resin packed into a Tricorn 10/300 column (GE Healthcare, Chalfont St. Giles, UK). The column was coupled to standard HPLC equipment (Shimadzu, Duisburg, Germany) operating in isocratic mode with the respective eluent and a flow rate of 0.5 ml/min. The peptides were detected by a fluorescence detector (RF-551) with an excitation at 275 nm and emission at 310 nm. All concentrations were determined using the UV-detector (SPD-10 AV, Shimadzu) operating at 635 nm and a standard curve of the QDs by determination of the areas under the curve of the particle fraction of the chromatograms.

#### *Cell culture*

The human breast cancer cell line MCF-7 and the human neuroblastoma cell line SK-N-MC were grown in Minimum Essential Medium containing Earl's salts (EMEM) and supplemented with 110 mg of pyruvate and 2.2 g of sodium bicarbonate per litre. The medium contained 5 and 10% of FCS for MCF-7 and SK-N-MC cells, respectively. The human breast cancer cell line MDA was maintained in McCoy's 5A medium supplemented with 2.2 g sodium bicarbonate per litre and 10% of FCS. For microscopic investigations, 5000 cells were seeded into 8-well  $\mu$  slides (Ibidi, Munich, Germany) one day before being placed in the corresponding medium. MCF-7 cells were grown with the addition of 1 nM estradiol to increase the Y1-receptor density [23].

#### *Confocal laser scanning microscopy*

All investigations were carried out in incubation medium at 37 °C. The samples were imaged using a Zeiss Axiovert 200M inverted epifluorescence microscope coupled with an LSM 510 laser scanning device using Axiovert Software (Zeiss, Oberkochen, Germany) and using a Plan-Apochromat X40 water-immersion objective (NA 1.2). The QDs were excited using a 488 nm Ar laser and fluorescence was collected using

a 650 nm longpass filter. SYTO 13 nucleic acid stain was excited at 543 nm and fluorescence was collected using a 505-550 nm bandpass filter. QDs and SYTO were imaged together in multi-track mode. Alexa488-Tf was excited at 488 nm and fluorescence was collected using a 505-530 nm band pass filter and was imaged together with the QDs in single-track mode. S0536-NPY was excited at 633 nm and emission was filtered using a 650 nm longpass filter.

### **Results and discussion**

In order to characterize the uptake of NPY-QDs by cells expressing the human NPY Y<sub>1</sub>-receptor, MCF-7 cells were counterstained and investigated by CLSM. In fig. 1, it can clearly be seen that the QDs, visualized in red, are bound to the cell membranes and are also entering the cells but cannot pass the nuclear membrane, since QDs cannot be found inside the nuclei, which were stained blue.

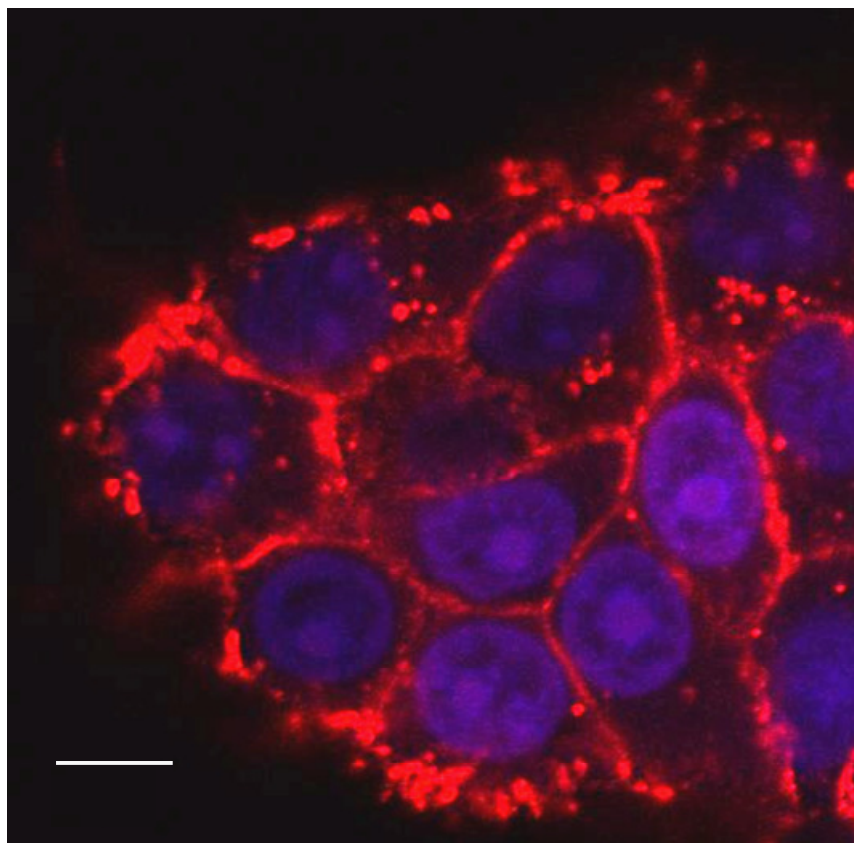
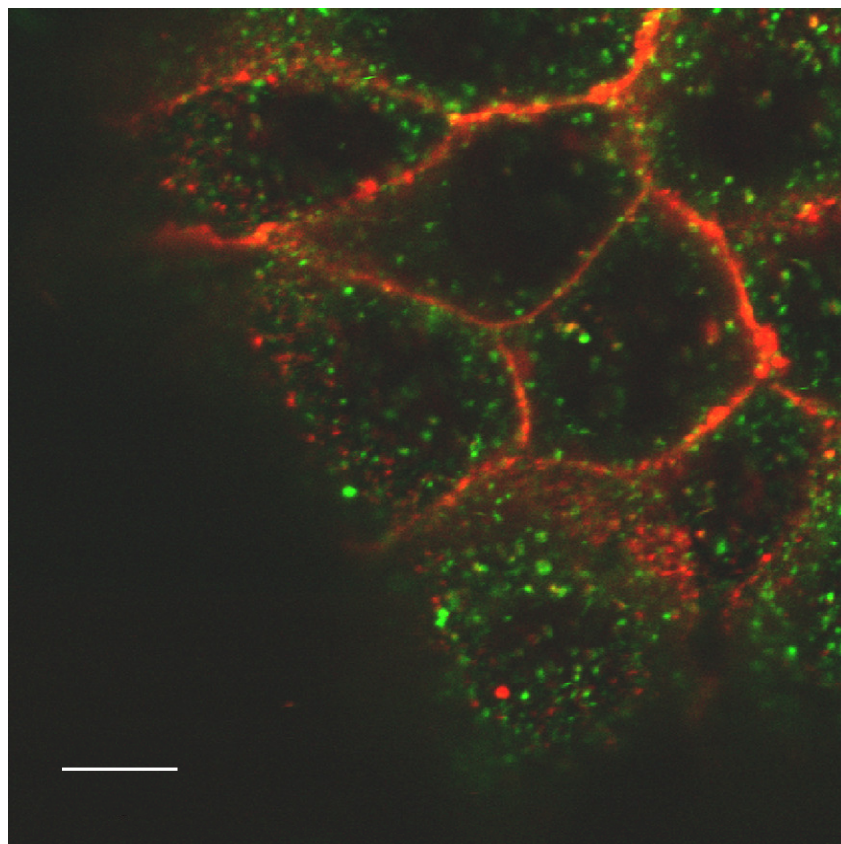


**Figure 1: Cellular uptake of NPY-QDs.** Cell nuclei of the MCF-7 cells are counterstained by SYTO 13 and visualized in blue. Binding of the QDs to the cell membranes and internalization is clearly visible. QDs do not enter the nuclei. Scale bar: 20  $\mu\text{m}$ .

It is known that after agonist binding, GPCRs are internalized into cells via clathrin coated pits and are subsequently present inside cells in endosomes [24]. Therefore, it was investigated whether QDs targeted towards these receptors take a similar route. Since transferrin is internalized into cells via receptor-mediated endocytosis as well, dye-labeled transferrin has become a frequently used marker of endosomes [15]. In fig. 2, green fluorescence is caused by Alexa488-Tf (green) which could be separated spectrally very well from the signal of the NPY-QDs which are shown in red. Both species are internalized into cells, since vesicular structures are visible throughout the cells, again with the exception of the nuclei which remain unstained. However, almost no colocalization of the NPY-QDs and Alexa488-Tf in endosomes was found which is indicated by the yellow color. Since transferrin and QDs seem to remain separated, this could suggest that the uptake of NPY-QDs would follow a route different from clathrin-mediated endocytosis. Moreover, the confocal

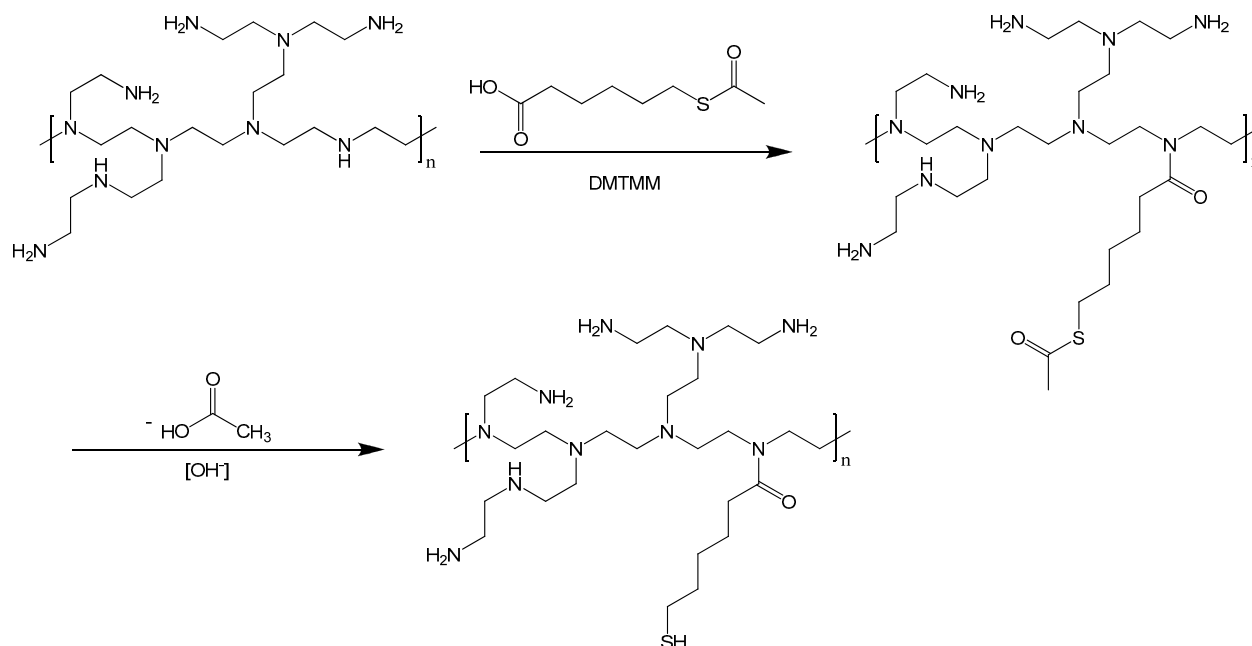


micrograph unambiguously proves that the NPY-QDs are taken up by the cells since they are localized on the same optical plane as the endosomes containing Alexa488-Tf.



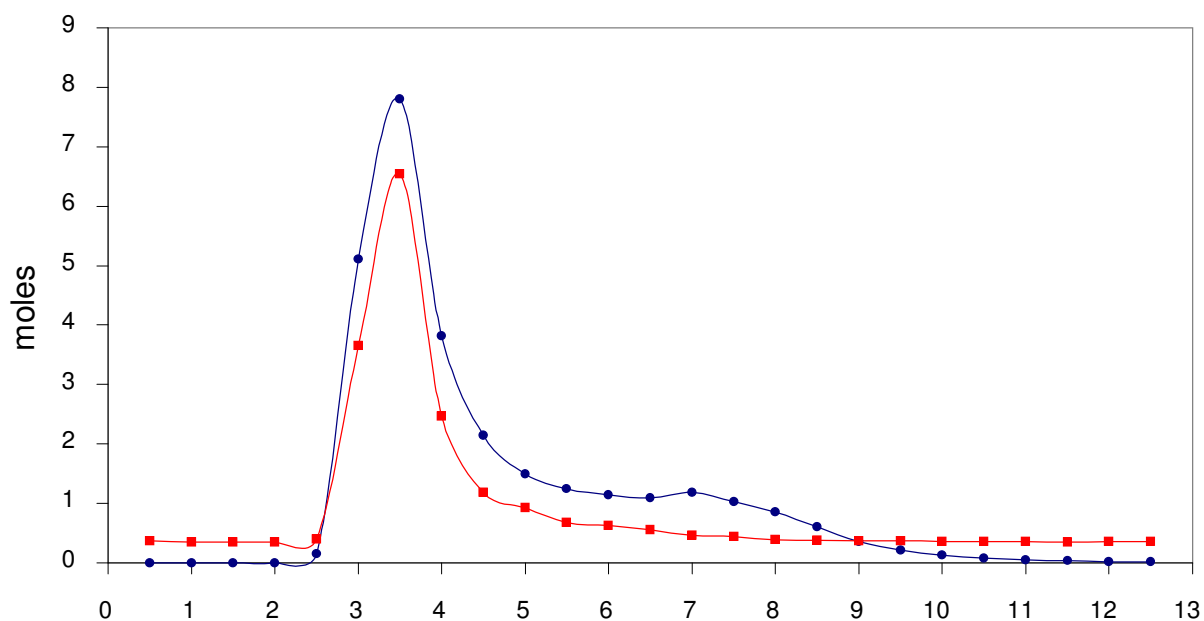
**Figure 2: NPY-QDs (red) and Alexa488-Tf labeled endosomes (green).** Though partially present in intracellular vesicles, the QDs are not colocalized in endosomes together with the labeled transferrin. Scale bar: 20  $\mu\text{m}$ .

For further characterization of the cellular uptake mechanism, the uptake of NPY-QDs was compared with that of the free ligand and QDs coated with PEI. This highly positively charged polymer is known for mediating cellular uptake without discriminating between cells. Therefore, this polymer has become a standard tool for cell transfection with nucleic acids [25]. While S0536-labeled pNPY has already been synthesized by Schneider *et al.* [19], the preparation of PEI-QDs had to be established. In order to bind the polymer to the QDs, PEI of a molecular weight of 1200 Da was modified with a thiolcarboxylic acid to introduce a thiol group. The reaction scheme is depicted in figure 3. After amide coupling of the PEI with the S-acetyl protected  $\epsilon$ -mercaptohexanoic acid, mediated by the coupling reagent DMTMM, the acetyl group was removed by basic hydrolysis to yield SH-PEI.



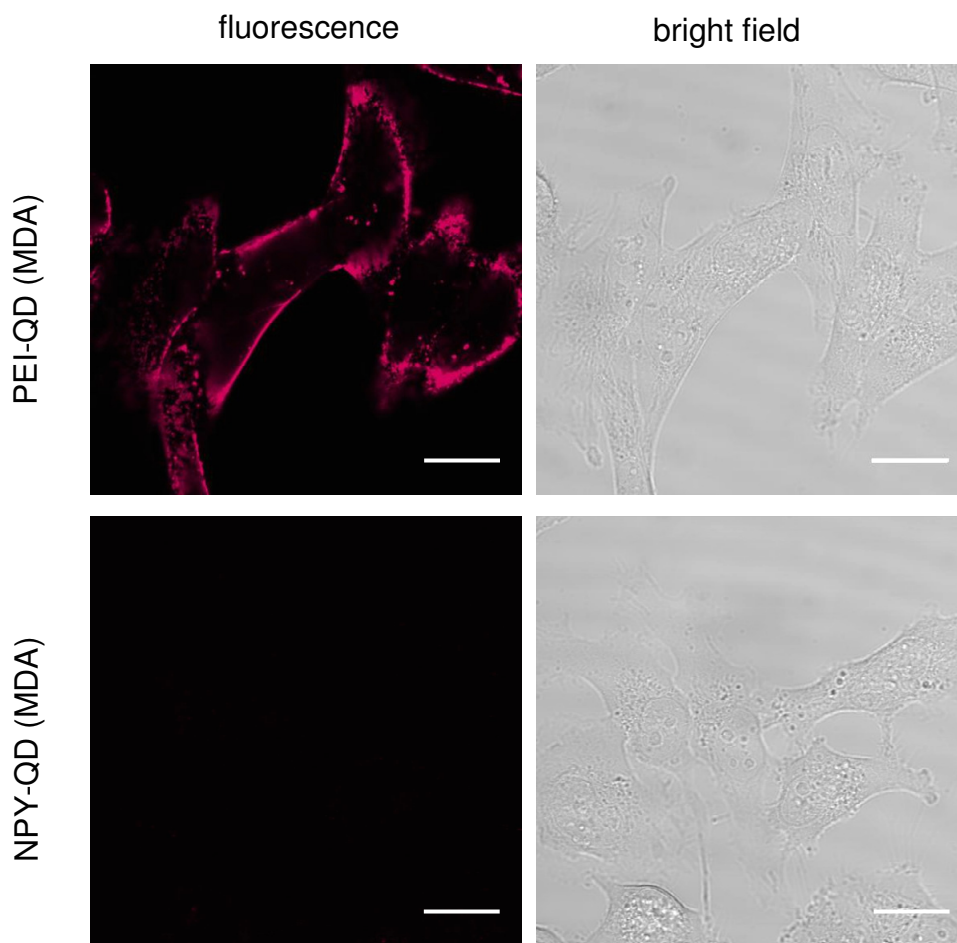
**Figure 3: Synthesis scheme of SH-PEI.** PEI (1200 Da) is acylated by S-acetylthiohexanoic acid mediated by the coupling reagent DMTMM. After this, deacetylation was obtained by basic hydrolysis to yield SH-PEI.

Fig. 4 shows the chromatogram of SH-PEI in the last purification step. The chromatogram shows a main peak at 3.5 ml representing the PEI. While the amount of thiols is depicted by the blue circles, the PEI content is shown by the red squares. Correlating both signals results in approx. 1.3 thiol groups per PEI molecule on average. By varying the ratio of 6-acetylthiohexanoic acid to PEI, the degree of thiol modification could be changed (not shown). The SH-PEI was subsequently bound to QDs.



**Figure 4: Purification and characterization of SH-PEI by size exclusion chromatography.** Fractions concerning the PEI-content (■) and the thiol-content (●) were analyzed. The calculated number of thiols per PEI molecule was 1.3.

To see whether the PEI-QDs prepared do indeed mediate non-specific cell binding and uptake, the interactions with the  $Y_1$ -receptor free human breast cancer cell line MDA were compared to their interactions of the NPY-QDs with the cells. In fig. 5, the PEI-QDs show strong binding to the cell surfaces and are also partially internalized into the cells. In contrast, no non-specific interactions of the NPY-QDs with the MDA cells can be seen.



**Figure 5: Binding and internalization of non-specific PEI-QDs and  $Y_1$ -receptor targeted NPY-QDs at  $Y_1$ -receptor negative MDA cells.** While the PEI-QDs are bound and internalized, the NPY-QDs specifically targeted towards  $Y_1$ -receptors show no interaction with the cells. Scale bar: 20  $\mu\text{m}$ .

In fig. 6, the uptake of NPY-QDs by  $Y_1$ -receptor positive MCF-7 cells is compared to the uptake of S0536-NPY and PEI-QDs. As for S0536-NPY, the NPY-QDs are found in vesicular structures inside the MCF-7 cells. However, the QDs seem to have accumulated at the cell membranes too while the S0536-NPY shows slightly lower concentration at the cell membranes. In contrast, the PEI-QDs are highly dispersed at the cell membranes, though diffuse fluorescence appears in the cytoplasm. Here, the tendency to form vesicular structures is lower than for the two GPCR-targeted species. This shows that the specific uptake of ligands and nanoparticles has a different appearance than non-specific uptake. When comparing PEI-QDs with NPY-QDs, it was found that the intensity of the first species was tremendously higher than

the NPY-QDs. This is because PEI-QDs, in contrast to the NPY-QDs, can only bind to a limited number of receptors.

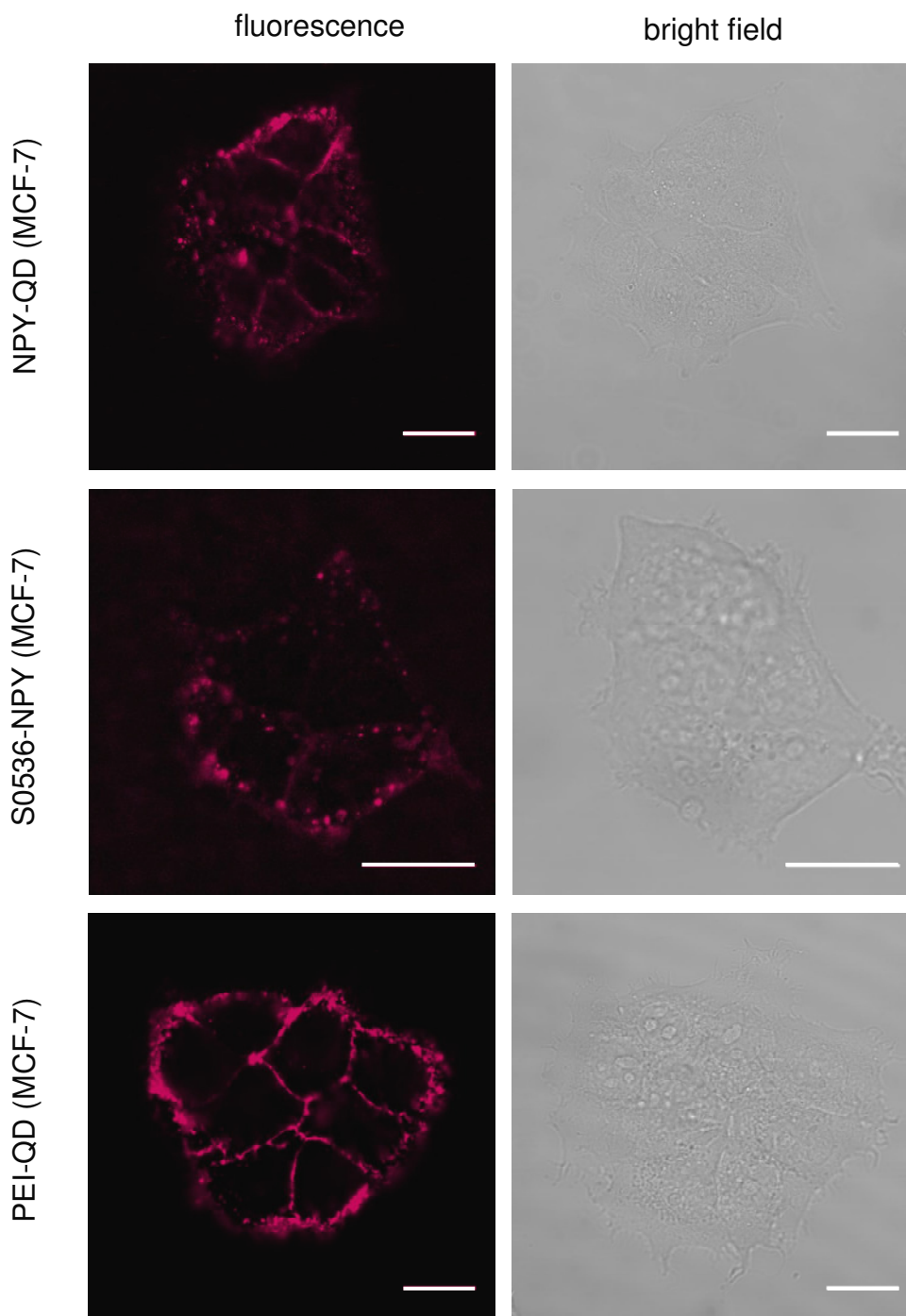


**Figure 6: Comparison of the binding and internalization of NPY-QDs, S0536-labeled pNPY and PEI-QDs by  $Y_1$ -receptor positive MCF-7 cells.** The  $Y_1$ -receptor targeted QDs and the dye-labeled agonist S0536-pNPY show similar internalization behavior and are localized in vesicles. In contrast, the PEI-QDs are mainly localized on the cell membranes. Scale bar: 20  $\mu\text{m}$ .

Similar findings were made when using SK-N-MC cells also expressing the  $Y_1$ -receptor (fig. 7). While the NPY-QDs are found inside intracellular vesicles, the PEI-QDs are found in large amounts on the cell membranes. However, internalization seems to take place as well. Again, the intensity of the fluorescence when regarding the cells was much higher than for the NPY-QDs.

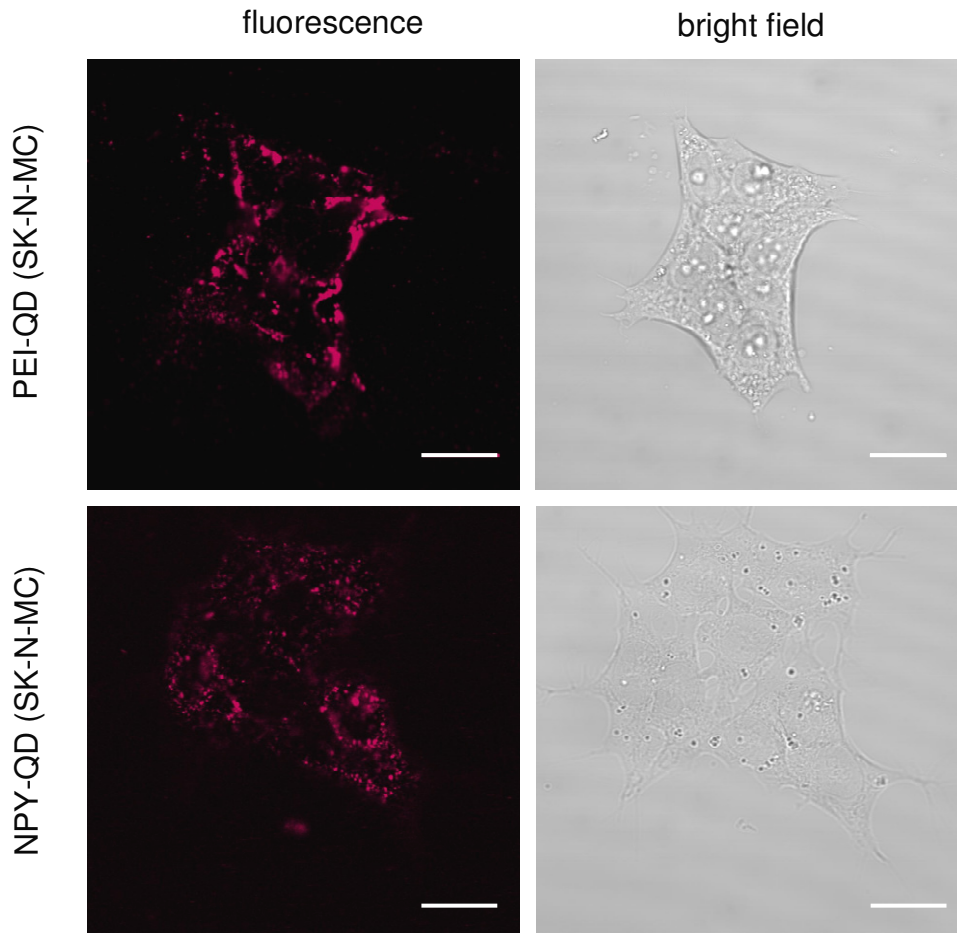


**Figure 7: Comparison of the binding and internalization of NPY-QDs and PEI-QDs at  $Y_1$ -receptor positive SK-N-MC cells.** While the majority of the PEI-QDs stick to the cell membranes and only a few substances are internalized, the NPY-QDs can be found inside the cells in higher amounts inside vesicular structures. Scale bar: 20  $\mu$ m.

**Summary and conclusion**

In summary, the specific uptake of QDs via NPY  $Y_1$ -receptors was studied by CLSM using endosome markers and free dye-labeled ligand as well as QDs modified with a custom-designed PEI. It was found that after endocytosis, the QDs modified with the GPCR-ligand are localized inside cells but not together with transferrin, a commonly used endosome marker. However, the appearance of the endosomes derived from QDs internalized by  $Y_1$ -receptors looks very similar to the ones obtained after uptake of the free dye-labeled agonist S0536-pNPY. These findings again make clear that endocytosis can occur in various forms, dependent upon the substance to be internalized. Since the pathway of internalization directly influences the fate of nanoparticles inside the cells, further investigations will be helpful to further elucidate the pathway of cellular uptake by GPCRs.

**References**

- [1] M. C. Lagerstroem and H. B. Schioeth, Structural diversity of G protein-coupled receptors and significance for drug discovery, *Nature Reviews Drug Discovery*, 7 (2008) 339-357.
- [2] R. T. Dorsam and J. S. Gutkind, G-protein-coupled receptors and cancer, *Nature Reviews Cancer*, 7 (2007) 79-94.
- [3] M. J. Marinissen and J. S. Gutkind, G-protein-coupled receptors and signaling networks: emerging paradigms, *Trends in Pharmacological Sciences* 22 (2001) 368-376.
- [4] B. K. Kobilka and X. Deupi, Conformational complexity of G-protein-coupled receptors, *Trends in Pharmacological Sciences*, 28 (2007) 397-406.
- [5] S. H. Young and E. Rozengurt, Qdot nanocrystal conjugates conjugated to bombesin or ANG II label the cognate G protein-coupled receptor in living cells, *Am. J. Physiol.*, 290 (2006) C728-C732.
- [6] C. Cabrele and A. G. Beck-Sickinger, Molecular characterization of the ligand-receptor interaction of the neuropeptide Y family, *Journal of Peptide Science*, 6 (2000) 97-122.
- [7] J. C. Reubi, M. Gugger, B. Waser, and J. C. Schaer, Y1-mediated effect of neuropeptide Y in cancer: breast carcinomas as targets, *Cancer Res.*, 61 (2001) 4636-4641.
- [8] T. Pedrazzini, F. Pralong, and E. Grouzmann, Neuropeptide Y: the universal soldier, *Cellular and Molecular Life Sciences*, 60 (2003) 350-377.
- [9] M. Koerner and J. C. Reubi, NPY receptors in human cancer: A review of current knowledge, *Peptides*, 28 (2007) 419-425.
- [10] J. Kitlinska, Neuropeptide Y (NPY) in neuroblastoma: Effect on growth and vascularization, *Peptides*, 28 (2007) 405-412.
- [11] M. Fabry, M. Langer, B. Rothen-Rutishauser, H. Wunderli-Allenspach, H. Hocker, and A. G. Beck-Sickinger, Monitoring of the internalization of neuropeptide Y on neuroblastoma cell line SK-N-MC, *Eur. J. Biochem.*, 267 (2000) 5631-5637.
- [12] H. Gicquiaux, S. Lecat, M. Gaire, A. Dieterlen, Y. Mely, K. Takeda, B. Bucher, and J. L. Galzi, Rapid internalization and recycling of the human neuropeptide Y Y1 receptor, *Journal of Biological Chemistry*, 277 (2002) 6645-6655.
- [13] R. Weissleder, K. Kelly, E. Y. Sun, T. Shtatland, and L. Josephson, Cell-specific targeting of nanoparticles by multivalent attachment of small molecules, *Nat. Biotechnol.*, 23 (2005) 1418-1423.



- 
- [14] B. L. Wolfe and J. Trejo, Clathrin-Dependent Mechanisms of G Protein-coupled Receptor Endocytosis, *Traffic*, 8 (2007) 462-470.
- [15] S. H. Hansen, K. Sandvig, and B. van Deurs, Molecules internalized by clathrin-independent endocytosis are delivered to endosomes containing transferrin receptors, *J. Cell Biol.*, 123 (1993) 89-97.
- [16] W. T. Godbey, K. K. Wu, and A. G. Mikos, Poly(ethylenimine) and its role in gene delivery, *Journal of Controlled Release*, 60 (1999) 149-160.
- [17] H. Duan and S. Nie, Cell-Penetrating Quantum Dots Based on Multivalent and Endosome-Disrupting Surface Coatings, *Journal of the American Chemical Society*, 129 (2007) 3333-3338.
- [18] L. A. Davies, G. McLachlan, S. G. Sumner-Jones, D. Ferguson, A. Baker, P. Tennant, C. Gordon, C. Vrettou, E. Baker, J. Zhu, E. W. Alton, D. D. Collie, D. J. Porteous, S. C. Hyde, and D. R. Gill, Enhanced Lung Gene Expression After Aerosol Delivery of Concentrated pDNA/PEI Complexes, *Mol Ther*, 16 (2008) 1283-1290.
- [19] E. Schneider, M. Mayer, R. Ziemek, L. Li, C. Hutzler, G. Bernhardt, and A. Buschauer, A simple and powerful flow cytometric method for the simultaneous determination of multiple parameters at G protein-coupled receptor subtypes, *ChemBioChem*, 7 (2006) 1400-1409.
- [20] R. M. Soll, M. C. Dinger, I. Lundell, D. Larhammer, and A. G. Beck-Sickinger, Novel analogues of neuropeptide Y with a preference for the Y1-receptor, *Eur. J. Biochem.*, 268 (2001) 2828-2837.
- [21] see chapter 8 of this thesis
- [22] B. Starcher, A Ninhydrin-Based Assay to Quantitate the Total Protein Content of Tissue Samples, *Analytical Biochemistry*, 292 (2001) 125-129.
- [23] H. Amlal, S. Farouqi, A. Balasubramaniam, and S. Sheriff, Estrogen up-regulates neuropeptide Y Y1 receptor expression in a human breast cancer cell line, *Cancer Research*, 66 (2006) 3706-3714.
- [24] S. D. Conner and S. L. Schmid, Regulated portals of entry into the cell, *Nature*, 422 (2003) 37-44.
- [25] U. Lungwitz, M. Breunig, T. Blunk, and A. Goepferich, Polyethylenimine-based non-viral gene delivery systems, *European Journal of Pharmaceutics and Biopharmaceutics*, 60 (2005) 247-266.



# **Chapter 10**

## **Summary and Conclusions**

## Summary

Targeted delivery of nanoparticles to specific cells has great potential to optimize drug therapy. Through this method, drawbacks in contemporary drug therapy could be overcome. Active substances would no longer be distributed to all regions in the body and thus the side-effects and toxic reactions could be decreased significantly. Moreover, such a delivery of nanoparticles would highly support new therapy strategies which need to be directed to specific cells, like gene therapy of diseased cells [1,2]. Though the idea of drug targeting has been existing for more than 100 years [3] and though promising nanoparticulate drug carriers have been developed [4,5], still the question has to be solved how to deliver these particles effectively to specific target cells.

For the investigation of the delivery of nanoparticles to specific kinds of cells, quantum dots (QDs), semiconductor nanocrystals, were reported to be promising tracers. QDs offer small and well-defined sizes and outstanding fluorescence properties. Due to these properties numerous studies enlightened the more or less specific delivery of QDs to cells by different cellular targets. In this context, the receptor-mediated endocytosis by distinct cell surface receptors was the most promising pathway for the delivery of nanoparticles into specific cells ([chapter 1](#)).

However, the largest class of receptors in the human genome [6], the G-protein coupled receptors (GPCRs), has only barely been investigated for their potential for being a specific portal into specific cells. Having access to this class of receptors for nanoparticle targeting would substantially increase the number of possible targets. Therefore, the main goal of this thesis was the development of ligand-modified QDs targeted to cells expressing a specific GPCR, the human neuropeptide Y (NPY) Y<sub>1</sub>-receptor which served as model receptor the class of GPCRs ([chapter 2](#)).

For this purpose, practical protocols for the synthesis of QDs were developed, based on their fabrication in non-coordinating and coordinating solvents. It turned out that QDs synthesized in the latter exhibited higher fluorescence quantum yields, which increases the sensitivity for their detection in biological studies ([chapter 3](#)).

In order to use these tracers as model colloids in biological systems, it was necessary to modify the particle surfaces to render the particles water-soluble. The investigations showed that introducing poly(ethylene glycol) (PEG) in the coating yielded highly stable QD-dispersions. A very convenient coating strategy was to use

PEG-modified phosphatidylethanolamines (PEG-PEs), as besides simple preparation of PEG-PE-QDs, the functionalization of the particles is very flexible, as PEG-PEs are available with numerous functional groups ([chapter 4](#)).

Having established the fabrication of stable PEGylated QDs, the exact characterization of the size-distribution of QDs for biological applications was of major interest, since the sizes of nanoparticles substantially influence their interactions with biological systems [7]. For this purpose, asymmetrical flow field-flow fractionation (AF4) was used. With this technique, a robust method for the separation of QDs as well as size-analysis was available. Moreover, for the first time, an estimation of the masses of QDs was presented, showing that QDs had molar masses of 300 kDa and higher ([chapter 5](#)).

The as-developed QDs subsequently had to prove their potential for use in cellular uptake studies in order to be an adequate model nanoparticle system. After microinjection it was found that the QDs could easily be detected inside living cells. The non-specific interactions with cells were extremely low, which was a decisive prerequisite for their use in studying specific interactions with cells. Additionally, the cytotoxicity of QDs was investigated, with the result that the toxic effects of the QDs were of minor significance when using the particles in concentrations up to 500 nM ([chapter 6](#)).

In order to explore whether QDs can be delivered into specific cells as model nanoparticles, the particles were modified with agonists or an antagonist of the human neuropeptide Y (NPY)  $Y_1$ -receptor. Interestingly, the particles showed extremely high affinity towards cells expressing the receptor, which was 5 orders of magnitude higher than the affinity of the free ligands. The nanoparticles were delivered into the cells by endocytosis when the ligand was an agonist. In the case of an antagonist, the particles remained on the cell surface. These findings successfully proved the enormous potential of GPCRs for targeted nanoparticles delivery ([chapter 8](#)).

The bioconjugation between the peptidic  $Y_1$ -receptor ligand and the nanoparticles is a decisive step, since in this step the specific targeting properties are bestowed upon the nanoparticles. The bioconjugation reaction was optimized using PEG-PE micelles and different pH values and the success of the coupling reaction was unequivocally proven by gel filtration chromatography and mass spectrometry. Through this, the first step towards a drug delivery system was taken, since micelles have already

been described as drug delivery vehicles [8,9]. The  $Y_1$ -receptor agonist-modified micelles exhibited specific delivery into the target cells by the GPCR ([chapter 7](#)).

Finally, the mechanism of QD-internalization by  $Y_1$ -receptor positive cells was investigated. It was found that there are several similarities between agonist-modified QDs and the free dye-labeled pNPY. Both were internalized and could be found inside intracellular vesicles. However, in contrast to the free ligand, the QDs were not colocalized with the endosome-marker transferrin. Comparison with non-specifically binding poly(ethyleneimine)-modified QDs (PEI-QDs) revealed that the specifically binding QDs are found inside the cells and yielded different characteristics in the fluorescence microscope ([chapter 9](#)).

## Conclusions

In conclusion, this thesis has successfully demonstrated that GPCRs are far more than just important targets in drug therapy – they also bear high potential for the targeted delivery of nanoparticles into specific cells. The results showed how to build stable QD-based model colloids that can be used for cellular uptake studies. Using bioconjugates between QDs and ligands of the human NPY  $Y_1$ -receptor, highly affine nanoparticle targeting and the delivery into cells expressing the GPCR were obtained.

The results have several implications that must be considered in future investigations. First of all, by introducing GPCRs into the field of nanoparticle targeting, a class of more than 800 candidates is accessible for specific targeting. Moreover, since the receptors discriminate between agonists and antagonists, it is possible to choose whether the particles are delivered into the cells for therapeutic purposes (agonist-conjugated nanoparticles) or whether they remain on the cell surfaces as diagnostic tag (antagonist-conjugated nanoparticles). The demonstrated multiligand-binding can be used for the combination of several different GPCR-ligands on one particle. This would open up the possibility of creating nanoparticles that fit to a very distinct receptor-pattern and would increase the cell-type selectivity enormously. Multiligand binding could also create a new class of receptor ligands, for ‘conventional’ therapeutic purposes, binding several orders of magnitude stronger than the ligands known up to now.

---

**References**

- [1] I. A. Khalil, K. Kogure, H. Akita, and H. Harashima, Uptake Pathways and Subsequent Intracellular Trafficking in Nonviral Gene Delivery, *Pharmacol. Rev.*, 58 (2006) 32-45.
- [2] Y. Dorsett and T. Tuschl, siRNAs: applications in functional genomics and potential as therapeutics, *Nat Rev Drug Discov*, 3 (2004) 318-329.
- [3] K. Strebhardt and A. Ullrich, Paul Ehrlich's magic bullet concept: 100 years of progress, *Nature Reviews Cancer*, 8 (2008) 473-480.
- [4] J. Rao, Shedding Light on Tumors Using Nanoparticles, *ACS Nano*, 2 (2008) 1984-1986.
- [5] K. Cho, X. Wang, S. Nie, Z. Chen, and D. M. Shin, Therapeutic Nanoparticles for Drug Delivery in Cancer, *Clinical Cancer Research*, 14 (2008) 1310-1316.
- [6] M. C. Lagerstroem and H. B. Schioeth, Structural diversity of G protein-coupled receptors and significance for drug discovery, *Nature Reviews Drug Discovery*, 7 (2008) 339-357.
- [7] W. Jiang, B. Y. S. Kim, J. T. Rutka, and W. C. W. Chan, Nanoparticle-mediated cellular response is size-dependent, *Nat. Nanotechnol.*, 3 (2008) 145-150.
- [8] T. Musacchio, V. Laquintana, A. Latrofa, G. Trapani, and V. P. Torchilin, PEG-PE Micelles Loaded with Paclitaxel and Surface-Modified by a PBR-Ligand: Synergistic Anticancer Effect, *Molecular Pharmaceutics*, 6 (2009) 468-479.
- [9] N. Nasongkla, E. Bey, J. Ren, H. Ai, C. Khemtong, J. S. Guthi, S. F. Chin, A. D. Sherry, D. A. Boothman, and J. Gao, Multifunctional Polymeric Micelles as Cancer-Targeted, MRI-Ultrasensitive Drug Delivery Systems, *Nano Lett.*, 6 (2006) 2427-2430.





# Appendix



**Abbreviations**

<sup>1</sup> H-NMR	Proton nuclear magnetic resonance spectroscopy
5HT	5-hydroxytryptamine
AFM	atomic force microscopy
Alexa488-Tf	Alexa Fluor 488-labeled human transferrin
AMPA	α-Amino-3-hydroxy-5-methyl-4-isoxazole-propionic acid
ANG II	angiotensin II
AT	angiotensin receptor
BIBP3226	selective NPY Y <sub>1</sub> -receptor antagonist
CCV	clathrin coated vesicle
Cd	Cadmium
CdO	cadmium oxide
CdSe	cadmium selenide
CHO	chinese hamster ovary
CHO	chinese hamster ovary cell line
CL-MUA-QDs	MUA-QDs exhibiting a surface crosslinked with lysine
CLSM	confocal laser scanning microscopy
CME	clathrin mediated endocytosis
CO <sub>2</sub>	carbon dioxide
CPP	cell penetrating peptide
cryo-TEM	Kryo-Transmissionselektronenmikroskopie
Cys-NPY	[Lys <sup>4</sup> ( <sup>α</sup> N-Acetyl-Cys), Arg <sup>6</sup> , Pro <sup>34</sup> ]-pNPY
Da	Dalton
DCC	<i>N,N'</i> -dicyclohexylcarbodiimide
DHLA	dihydrolipoic acid
DLS	dynamic light scattering
DLS	dynamic light scattering
DMF	dimethylformamide
DMSO	dimethylsulfoxide
DMTMM	4-(4,6-Dimethoxy-1,3,5-triazin-2-yl)-4-methylmorpholinium chloride
DNA	desoxyribunucleic acid
DTNB	5,5'-dithiobis(2-nitrobenzoic acid)

## Appendix

---

EDC	1-ethyl-3-(3-dimethylaminopropyl) carbodiimide
EGF	epidermal growth factor
EGFR	epidermal growth factor receptor
EMEM	minimum essential medium containing Earl's salts
EPR	enhanced permeability and retention
erbB1	Epidermal growth factor subtype
FACS	fluorescence activated cell sorting
FCS	Fetal calf serum
FR	folate receptor
FWHM	full width at half maximum
GFC	gel filtration chromatography
GPCR	G-protein coupled receptor
HDA	hexadecylamine
HEK	human embryonic kidney
Her2	human epidermal growth factor receptor 2
HIV	human immunodeficiency virus
HIV TAT	human immunodeficiency virus transactivator protein
IL-2	interleukin-2
K <sub>2</sub> CO <sub>3</sub>	potassium carbonate
LDL	low-density lipoprotein
MALDI-ToF	matrix assisted laser desorption/ionization time of flight mass spectrometry
MCF-7	human breast cancer cell line
MDA	human breast cancer cell line
MLS	mitochondrial localization signal
MMP	matrix metalloprotease
MRI	magnetic resonance imaging
MUA	11-mercaptopundecanoic acid
MUA-QDs	quantum dots hydrophilized by mercaptopundecanoic acid
NGF	nerve growth factor
NHS	N-hydroxysuccinimide
NIR	near infrared
NLS	nuclear localization signal

## Appendix

---

NMR	nuclear magnetic resonance
NPY	neuropeptide Y
OA	oleic acid
PEG	poly(ethylene glycol)
PEG	polyethylene glycol
PEG-PE	PEGylated phosphatidylethanolamine
PEG-PE-QDs	quantum dots hydrophilized by PEG-PE
PEI	poly(ethyleneimine)
PET	positron emission tomography
PL	photoluminescence
pNPY	porcine neuropeptide Y
PO-PEG	phosphine oxide-modified PEG
PO-PEG-QDs	quantum dots hydrophilized by phosphine oxide-modified PEG
PSMA	prostate specific membrane antigen
PTD	protein transduction domain
QD	quantum dot
RES	reticulo endothelial system
ROS	reactive oxygen species
S	sulfur
SERT	serotonin transporter protein
SH-PEI	thiol-modified PEI
SK-N-MC	human neuroblastoma cell line
SNAC	serotonin-labeled CdSe nanocrystals
SPECT	single photon emission computerized tomography
SPION	superparamagnetic iron oxide nanoparticle
sulfo-SMCC	sulfosuccinimidyl-4-(N-maleimidomethyl)-cyclohexane-1-carboxylate
SV40	simian virus 40
TAMRA	5(6)-carboxytetramethylrhodamine
TAMRA-PEG-PE	5(6)-carboxytetramethylrhodamine-labeled PEGylated phosphatidylethanolamine
TEM	transmission electron microscopy
Tf	transferrin

TfR	transferrin receptor
THF	tetrahydrofurane
TOP	trioctylphosphine
TOPO	trioctylphosphine oxide
TOPS	trioctylphosphine sulfide
TOPSe	trioctylphosphine selenide
tris	Tris(hydroxymethyl)aminomethane
TRK	receptor tyrosine kinase
UV	ultraviolet light or irradiation
Zn	zink
ZnS	zinc sulfide

## Curriculum vitae

Name: Wolfgang Alexander Hild  
Date of birth: July 07, 1981  
Place of birth: Freising, Germany  
Nationality: German  
Marital status: Single

### *Education*

09/1987 – 07/1991 Elementary School Landshut Berg, Landshut  
09/1991 – 06/2000 Hans Carossa Grammar School, Landshut  
06/2000 University-entrance diploma (Abitur)

### *Professional Training*

10/2000 – 10/2004 Studies of Pharmacy, University of Regensburg  
11/2004 – 04/2005 Practical Training, Hofberg Apotheke Landshut  
05/2005 – 04/2009 PhD program, Department of Pharmaceutical Technology,  
University of Regensburg  
Member of Research Training Group of the German  
Research Foundation (DFG), GRK 760 Medicinal  
Chemistry: Molecular Recognition-Ligand-Receptor  
Interactions”  
12/2005 Acquisition of license to practice as pharmacist  
since 05/2009 Dr. R. Pfleger Chemische Fabrik GmbH  
Head of Packaging Department





W. Hild, K. Pollinger, A. Caporale, C. Cabrele, M. Breunig, J. Teßmar, A. Göpferich: Peptide-mediated nanoparticle delivery by G-protein coupled receptors (GPCRs). 4th Summer School "Medicinal Chemistry", Regensburg (2008) – **Poster**

W. Hild, K. Pollinger, A. Caporale, C. Cabrele, M. Breunig, J. Teßmar, A. Göpferich: G-Protein Coupled Receptors – New Portals for Nanoparticles in Cellular Drug Targeting?. 2nd World Conference on Magic Bullets - Ehrlich II, Nuremberg (2008) – **Talk**

W. Hild, K. Pollinger, A. Caporale, C. Cabrele., M. Breunig, J. Teßmar, A. Göpferich: Targeting Cells with Nanoparticles using G-Protein coupled Receptors (GPCRs). Controlled Release Society, German Chapter, Halle (2009) – **Talk**

W. Hild, K. Pollinger, A. Caporale, C. Cabrele, M. Breunig, J. Teßmar, A. Göpferich: Nanoparticle Delivery into Target Cells by G-Protein Coupled Receptors. 36th Annual Meeting and Exposition of the Controlled Release Society, Copenhagen (2009) – **Poster**

*Presentations – Research Training Group*

W. Hild, Cellular Uptake of Nanoparticles by G-Protein Coupled Receptors, Regensburg (December 2005) – **Poster**

W. Hild, Surface Modifications of Quantum Dot Colloids, Regensburg (May 2006) – **Talk**

W. Hild, Characterization of quantum dot micelles for cellular studies, Regensburg (November 2006) – **Talk**

W. Hild, Development and Characterization of Water-soluble Quantum Dots, Regensburg, (May 2007) – **Talk**

W. Hild, Towards Targeted Nanoparticles for Intracellular Delivery, Regensburg (October 2007) – **Talk**

W. Hild, Towards Peptide-modified Nanocrystals For Drug Targeting Applications, Regensburg (April 2008) – **Talk**

W. Hild, G-Protein Coupled Receptors – New Portals for Nanoparticles in Cellular Drug Targeting?, Regensburg (October 2008) – **Talk**

## Acknowledgements

I especially thank Prof. Dr. Achim Göpferich for giving me the opportunity of working in his research team and for committing this fascinating project to me. I also appreciate his enthusiasm, the inspiring discussions and his unconfined view concerning new ideas. Moreover, I acknowledge the excellent training in scientific presentation and the motivation to take part in numerous scientific conferences.

My deep thank is due to Dr. Jörg Teßmar for his excellent scientific support and his patience when advice was needed. He was decisively responsible for the great working atmosphere at the department and for keeping things go in the lab routine.

I sincerely thank Dr. Miriam Breunig for her continuous scientific contribution and the valuable discussions as well as her support in the preparation of the manuscripts.

I also thank Dr. Torsten Blunk for his interest in my work and the valuable discussions during and after work.

I would like to thank the whole Research Training Group GRK 760 Medicinal Chemistry: Molecular Recognition-Ligand-Receptor Interactions", all colleagues and supervisors, especially Prof. Dr. Armin Buschauer, for creating an inspiring and cooperative scientific working atmosphere and many critical and helpful discussions.

Moreover, I would like to thank Prof. Dr. Chiara Cabrele for the synthesis of the peptides and for the helpful discussions. Many thanks as well are due to Dr. Andrea Caporale for conducting the peptide synthesis.

My sincere thanks are due to Renate Liebl who introduced me to working techniques in cell culture. I could count on her friendly help in busy work days in the lab and on her helpful advice for the experiments.

Moreover, I would like to thank Prof. Deutzmann, Eduard Hochmuth, Angelika Berrié and Josef Kiermaier for the mass analysis, Stephanie Bauer for the introduction into the microinjection technique and Prof. Dr. Ralph Witzgall for providing the microinjection unit, Dr. Markus Drechsler, University of Bayreuth, for the cryo-TEM measurement and Dr. Reinhard Rachel for the TEM measurement.

I would like to thank Dr. Robert Lang, Department of Pharmaceutical Technology of Prof. Dr. Gerhard Winter at the University of Munich, for his help with the AF4 measurements.

I sincerely thank our secretaries Lydia Frommer and Liane Öttl for always being helpful and for the organization of the every day routine.

Many thanks are due to Katharina Zenger for actively taking part in the research for half a year during her practical training. It was a great time working together.

My thanks also go to Patrick Spicer, to Christoph Luschmann and Anja Huber, to Ralph Bauer and Michael Schmalzbauer, to Andrea Poxleitner and Julia Scharnowell, to Laure Viguerie, to Julia Häring and to Florian Schlenk, for their active

contributions to the project during their internships. It was a pleasure for me working with them and I appreciate their help in the lab work.

I express my deep gratitude to all my former and present colleagues in the workgroup of the Department of Pharmaceutical Technology. They created an atmosphere of companionship and made the time at the department valuable and unforgettable for me. My special thanks go to the following colleagues:

My former lab mate Dr. Bernhard Appel for the great time and the best coffee available at the university

My lab mate Julia Baumer for her support and the good talks

Ferdinand Brandl for the great time and the helpful discussions during and after work

Axel Ehmer for being a great colleague and for giving me motivation to start running

Klaus Pollinger for his cooperation in the project, the great time in the last year of my work and for continuing this project

Dr. Stefan Rothschenk for the great time and his help handling the HPLC

Grateful acknowledgements are due the financial support of the German Research Foundation (DFG) for the grant during the first three years of my research and for supporting travels to all the conferences and courses.

Special thanks are due to Dr. Leon Bellan, Adam Cerkeliunas, Dr. Johnna Temenoff and Dr. Cornelia Zeltner for the critical revision of the manuskripts and parts of this thesis.

Finally I want to express my deep thank to my parents Elfriede and Jürgen Hild for their support and assistance during my study years and the PhD period and for encouraging me to follow this path.

